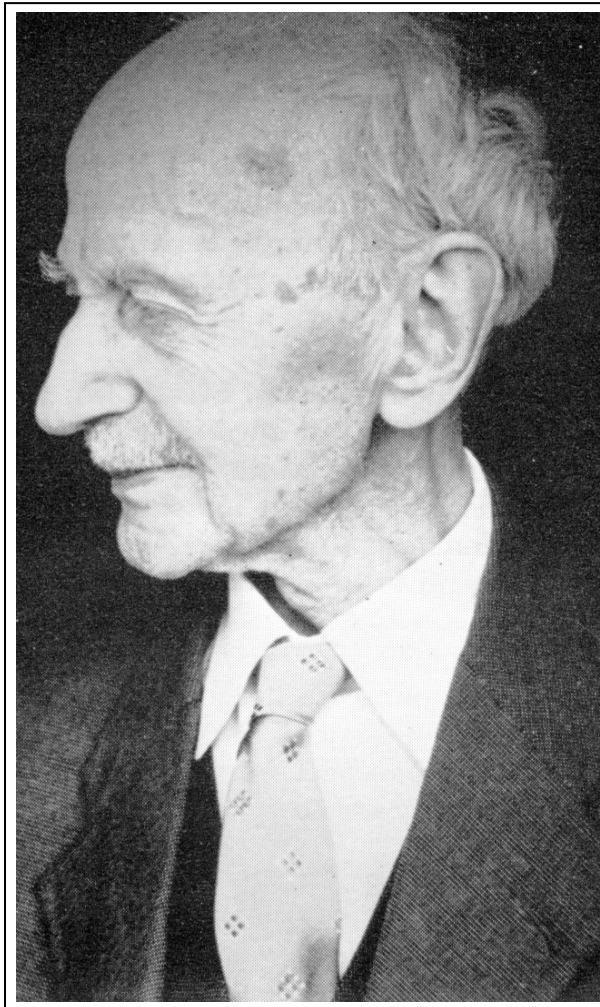

MOLECULAR AND BIOCHEMICAL INVESTIGATIONS INTO VMD2,

THE GENE ASSOCIATED WITH BEST DISEASE

**DISSERTATION ZUR ERLANGUNG DES
NATURWISSENSCHAFTLICHEN DOKTORGRADES
DER BAYERISCHEN JULIUS-MAXIMILIANS-UNIVERSITÄT WÜRZBURG**

**VORGELEGT VON
FRANZISKA KRÄMER
AUS MARKTREDWITZ**

WÜRZBURG 2003



„Über eine hereditäre Maculaaffection“

*Die Augenerkrankung Morbus Best wurde erstmalig von
Priv.-Doz. Dr. Friedrich Best im Jahre 1905 in der
Zeitschrift für Augenheilkunde beschrieben.*

Eingereicht am 27. März 2003

Bei der Fakultät für Biologie

Mitglieder der Promotionskommission

Vorsitzender: Prof. Dr. Rainer Hedrich

Gutachter: Prof. Dr. Bernhard H.F. Weber

Gutachter: Prof. Dr. Peter Seibel

Tag des Promotionskolloquiums: 21. Mai 2003

Doktorurkunde ausgehändigt:

Erklärung gemäß §4, Absatz 3 der Promotionsordnung für die Fakultät für Biologie der Universität Würzburg:

Hiermit erkläre ich, dass ich die vorliegende Dissertation selbständig durchgeführt und verfasst habe.

Andere Quellen als die angegebenen Hilfsmittel und Quellen wurden nicht verwendet.

Die Dissertation wurde weder in gleicher noch in ähnlicher Form in einem anderen Prüfungsverfahren vorgelegt.

Es wurde zuvor kein anderer akademischer Grad erworben.

Die vorliegende Arbeit wurde am Institut für Humangenetik der Universität Würzburg unter der Leitung von Prof. Bernhard H.F. Weber angefertigt.

Würzburg, den 27. März 2003

VIELEN DANK! THANK YOU! DOBRY DEN!

An dieser Stelle möchte ich mich bei allen Personen recht herzlich Bedanken, die im Laufe der Jahre in irgendeiner Art und Weise am Gelingen dieser Arbeit beteiligt waren.

*In erster Linie gilt Prof. Dr. **Bernhard Weber** mein besonderer Dank für die Möglichkeit in seiner Arbeitsgruppe die Dissertation anzufertigen. Weiterhin möchte ich mich für die hervorragende fachliche Betreuung und sein zeitliches Engagement bedanken.*

*Mein Dank sei an Prof. **Peter Seibel** als Vertreter der Fakultät für Biologie für die kurzfristig Übernahme der Begutachtung dieser Arbeit gerichtet.*

*Ein Teil der Disseration wurde in der Arbeitsgruppe von Dr. Burkard Kneitz angefertigt. Bei **Burkard** sowie seinen Mitarbeiterinnen **Anja** und **Martina** möchte ich mich für die Einführung in die Welt der ES Zellkultur, für die Nutzung der Laborräumlichkeiten und für die freundliche Zusammenarbeit bedanken.*

*Bedanken möchte ich mich weiterhin bei allen jetzigen und ehemaligen KollegInnen der AG Weber. Ihr habt ein wunderbares Arbeitsklima geschaffen, in dem man sich sehr wohl fühlt, gerne viel Zeit verbringt und man sich stets auf fachliche Hilfestellung verlassen kann. **Andrea Gehrig**, danke für die wissenschaftlichen Tipps und das große Interesse meiner Versuchsplanung und -durchführung, **Andrea Rivera**, für die vielen Selbstverständlichkeiten, **Birgit Geis**, für die Weiterführung einiger Teilprojekte, **Nicole Mohr**, für die Durchführung der Mutationsanalysen und **Vladimir Milenkovic** für die Bereitschaft die Mäuse zu präparieren und für seine Computerhilfen aller Art. Für das mühsame Korrekturlesen möchte ich mich vor allem bei **Heidi Schulz** und **Jelena Stojic** bedanken.*

*Auch ein Dankeschön an die Mitarbeiter der Nachbarlabors im 3. und 4. Stock - vor allem an **Birgit Halliger-Keller**, die immer einen hilfreich Rat in allen Lebens- und Labor(not)lagen hat und die mich alljährlich mit den allerbesten Weihnachtsplätzchen versorgt! Bei **Indrajit Nanda** möchte ich mich für die netten Kaffee-mit-Hörnchen-Pausen am Wochenende bedanken.*

*Ein riesengroßes Dankeschön an all meine Freunde sowie meine Familie, an meine **Oma**, meine **Mutter**, **Andreas**, meine Schwester **Ina** und **Martin**. Danke, dass ihr in guten wie in schlechten „Versuch-klappt-nicht“-Zeiten für mich da wart! Meinem Freund **Frank** danke ich für die unendlich große Unterstützung und die superschöne Zeit die wir zusammen haben.*

DIE ARBEIT WIDME ICH MEINEM VATER, OTTO KRÄMER

TABLE OF CONTENTS

I SUMMARY	1
II ZUSAMMENFASSUNG	3
III INTRODUCTION	5
1 THE RETINA AND RETINAL DEGENERATION	5
2 BEST DISEASE	8
2.1 CLINICAL FEATURES OF BEST DISEASE.....	8
2.2 ELECTROPHYSIOLOGY IN BEST DISEASE.....	9
2.3 GENETICS OF BEST DISEASE.....	10
2.4 BIOCHEMISTRY OF BESTROPHIN.....	11
3 GOAL OF THE THESIS	14
IV RESULTS	16
1 MUTATIONAL ANALYSIS OF HUMAN VMD2	16
1.1 NOMENCLATURE.....	16
1.2 CLASSIFICATION OF MUTATIONS, RARE VARIANTS AND COMMON POLYMORPHISMS.....	16
1.3 IDENTIFICATION OF SEQUENCE CHANGES IN THE <i>VMD2</i> GENE.....	17
1.4 EVALUATION OF NOVEL DISEASE-ASSOCIATED MUTATIONS.....	20
1.5 EVALUATION OF NOVEL RARE SEQUENCE VARIANTS.....	20
1.6 FUNCTIONAL ASSAY TO EVALUATE THE 624G>A TRANSITION.....	21
1.7 DETERMINATION OF ALA243VAL FREQUENCY IN A CONTROL POPULATION.....	24
1.8 THE VMD2 MUTATION DATABASE.....	25
1.9 FREQUENT POLYMORPHISMS IDENTIFIED IN THE <i>VMD2</i> GENE.....	27
2 FUNCTIONAL ANALYSIS OF HUMAN BESTROPHIN	28
2.1 ANTIBODY REPERTOIRE AGAINST HUMAN AND BOVINE BESTROPHIN.....	28
2.1.1 Selection of antigens and production of polyclonal antibodies.....	28
2.1.2 Recombinant partial and full length bestrophin.....	30
2.1.3 Characterization of polyclonal antisera.....	31
2.2 HETEROLOGOUS EXPRESSION OF MUTANT BESTROPHIN.....	34
2.3 SUBCELLULAR LOCALIZATION OF BESTROPHIN.....	36
2.3.1 Membrane fractionation.....	36
2.3.2 Immunocytochemistry.....	37
3 IDENTIFICATION AND CHARACTERIZATION OF THE MURINE VMD2-RFP-TM FAMILY	39
3.1 <i>IN SILICO</i> CHARACTERIZATION OF THE MURINE RFP-TM GENE FAMILY.....	39
3.1.1 Identification, genomic organisation and chromosomal localization.....	39
3.1.1.1 Murine Vmd2.....	39
3.1.1.2 Murine Vmd2L1.....	44
3.1.1.3 Murine Vmd2L2.....	48
3.1.1.4 Murine Vmd2L3.....	53
3.2 <i>IN SILICO</i> CHARACTERIZATION OF THE MURINE RFP-TM PROTEIN FAMILY.....	58
3.2.1 Syntenic grouping.....	58
3.2.2 Multiple sequence alignment and analysis of transmembrane domains.....	59
3.2.3 Phylogenetic tree.....	62
3.3 EXPRESSION PROFILE OF MURINE <i>VMD2</i> , <i>VMD2L1</i> AND <i>VMD2L3</i> BY REAL-TIME QUANTITATIVE REVERSE TRANSCRIPTASE POLYMERASE CHAIN REACTION (QRT PCR).....	62
4 VMD2 KNOCK-IN AND KNOCK-OUT MICE	70
4.1 GENERATION OF MURINE KNOCK-IN AND KNOCK-OUT CONSTRUCTS.....	70
4.1.1 Cloning strategy for the knock-in construct.....	71

4.1.2 Cloning strategy for the knock-out construct	74
4.2 TRANSFECTION OF EMBRYONIC STEM (ES) CELLS WITH MUTANT CONSTRUCTS.....	76
4.3 SCREENING FOR ES CELLS CONTAINING HOMOLOGOUS RECOMBINATION EVENTS WITH MUTANT CONSTRUCTS.....	78
4.3.1 Screening for knock-in ES cells	78
4.3.2 Screening for knock-out ES cells	79

V DISCUSSION..... 81

1 MOLECULAR STUDIES OF HUMAN VMD2.....	82
1.1 MUTATIONAL ANALYSIS OF THE HUMAN VMD2 GENE	82
1.1.1 Novel disease-associated missense mutations.....	83
1.1.2 Novel disease-causing deletion	86
1.1.3 Novel rare variants identified in human VMD2.....	87
1.1.4 Topology of bestrophin and the distribution of mutations	88
1.2 GENOTYPE/PHENOTYPE CORRELATIONS	90
1.3 VMD2 MUTATIONS CAUSATIVE FOR OTHER MACULOPATHIES.....	91
1.4 MUTATION DETECTION RATES	92
1.5 FUNCTIONAL ANALYSIS OF BESTROPHIN	93
1.5.1 VMD2-specific antibodies	93
1.5.2 Heterologous expression of mutant and wild-type VMD2.....	94
1.5.3 Immunocytochemistry.....	94
1.6 PROPOSED MOLECULAR MECHANISMS/PATHOMECHANISMS OF HUMAN VMD2	95
1.6.1 Is bestrophin a subunit of a homo/hetero-oligomeric channel?.....	95
1.6.2 Is bestrophin a calcium sensitive chloride channel?.....	96
1.6.3 Is bestrophin interacting with protein phosphatase 2A?.....	97
2 THE MOUSE VMD2 RFP-TM PROTEIN FAMILY	98
2.1 THE MOUSE GENOME SEQUENCING CONSORTIUM (MGSC).....	98
2.2 THE MURINE VMD2 RFP-TM PROTEIN FAMILY.....	98
2.3 COMPARATIVE ANALYSIS OF THE MOUSE AND HUMAN GENOME: GENE, EXON AND INTRON SIZES	99
2.4 ESTABLISHMENT OF THE SEQUENCE BEYOND EXON NINE OF THE VMD2 RFP-TM GENE FAMILY	101
2.5 EXPRESSION PROFILE OF MURINE VMD2 AND ITS FAMILY MEMBERS.....	101
2.6 IS MURINE VMD2L2 A PSEUDOGENE?	103
2.7 DIFFERENTIAL SPLICING OF MURINE VMD2L3	104
3 THE RELEVANCE OF KNOCK-IN AND KNOCK-OUT MOUSE MODELS	105

VI MATERIALS AND METHODS 109

1 CLINICAL DATA OF PATIENTS	109
2 GENERAL METHODS OF MICROBIOLOGY	109
3 DNA-SPECIFIC METHODS OF MOLECULAR BIOLOGY.....	109
3.1. DNA EXTRACTION.....	109
3.1.1 Extraction of human genomic DNA.....	109
3.1.2 Extraction of PAC DNA.....	110
3.1.3 Extraction of plasmid DNA.....	110
3.2 QUANTIFICATION OF DNA.....	110
3.3 RESTRICTION ENZYME DIGESTION	111
3.4 SOUTHERN BLOT.....	111
3.4.1 Labeling of DNA probes	111
3.4.2 DNA transfer (Southern blotting).....	112
3.4.3 Hybridization and washing.....	112
3.5 ISOLATION OF GENOMIC PAC CLONES.....	112

3.6	PCR AMPLIFICATION.....	113
3.7	DIRECT SEQUENCING OF PCR PRODUCTS.....	113
3.8	MUTATION SCREENING OF HUMAN VMD2.....	115
3.9	CLONING OF PCR PRODUCTS.....	115
3.9.1	T-overhang cloning.....	115
3.9.2	Cloning by introducing restriction sites.....	116
3.9.3	Vector modifications.....	116
3.9.4	Ligation.....	117
3.10	SITE-DIRECTED MUTAGENESIS.....	117
4	RNA-SPECIFIC METHODS.....	118
4.1	TOTAL RNA ISOLATION.....	118
4.2	NORTHERN BLOTTING.....	119
4.3	FIRST STRAND CDNA SYNTHESIS.....	119
4.4	3'-RAPID AMPLIFICATION OF CDNA ENDS (3'-RACE).....	120
4.5	REVERSE TRANSCRIPTASE (RT) PCR.....	120
4.6	REAL TIME QUANTITATIVE RT PCR.....	121
5	MAMMALIAN CELL CULTURE.....	122
5.1	COS7 CELL CULTURE.....	122
5.1.1	Transient Transfection of COS7 cells.....	122
5.1.2	The Exon Trapping System.....	123
5.2	EMBRYONIC STEM CELL CULTURE.....	124
5.2.1	Handling of feeder cells.....	124
5.2.2	Handling of ES cells.....	124
5.2.3	Establishment of stable cell lines.....	125
5.2.3.1	Preparation of targeting DNA.....	125
5.2.3.2	Electroporation.....	125
5.2.3.3	DNA extraction of stable ES cell lines.....	126
5.2.3.4	Screening for homologous recombination events in stable ES cell lines.....	126
6	PROTEIN BIOCHEMISTRY.....	126
6.1	PREPARATION OF PROTEIN EXTRACTS.....	126
6.1.1	Bacterial lysates.....	127
6.1.2	Whole cell protein extracts of COS7 cells.....	127
6.1.3	Membrane fractionation of COS7 cells.....	127
6.1.4	RPE tissue extracts.....	128
6.2	WESTERN BLOTTING.....	128
6.2.1	Sodium dodecyl sulfate polyacrylamide gel electrophoresis (SDS-PAGE).....	128
6.2.2	Antibody generation.....	129
6.2.3	Purification of antibodies by affinity chromatography.....	129
6.2.4	Immunoblotting.....	129
6.3	IMMUNOCYTOCHEMISTRY.....	130
7	METHODS OF BIOCOMPUTATION.....	130
<u>VII REFERENCES.....</u>		<u>132</u>
<u>VIII APPENDIX.....</u>		<u>142</u>
1	CDNA AND PUTATIVE AMINO ACID SEQUENCE OF BOVINE VMD2.....	142
2	ABBREVIATIONS.....	144
<u>IX CURRICULUM VITAE.....</u>		<u>145</u>
<u>X LIST OF PUBLICATIONS.....</u>		<u>146</u>

I SUMMARY

Best disease (OMIM 153700) is an early-onset, autosomal dominant maculopathy characterized by bilateral egg yolk-like lesions in the central retina. The disease gene, the vitelliform macular dystrophy gene type 2 (*VMD2*), encodes a 585-aa VMD2 transmembrane protein, termed bestrophin. The protein is predominantly expressed on the basolateral side of the retinal pigment epithelium (RPE) and is thought to be involved in the transport of chloride ions across the plasma membrane. Bestrophin as well as three closely related VMD2-like proteins (*VMD2L1-L3*) contain multiple putative transmembrane (TM) domains and an invariant tripeptide motif of arginine (R), phenylalanine (F) and proline (P) in the N-terminal half of the protein. This and the tissue-restricted expression to polarized epithelial cells are typical features of the VMD2 RFP-TM family.

Best disease is predominantly caused by missense mutations, clustering in four distinct „hotspots“ in the evolutionary highly conserved N-terminal region of the protein. To further augment the spectrum of mutations and to gain novel insights into the underlying molecular mechanisms, we screened VMD2 in a large cohort of affected patients. In total, nine novel VMD2 mutations were identified, raising the total number of known Best disease-related mutations from 83 to 92. Eight out of nine novel mutations are hotspot-specific missense mutations, underscoring their functional/structural significance and corroborating the dominant-negative nature of the mutations. Of special interest is a one-basepair deletion (Pro260fsX288) encoding a truncated protein with a deletion of an important functional domain (TM domain four) as well as the entire C-terminal half of bestrophin. For the first time, a nonsense mutation leading to a 50 % non-functional protein has been identified suggesting that on rare occasions Best disease may be caused by haploinsufficiency.

Molecular diagnostics strongly requires a reliable classification of VMD2 sequence changes into pathogenic and non-pathogenic types. Since the molecular pathomechanism is unclear at present, the pathogenicity of novel sequence changes of VMD2 are currently assessed in light of known mutations. We therefore initiated a publicly accessible VMD2 mutation database (<http://www.uni-wuerzburg.de/humangenetics/vmd2.html>) and are collecting and administrating the growing number of mutations, rare sequence variants and common polymorphisms.

Missense mutations may disrupt the function of proteins in numerous ways. To evaluate the functional consequences of VMD2 mutations in respect to intracellular mislocalization and/or

protein elimination, a set of molecular tools were generated. These included the establishment of an *in vitro* COS7 heterologous expression assay, the generation of numerous VMD2 mutations by site-directed mutagenesis as well as the development of bestrophin-specific antibodies. Surprisingly, membrane fractionation/Western blot experiments revealed no significant quantitative differences between intact and mutant bestrophin. Irrelevant of the type or location of mutation, incorporation of mutant bestrophin to the membranous fraction was observed. These experiments provide first indications that impaired membrane integration may be ruled out as causative pathomechanism of Best disease consistent with a dominant-negative effect of the mutations.

In a different approach, efforts were directed towards identifying and characterizing the VMD2 RFP-TM protein family in mouse. While clarification of the genomic organization of murine *Vmd2* was required as basis to generate *Vmd2*-targeted animals (see below), the study of closely related proteins (*Vmd2L1*, *Vmd2L2* and *Vmd2L3*) may provide further clues as to the function of bestrophin. Biocomputational analyses (EST assembly, TM domain predictions, syntenic grouping, etc.), supplemented by RT PCR analysis were used to identify, characterize and independently confirm the four novel murine orthologues. Moreover, the novel genes were analyzed by real time quantitative RT PCR, displaying predominant expression in testis, colon and skeletal muscle of *Vmd2*, *Vmd2L1* and *Vmd2L3* transcripts, respectively as well as in eye tissue. Interestingly, neither an ORF was determined for murine *Vmd2L2* nor was the transcript present in a panel of 12 mouse tissues, suggesting that murine *Vmd2L2* may represent a functionally inactive pseudogene. The murine *Vmd2L3* gene, as its human counterpart, is a highly differentially spliced transcript.

Finally, generating mouse models of Best disease will provide essential tools to investigate the pathophysiology of bestrophin *in vivo*. We have initiated the generation of two different mouse lineages, one deficient of *Vmd2* (knock-out) and the other carrying a human disease-related mutation (Tyr227Asn) in the orthologous murine gene (knock-in). Genetic engineering of both constructs has been achieved and presently, four ES clones harboring the homologous recombination event (*Vmd2*^{+/-}) have been isolated and are ready for the subsequent steps to generate chimeric animals. The resulting *Vmd2*-deficient knock-out and the Tyr227Asn-containing knock-in mouse lineages will represent two key models, opening an entirely new field of experimental possibilities to elucidate the functional role of bestrophin in Best disease, in RPE development and physiology.

II ZUSAMMENFASSUNG

Morbus Best (OMIM 153700) ist eine autosomal dominant vererbte Makulopathie mit juvenilem Beginn. Charakteristisch sind beidseitige, Eidotter-ähnliche Läsionen im zentralen Bereich der Retina. Das krankheitsverursachende Gen, das vitelliforme Makuladystrophie-Gen Typ 2 (*VMD2*), kodiert für ein 585 Aminosäuren langes Transmembranprotein. Das als Bestrophin bezeichnete Protein ist vorwiegend auf der basolateralen Seite des retinalen Pigmentepithels (RPE) exprimiert und wahrscheinlich am Transport von Chloridionen über die Plasmamembran beteiligt. Bestrophin wie auch die drei eng-verwandten *VMD2*-ähnlichen Proteine (*VMD2L1-L3*) enthält in seiner N-terminalen Hälfte mehrere putative Transmembrandomänen (TM) und ein invariables Tripeptid aus Arginin (R), Phenylalanin (F) und Prolin (P). Diese Sequenzeigenschaften sowie die auf polarisierte Zelltypen beschränkte Expression kennzeichnen die Familie der *VMD2* RFP-TM Proteine.

Morbus Best wird hauptsächlich durch „missense“ Mutationen verursacht die in vier Bereichen („hotspots“) innerhalb der evolutionär stark konservierten N-terminalen Region des Proteins akkumulieren. Um das Mutationsspektrum zu erweitern und darüber hinaus den zugrundeliegenden molekularen Mechanismus weitergehend aufzuklären, wurde das *VMD2* Gen in einer großen Anzahl betroffener Patienten untersucht. Insgesamt wurden neun bisher nicht beschriebene Mutationen identifiziert, wodurch sich die Anzahl der bekannten krankheitsassoziierten Mutationen auf 92 erhöhte. Wie die meisten der bisher bekannten Mutationen befinden sich acht „missense“ Mutationen in den sogenannten „hotspots“ des Gens. Dies unterstreicht die funktionelle bzw. strukturelle Bedeutung der betroffenen Regionen sowie den dominant-negativen Effekt der Mutationen. Bemerkenswert ist eine atypische 1-Basenpaar-Deletion (Pro260fsX288). Der fehlerhafte Leserahmen kodiert für ein verkürztes Protein, dem die funktionell wichtige vierte Transmembrandomäne und die gesamte C-terminale Hälfte fehlt. Erstmals wurde somit eine „nonsense“ Mutation im *VMD2* Gen identifiziert, die 50 % nicht-funktionelles Protein zur Folge hat. In seltenen Fällen kann daher die durch „nonsense“ Mutationen bedingte Haploinsuffizienz der Krankheit zugrunde liegen.

Die molekulare Diagnostik verlangt eine zuverlässliche Einteilung der *VMD2* Sequenzänderungen in pathogene und nicht-pathogene Gruppen. Da der molekulare Pathomechanismus zurzeit weitgehend ungeklärt ist, wird die Pathogenität neuer Sequenzänderungen aufgrund bereits bekannter Mutationen eingestuft. Es wurde daher eine öffentlich zugängliche *VMD2* Mutationsdatenbank eingerichtet (<http://www.uni-wuerzburg.de/humangenetics/vmd2.html>), in der die wachsende Zahl an Mutationen, Sequenzvarianten und Polymorphismen gesammelt und verwaltet wird.

„Missense“ Mutationen können die Proteinfunktion auf verschiedene Weise beeinträchtigen. Geeignete molekulare Assays wurden daher etabliert, um die funktionellen Auswirkungen der VMD2 Mutationen in Hinblick auf die intrazelluläre Lokalisation und/oder den Proteindegredation zu untersuchen. In der vorliegenden Arbeit wurde ein heterologes COS7 Expressionssystem entwickelt, es wurden verschiedene Mutationen mittels „site-directed mutagenesis“ generiert sowie Bestrophin-spezifische Antikörper hergestellt. Überraschenderweise konnte anhand von Membranfraktionierungs- und Westernblot-Analysen keine signifikanten quantitativen Unterschiede zwischen intakten und mutierten Bestrophin nachgewiesen werden. Unabhängig von Art oder Position der Mutation konnte der Einbau von mutiertem Bestrophin in die Membran gezeigt werden. Die Experimente deuten erstmalig darauf hin daß eine fehlerhafte Membranintegration als kausaler krankheitsverursachender Mechanismus ausgeschlossen werden kann. Dies liegt in Übereinstimmung mit dem dominant-negativen Effekt der Mutationen.

In einem alternativen Ansatz wurde die VMD2 RFP-TM Proteinfamilie im Mausgenom identifiziert und charakterisiert. Während die Aufklärung der genomischen Struktur des *Vmd2* Gens die Grundlage zur Herstellung *Vmd2* transgener Mäuse darstellte (siehe unten), gewährte die Charakterisierung der eng verwandten *Vmd2L1-L3* Mausgene weitere Einblicke in die Funktion des Bestrophins. Anhand von bioinformatische Analysen („EST-Assembly“, TM Vorhersagen, syntenische Gruppierungen usw.) zusammen mit RT PCR Untersuchungen konnten die vier orthologen Gene in Maus erstmalig identifiziert, charakterisiert und in unabhängigen Experimenten bestätigt werden. Darüber hinaus wurde die präferentielle Expression der jeweiligen Transkripte in Testis, Kolon und Skelettmuskel sowie Augengewebe anhand von „real-time quantitative“ RT PCR nachgewiesen. Interessanterweise konnte für *Vmd2L2* weder ein offenes Leseraster noch ein Transkript in 12 untersuchten Mausgeweben detektiert werden. *Vmd2L2* stellt wahrscheinlich ein funktionell inaktives Pseudogen dar. Ähnlich wie sein humanes Gegenstück wird das Maus *Vmd2L3*-Transkript auf mRNA Ebene differentiell prozessiert.

Mausmodelle für Morbus Best stellen grundlegende Hilfsmittel dar, die Pathophysiology von Bestrophin *in vivo* zu untersuchen. Es wurde die Herstellung zweier verschiedener Mauslinien initiiert: zum einen ein *Vmd2*-defizientes „knock-out“ Modell, zum anderen eine „knock-in“ Maus, die eine humane krankheitsassoziierte Mutation (Tyr227Asn) im mausorthologen Gen trägt. Die entsprechenden Konstrukte wurden hergestellt und in ES Zellen eingeschleust. Ausgehend von bislang vier isolierten ES Klonen, die den *Vmd2*^{+/-} Genotyp tragen, können nun in nachfolgenden Schritten chimäre Tiere generiert werden. Die resultierenden *Vmd2*-defizienten „knock-out“ sowie die Tyr227Asn-tragende „knock-in“ Mauslinien repräsentieren neue experimentelle Ansätze, die funktionelle Rolle des Bestrophins in Morbus Best sowie in der Entwicklung und Physiology des RPEs aufzuklären.

III INTRODUCTION

1 THE RETINA AND RETINAL DEGENERATION

The human eye is a highly developed sensory organ (Fig. 1). Different ocular structures including the iris, cornea, lens, pupil, vitreous body, sclera and retina are required for proper vision. Of these structures, the retina is a specialized multi-layered sensory tissue (Fig. 2, right), converting incident light energy into electrical signals and transmitting them to the brain via the optic nerve. This light-sensitive tissue consists of ten discrete layers composed of multiple specialized cell types. Rod photoreceptors with the photopigment rhodopsin and cone photoreceptors with the photopigment iodopsin are primarily involved in converting light to electrical impulses producing black-and-white and colored images, respectively. Bipolar and ganglion cells function as conducting neurons, while Muller's and neuroglial cells are supporting cells. Horizontal and amacrine cells function as association cells to other neurons.

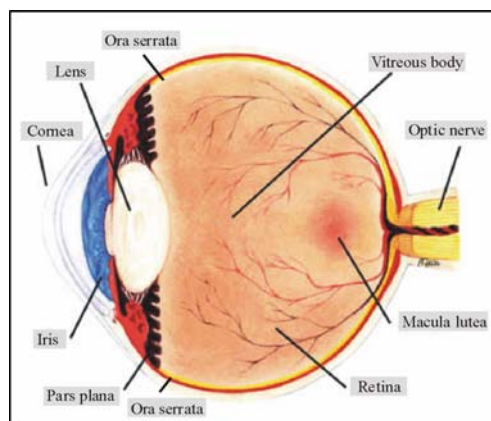


Fig. 1 The human eye and vision

The cornea is a window-like, transparent region allowing light to enter the eye. The amount of light entering the eye, is regulated by the iris, controlling the size of the pupil by means of contraction and expansion. The crystalline lens is responsible for focusing light onto the retina. Then, light passes through the vitreous body, a clear jelly-like substance filling the eye's cavity. The retina lines the inside wall of the eye, and it functions primarily as converter of light signals to electrical impulses. The optic nerve carries these electric impulses to the brain, where processing of electrical impulses takes place. In the central area of the retina, the macula lutea is located, responsible for highest visual acuity. Figure taken from: <http://www.vrmny.com/anatomy.htm>.

All parts of the retina are responsible for vision, but the macula lutea is essential for visual acuity and color perception (Cavallerano et al. 1997). The 5 – 6 mm sized macula is located almost in the centre of the retina with a unique photoreceptor composition (Fig. 2, left). While the largest part of the retina is formed by approximately 120 million rods, the macula lutea predominantly consists of 6 – 7 million cones. The fovea centralis, a small rod-free area of 0.4 mm in diameter, is found in the very centre of the macula. Here, the cones are most densely packed, thinner and individually connected to nerve fibers, resulting in maximum visual acuity and color sensitivity. Another unique characteristic of the fovea centralis is the absence of blood vessels, allowing a direct light path to the photoreceptors.

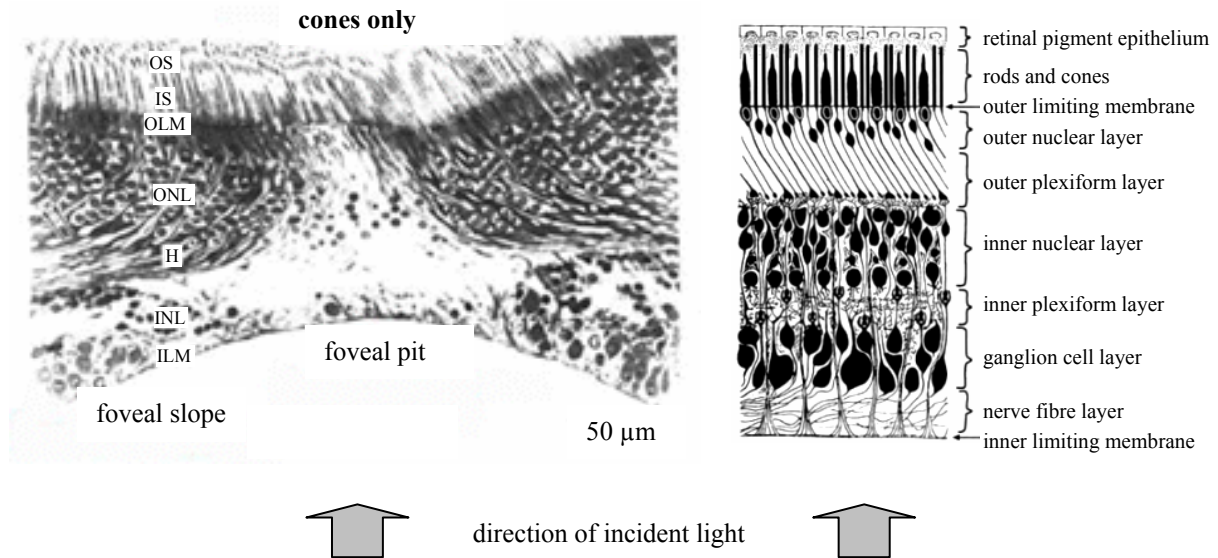


Fig. 2 Vertical section of the human macula (left) and schematic of the ten layers of the retina (right)

As shown on the left, special structures of the macula lutea are the foveal slope and rod-free foveal pit. Cell types of the macula include the outer segments (OS), inner segments (IS), outer limiting membrane (OLM), outer nuclear layer (ONL), Henle fibre layer (H), inner nuclear layer (INL) and inner limiting membrane (ILM). Figure taken from: <http://webvision.med.utah.edu/sretina.html>. The schematic on the right shows ten histologically distinct layers composing the neuronal retina.

Figure taken from: <http://www3.umdj.edu/histsweb/lab13/lab13ey2.html>.

Retinal degeneration is the most common cause of incurable vision loss in the industrialized world and accounts for more than 50 % of registered blindness. Generally, retinal degeneration encompasses disorders associated with the progressive loss of retinal cell types. Several hundred distinct entities exist within this group which vary in age of onset, disease progression and severity of symptoms. Retinal degenerations are heterogeneous, not only clinically but also genetically. Some are monogenic disorders with simple patterns of Mendelian inheritance, others are complex diseases resulting from environmental as well as genetic factors. Single genes may account for multiple disease phenotypes, and vice versa, multiple genetic deficiencies may cause similar retinal phenotypes. To date, over 85 retinal genes have been cloned and an additional 130 retinal disease loci have been mapped awaiting their identification (RetNet database¹). In most cases, the underlying disease-causing mechanisms are still unclear.

Due to the complex processes underlying the retinal degenerations, no general rules of systematic classification exist. Inherited retinal degenerations may be classified according to their age of onset (congenital, early childhood or late in adult life), their inheritance pattern (autosomal dominant, autosomal recessive or X-linked), their clinical symptoms or their

¹ RetNet (Retinal Information Network): <http://www.sph.uth.tmc.edu/Retnet/home.htm>

underlying genetic defects. Based on a classification scheme by Kellner (1997a, 1997b and website²), retinal degenerations are subdivided into two main categories, the „generalized retinal/choroid types” predominantly affecting peripheral and night vision (e.g. retinitis pigmentosa) and the „regionally defined types” primarily affecting central vision (e.g. Stargardt disease) (Fig. 3). Both, the generalized type as well as the regionally defined type, are subdivided into two categories depending on the region of the retina which is initially afflicted. The primary site of onset may either be located centrally or in the periphery of the retina.

<u>CLASSIFICATION OF RETINAL DEGENERATIONS</u>	
Generalized:	peripheral onset <i>retinitis pigmentosa</i> <i>atrophia gyrata</i>
	central onset <i>cone dystrophy</i> <i>Sorsby fundus dystrophy</i>
Regionally-restricted:	peripheral onset <i>autosomal dominant vitreoretinopathopathy</i>
	central onset <i>Stargardt disease</i> <i>Best disease</i> <i>autosomal dominant cystoid macular dystrophy</i>
Stationary:	<i>Oguchi disease</i> <i>blue cone monochromasy</i>
Syndromes:	<i>Usher syndrome</i> <i>Kearns-Sayre syndrome</i>
Other types (multifactorial):	<i>age-related maculadegeneration (AMD)</i>

Fig. 3 Classification scheme of inherited retinal degenerations

According to Kellner’s classification scheme (1997a, 1997b, website²), retinal degenerations are subdivided into five main groups, namely, (i) the generalized types, (ii) the regionally-restricted types, (iii) the stationary types, (iv) syndromes and (v) other types, e.g. multifactorial diseases. For each main group a few examples are given.

Inherited retinal degenerations affecting the central fundus of the retina, the macula lutea, are referred to as macular degenerations (MD). According to Kellner’s classification, MD is either a condition with generalized manifestations but onset in the central retina (e.g. cone dystrophy, cone-rod dystrophy, Sorsby fundus dystrophy) or a regionally-restricted condition with central onset (Stargardt disease, Best disease, congenital X-linked retinoschisis, pattern dystrophy of the retinal pigment epithelium). Generally, MD is characterized by loss of central vision while peripheral vision is typically preserved. The final

² Classification of retinal degeneration: <http://retinadiagnostic.de/>

stages of MD, especially those of the generalized types, are often associated with the degeneration and functional loss of all photoreceptors, leading to severe impairment of vision or to blindness.

Best disease is a regionally-restricted type of retinal degeneration with central onset. It is a rare disease and shares histological and clinical features with age-related macular degeneration (AMD), the leading cause of blindness in industrialized countries. In contrast to Best disease, AMD is a complex, heterogeneous and multifactorial disorder caused by both environmental as well as genetic factors (Gorin et al. 1999). Elucidating the pathogenic mechanisms in Best disease may also contribute to a better understanding of the genetic components predisposing to AMD. Similar to other age-related diseases such as Alzheimer disease, cancer or diabetes, AMD will have an ever-increasing impact in a society in which the average lifespan is increasing.

2 BEST DISEASE

Best disease, also known as Best macular dystrophy (BMD) or vitelliform macular dystrophy type 2 (VMD2, OMIM³ 153700), is an autosomal dominantly inherited macular disorder. BMD manifests in teenage years and displays a great variability in expression and penetrance. The disease is named after the German ophthalmologist Friedrich Best who reported the first multigeneration pedigree (Best 1905). Clinically, the disease is characterized by striking yellowish vitelliform lesions of the macula associated with a gradual decline of central vision. Histopathologically, aberrant remnants of heterogeneous material, including proteins, lipids and lipofuscin-containing material, are found in the central area of the retina (macula) and the tissue beneath, the retinal pigment epithelium (RPE). The deposits are thought to derive from incomplete enzymatic digestion of rod outer segments (Weingeist et al. 1982).

2.1 CLINICAL FEATURES OF BEST DISEASE

The typical vitelliform, egg-yolk-like lesions of Best disease patients is a pronounced feature in a series of disease stages (Fig. 4). Not all patients follow these stages chronologically. Some patients do not progress beyond the early stages whereas others progress rapidly from an early to a late stage. At stage 0, Best disease patients are funduscopically asymptomatic. The first symptoms are subtle changes of the RPE (stage 1). In

³ OMIM: <http://www.ncbi.nlm.nih.gov/Omim/searchomim.html>

the vitelliform stage (stage 2a), a lipofuscin-containing cyst is formed in the area of the fovea centralis having the appearance of an egg-yolk. The cyst is round, 0.5 – 5 mm in diameter and usually well circumscribed. The vitelliruptive stage (2b) describes the disintegration of the uniform cyst which then resembles a scrambled egg. A pseudohypopyon may form representing an accumulation of yellowish, lipofuscin-containing fluid in the subretinal space (stage 3). The later stages of Best disease are less characteristic and often indistinguishable from other MDs. After the disappearance of yellowish material, the fundus may develop atrophic lesions (stage 4a), fibrous macular scars may form (stage 4b, not shown) and choroidal subretinal neovascularization may develop (stage 4c, not shown) (Godel et al. 1986; Mohler and Fine 1981).

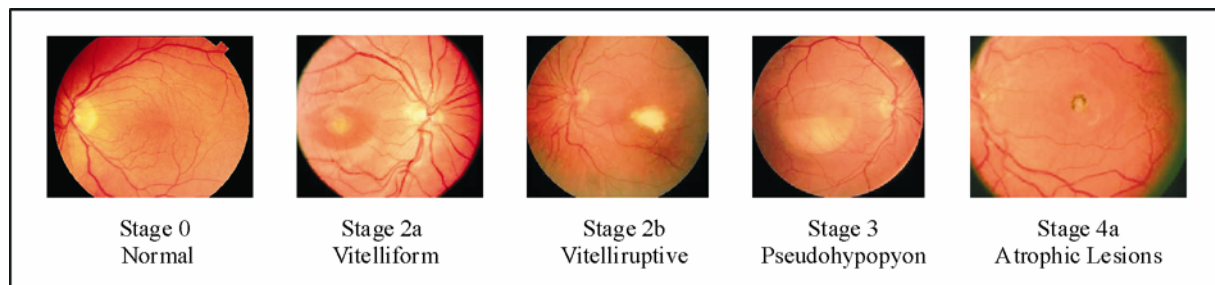


Fig. 4 Fundus photography of multiple stages of Best disease

Stage 0 displays a fundus without pathological findings. Stages 2a and 2b depict the classic appearances of Best disease as egg-yolk and scrambled egg stages. The egg-yolk stage describes a vitelliform oval lesion (cyst) formed by an accumulation of lipofuscin within the RPE and the sub-RPE space. At some point of time the cyst ruptures and then looks like a scrambled egg (vitelliruptive stage). Stage 3 denotes the formation of pseudohypopyon lesions and in stage 4a atrophy of the RPE is seen (see text for details).

The disease progression is accompanied by a gradual reduction of visual acuity. Normal visual acuity is found in stages 0 and 1 (20/20), is reduced in stages 2a, 2b and 3 (20/20 – 20/100) and may be below 20/200 in stages 4a, 4b and 4c (Emedicine⁴). Visual acuity is measured in a standardized manner with a Snellen chart, a chart of progressively smaller letters (Spalton et al. 1994). A test subject with vision acuity of 20/200 recognizes the same letter size at a distance of 20 feet as a normal person would at a distance of 200 feet. Officially, legal blindness is defined as central visual acuity not exceeding 20/200 in the better eye with best correction.

2.2 ELECTROPHYSIOLOGY IN BEST DISEASE

Not all cases of Best disease follow the same course of disease stages as described above. Especially the later stages are sometimes difficult to distinguish from other similar MD

⁴ Emedicine: <http://www.emedicine.com/OPH/topic700.htm#section~introduction>

phenotypes like adult vitelliform macular dystrophy (AVMD) or AMD. A hallmark of Best disease, however, is the characteristic abnormal electro-oculography (EOG) in combination with a normal electro-retinography (ERG) in all stages of disease progression from phenotypically normal carriers to patients with acute vision impairment. With the ERG, electrical responses of retinal cell types to a standardized light stimulus are recorded and therefore reflect the function of photoreceptor cells, Müller cells and bipolar cells (Leydhecker et al. 1988). Typically reduced or absent amplitudes are seen in retinitis pigmentosa patients with deteriorated photoreceptors. In contrast, the EOG measures the transepithelial potential over the RPE and reveals the late response of the eye to light-induced depolarization of the basal membrane of the RPE. While intact EOG recordings display a light peak to dark trough ratio (Arden ratio) of approximately 1.8, pathologic values of Best disease patients are in the range between 1.1 to 1.5 (Arden et al. 1962). The pathological EOG in Best disease indicates the primary defect to reside in the RPE (Berson et al. 1992).

2.3 GENETICS OF BEST DISEASE

Initially, the disease locus was mapped to a region of 26 cM on chromosome 11q13 (Forsman et al. 1992; Stone et al. 1992). Subsequent genetic, physical and radiation hybrid mapping further refined the disease region to an interval less than one million basepairs or 2 cM flanked by the microsatellite marker D11S4076 and the uteroglobin (*UGB*) gene (Graff et al. 1994; Graff et al. 1997; Hou et al. 1996; Nichols et al. 1994; Stöhr and Weber 1995; Weber and Mar 1994a; Weber et al. 1994b). Detailed transcript maps covering the critical candidate region were generated by direct cDNA selection and EST mapping, resulting in the identification of multiple candidate genes expressed in the retina and/or the RPE (Stöhr et al. 1998; Cooper et al. 1997). The identification of the *VMD2* gene was finally achieved by identifying a novel retina-specific expressed sequenced tag (EST), named *TUI5B* (EST database, NCBI), which mapped to the critical region of Best disease (Marquardt et al. 1998). Independently, Petrukhin and coworkers (1998) identified the *VMD2* gene using a similar approach. By genetic analyses of patients diagnosed with Best disease both research groups identified distinct mutations and thus confirmed the *VMD2* gene to be causative of Best disease.

VMD2 is located on the long arm of chromosome 11 (11q12.1-13) and is flanked by *FADS3* on the centromeric and *FTH1* on the telomeric side. Interestingly, the 3'-UTRs of *VMD2* and *FTH1* overlap in an antisense tail-to-tail fashion. However, no regulatory role of

gene expression via RNA stability has been described to date (Petrukhin et al. 1998). The *VMD2* gene spans a genomic region of 14 kb and comprises a first non-coding exon and ten coding exons. The ten intervening sequences range from 0.3 kb (smallest, IVS8) to 3.1 kb (largest, IVS2). The *VMD2* mRNA of 2.2 kb is found to be expressed predominantly in the RPE (Marquardt et al. 1998). Signals of *VMD2* expression are also identified by reverse transcriptase polymerase chain reaction (RT PCR) and Northern blot analysis in tissues other than the RPE, i.e. in retina, brain, testis (Petrukhin et al. 1998; Stöhr et al. 2002). The VMD2 protein, designated bestrophin, consists of 585 amino acid residues and has an approximate molecular mass of 68 kDa. Based on immunohistochemistry of macaque and porcine eye sections, bestrophin is exclusively localized to the basal and lateral plasma membrane of the RPE (Marmorstein et al. 2000).

In silico protein analyses reveals that bestrophin is an evolutionary highly conserved protein. It is closely related to a family of proteins first described in *Caenorhabditis elegans* with unknown function (Marquardt et al. 1998; Petrukhin et al. 1998). All members of this so-called RFP-TM protein family exhibit a conserved region of approximately 350 – 400 residues, encoding an invariant tripeptide motif (arginine R, phenylalanine F, proline P) as well as multiple transmembrane (TM) spanning regions (Sonnhammer and Durbin 1997). Besides human bestrophin, other closely related proteins have recently been identified in the human genome, namely the VMD2-like proteins VMD2L1, VMD2L2 and VMD2L3 (Stöhr et al. 2002). The genes are mapped by fluorescence *in situ* hybridization (FISH) to chromosomes 19p13.2-13.12, 1p32.3-p33 and 12q14.2-q15, respectively. VMD2 as well as VMD2L1 and VMD2L2 have a restricted expression to polarized epithelial cells such as the RPE, colon tissue and testis. Therefore, proteins belonging to the VMD2 RFP-TM family may play an important functional role especially in cells divided into distinct apical and basolateral regions (Stöhr et al. 2002).

2.4 BIOCHEMISTRY OF BESTROPHIN

First insight into structure and function of bestrophin can be obtained from bioinformatics. Hydrophobicity profiling identified several α helices in the N-terminal half of the protein, suggesting bestrophin to encode an integral membrane protein with multiple transmembrane domains (Bakall et al. 1999; Krämer et al. 2000; Marquardt et al. 1998, Petrukhin et al. 1998 and White et al. 2000). As shown in Fig. 5, two topological models have been proposed. In model A, four TM domains are predicted for bestrophin with the N- and C-

termini located intracellularly. The alternate five-TM domain model (B) contains an additional fifth putative TM domain (TM2a) between TM domain two and three. In model B, the N- and C-termini are located on either side of the plasma membrane. Independent of the model, the short N-terminus of bestrophin (31 amino acid residues) is located within the cytosol and the N-terminal moiety of bestrophin is membrane-associated (amino acid residue 1 – 290). Based on the *in silico* data as well as labeling experiments by Marmorstein (2000) (for further details see Discussion 1.1.4), model A is currently regarded to be the most likely model for bestrophin.

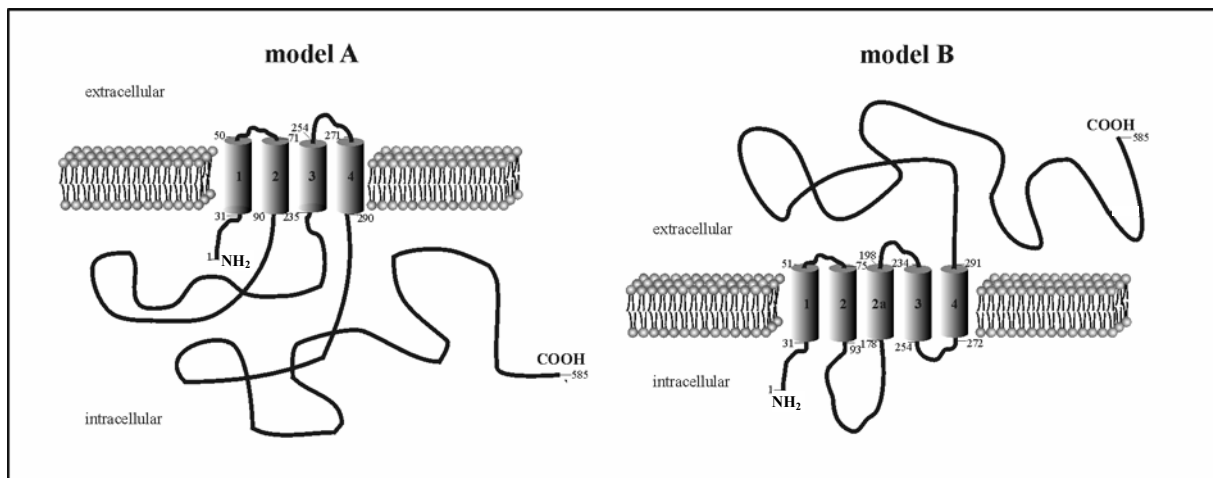


Fig. 5 Predicted topology of bestrophin

Several TM domain prediction programs (DAS, HMMTOP, SOSUI, TMHMM) suggest four TM helices (model A, left) for bestrophin, while one program (TMpret) predicts five TM domains (model B, right). Accordingly, the C-terminal half of bestrophin (residue ~290 – 585) is either inside (model A) or outside (model B) the cell. All programs prognosticate the N-terminus of VMD2 to be located within the cytosol. The URL addresses of the five TM prediction programs are found in Materials and Methods, Table 17. Previously, model A was published by Petrukhin et al. 1998 and Bakall et al. 1999 and model B by Krämer et al. 2000 and White et al. 2000.

Preliminary experimental evidence suggests that bestrophin may act as anion channel, in particular as a calcium-sensitive chloride channel (Sun et al. 2002). In a series of heterologous expression experiments, HEK cells were transiently transfected with plasmid constructs containing human, *Ceanorhabditis elegans* and *Drosophila melanogaster* VMD2 as well as the human VMD2-like gene VMD2L1. The subsequent recording of whole cell currents revealed chloride conductances with distinctive current-voltage relations and/or ion selectivity. Similar to the dominant trait of Best disease, a dominant inhibition of mutant bestrophin upon the chloride conductance of intact bestrophin was observed. Furthermore, the four or five subunits of bestrophin are thought to oligomerize, forming chloride channels; however, the exact homooligomeric or heterooligomeric nature of the channel was not fully resolved. Experimentally, bestrophin also associated with human VMD2L1 and bestrophin from other species with decreasing efficiency (Sun et al. 2002). In spite of theoretical

proposals that an increased chloride conductance accounts for the typically depressed EOG in Best disease (Gallemore et al. 1998), independent confirmational evidence is required for the proposed function of bestrophin and the VMD2 RFP-TM protein family as a novel chloride channel protein family.

By performing *in silico* analyses, i.e. refined bioinformatical queries and profile sequence comparisons, two functional properties have been ascribed to the N- and C-terminal half of bestrophin, respectively. At the N-terminal part of bestrophin, Gomez et al. (2001) identified weak correlations to Na/Ca-K exchanger motifs, while the C-terminus revealed some similarity to putative cyclic nucleotide binding sites. The comparative *in silico* data therefore suggest that bestrophin may function as Na/Ca-K exchanger rather than chloride channel. This would be in accordance with two other integral proteins located within the outer segments of photoreceptors namely the rod Na/Ca-K exchanger and cGMP-gated channels. These proteins are involved in phototransduction by regulating intracellular calcium levels (Kim et al. 1998).

More recently, Marmorstein et al. (2002) reported of an interaction between bestrophin and protein phosphatase 2A (PP2A). By immunoaffinity purification, a bestrophin complex was isolated from the porcine RPE and by matrix-assisted laser desorption ionization time-of-flight mass spectrometry (MALDI-TOF MS) the complex was found to contain peptides matching to bestrophin as well as to protein phosphatase 2A catalytic subunit (β isotype). Evidence of an interaction between the C-terminal region of bestrophin and PP2A was given by reciprocal co-immunoprecipitation. Furthermore, phosphorylation and dephosphorylation of bestrophin by PP2A as well as the inhibition of PP2A activity by ocadaic acid could also be experimentally verified. Bestrophin is therefore proposed to be part of a phosphorylation-dependent signaling cascade (Marmorstein et al. 2002). An as yet unknown pathway is thought to transmit light-induced secretory signals from the photoreceptors of the retina, via the apical to the basolateral plasma membrane of the RPE. By means of EOG, the resulting light-dependent depolarization of the basolateral plasma membrane of the RPE is then detectable. This pathway is thought to be disrupted in Best disease, in agreement with markedly reduced or absent light-induced EOG potentials in affected patients. In which manner the defective phosphorylation cascade may account for Best disease remains to be elucidated.

3 GOAL OF THE THESIS

A great number of studies have shown that missense mutations in VMD2 are predominantly associated with Best disease. Only a few other types of mutations including in-frame deletions and frameshift mutations are found in a minority of Best disease patients. Furthermore, most of the known disease-associated mutations reside in the N-terminal moiety of bestrophin, in close proximity to putative transmembrane domains. To further extend the spectrum of disease-associated VMD2 mutations, a large number of Best disease patients were analyzed in the course of this thesis. This further allowed the identification and evaluation of sequence alterations in the *VMD2* gene. In addition, *in vitro* heterologous expression assays were established facilitating the assessment of functional consequences of VMD2 mutations.

To initiate functional studies of bestrophin, VMD2-specific polyclonal antibodies were raised, permitting Western blot and immunocytochemical analyses. As the subcellular localization of a protein provides first clues as to its function, bestrophin was studied by membrane fractionation experiments. Moreover, to understand the molecular pathology of the mutations identified in Best disease, a series of VMD2 mutations were analyzed for their ability to incorporate into the membrane.

Presently, several different functions have been assigned to bestrophin, including its role as chloride channel (Sun et al. 2002) or as ion exchanger (Gomez et al. 2001). The proposed functions may be regulated by calcium-sensitive mechanisms (Sun et al. 2002), by phosphorylation/dephosphorylation (Marmorstein et al. 2002) or by putative nucleotide binding sites (Gomez et al. 2001). All data primarily rely on *in silico* and *in vitro* studies and further experimental confirmation by using different approaches and systems are needed. Therefore, an alternate approach to study the function of a protein is to elucidate the role of close family members in the respective tissues with predominant expression. This requires the molecular and biochemical characterization of the immediate family members, the VMD2-like RFP-TM proteins. To this end, the identification and characterization of the Vmd2-like RFP-TM protein family in mouse has been initialized in the course of this thesis.

Finally, the long-term goal of this thesis was directed towards generating mouse models of Best disease. This is being achieved by targeting the endogenous murine *Vmd2* gene in two ways, by generating knock-out mice deficient in bestrophin and knock-in mice carrying a missense mutation homologous to a mutation found in a large Best disease pedigree. Histological, immunohistochemical and electron-microscopical characterization of these mouse lines will provide insight into the function and pathology of normal and mutant bestrophin, respectively.

IV RESULTS

1 MUTATIONAL ANALYSIS OF HUMAN VMD2

1.1 NOMENCLATURE

The HUGO Gene Nomenclature Committee (HGNC⁵) is a central organization providing general agreements and guidelines on how to classify and name the estimated number of 26,000 to 40,000 genes (Wain et al. 2002). Based on the HGNC guidelines, the termini and symbols used for the VMD2 disease locus, both the gene and protein nomenclature are defined as follows. The locus of Best disease referring to the map position on chromosome 11 is designated as VMD2. The human Best disease gene is written in capital letters and italics (*VMD2*), while the orthologous mouse gene is written in small letter and italics (*Vmd2*). Human and mouse protein symbols are written in standard font and are distinguishable from one another by either capital letters (VMD2) or small letters (Vmd2), respectively. Approved by HGNC, the word „bestrophin” may be used as synonym for the human VMD2 and mouse Vmd2 protein.

1.2 CLASSIFICATION OF MUTATIONS, RARE VARIANTS AND COMMON POLYMORPHISMS

In the absence of functional assays, the discrimination between pathogenic and non-pathogenic sequence variants is often difficult. Newly discovered sequence changes are generally classified into three categories, namely common polymorphisms, mutations with disease-causing effects and rare sequence variants with unknown pathogenicity. Sequence variants identified in both affected and control patients with allele frequencies above 1 % are referred to as common polymorphisms. Sequence variants identified exclusively in affected subjects but at low allele frequencies (< 1 %) may or may not be causally linked to a disease.

Inclusion criteria used to define the group of disease-causing mutations are based on modified recommendations by Kazazian et al. (2000). Primarily, the functional consequence of a sequence variant is predicted on mRNA and protein level. Premature truncated proteins resulting from deletions, insertions, nonsense mutations or splicing mutations most likely have a pathologic effect and are generally classified as disease-causing mutations. In contrast, aberrant proteins altered by only one amino acid exchange (missense mutations) may have a less severe or no impact on the protein function and need to be subjected to further analytical

⁵ HGNC: <http://www.gene.ucl.ac.uk/nomenclature/>

criteria. These may include: (i) the interspecies conservation of affected amino acid residues, (ii) the conservation of affected amino acid residues within paralogous proteins, (iii) the localization of affected amino acid residues within known mutational hotspots, (iv) the finding that different affected amino acid exchanges of one and the same codon are independently identified in unrelated, affected families and (v) the fact that affected amino acid residues are exclusively segregating with the phenotype in multiple generations. All these criteria may underscore the functional importance of a respective residue within the protein and its putative involvement in disease development. Vice versa, a sequence variant not segregating with the phenotype may be excluded as disease-causing mutation with high confidence.

1.3 IDENTIFICATION OF SEQUENCE CHANGES IN THE *VMD2* GENE

In the course of mutational analyses performed between 1999 and 2002, the human *VMD2* gene was analyzed by bidirectional sequencing of all ten coding exons and adjacent splice sites in 47 unrelated patients in a total of 57 cases. Besides 37 clinically diagnosed Best disease cases, the analysis was also done in five cases with an unspecified phenotype of vitelliform macular degeneration, two cases with suspected AVMD, one case with Bull's eye maculopathy, one case affected with pattern dystrophy and one case with unclassified macular degeneration. An overall number of 181 sequence changes (on average 3.85 sequence changes per patient) and a total number of 30 unique sequence changes were identified in the *VMD2* gene. By comparison to previous reports⁶, nine of the 30 identified unique sequence changes (or 153 out of a total of 181 sequence changes) are classified as common polymorphisms (see Results 1.9). The remaining 21 unique sequence changes (or 28 out of a total of 181 sequence changes) are further classified into 15 unique disease-associated mutations and six unique rare sequence variants.

When considering all recurrent sequence changes except for the common polymorphisms identified in the *VMD2* gene (28), 21 are classified as disease-causing mutations and seven as rare sequence variants. Of the 21 disease-associated mutations, 13 are non-recurrent, while each of the remaining two mutations are found four times in unrelated patients. Due to this recurrency, the number of unique disease-associated mutations decreased from 21 to 15. Nine of the 15 unique disease-associated mutations are novel and six have

⁶ *VMD2* mutation database: <http://www.uni-wuerzburg.de/humangenetics/vmd2.html>

previously been described in unrelated Best disease patients (VMD2 mutation database⁷). The seven rare variants include five non-recurrent and two recurrent mutations, thus, a total number of six rare sequence variants are unique. These have not been reported previously. All sequence changes except for the common polymorphisms identified in the analysis, i.e. 15 disease-associated mutations plus six rare sequence variants are given in Table 1.

As indicated, not all mutation carriers are clinically affected with Best disease (Table 1). Besides 19 mutations (Gly26Arg, Tyr29His, Leu100Arg, Trp102Arg, Asp104His, Ala195Val, Arg218Ser, Thr237Arg, Thr241Asn, 3 x Ala243Val, Pro260fsX288, 4 x Ile295del, Leu294Val, Phe298Ser) identified in 37 Best disease patients, one mutation (Ala243Val) was identified in a single case of pattern dystrophy and one mutation (Asn11Ile) is found in one patient affected with Bull's eye maculopathy. No mutations were identified in the group of patients affected with unspecified vitelliform macular dystrophy (5), AVMD (2) and with unclassified macular degeneration (1).

Of the 47 patients affected with Best disease or related maculopathies, 14 patients have a positive family history, in nine patients the family history is negative and in the remaining 24 patients the familial situation has not been ascertained. Mutations are detected in 9/14 (64 %) patients with positive family history. Of the nine mutation carriers, one patient is affected with Bull's eye maculopathy, one with pattern dystrophy and the remaining seven with Best disease. In 3/9 (33 %) cases, a mutations were found in Best disease patients with a negative family history. Thus, higher mutation detection rates are found in the patients with a positive family history.

⁷ VMD2 mutation database: <http://www.uni-wuerzburg.de/humangenetics/vmd2.html>

Table 1 Sequence changes identified in the *VMD2* gene in 47 unrelated patients affected by Best disease (BMD) and related maculopathies

Patient ID	Nationality	Family history	Phenotype	Exon	IVS	Nucleotide Change ^a	Amino Acid Change ^a	AA Conservation ^b interspecies/ protein family	Number of Alleles (n=94)	Segregation ^c	Hotspots	Mutation (M) or Rare Variant (V)	Literature
G99-1200	West. E	yes	Bull's eye maculopathy	2		32 A>T	Asn11Ile	yes/yes	1	yes	yes	M	novel
G01-0251^d	West. E	no	BMD	2		76 G>C	Gly26Arg	yes/yes	1	n.d.	yes	M	novel
G00-0041	West. E	no	BMD	2		85 T>C	Tyr29His	yes/yes	1	n.d.	yes	M	novel
G01-0185^d	East. E	yes	BMD		3	-12 C>T ^e	-	-	2	n.d.	-	V	novel
G88-0222^c	West. E	yes	BMD		3	-17 C>T	-	-	1	n.d.	-	V	novel
G01-0251^d	West. E	no	BMD		3	-26 C>T	-	-	1	n.d.	-	V	novel
G01-1259^d	West. E	yes	pattern dystrophy		3	-26 C>T	-	-	1	n.d.	-	V	novel
G88-0222^c	West. E	yes	BMD		3	-32 C>T ^e	-	-	1	n.d.	-	V	novel
G99-0723	West. E	yes	BMD	4		299 T>G	Leu100Arg	yes/no	1	yes	yes	M	Krämer ^f
G01-1102	West. E	unknown	BMD	4		304 T>C	Trp102Arg	yes/no	1	n.d.	yes	M	novel
G99-0489	West. E	unknown	BMD	4		310 G>C	Asp104His	yes/yes	1	n.d.	yes	M	novel
G01-1456	West. E	unknown	BMD	5		584 C>T	Ala195Val	yes/yes	1	n.d.	yes	M	Lotery ^f
G01-1378	West. E	unknown	BMD	5		624 G>A	Gln 208 Gln	-	1	n.d.	-	V or M?	novel
G00-1843	West. E	yes	BMD	6		652 C>A	Arg218Ser	yes/yes	1	n.d.	yes	M	Bakall ^f and Krämer ^f
G99-0335	West. E	yes	BMD	6		710 C>G	Thr237Arg	yes/yes	1	yes	yes	M	Krämer ^f
G02-2492^d	West. E	yes	BMD	7		720 G>C	Val 240Val ^e	yes/yes	1	n.d.	-	V	novel
G02-2492^d	West. E	yes	BMD	7		722 C>A	Thr241Asn	yes/yes	1	yes	yes	M	novel
G99-1228	West. E	yes	BMD							yes			
G01-1259 ^d	West. E	yes	pattern dystrophy	7		728 C>T	Ala243Val	yes/yes	4	yes	yes	M	Krämer ^f
G00-0144	West. E	unknown	BMD							n.d.			
G01-0185 ^d	East. E	yes	BMD							n.d.			
G02-0482	West. E	unknown	BMD	7		779 delC	Pro260fsX288	-	1	n.d.	yes	M	novel
G00-0433	West. E	unknown	BMD	8		880 C>G	Leu294Val	yes/yes	1	n.d.	yes	M	novel
G99-0803	West. E	yes	BMD							yes			
G99-0551	East. E	unknown	BMD	8		884delTCA	Ile295del	yes/yes	4	n.d.	yes	M	Marquardt ^f and Krämer ^f
G02-0177	West. E	unknown	BMD							n.d.			
G00-0989	West. E	no	BMD							n.d.			
G99-0273	East. E	unknown	BMD	8		893 T>C	Phe298Ser	yes/yes	1	n.d.	yes	M	novel

Novel mutations are indicated in bold letter and are not yet entered into the VMD2 mutation database. ^a The adenosine of start codon ATG is numbered base 1 and ATG coding for methionine is numbered residue 1. ^b "Interspecies" conservation is based on human, bovine and mouse bestrophin sequences (Fig.10) and "protein family" conservation denotes a multiple sequence alignment of the human and murine Vmd2 RFP-TM protein family (Fig. 31). ^c "yes" denotes mutations segregating in at least two generations with Best disease phenotype; n.d. not determined. ^d Individuals are carriers of a disease-associated mutation as well as a novel rare sequence variant. ^e Nucleotide exchanges -12 C>T and -32 C>T are found in one person. Phase is not determined. ^f Bakall et al. 1999, Krämer et al. 2000, Lotery et al. 2000, Marquardt et al. 1998.

1.4 EVALUATION OF NOVEL DISEASE-ASSOCIATED MUTATIONS

Eight out of nine unique novel disease-associated mutations are predominantly missense mutations, residing in exon two (Asn11Ile, Gly26Arg and Tyr29His), exon four (Trp102Arg and Asp104His), exon seven (Thr241Asn) and exon eight (Leu294Val and Phe298Ser). In most (if not all) cases the criteria for classifying these sequence changes as „disease-associated” mutations are fulfilled (Table 1). All missense mutations are located within mutational hotspots of *VMD2* and interspecies conservation is given. Within the human *VMD2* RFP-TM protein family, only codon 100 (leucine) of missense mutation Leu100Arg is not entirely conserved. At codon position 100, human *VMD2* and *VMD2L3* have leucine, whilst *VMD2L1* has methionine and *VMD2L2* has isoleucine as residue. Segregation of missense mutations Asn11Ile and Thr241Asn is established in two and three generations of Best disease families, respectively.

The ninth novel disease-associated mutation is a heterozygous deletion of one basepair identified in exon seven (779delC). Interestingly, this is the first finding of an out-of-frame deletion in the N-terminal moiety of the protein in a Best disease patient. The deletion of cytosine (779delC) probably causes a frameshift, resulting in a premature stop codon after 28 altered amino acid residues with the entire C-terminal half including TM domain four missing. The hypothetical truncated protein consists of 287 amino acid residue. According to novel nomenclature recommendations (den Dunnen and Antonarakis 2001), the 779delC mutation is described as Pro260fsX288.

1.5 EVALUATION OF NOVEL RARE SEQUENCE VARIANTS

Six novel rare sequence variants with unknown functional consequences for pathogenicity are found in intervening sequence three (-12 C>T, -17 C>T, -26 C>T and -32 C>T), in exon five (624 G>A) and in exon seven (720 G>C) of *VMD2* (Table 1). The four intronic sequence changes are located beyond the critical 3'-acceptor splice motifs, suggesting that splicing may not be affected. The fifth novel silent exchange (720G>C) is classified as neutral rare sequence variant due to the presence of a disease-associated mutation, segregating in three generations of a typical Best disease family. Patient G02-2492 is carrier of both, the silent 720G>C sequence change and a disease-associated missense mutation (Thr241Asn) in exon seven of *VMD2*. Finally, the sixth novel sequence variant (624G>A) in exon five is also a silent exchange (Gln208Gln) and classified as rare variant. Although not supported by the inclusion criteria of disease-associated mutations, some arguments suggest that the silent

mutation 624G>A may be associated with the disease phenotype. Firstly, the carrier of the heterozygous G to A transition shows typical phenotypic features of BMD, including vitelliform, yellowish central lesions in both eyes. Secondly, the carrier seems to have a positive family history for Best disease. A further family member suffers from maculopathy but did not volunteer for ophthalmological examinations. This and the fact that no other, more likely disease-associated sequence change was identified in *VMD2* has led us to further analyze the 624G>A mutation.

1.6 FUNCTIONAL ASSAY TO EVALUATE THE 624G>A TRANSITION

A functional test was established to analyze the significance of the novel sequence variant 624G>A on the splicing behaviour of maturing pre-messenger RNA. It is based on an exon trapping system in which the effect of any given sequence variant on mRNA splicing can be evaluated. Here, we tested whether the nucleotide substitution at position 624 creates a novel or alternative splice acceptor site (nucleotide position 625-626, AG). Wild-type and mutant genomic *VMD2* sequence encompassing the putative splice variant in exon five (from intron four to intron six) is cloned into the mammalian expression vector pSPL3b. Subsequently, both wild-type and mutant constructs are introduced into COS7 cells via electroporation and the resulting spliced RNA products are analyzed by RT PCR and direct sequencing (Fig. 6a, 6b). By using vector-specific primers SD6 and SA2, two bands (496 bp and 263 bp) are amplified using wild-type RNA template and three bands (496 bp, 341 bp and 263 bp) are amplified using the mutant RNA template. With primer combination SD6/mVMD2-R1 similar results are generated. A 288 bp RT PCR product is generated in both wild-type and mutant constructs, while a 133 bp product is exclusively found in the mutant DNA. No marked quantitative differences are observed between wild-type and mutant RT PCR products of 496 bp (primer pair SD6/SA2) and 288 bp (primer pair SD6/mVMD2-R1), respectively. The RT PCR products of 496 bp and 288 bp in size represent normal splicing variants in which IVS4, IVS5 and IVS6 are correctly removed by the splicing machinery. Similarly, the 263 bp band seen in both wild-type and mutant constructs were found to be generated by the strong donor and acceptor splicing sites of the pSPL3b vector.

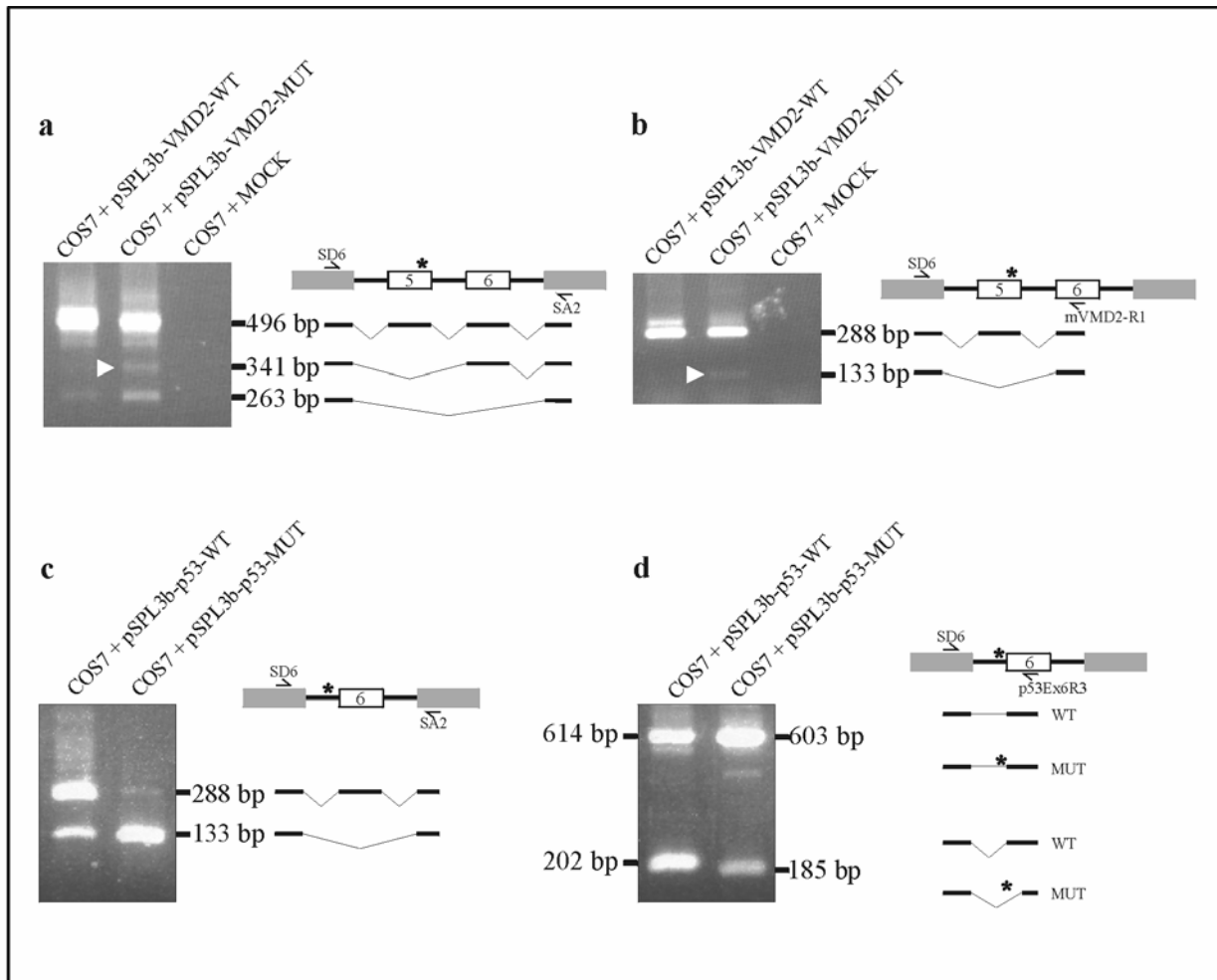


Fig. 6 Evaluation of putative novel splice acceptor sites

The splicing behaviour of the wild-type (pSPL3b-VMD2-WT) and mutant (pSPL3b-VMD2-MUT) constructs are shown in (a) and in (b) by RT PCR (left) and as schematic representations (right). The 496 bp PCR product amplified with primer pair SD6/SA2 (a) and the 288 bp PCR fragment amplified with primers SD6 and mVMD2-R1 (b) are present in about equal amounts in the wild-type (COS7 + pSPL3b-VMD2-WT) and mutant (COS7 + pSPL3b-VMD2-MUT) RT PCR products. Indicated by a white arrow, an additional band of 341 bp (a) and 133 bp (b) is observed in the mutant RT PCR product. Furthermore, a band of 263 bp is detected with the primer pair SD6/SA2 in both wild-type and mutant constructs (a). In (b), a RT PCR product above the 288 bp fragment (approximately 300 bp) is noticed. The 288 bp and ~300 bp bands were technically not separable by agarose gel excision and therefore not further analyzed.

The splicing behaviour of the wild-type (pSPL3b-p53-WT) and mutant (pSPL3b-p53-MUT) constructs are shown in (c) and in (d) by RT PCR (left) and as schematic representations (right). (a) Due to the deleted acceptor splice site in the mutant construct (COS7 + pSPL3-p53-MUT), the 288 bp PCR fragment amplified with primers SD6/SA2 is exclusively detected in the wild-type (COS7 + pSPL3-p53-WT) construct. In comparison to the wild-type RT PCR, a much higher amount of the 133 bp-PCR fragment representing the skipping of the entire exon six is found in the mutant construct. (b) A clear difference is shown by RT PCR with primers SD6/p53Ex6R3 between the wild-type (COS7 + pSPL3-p53-WT) and the mutant (COS7 + pSPL3-p53-MUT) construct resulting in a 202 bp and a 185 bp fragment, respectively.

Of interest are those bands exclusively identified with the mutant templates (Fig. 6a, 6b). The faint 341 bp and 133 bp bands generated with primers SD6/SA2 and SD6/mVMD2-R1, respectively (Fig. 6a, 6b), were excised from the agarose gel, reamplified and directly sequenced. Both bands reveal the skipping of exon five in the mutant construct, suggesting that the 624G>A transition has a weak but defined effect on exon definition. To

test whether the sequence variant 624G>A may be located within the context of an exon splicing enhancer (ESE) element, the sequence surrounding the 624G>A variant in exon five of *VMD2* is analyzed with the bioinformatics tool ESEfinder[®] (Cartegni et al. 2002). Numerous ESE elements of serine/arginine-rich (SR) proteins (SF2/ASF, SC35, SRp40 and SRp55) are identified in *VMD2* exon five displaying scores above default threshold values (SF2/ASF: 1.956, SC35: 2.383, SRp40: 2.670 and SRp55: 2.676) (Fig. 7). Scores above the given threshold values are thought to significantly discriminate ESE motifs from any random sequence. The sequence variant 624G>A in exon five lies within one of the putative binding sites of SC35. While the wild-type sequence motif of 8 bp (5'-TGCTCCAG) has a score value of 3.148, the value of the mutant ESE element (5'-TGCTCCAA) is slightly reduced (2.698).

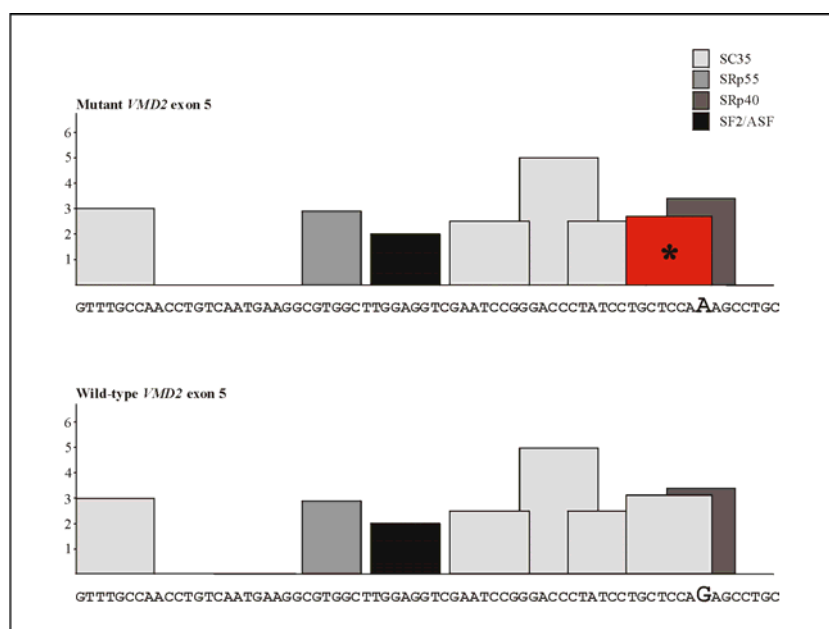


Fig. 7 Putative ESE motifs in exon five of *VMD2*

In search for putative ESE motifs, a partial sequence of wild-type and mutant (624G>A) *VMD2* exon five (nt 561-631) is analyzed with the bioinformatics tool ESEfinder[®]. ESE motifs with scores (y-axis) above the respective threshold values (see text) are indicated. The width of the bars indicate the length of the motifs and the height of the bars are numerical values calculated by ESEfinder[®]. An asterisk denotes the SC35 motif (red) which is affected by the 624A>G sequence variant.

The efficiency of the pSPL3b exon trapping assay is demonstrated with a control construct containing a DNA fragment mutated in the sequence for the splice acceptor site. This DNA fragment was derived from a Li Fraumeni syndrome patient (G01-0672) carrying a heterozygous deletion of 11 bp in intron five (IVS5-11_-1del) of the *TP53* gene. Two primer combinations SD6/SA2 and SD6/p53Ex6R3 are used to analyse the splicing behaviour by RT PCR analysis (Fig. 6c, 6d). Normal splicing of exon five is seen in the wild-type RNA templates, reflected by the 288 bp and 614 bp RT PCR products amplified with primer pairs SD6/SA2 and SD6/p53Ex6R3, respectively. The skipping of exon five is also observed in the wild-type RNA templates, probably due to strong vector-specific splice acceptor and donor

⁸ ESEfinder[®]: <http://exon.cshl.edu/ESE/>

sites. Sequencing of the 133 bp RT PCR product (SD6/SA2) predominantly found in mutant RNA template reveals that exon five is skipped due to the 11 bp deletion (Fig. 6c). Sequencing of the 185 bp RT PCR product (SD6/p53Ex6R3) shows that the splicing machinery uses a novel 3'-acceptor splice site 17 bp downstream of the native splice site (Fig. 6d). In both cases the resulting p53 protein is truncated, either consisting of 190 amino acid residues (exon skipping) or 202 amino acid residues (alterative splice site usage). In comparison, the wild-type protein contains 394 amino acid residues.

1.7 DETERMINATION OF ALA243VAL FREQUENCY IN A CONTROL POPULATION

Ala243Val represents one of the most common VMD2 mutations identified in our unrelated patient cohort. In this study, it is found in four unrelated subjects and previously it was found in five unrelated Best disease patients as well as in four unrelated AVMD patients (Krämer et al. 2000). The high allele frequency of Ala243Val, the similar chemical properties of alanine and valine (both are hydrophobic, aliphatic residues with similar molecular weights) and the localization of the mutation outside of a hotspot region has led to the notion that this mutation may in fact represent a benign polymorphism. Therefore, the frequency of Ala243Val was investigated in a large population of clinically unaffected Best disease cases. To examine exon seven of *VMD2* in 251 control DNAs, a restriction enzyme assay (*Aci* I) was established (Fig.8). No Ala243Val mutations were identified in 502 control alleles, providing further evidence that Ala243Val is likely to be a disease-associated mutation.

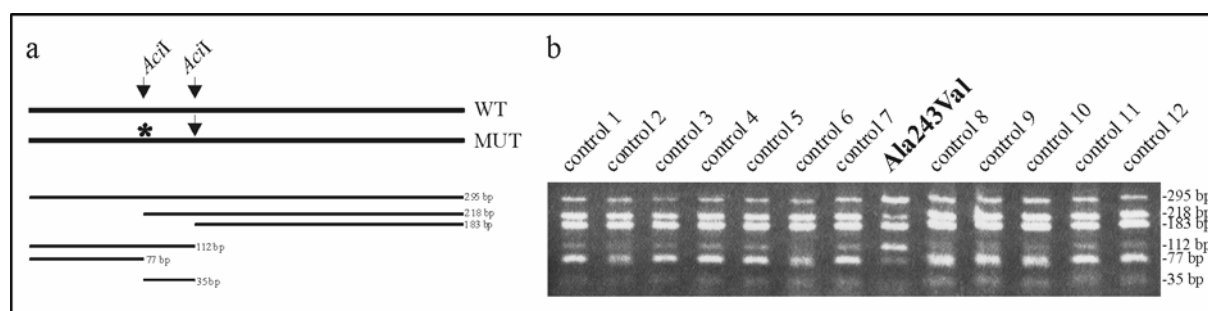


Fig. 8 Schematic diagram and agarose gel electrophoresis of *Aci* I digestion assay

(a) Indicated by arrows, the wild-type (WT) *VMD2* exon seven PCR product (295 bp) contains two *Aci* I restriction sites (GCGG) and the mutant (MUT) exon seven PCR product contains one *Aci* I site. *Aci* I digestion of WT results in three digested products of 35 bp, 77 bp and 183 bp. Due to incomplete digestion, two further digestion products of 112 bp and 218 bp as well as the undigested PCR product (295 bp) are generated. The heterozygous Ala243Val exchange (GCG→GTG) eliminates the first *Aci* I cutting site (*), resulting in two digested products of 112 bp and 183 bp. (b) Different digestion patterns are observed between two WT alleles (control 1 – 12) and a heterozygous Ala243Val carrier (positive control) with one WT and one Ala243Val allele.

1.8 THE VMD2 MUTATION DATABASE

In 1998 our laboratory designed and established a HUGO-affiliated VMD2 mutation database⁹ on behalf of the Mutation Database Initiative (MDI) (now: Human Genome Variation Society). For the last two years the database is officially curated by me and an update takes place on a regular basis (Fig. 9). To increase the usage of such databases worldwide, links from commonly used URL addresses like The Human Gene Mutation Database¹⁰ and GeneCards¹¹ refer to the VMD2 mutation database. The database comprises a detailed description of mutations, polymorphisms and rare variants identified in the *VMD2* gene as well as additional information such as segregation of mutations, allele frequencies of polymorphisms and origin and phenotype of patients analyzed.

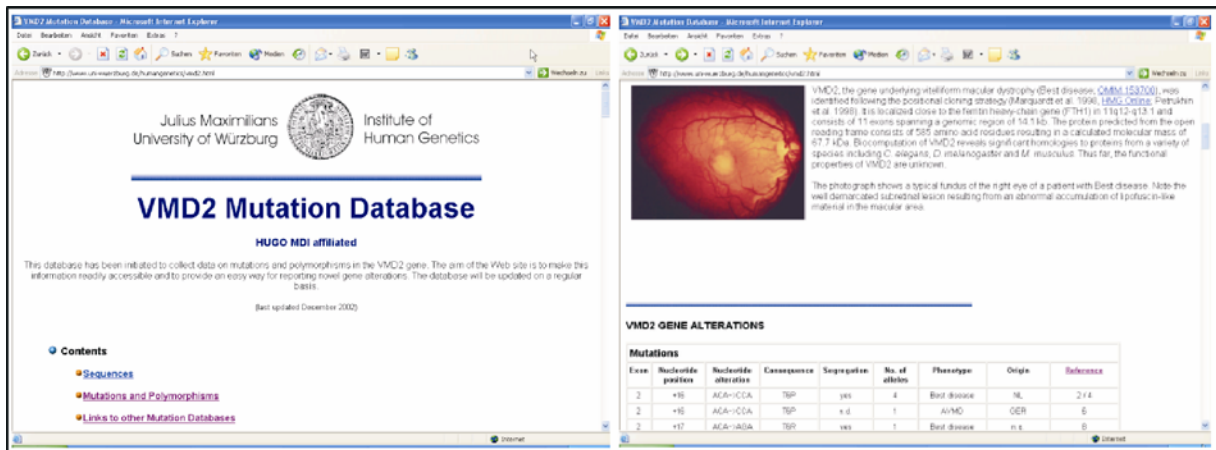


Fig. 9 Screen shot of VMD2 mutation database

The comprehensive VMD2 mutation database is regularly updated and to date contains 118 unique sequence variants identified in human *VMD2*. Besides data on mutations and polymorphisms, the web page provides the cDNA and putative protein sequence of VMD2, links to other mutation databases, a data submission form and a comprehensive reference list.

To date, 12 studies on VMD2 mutation analysis have contributed to the VMD2 mutation database (December 2002), providing a total number of 118 entries of unique sequence changes. Not yet included are the 15 novel sequence changes presented in this thesis. The sequence changes of *VMD2* are classified into the three defined major categories (see Results 1.2), into (i) disease-associated mutations identified in both Best disease patients and other maculopathies such as AVMD, (ii) rare variants of unknown pathogenic consequence found in patients and/or controls at allele frequencies below 1 % and (iii) frequent polymorphisms with allele frequencies greater than 1 %, found in patients and control individuals in comparable frequencies.

⁹ VMD2 mutation database: <http://www.uni-wuerzburg.de/humangenetics/vmd2.html>

¹⁰ The Human Gene Mutation Database (HGMD): <http://archive.uwcm.ac.uk/uwcm/mg/search/133795.html>

¹¹ GeneCard: <http://bioinfo.weizmann.ac.il/cards-bin/carddisp?VMD2&search=vmd2&suff=txt>

In the VMD2 mutation database, category (i) comprises a total number of 83 distinct, disease-associated mutations. Of these, 78 mutations are associated exclusively with Best-disease and three mutations are exclusively associated with AVMD. A further two mutations were identified in both Best disease and AVMD. In category (ii) a total number of 20 distinct sequence changes are listed, including six silent mutations, eight missense mutations, one nonsense mutation as well as two non-coding nucleotide substitutions, two non-coding insertions and one non-coding deletion. These rare sequence changes are found in patients affected with AMD, Bulls eye maculopathy, Best disease, unspecified maculopathy and controls. Category (iii) consists of a total number of 15 common polymorphisms, including seven sequence changes found in the 5'-UTR, IVS4, IVS6 and 3'-UTR and eight silent mutations located in exons two, three, nine and ten. Interestingly, no common polymorphisms affecting coding exons four to eight and ten have yet been identified.

In the following, the mutational spectrum and distribution of disease-associated mutations (category i) and rare sequence variants (category ii) are assessed in respect to different phenotypes. For Best disease, four different types of mutations have been identified, including 75 disease-associated missense mutations in exons two to eight (95 %), three disease-associated 3 bp in-frame deletion mutations in exons seven and eight (4 %, delPhe281, delIso295 and delAsp301), one splice-site mutation in IVS5 (1 %, IVS5+1 G→C) and one frameshift mutation in exon ten (1 %, Leu489fsX513). Deduced from the frequency of mutation types, Best disease is predominantly caused by missense mutations and single amino acid residue deletions. The other types of mutations seem to play a minor role. In addition, one rare sequence variant (silent mutation) was reported to be located in exon five of two unrelated Best disease patient (category ii). For AVMD, five distinct disease-associated missense mutations have been identified in exons two, four, seven and eight. Of these, three missense mutations (Arg47His, Ala146Lys, Asp312Asn) are AVMD-specific and two missense mutations (Thr6Pro and Ala243Val) are present in both AVMD and Best disease patients. In AMD patients, a total number of 15 rare sequence variants of unknown pathogenicity have been identified in the *VMD2* gene. Five missense mutations are located in exons four, six, seven and ten, five silent mutations are located in exons three, six, eight and nine, one nonsense mutation is located in exon four, two insertions are found in IVS6 and the 3'-UTR. Two single nucleotide substitutions are found in IVS5 and IVS10. Single cases of sequence variants have been identified in Bulls eye maculopathy (one missense mutation, exon four) as well as in unspecified maculopathy (two silent mutations, exons three and six).

In control DNAs, three missense mutations in exon ten and a non-coding 1 bp deletion in IVS8 have been identified.

1.9 FREQUENT POLYMORPHISMS IDENTIFIED IN THE *VMD2* GENE

Nine unique common polymorphisms, including 109 T>C in exon two, 201 G>C and 219 C>A in exon three, -24C>T in the IVS4, -9 del(TCC)₃ in IVS6, 1023 C>T in exon nine and 1410 G>A, 1557C>T and 1608T>C in exon ten were identified in the group of 47 unrelated patients affected by Best disease and related maculopathies (see Results 1.3). All of the common polymorphisms were previously reported and are listed in the VMD2 mutation database¹². In the 94 chromosomes of unrelated patients, the allele frequencies of common polymorphisms are generally consistent with previously reported allele frequencies in the VMD2 mutation database. However, due to the low number of alleles (n = 92), differences in frequencies are partially observed. For example, polymorphisms 109 T>C in exon two displays an allele frequency of 31 % in this group of patients (n = 92) versus an allele frequency of 4 % previously reported (n = 620). Similarly, differences in allele frequencies are seen in polymorphisms -9del(TCC)₃ of IVS6 (1 % in this group versus 8 % in previous reports), in 1023 C>T of exon nine (4 % vs. 0.7 %), and in 1410 G>A of exon ten (51 % vs. 28 %). Polymorphisms 201 G>C of exon three (1 % vs. 3 %), 219 C>A of exon three (9 % vs. 7 %), -24C>T of IVS4 (14 % vs. 18 %), 1557C>T of exon ten (20 % vs. 24 %) and 1608T>C of exon ten (32 % vs. 35 %) lie approximately in the same ranges of allele frequencies.

¹² VMD2 mutation database: <http://www.uni-wuerzburg.de/humangenetics/vmd2.html>

2 FUNCTIONAL ANALYSIS OF HUMAN BESTROPHIN

Efforts directed towards elucidating the physiological function of normal and mutant human bestrophin are presented in this chapter. This includes the generation of specific antibodies against bestrophin as a prerequisite to study functional aspects of the VMD2 protein. By means of site-directed mutagenesis, a series of mutant VMD2 constructs are generated that represent disease-causing mutations identified in Best disease patients. A heterologous COS7 expression system is established to examine the localization of the transiently expressed mutant and wild-type VMD2 proteins. Post-transfection, the incorporation of mutant and wild-type VMD2 into the membranes of COS7 cells is monitored by isolating the membraneous fraction and by performing fluorescence immunocytochemistry.

2.1 ANTIBODY REPERTOIRE AGAINST HUMAN AND BOVINE BESTROPHIN

2.1.1 Selection of antigens and production of polyclonal antibodies

Here, the aim was to generate a repertoire of polyclonal antibodies, directed against different epitopes of bestrophin in various species, i.e. in human, cow and mouse. First, appropriate epitopes need to be identified in the given protein sequence. The selection of a suitable epitope sequence is a critical step that has an impact on the successful outcome of antibody specificity. Hydrophobic regions are avoided, because these regions potentially span membranes and are therefore likely to be inaccessible for antibodies. To prevent cross-reactivity of the antibodies with the VMD2 RFP-TM family members VMD2L1, VMD2L2 and/or VMD2L3 (see Introduction 2.3), a multiple sequence alignment of the protein family was done (Fig. 10). Regions of high homology are not taken into consideration as suitable antigenic sequences and all epitopes designed for antibody production are shown in the multiple sequence alignment of human, murine and bovine bestrophin.

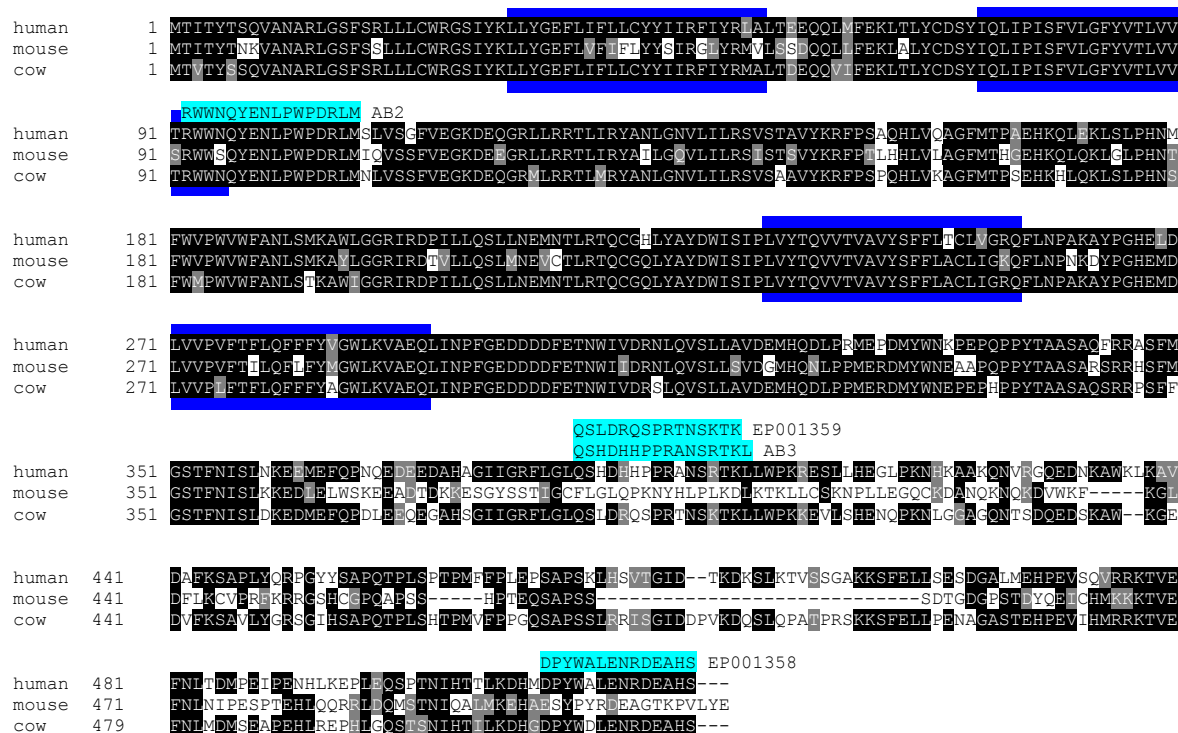


Fig. 10 Multiple Sequence Alignment of human, murine and bovine bestrophin indicating the location of suitable epitopes for antibody production

Multiple sequence alignment of human (NP_004174), murine (Fig 18) and bovine (unpublished, see Appendix) bestrophin is generated by using the bioinformatic tools T-COFFEE¹³ and boxshade¹⁴. The localization of four transmembrane domains predicted by TMHMM¹⁵ are represented by blue rectangles); the sequence of the four epitopes is shown in turquoise. Please note that synthetic peptides AB2, AB3 and EP001358 are deduced from human bestrophin, while EP001359 is based on the bovine sequence.

Anti-bestrophin polyclonal antibodies (pAb) are raised in four New Zealand rabbits immunized with synthetic polypeptides. Two rabbits are immunized with human polypeptide sequences (i) human AB2 (NH₂-RWWNQYENLPWPDRLM-COOH) located in the second loop between TM2 and TM3 and (ii) human AB3 (NH₂-QSHDHHPPRANSRTKL-COOH) located within the C-terminal tail after TM4. Another two rabbits are immunized with a mixture of human and bovine polypeptide sequences: (iii) bovine EP001359 (NH₂-CQSLDRQSPRTNSKTK-CONH₂) located 106 residues after TM domain four of bovine VMD2 and (iv) human EP001358 (NH₂-CDPYWALENRDEAHS-COOH) located at the C-terminus of human VMD2 (Fig. 10). The four New Zealand rabbits produced four polyclonal antisera, terminated pAB2, pAB3, pAB-333 and pAB-334. The resulting polyclonal antibodies are directed against the following epitopes: pAB2 is directed against human AB2, pAB3 is directed against human AB3, and polyclonal antibodies pAB-333

¹³ T-Coffee: <http://www.ch.embnet.org/software/TCoffee.html>

¹⁴ boxshade: http://www.ch.embnet.org/software/BOX_form.html

¹⁵ TMHMM: <http://www.cbs.dtu.dk/services/TMHMM/>

and pAB-334 are both directed against the human and bovine epitopes EP001358 and EP001359 (Fig. 10, 11e and 11f).

2.1.2 Recombinant partial and full length bestrophin

To test the specificity of rabbit polyclonal antisera, various recombinant VMD2 fusion proteins are generated using the bacterial pGEX and pMAL expression systems. Partial sequences encoding antigenic regions of VMD2 are cloned in-frame into a vector either encoding the maltose binding protein (MBP) or the glutathione S-transferase protein (GST). Table 2 lists all fusion proteins constructed for testing the immunoresponse of rabbit polyclonal antisera; oligonucleotide primer sequences used for engineering the constructs are summarized in Table 11A. *Escherichia coli* strain XL1-blue is transformed with the pGEX and pMAL constructs and large amounts of fusion proteins are produced by inducing the protein expression with IPTG. Bacterial lysates are then denatured with β -mercaptoethanol and preheated prior to SDS-PAGE.

Table 2 Recombinant fusion proteins

Plasmid construct	LabCode	Species	Epitope	Fusion Protein	aa – aa	Predicted size of protein (kDa)	Antibodies
pGEX-4T3-hAB2	21-2;21-3	human	AB2	GST-hAB2	78 - 116	26 + 6 = 32	pAB2
pGEX-4T3-hAB3	23-1;23-3	human	AB3	GST-hAB3	361 - 446	26 + 11 = 37	pAB3
pGEX-4T3-bAB3	1; 14	bovine	AB3	GST-bAB3	361 - 446	26 + 11 = 37	pAB-333/-334
pMAL-cxh-bAB3	1-1; 1-2	bovine	EP001359	MBP-bAB3	361 - 446	43 + 11 = 54	pAB-333/-334
pGEX-4T3-h-bov4	h4G5; 6-1	human	EP001358	GST-hbov4	538 - 585	26 + 6 = 32	pAB-333/-334
pGEX-4T3-b-bov4	7-3	bovine	EP001358	GST-bbov4	538 - 585	26 + 6 = 32	pAB-333/-334
pMAL-cxh-h-bov4	8-1	human	EP001358	MBP-hbov4	538 - 585	43 + 6 = 49	pAB-333/-334 pAB-334(AP3)
pMAL-cxh-b-bov4	9-1	bovine	EP001358	MBP-bbov4	538 - 585	43 + 6 = 49	pAB-333/-334

Furthermore, full-length VMD2 is expressed in prokaryotic and eukaryotic expression systems (Table 3). (i) For bacterial expression, the entire human *VMD2* cDNA is cloned into the pQE30 vector (Qiagen) and expressed in *Escherichia coli* strains M15/pREP4 and SG13009/pREP4. In the presence of bestrophin, bacterial growth is inhibited, suggesting that bestrophin has a toxic effect on growth. (ii) In yeast, full length bovine VMD2 is expressed by cloning the *VMD2* cDNA into the pGADT7 vector (Clontech). The coupling of VMD2 to the activating domain (AD), a necessity for the yeast-two-hybrid system, results in a protein size of 87 kDa. (iii) To express bestrophin in a mammalian cell line (COS7), a third construct is engineered by inserting human *VMD2* cDNA into the pcDNA3 vector (Invitrogen).

Table 3 Full length VMD2 protein expression systems

Plasmid construct	Species	Host	Fusion protein	aa - aa	Predicted size (kDa)	provided by
pQE30-hVMD2	human	<i>Escherichia coli</i>	fl-hVMD2	1 - 585	68	Dr. S. Herterich
pGAD-BEST	bovine	yeast	fl-bVMD2	1 - 585	87	A. Gehrig
pcDNA3-VMD2	human	mammalian cells	fl-hVMD2	1 - 585	68	Dr. H. Stöhr

2.1.3 Characterization of polyclonal antisera

The specificity of the four polyclonal antisera pAB2, pAB3, pAB-333 and pAB-334 are tested on multiple VMD2-containing extracts. As shown in Fig. 11a, polyclonal antisera pAB2 and pAB3 specifically recognize the fusion proteins GST-hAB2 (21-2 and 21-3) and GST-hAB3 (23-1 and 23-3) by Western blot analysis, respectively. However, in RPE extracts no signals are detected at 68 kDa, the calculated molecular mass of bestrophin.

Specific labeling of unpurified polyclonal antisera pAB-333 and pAB-334 is tested with fusion proteins containing human and bovine-specific antigenic regions. Unpurified polyclonal antisera pAB-334 reveals specific signals labeling both, human (MBP-hbov4 (8-1) and GST-hbov4 (h4G5)) as well as bovine (MBP-bbov4 (9-1) and GST-bbov4 (7-3)) fusion proteins generated against the C-terminus of bestrophin (Fig. 11b). Because human antigen EP001358 differs from the bovine sequence in only one amino acid residue, a polyclonal antibody is generated with cross-reactivity for VMD2 in both species. Furthermore, pAB-334 specifically detects fusion protein GST-bAB3, which contains the bovine polypeptide sequence of antigen EP001359. However, fusion protein GST-hAB3 containing the analogous human sequence is not specifically stained. This is probably due to the low homology of nine out of 15 residues between human and bovine epitopes in this region. As for pAB2 and pAB3, bestrophin is not detected by pAB-334 in human RPE extracts. Immunoblotting with polyclonal antisera 333 (pAB-333) displays the same pattern of binding specificity, suggesting that both rabbits gave immunoresponses against the injected antigens (data not shown).

To improve specificity, polyclonal antisera 334 (pAB-334) is purified by affinity chromatography against the human-specific fusion protein MBP-hbov4 (8-1). Purified pAB-334(AP3) is tested by immunoblotting against a variety of protein extracts containing partial and full-length human and bovine VMD2 (Table 2 and 3) as well as against a bovine RPE protein extract (Fig. 11c). Strong and specific signals of the expected sizes are found in bacterial, yeast and COS7 cell lysates; a faint band migrating at the expected size of approximately 68 kDa labels VMD2 in the bovine RPE extract. In control experiments the

specificity of pAb-334(AP3) is demonstrated by blocking the immunoaffinity with competing antigens prior to primary antibody labeling (Fig. 11d). Without pretreatment of the fusion protein MBP-hbov4, pAB-334(AP3) specifically detects full length human bestrophin expressed in the COS7 cell line, full length bovine bestrophin in yeast extracts and bacterially expressed fusion protein MBP-hbov4. A treatment with excess of fusion protein (MBP-hbov4) saturates the binding capacity of pAB-334(AP3) and results in unlabeled bestrophin in the immunoblot.

Fig. 11 Characterization of anti-bestrophin antibodies (see following page)

The binding specificity of polyclonal antibodies raised against various human and bovine bestrophin epitopes is evaluated by Western blot analysis. Protein lysates deriving from bacteria, yeast cells, COS7 cells and RPE tissues are separated by electrophoresis in a SDS-containing 10 %-PAA-gel. The proteins are then transferred to a nylon membrane and incubated with different dilutions of first antibodies as depicted below each blot. Otherwise, the protein gels are stained with Coomassie® brilliant blue. (a) The blot on the left is probed with pAB2 and the one on the right with pAB3. Specific signals of 32 kDa and 37 kDa label the respective fusion proteins. In addition, a number of distinct but unspecific signals are found in the protein extracts with (GST-AB2 or -AB3) and without the epitope of interest (GST). Unspecific labeling of pAB3 is seen as a distinct 37 kDa band in the human RPE extract. (b) Similarly to (a), multiple bacterial lysates and RPE extracts are probed with unpurified pAB-334 to determine its specificity. (c) Specific labeling of purified pAb-334(AP3) is confirmed by Western blot analysis (right) of a human VMD2 transfected COS7 cell homogenate, a yeast lysate overexpressing bovine VMD2, a bacterial lysate overexpressing the fusion protein MBP-hbov4 and a bovine RPE extract (white arrow). Protein loadings are depicted in a Coomassie-stained gel (left). (d) Further evidence of specific labeling is demonstrated by pretreating the purified primary antibody pAB-334(AP3) with MBP-hbov4 protein extracts followed by primary and secondary staining of the blot. A surplus of MBP-hbov4 binds the specific antibodies, resulting in no staining of the subsequent immunoblot (left). Without pretreating the antibody with MBP-hbov4 (right), pAB-334(AP3) specifically detects full-length human VMD2 (68 kDa), full-length bovine VMD2 (87 kDa) and the fusion protein MPB-hbov4 (49 kDa). To illustrate the binding sites of antibodies pAB2, pAB3, pAB-333, pAB-334 and pAB-334(AP3) schematically, the four TM domain model of human (e) and bovine (f) VMD2 are shown. Antigens AB2, AB3, EP001358 and EP001359 are indicated by yellow (human) and orange (bovine) rectangles.

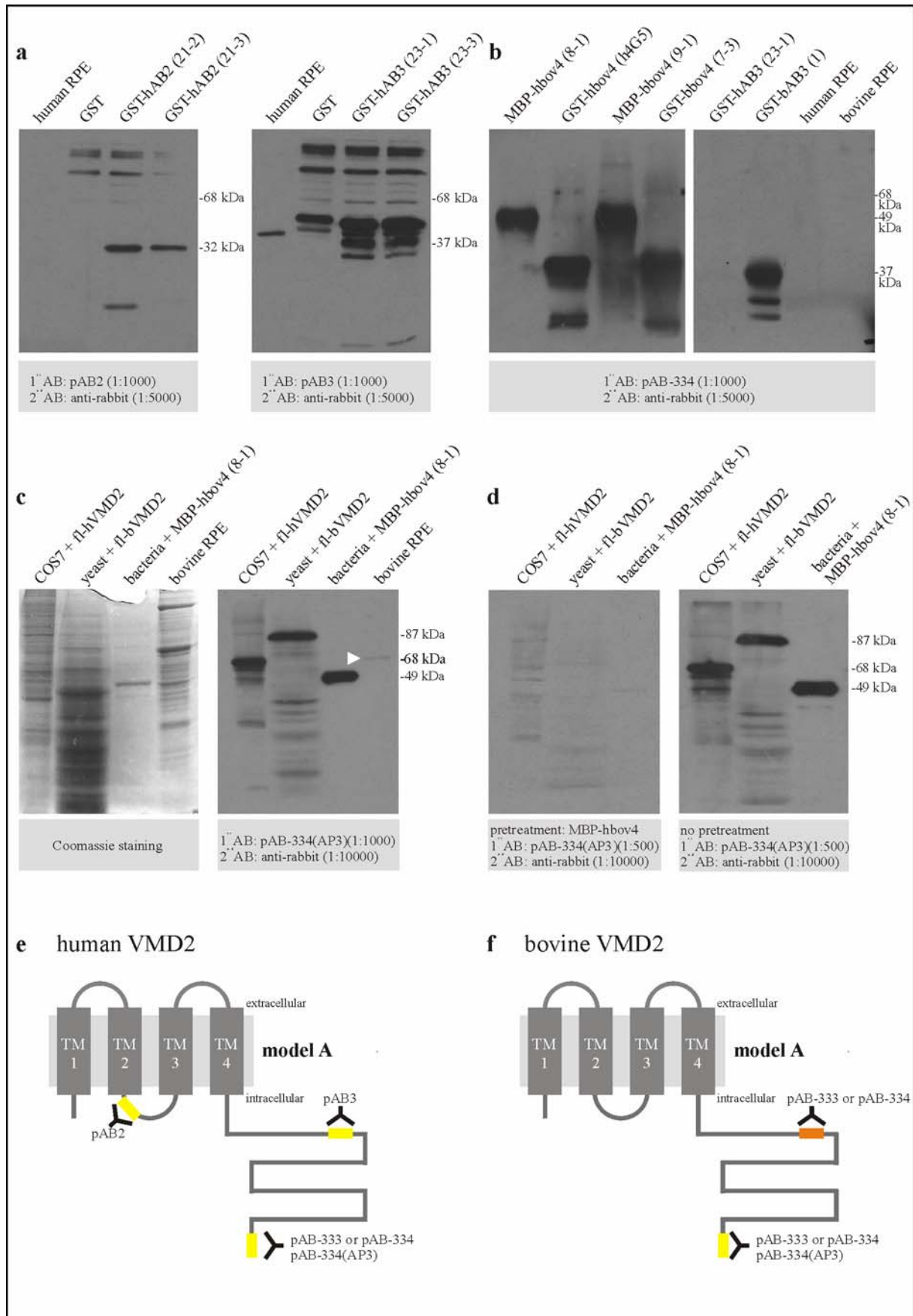


Fig. 11 Characterization of anti-VMD2 antibodies (see preceding page)

2.2 HETEROLOGOUS EXPRESSION OF MUTANT BESTROPHIN

To gain first insight into the functional consequences of mutant VMD2, an *in vitro* heterologous expression system was established. The cell model system consists of native COS7 cells, COS7 cells transiently transfected with wild-type VMD2 and a series of VMD2 mutants. The COS7 cell line is chosen as suitable system as no endogenous VMD2 expression is detectable in the cell line (see below). Using the technique of site-directed mutagenesis, 23 distinct mutations are generated and cloned into the mammalian expression vector pcDNA3 as full-length *VMD2* transcripts (Table 4).

Table 4 Best-disease-associated mutations generated by site-directed mutagenesis

Name of Construct	Lab Code	Mutation	type of mutation	Localization according to:			
				Model A		Model B	
pcDNA3-empty	3.1	-	-	-	-	-	-
pcDNA3-VMD2	2.2	-	-	-	-	-	-
pcDNA3-VMD2-T6P	T6P	Thr6Pro	missense	N-terminus	cytosolic	N-terminus	cytosolic
pcDNA3-VMD2-A10T	1.1	Ala10Thr	missense	N-terminus	cytosolic	N-terminus	cytosolic
pcDNA3-VMD2-L21V	2a	Leu21Val	missense	N-terminus	cytosolic	N-terminus	cytosolic
pcDNA3-VMD2-W24C	3b	Trp24Cys	missense	N-terminus	cytosolic	N-terminus	cytosolic
pcDNA3-VMD2-R25Q	4a	Arg25Gln	missense	N-terminus	cytosolic	N-terminus	cytosolic
pcDNA3-VMD2-R47H	5a	Arg47His	missense	TM1	membrane	TM1	membrane
pcDNA3-VMD2-L82V	6c	Leu82Val	missense	TM2	membrane	TM2	membrane
pcDNA3-VMD2-Y85H	7a	Tyr85His	missense	TM2	membrane	TM2	membrane
pcDNA3-VMD2-R92S	8a	Arg92Ser	missense	LOOP2	cytosolic	TM2	membrane
pcDNA3-VMD2-P101T	9b	Pro101Thr	missense	LOOP2	cytosolic	LOOP2	cytosolic
pcDNA3-VMD2-R218C	10a	Arg218Cys	missense	LOOP2	cytosolic	LOOP3	extracellular
pcDNA3-VMD2-L224M	11b	Leu224Met	missense	LOOP2	cytosolic	LOOP3	extracellular
pcDNA3-VMD2-Y227N	2.6	Tyr227Asn	missense	LOOP2	cytosolic	LOOP3	extracellular
pcDNA3-VMD2-V235M	13a	Val235Met	missense	LOOP2	cytosolic	TM3	membrane
pcDNA3-VMD2-T237R	14b	Thr237Arg	missense	TM3	membrane	TM3	membrane
pcDNA3-VMD2-A243V	15a	Ala243Val	missense	TM3	membrane	TM3	membrane
pcDNA3-VMD2-F276L	16a	Phe276Leu	missense	TM4	membrane	TM4	membrane
pcDNA3-VMD2delF281	17a	Phe281del	deletion	TM4	membrane	TM4	membrane
pcDNA3-VMD2-delI295	3.2	Ile295del	deletion	C-terminus	cytosolic	C-terminus	extracellular
pcDNA3-VMD2-P297A	19a	Pro297Ala	missense	C-terminus	cytosolic	C-terminus	extracellular
pcDNA3-VMD2-D301E	20a	Asp301Glu	missense	C-terminus	cytosolic	C-terminus	extracellular
pcDNA3-VMD2-F305S	21a	Phe305Ser	missense	C-terminus	cytosolic	C-terminus	extracellular
pcDNA3-VMD2-V311G	22a	Val311Gly	missense	C-terminus	cytosolic	C-terminus	extracellular

As indicated in Fig. 12, the 21 missense mutations and two in-frame deletions selected for testing are representative of the mutational spectrum found in Best disease patients. Based on model A, the majority of mutations are either on the cytosolic side or within membrane-spanning regions of bestrophin. Five mutations (Thr6Pro, Ala10Thr, Leu21Val, Trp24Cys and Arg25Gln) are located prior to TM1, six mutations (Pro92Ser, Pro101Thr, Arg218Cys, Leu224Met, Tyr227Asn and Val235Met) are located in the second loop between TM2 and TM3 and five mutations (Ile295del, Pro297Ala, Asp301Glu, Phe305Ser and Val311Gly) are found directly after TM4. Mutations affecting membrane-spanning regions of VMD2 are Arg47His (TM1), Leu82Val and Tyr85His (TM2), Thr237Arg and Ala243Val (TM3) as well

as Phe276Leu and Phe281del (TM4). Model B places mutations Arg218Ser, Leu224Met and Tyr227Asn on the extracellular instead of the intracellular side; and mutations Ile295del, Pro297Ala, Asp301Glu, Phe305Ser and Val311Gly would be located outside the cell (Table 4). Furthermore, Arg92Ser shifts from LOOP2 to TM2 and Val235Met from LOOP2 to TM3.

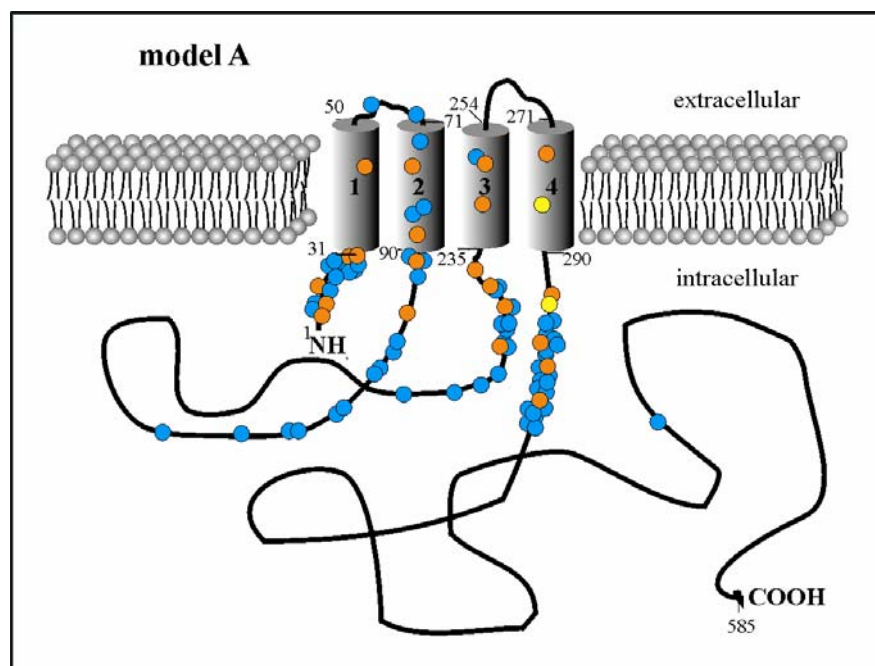


Fig. 12 Best disease-associated mutations relative to model A of bestrophin

In the four TM domain model A of bestrophin, the localization of all mutations (colored circles) so far identified to be associated with Best disease are displayed (VMD2 mutation database). Mutations selected for site-directed mutagenesis include 21 missense mutations (orange circles) and two in-frame deletions (yellow circles) located in mutational hotspots in close proximity to or within TM domains one to four.

COS7 cells are transiently transfected with mutant and wild-type pcDNA3-VMD2 constructs, an expression vector that contains the human *VMD2* cDNA under the control of the cytomegalovirus (CMV) promoter. As negative controls, COS7 cells are transfected with water (MOCK) and with the pcDNA3 expression vector without insert. After an incubation period of 48 hrs, the transfected cells are harvested. One half of the harvested cells is used to isolate total RNA and the other half is lysed in a SDS-containing buffer to obtain whole protein extracts. For example, the transfection assays and Western blot analyses performed with wild-type VMD2 and the mutants, demonstrate specific labeling of normal and mutant VMD2 (Ala10Thr, Tyr227Asn, Ala243Val and Ile295del) with purified polyclonal antibody pAB-334(AP3) (Fig. 13a). No staining is detected in the negative controls. Under reducing conditions, mutant and wild-type VMD2 protein are present at similar levels and migrate with the apparent molecular mass of 68 kDa. By Northern blot analysis, a specific band of approximately 2.5 kb is detected in all mutants as well as in wild-type *VMD2* (Fig. 13b). Variations in expression, probably resulting from differences in total RNA loadings (see control), are observed, but in each case a mutant *VMD2* (and wild-type *VMD2*) transcript is

detectable. In conclusion, the presence of Best disease-associated mutations seem to have no severe effect on the expression of exogenous bestrophin, neither in form of protein nor mRNA transcript synthesis.

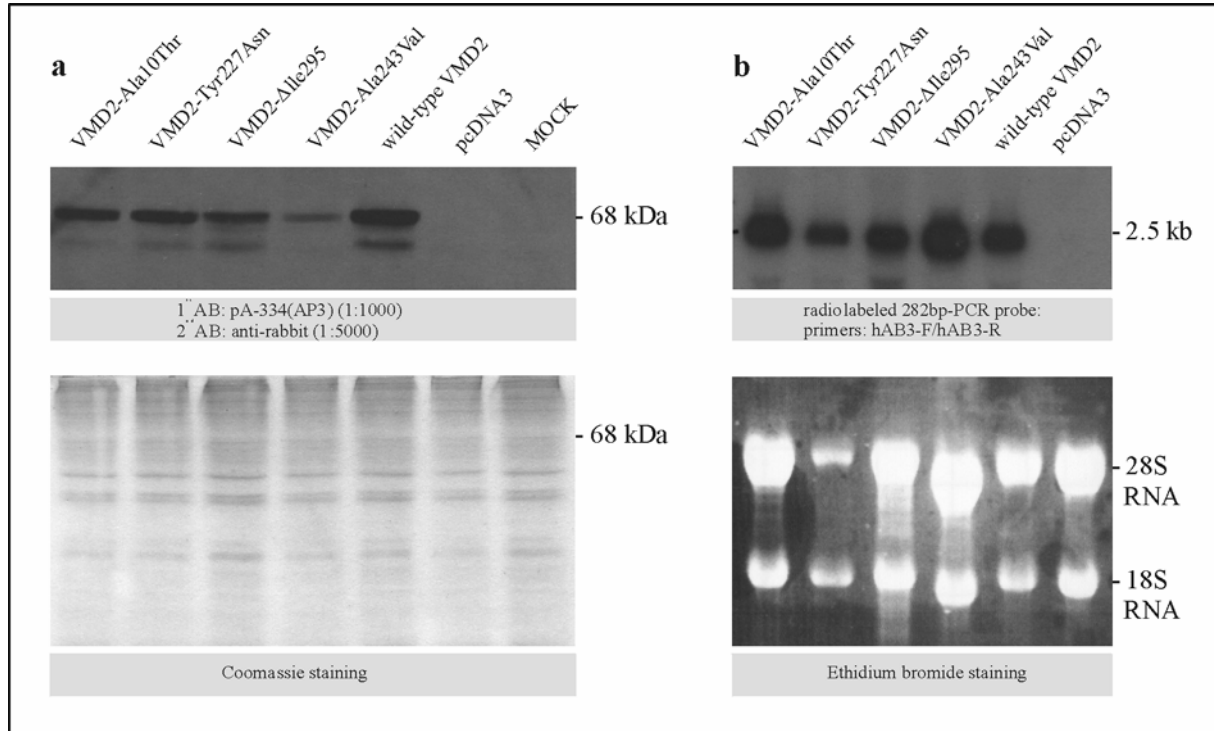


Fig. 13 Expression of wild-type and mutant VMD2 in transiently transfected COS7 cells

Heterologous expression of four mutants (Ala10Thr, Tyr227Asn, Al243Val and Ile295del), wild-type VMD2, the empty vector (pcDNA3) and MOCK is performed in the COS7 cell system. The protein and RNA extracts are analyzed by Western blot (a) and Northern blot (b). (a) Protein extracts of transfectants are separated by SDS-PAGE and probed with pAB-334(AP3) and below, equal loadings of protein extracts are depicted in a Coomassie-stained PAA-gel. Scored by immunocytochemical staining of transfected cells (Fig. 6), the transfection efficiency is approximately 10 %. (b) Total RNA is isolated from the transfected cells and separated electrophoretically in a formaldehyde-containing agarose gel. A 282 bp PCR probe (primers hAB3-F/hAB3-R) specifically labels the human VMD2 transcript (2.5 kb). Below, RNA quantification is determined in an ethidium bromide-stained agarose gel.

2.3 SUBCELLULAR LOCALIZATION OF BESTROPHIN

2.3.1 Membrane fractionation

Both biocomputational transmembrane domain predictions (Fig. 5) as well as in situ hybridizations of the macaque and porcine RPE (Marmorstein et al. 2000), provide evidence that VMD2 is indeed an integral membrane-spanning protein and may be restricted to the basolateral regions of RPE cells. To localize VMD2 in the established *in vitro* COS7 cell system and to assess the effects of various mutations on the subcellular localization of bestrophin, membrane fractionation using high speed centrifugation is applied. COS7 cells are transiently transfected with the wild-type construct (pcDNA3-VMD2), mutant constructs (pcDNA3-VMD2-Arg47His, -Arg92Ser, -Tyr227Asn and -Val235Met) and the empty vector

pcDNA3. Then, whole cell crude extracts are separated by ultracentrifugation in a sucrose column consisting of two distinct sucrose concentrations of 5 % and 60 %. A whitish cloud of proteins is present at the border between the 5 % and 60 % sucrose, representing the membrane fraction. The soluble fraction of proteins is isolated from the upper 5 % sucrose solution. Western blot analysis reveals the presence of normal and mutant bestrophin exclusively in membrane fractions (Fig.14). Similarly, VMD2 mutants carrying the Arg25Gln, Leu82Val, Pro101Thr and Phe281del mutations are retrieved from the membraneous fractions isolated in the same way (data not shown). These experiments confirm that wild-type VMD2 associates with cellular membranes in COS7 cells and that the VMD2 missense mutations Arg25Gln, Arg47His, Leu82Val, Arg92Ser, Pro101Thr, Tyr227Asn and Val235Asn and the deletion Phe281del do not grossly interfere with the incorporation of the protein into the membrane. Significant quantitative and/or qualitative differences in localization of proteins with mutations located within a TM domain (Arg47His in TM1, Leu82Val in TM2, Arg92Ser in TM3, Val235Met and Phe281del in TM4) and a mutation located in close proximity to a TM domain (Arg25Gln, Pro101Thr, Tyr227Asn) are not observed.

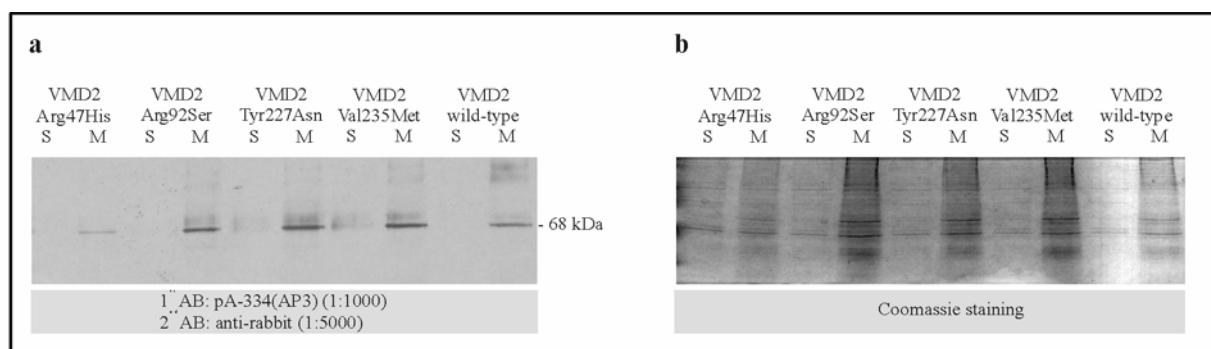


Fig. 14 Isolation of membrane and soluble fraction of COS7 cells transiently transfected with wild-type and mutant VMD2

Membrane-associated and soluble proteins are isolated by ultracentrifugation in two sucrose layers, consisting of 60 % sucrose (bottom layer) and 5 % sucrose (top layer). The protein extracts are separated by SDS-PAGE. (a) Wild-type and mutant VMD2 is labeled in the membrane (M) fraction but not in the soluble (S) fraction with polyclonal antibody pAB-334(AP3). (b) Protein loadings are depicted in the Coomassie-stained PAA-gel. The weak labeling of the mutant Arg47His and wild-type VMD2 visible on the Western blot is explained by the lower protein concentrations visible by Coomassie staining.

2.3.2 Immunocytochemistry

While *in vivo* localization studies localize bestrophin to the basolateral plasma membrane of RPE cells (Marmorstein et al. 2000), *in vitro* expression of bestrophin displays no plasma membrane association (Sun et al. 2002). Sun and coworkers transiently expressed bestrophin in human epithelial kidney cells (HEK293) and observed that bestrophin localizes

to intracellular membranes. To further clarify the subcellular localization of bestrophin in the COS7 heterologous expression assay, the VMD2 protein is first transiently expressed in COS7 cell and then detected by fluorescence immunocytochemistry. The subcellular localization of bestrophin reveals specific labeling of COS7 cells expressing VMD2. No signals are detected in non-transfectants or negative control experiments. Transfected cells display an intensive perinuclear staining as well as uniform staining of the cell surface and no staining of the nucleus (Fig. 15), indicating an association of the VMD2 protein to intracellular membranes (e.g. the endoplasmatic reticulum) as well as to the plasma membrane of COS7 cells.

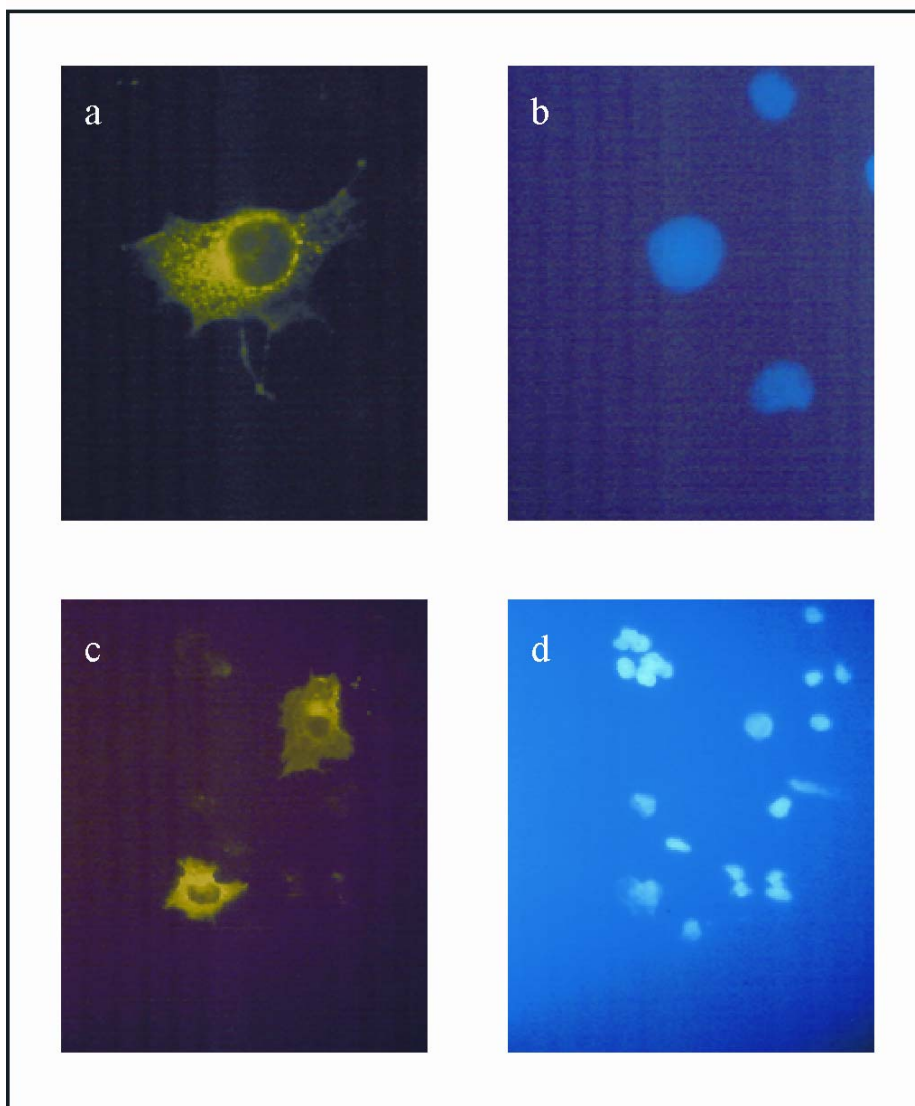


Fig. 15 Heterologous expression of VMD2 in COS7 cells

25x (a, b) and 100x (c, d) magnification of COS7 cells subjected to transient transfection experiments.

Polyclonal antibody pAB-334 specifically detects those Vero cells expressing VMD2 (a, c) and DAPI counter-staining labels the nucleus of all cells (b, d).

A transfection efficiency of approximately 10 % is calculated by dividing the number of specifically labeled cells by the total number of DAPI-stained cells.

3 IDENTIFICATION AND CHARACTERIZATION OF THE MURINE VMD2-RFP-TM FAMILY

In humans, bestrophin was the first member reported revealing typical features of the RFP-TM protein family, a protein family formerly described in *Caenorhabditis elegans* (see Introduction 2.3). By performing BLASTX searches with the cDNA of human *VMD2* in the human draft sequence, three further human *VMD2*-like proteins closely related to bestrophin were identified (Stöhr et al. 2002). As in the case of human *VMD2*, the human *VMD2*-like proteins (*VMD2L1*, *VMD2L2* and *VMD2L3*) possess a highly conserved region of 370 amino acid residues with four predicted transmembrane domains and an invariant RFP motif. Here, it was aimed at identifying and characterizing the RFP-TM gene/protein family in mouse. Detailed knowledge of the murine counterparts is regarded as an essential tool for performing genetic and biochemical experiments that are not possible in humans, such as sublocalization studies of bestrophin and its relatives on eye cross sections, spatial and temporal expression studies and protein interaction studies among the family members and/or other proteins. In the long run, the generation of targeted knock-in and knock-out mouse models for the *Vmd2*-like proteins is aspired.

3.1 *IN SILICO* CHARACTERIZATION OF THE MURINE RFP-TM GENE FAMILY

Murine genes orthologous to the respective human *VMD2*, *VMD2L1*, *VMD2L2* and *VMD2L3* genes are identified by performing extensive *in silico* analyses. By means of BLASTN and BLASTX searches in NCBI¹⁶ databases and BLAT searches in the UCSC¹⁷ genomic mouse DNA database, the corresponding genomic sequences are identified and the organization and localization of the murine genes is determined. This includes the prediction of the exonic and intronic sequences and the accompanying splice donor and acceptor sites, the identification of putative start codons, of alternative start codons and of stop codons and the prediction of the entire ORF of the genes or differentially spliced transcripts.

3.1.1 *Identification, genomic organisation and chromosomal localization*

3.1.1.1 *Murine Vmd2*

At the time the search for the murine *Vmd2* gene was initiated, neither murine ESTs nor cDNA entries corresponding to the gene were available in the public sequence databases. Therefore, genomic clones containing murine *Vmd2* are first identified in a murine P1-derived bacterial artificial chromosome (PAC) library (RCPI-21 Mouse PAC library, Rosswell Park Cancer Institute) by screening with a radiolabeled 1.3 kb probe PCR-amplified with primers

¹⁶ NCBI: <http://www.ncbi.nlm.nih.gov/80/>

¹⁷ UCSC: <http://genome.ucsc.edu/index.html?org=Human&db=hg13&hgsid=15995042>

TU15newF2 and mVMD2-R1 using murine genomic DNA as template. Four positive PAC clones (472E12, 472P7, 586H16 and 599E13) are identified in the initial screen and three of them (472E12, 472P7 and 599E13) are verified by Southern blotting (Fig. 16).

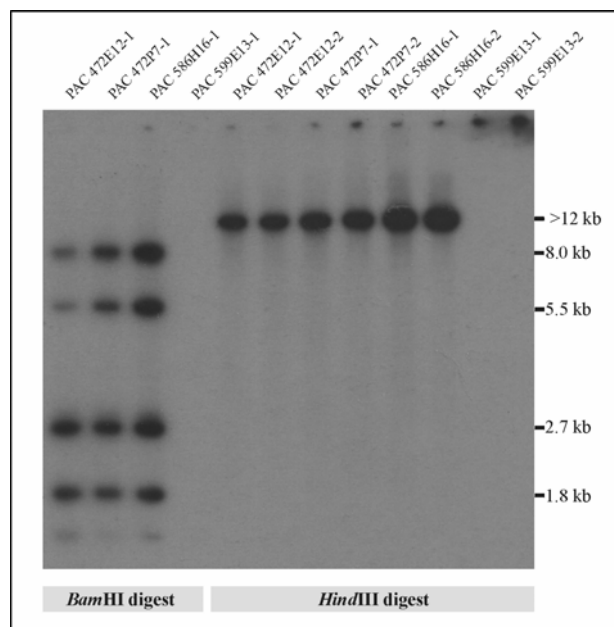


Fig. 16 Southern blot analysis of PAC clones containing the murine *Vmd2* gene

DNA of PAC clones 472E12, 472P7, 586H16 and 599E13 is digested with restriction enzymes *Bam*HI and *Hind*III, respectively, separated by agarose gel electrophoresis and subsequently transferred to a Nylon membrane. The radiolabeled 1.3 kb probe (a PCR product amplified with primer pair TU15newF2/VMD2-R1 and containing murine genomic DNA from *Vmd2* exon four to exon six) specifically detects murine *Vmd2* in PAC clones 472E12, 472P7, 586H16 but not in PAC clone 599E13.

PCR amplification and direct sequencing of PAC clones 472E12 and 586H16 with different combinations of murine-specific walking primers and known human-specific *VMD2* primers (bov4-b, TU15newR2, mVMD2-F3, -F5, -F6, -F8, -F11, -F12, -R1, -R2, -R3, -R4, -R5, -R7, -R8, -R9, -R10, -R12, -R13) provides novel sequence data of approximately 6 kb (Fig. 17a). Later, a cDNA clone (AK006549) is identified in a male testis cDNA RIKEN full-length enriched library with the help of BLASTN searches in the NCBI database (Fig. 17b). Sequence alignment between clone AK006549 and the murine genomic DNA sequence allows the corroboration of coding exons three to 12.

Due to the availability of novel murine draft genomic sequences from UCSC¹⁸, putative murine *Vmd2* exons one and two are assembled by performing BLAT search analyses with the human counterparts. Murine exon two, which is highly conserved, is readily identified. 929 bp upstream of murine exon two, a sequence homologous to human exon one is identified. However, sequence identity between the orthologous exons diverges towards the 3'-end of putative exon one, making it impossible to determine the exact splice donor site. Two alternative sequences may be used as 5'-donor splice sequence, resulting in either a

¹⁸ USCS: <http://genome.ucsc.edu/index.html?org=Human&db=hg13&hgsid=15995042>

longer (69 bp) or a shorter (49 bp) exon one. Both proposed splice site sequences display similar discrimination scores of 5.3 and 5.8, respectively (Table 5). However, which of these is utilized *in vivo* remains to be elucidated.

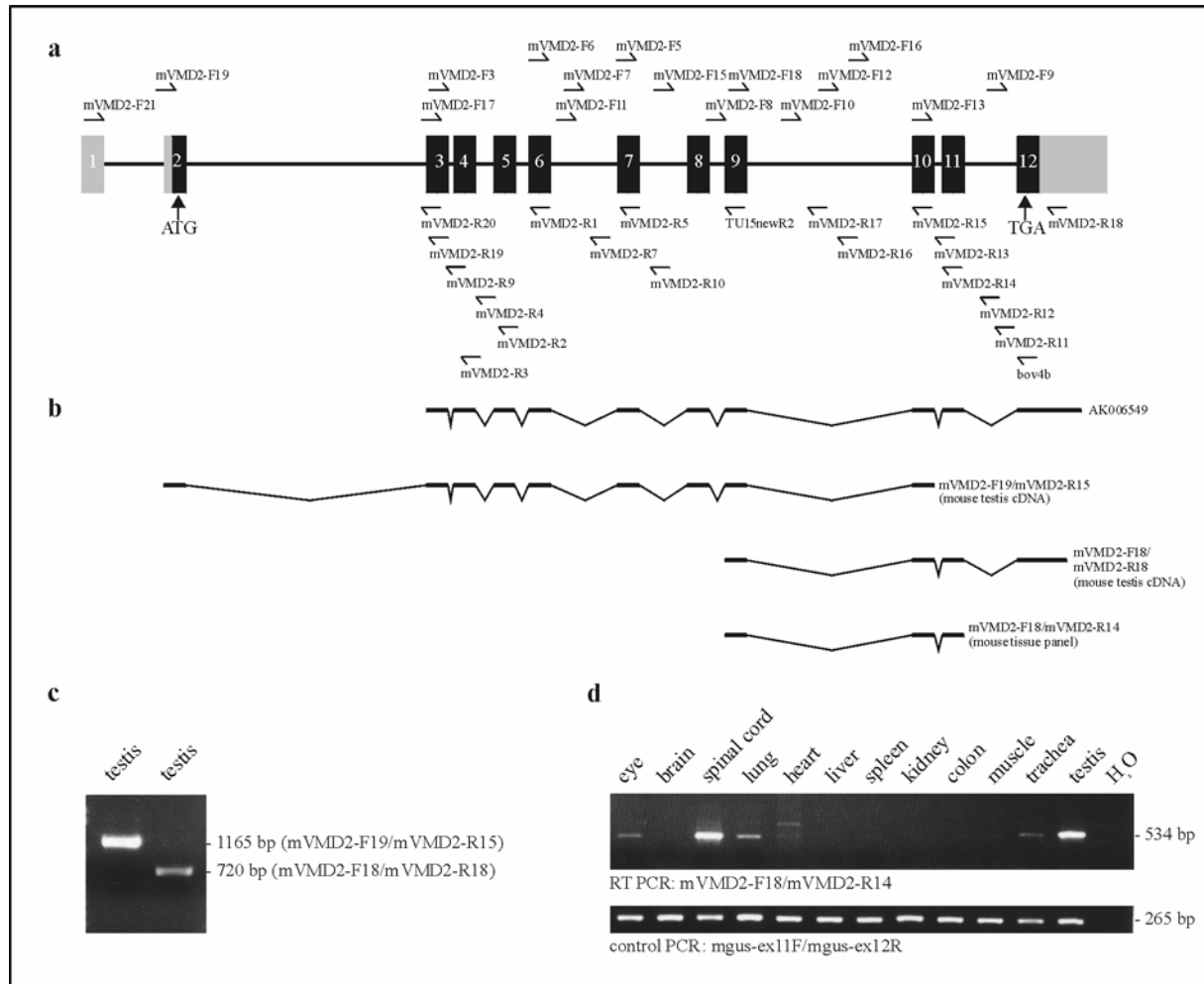


Fig. 17 Genomic organization and expression of murine *Vmd2*

(a) The gene structure of murine *Vmd2* is schematically demonstrated: protein encoding exons are represented by equally-sized black boxes, non-coding exons are represented by grey boxes and the relative position of all primers that are used to amplify the *Vmd2* gene are given above (forward primers) and below (reverse primers) the schematic. (b) The cDNA structure of murine *Vmd2* is based on cDNA clones (e.g. AK006549, NCBI database) as well as several RT PCR products amplified with testis cDNA and primers mVMD2-F19/mVMD2-R15, mVMD2-F18/mVMD2-R18 and mVMD2-F18/mVMD2-R14, plus numerous other combinations (not shown). In (c), some of the RT PCR products (mVMD2-F19/mVMD2-R15 and mVMD2-F18/mVMD2-R18) are shown by agarose gel electrophoresis. (d) In a panel of 12 murine tissues, the expression of *Vmd2* is restricted to eye, spinal cord, lung, heart, trachea and testis tissue. An additional band observed in heart tissue may represent a splice variant of the *Vmd2* transcript but was not further analyzed. Amplification of ubiquitously expressed murine β -glucuronidase (β -*Gus*) serves as positive control.

The resulting full-length cDNA contains an ORF of 1653 bp and encodes a 551 amino acid protein (Fig. 18). The highly conserved ATG initiation site in exon two (CAAGCCATGA) only partially matches to the preferred Kozak consensus sequence GCC(A/G)CCATGG (Kozak 1991; Kozak et al. 1996). Because the sequence is conform in at

least one of the two key positions (in bold, G⁻³ and A⁺⁴), it is classified as ‘not strong’ but ‘adequate’ Kozak motif. An in-frame stop codon is identified 234 bp upstream of the putative initiation site (ATG) in the 5′-UTR. The predicted splice junctions are mostly concordant with the consensus 5′-donor (AG**gt**) and 3′-acceptor (**ag**G) splice sites (Table 5). Splice site discrimination scores are calculated for all donor and acceptor sequences. 3′-acceptor splice scores (6.8 – 14.6) and 5′-donor splice scores (1.0 – 5.8) of murine *Vmd2* lie below the threshold values of 20 and 11, respectively (Berg and von Hippel 1988; Penotti 1991).

Table 5 Exon sizes, intron sizes and splice sites of murine *Vmd2*

Exon		3′-Acceptor Splice Site ^a		5′-Donor Splice Site ^a		Intron	
No.	Size (bp)	Sequence	Score ^b	Sequence	Score ^b	No.	Size (bp)
1 ^c	49 ^d			TGT gt gagc	5.8	1	929
1 ^c	69 ^d			CAG gt ggac	5.3	1	909
2	188	tctgcctgctcacc ag G	11.9	CAG gt aaga	1.0	2	>3000
3	95	gcctcaccacgccc ag A	13.6	TGG gt gagc	3.6	3	228
4	234	ccttctctctcccc ag G	7.5	CAG gt tggc	5.7	4	554
5	155	ccactctgcccggc ag G	12.2	AAT gt gagc	3.4	5	342
6	78	ctttcccgcaccatc ag G	11.0	CAG gt aaga	1.0	6	1016
7	153	ccttttctccttcc ag G	6.8	AAG gt gaga	1.3	7	791
8	81	ctctccccacctct ag G	10.4	CAG gt ataa	5.8	8	328
9	152	ggctccttggcaacc ag G	14.4	CAG gt tagac	5.2	9	2123
10	344	tctcttttctctcc ag C	8.2	CAG gt atgg	3.1	10	279
11	175	gttaaattgttctc ag G	14.6	CAG gt ctgt	5.6	11	775
12 ^c	37	gaatactctcccac ag G	11.9				

^a Exonic and intronic sequences are given in upper and lower case letters, respectively.

^b Score of perfect consensus = 0; worst score for acceptors: 42.5 (99 %: 0-20), for donors: 31.1 (99 %: 0-11) (Berg and von Hippel 1988; Penotti 1991). For calculations, an Excel[®]-based spreadsheet is used (Sauer, 2001).

^c Exon size calculations in exon one and exon 12 exclude the 5′-UTR and 3′-UTR, respectively.

^d Two possible 5′-donor splice sites of intron one result in a shorter (49 bp) or longer (69 bp) exon one.

Finally, RT PCR analysis is performed to confirm the novel *Vmd2* cDNA sequence experimentally. Using murine cDNA (testis) as template, primer sets mVMD2-F19/mVMD2-R15 and mVMD2-F18/mVMD2-R18 yielded two RT PCR products of 1165 bp and 720 bp, respectively (Fig. 17c). Cloning and sequencing of these bands reveals sequences matching exactly to the *in silico* predicted cDNA. Furthermore, RT PCR analysis is performed to establish the expression profile of *Vmd2* in a wide range of adult murine tissues. Specific PCR products (534bp) are obtained with primers mVMD2-F18 and mVMD2-R14 in eye, spinal cord, lung, heart, trachea and testis, while no PCR amplification is observed in brain, liver, spleen, kidney, colon and muscle tissue (Fig. 17d).

```

-270 GCTGCTGATTTTGGAGCAGATGACAGGAGGGGCTGAGACAATGGCTTCTTTGTAGAACCTTTTGTCTTAGAAAGTCAGGTGATAACTCAGCA
•exon 1
-180 CTATCTAGGTGGGCAGTGCCAGCCTCCAAGTATGGGCAAGGGTACCTGCCCCAGGGTCTCAGAAAGTCCCATCAACATAGTGGCCAGAGC
•exon 2
-90 TTTTATGGGGTTACCTGAACTGCTGGAACCTGTGTGAGCAGGGGCTGCCCCAGGACCCAAGCCCACCTACTGCTGCCAGTGCCAAGCC
1 ATGACTATCACCTACACAAACAAAGTAGCCAAATGCCCGCCTCGGTTCTGTTCTCGTCCCTCCTCTGTGCTGGCGAGGCAGCATCTACAAG
M T I T Y T N K V A N A R L G S F S S L L L C W R G S I Y K 30
•exon 3
91 CTGCTGTATGGAGAATTCCTTGTCTTCATATTCCTCTACTATTCCATCCGTGGACTCTACAGAATGGTTCCTCGAGTGATCAGCAGCTG
L L Y G E F L V F I F L Y Y S I R G L Y R M V L S S D Q Q L 60
•exon 4
181 TTGTTTGGAGAAGCTGGCTCTGTACTGCGACAGCTACATCCAGTCTATCCCTATATCCTTCGTTCTGGGTTTCTATGTTACATTGGTGGTG
L F E K L A L Y C D S Y I Q L I P I S F V L G F Y V T L V V 90
271 AGCCGCTGGTGGAGCCAGTACGAGAAGTTCGCGTGGCCCGACCCGCTCATGATCCAGGTGTCTAGTTCGTTGGAGGGCAAGGATGAGGAA
S R W W S Q Y E N L P W P D R L M I Q V S S F V E G K D E E 120
361 GGCCGTTTGTGCGGCGCACGCTCATCCGCTACGCCATCCTGGGCCAAGTGCTCATCTGCGCAGCATCAGCACCTCGGTCTACAAGCGC
G R L L R R T L I R Y A I L G Q V L I L R S I S T S V Y K R 150
•exon 5
451 TTTCCCACTCTTACCACCTGGTGTAGCAGGTTTATGACCCATGGGGAACATAAGCAGTTGCAGAAGTTGGGCTACCACACAACACA
F P T L H H L V L A G F M T H G E H K Q L Q K L G L P H N T 180
541 TTCTGGGTGCCCTGGGTGTGGTTTGCCAATTGTCAATGAAGCCATCTTGGAGGTGCAATCCGGGACACCGTCTGTCCAGAGCCTG
F W V P W V W F A N L S M K A Y L G G R I R D T V L L Q S L 210
•exon 6
631 ATGAATGAGGTGTGTACTTTGCGTACTCAGTGTGGACAGCTGTATGCCTACGACTGGATAAGTATCCCATTTGGTGTACACACAGGTGGTG
M N E V C T L R T Q C G Q L Y A Y D W I S I P L V Y T Q V V 240
•exon 7
721 ACAGTGGCAGTATACAGCTTTTTTCTTGCATGCTTGATCGGGAAGCAGTTTCTGAACCCAAACAAGGACTACCCAGGCCATGAGATGGAT
T V A V Y S F F L A C L I G K Q F L N P N K D Y P G H E M D 270
•exon 8
811 CTGGTGTGCTCTTCTTACAAATCCTGCAATTCTTATTCTACATGGGCTGGCTGAAGGTGGCAGAACAGCTCATCAACCCCTTCGGGGAG
L V V P V F T I L Q F L F Y M G W L K V A E Q L I N P F G E 300
•exon 9
901 GACGATGATGATTTTGGAGACTAACTGGATCATTGACAGAAACCTGCAGGTGTCCCTGTGTCCGTTGGATGGGATGCACCAGAAGTTCCT
D D D D F E T N W I I D R N L Q V S L L S V D G M H Q N L P 330
991 CCCATGGAACGTGACATGTACTGGAACGAGGCAGCGCCTCAGCCGCCCTACACAGCTGCTTCTGCCAGGTCTCGCCGGCATTCCCTTCATG
P M E R D M Y W N E A A P Q P P Y T A A S A R S R R H S F M 360
•exon 10
1081 GGCTCCACCTTCAACATCAGCCTAAAGAAAGAAGACTTAGAGCTTTGGTCAAAGAGGAGGCTGACACGGATAAGAAAGAGAGTGGCTAT
G S T F N I S L K K E D L E L W S K E E A D T D K K E S G Y 390
1171 AGCAGCACCATAGGCTGCTTCTTAGACTGCAACCCAAAACTACCATCTTCCCTTGAAAGACTTAAAGACCAAACTATTGTGTTCTAAG
S S T I G C F L G L Q P K N Y H L P L K D L K T K L L C S K 420
1261 AACCCCTCCTCGAAGGCCAGTGTAAAGGATGCCAACCGAGAAACAGAAAGATGTCTGAAATTTAAGGGTCTGGACTTCTTGAATGT
N P L L E G Q C K D A N Q K N Q K D V W K F K G L D F L K C 450
1351 GTTCCAAGGTTTAAAGAGGAGAGGCTCCCATTTGTGGCCACAGGCACCCAGCAGCCACCTACTGAGCAGTACAGCACCTCCAGTTCAGAC
V P R F K R R G S H C G P Q A P S S H P T E Q S A P S S S D 480
•exon 11
1441 ACAGGTGATGGGCTTCCACAGATTACCAAGAAATCTGTACATGAAAAAGAAAAGTGTGGAGTTTAACTTGAACATTCCAGAGAGCCCC
T G D G P S T D Y Q E I C H M K K K T V E F N L N I P E S P 510
exon 12
1531 ACAGAACATCTTCAACAGCGCCGTTTGGACCAGATGTCAACCAATATACAGGCTCTAATGAAGGAGCATGCAGAGTCCCTATCCCTACAGG
T E H L Q Q R R L D Q M S T N I Q A L M K E H A E S Y P Y R 540
1621 GATGAAGCTGGCACCAACCTGTTCTCTATGAGTGA
D E A G T K P V L Y E & 551

```

Fig. 18 cDNA and protein sequence of murine *Vmd2*

The putative amino acid sequence is shown below the coding DNA sequence of murine *Vmd2*. The numbering of nucleotides, beginning with position one at the adenine of the start codon ATG is shown on the left; the numbering of the amino acid residues is shown on the right. The beginning of each exon is denoted with a dot and the putative start (ATG) and stop (TGA) codons are framed. The sequence of the longer exon one is selected to be „more likely” for two reasons: (i) its discrimination score at the 5’-donor site is lower (5.3) and (ii) the shorter exon one would encode an in-frame alternative start signal resulting in a prolonged murine *Vmd2* protein by 22 amino acid residues. No homology to this 22 amino acid sequence is found in any member of the human VMD2 RFP-TM protein family.

The murine *Vmd2* gene consists of 12 exons spanning a genomic region of approximately 12 kb on mouse chromosome 19 (Fig. 19). In total, the murine *Vmd2* gene

locus (12.1 kb) is 1.6 kb smaller than the human *VMD2* orthologue (13.7 kb). High sequence conservation in both sequence identity (83 %) and the pattern of exon distribution is observed for exons one to nine of human and murine *Vmd2*. The intronic sequence distances between two exons are proportionally smaller in mouse than in human, but display an overall similar pattern. For example, in both genes the longest intervening sequences are located between exons one and two (1.4 x the size of human IVS1), between exons two and three (1.1 x larger) and between exons nine and ten (1.1 x larger). Beyond exon nine the sequence identity of the coding exons drops below 60 % and in mouse *Vmd2* an additional exon 12 is identified.

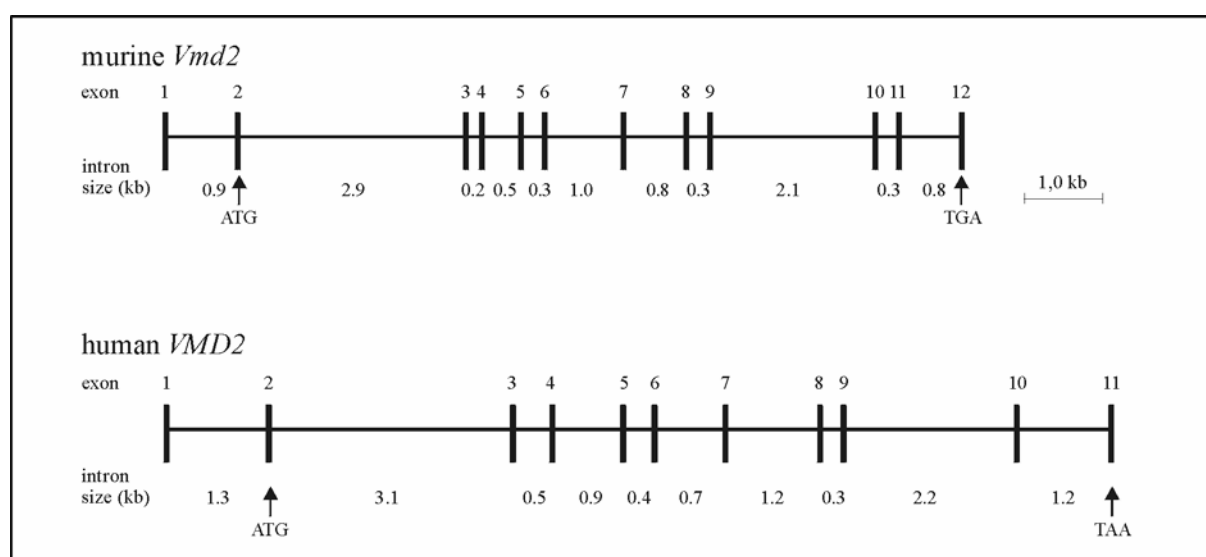


Fig. 19 Comparison between the genomic organization of murine *Vmd2* and human *VMD2*

In the schematic representation of murine and human *VMD2* the vertical black bars represent the distribution of exons one to 12 (mouse) and exons one to 11 (human) within the intronic sequence (horizontal line). Exon sizes are not to scale. The sizes of murine *Vmd2* exons are found in Table 5; human *VMD2* exon sizes are published by Marquardt et al. (1998). The arrows indicate the position of putative start and stop codons.

3.1.1.2 Murine *Vmd2L1*

Initially, the human *VMD2L1* protein sequence (AF440756) is used as query sequence for BLAT homology searches in the murine draft sequence database (UCSC¹⁹). A genomic sequence representing significant homology to human *VMD2L1* is identified on murine chromosome eight. This genomic region reveals nine predicted murine *Vmd2L1* exons, beginning with the start codon ATG in the putative exon two. An upstream, in-frame stop codon homologous to the stop codon of human *VMD2L1* is not identified. Therefore, further cycles of BLASTN searches are performed in the NCBI²⁰ EST mouse and nr databases with the assembled, incomplete murine *Vmd2L1*-cDNA. Five similar cDNA clones (BC036163, NM_145388, BC036157, BC019528 and BC031186) and four overlapping EST clones

¹⁹ USCS: <http://genome.ucsc.edu/index.html?org=Human&db=hg13&hgsid=15995042>

²⁰ NCBI: <http://www.ncbi.nlm.nih.gov/80/>

(BG965806, BG961794, BG923094 and BF582102) are detected (Fig. 20b). These sequences facilitate the assembly of the full-length cDNA transcript (Fig. 20a and 21) as well as the entire genomic organization of murine *Vmd2L1* (Fig. 22).

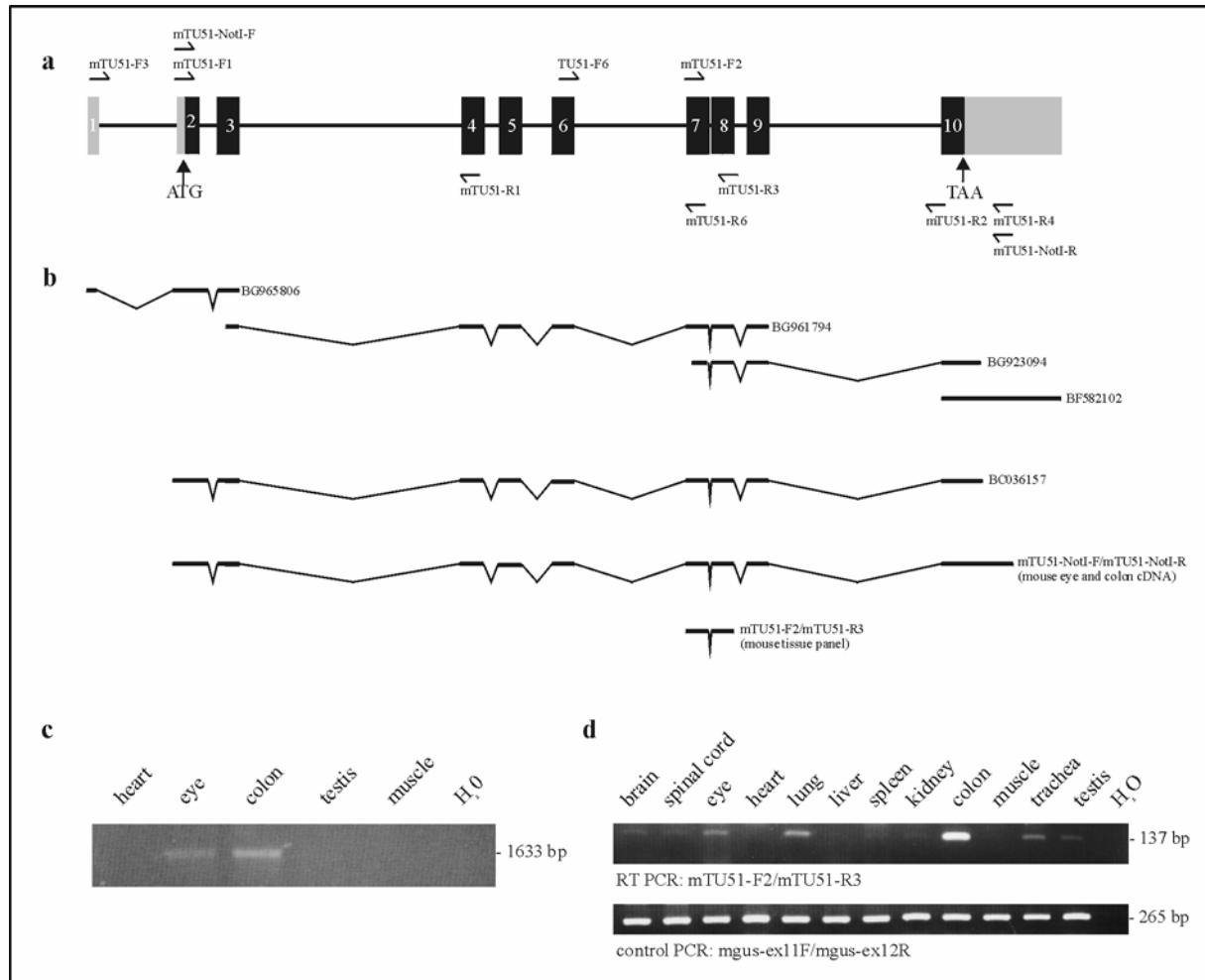


Fig. 20 Genomic organization and expression of murine *Vmd2L1*

(a) Schematic showing the exon/intron structure of murine *Vmd2L1*. The gene consists of nine coding exons (exons two to ten, black bars) and non-coding regions including exons one, two and the 5'- and 3'-UTRs (grey bars). The position of *Vmd2L1*-specific forward and reverse primers is given above and below the exons, respectively. Introns are given to scale and the putative start and stop codons are indicated by arrows. (b) EST clones (BG965806, BG961794, BG923094 and BF582102), cDNA clone (BC036157) and full length RT PCR product (mTU51-NotI-F/mTU51-NotI-R) correspond to the putative murine *Vmd2L1* transcript. (c) The full length *Vmd2L1* cDNA is RT PCR amplified with mTU51-NotI-F/mTU51-NotI-R primers in murine colon and eye tissue, but not in heart, muscle and testis tissue. (d) RT PCR analysis is performed in a panel of 12 murine tissues, revealing *Vmd2L1*-specific amplification (mTU51-NotI-F/mTU51-NotI-R) in colon, eye as well as in lung, trachea and testis. To demonstrate RNA integrity, the tissue panel is amplified with β -*Gus*-specific primers (mgus-ex11F/mgus-ex12R).

Novel sequence information is obtained from EST clone BG965806 and BF582102 corresponding to the 5'- and 3'-UTR, respectively, while EST clones BG961794 and BG923094 and cDNA clone BC036163 confirm the formerly predicted exon/intron boundaries. An additional exon, 798 bp upstream of putative start codon in exon two, is found

by alignment of EST clone BG965806 and genomic murine sequences. This reveals the exact size of intron one (672 bp), the 5'-donor and 3'-acceptor sites as well as the complete size of exon two (205 bp). EST clone BF582102 includes the stop codon (TGA) and extends the 3'-UTR by 582 bp (Fig. 20a, 20b). The assembled sequence of the entire coding region of murine *Vmd2L1* is verified by RT PCR amplification and sequencing. RT PCR analysis with primers that span the *Vmd2L1* ORF (mTU51-NotI-F/mTU51-NotI-R) result in specific PCR fragments of expected sizes using murine cDNAs derived from colon and eye (Fig. 20c). The expression of *Vmd2L1* is then analyzed in a larger panel of cDNAs derived from different mouse tissues (Fig. 20d). A high level of the *Vmd2L1* transcript is observed in colon tissue, while low levels of expression are observed in eye, lung, trachea and testis tissue.

The predicted initiation codon ATG in exon two differs from the preferred Kozak consensus sequence (GCC(A/G)CCATGG) by three nucleotides, at positions -4, -1 and +4 (GCAGCGATGA) (Kozak 1991; Kozak et al. 1996). However, high sequence homology to its human counterpart strongly suggests that this putative start codon is used as site of translation initiation. An in-frame stop codon (TAA) is detected 42 bp upstream of this ATG codon and no further ATGs are identified within this region. Generally, all putative exon/intron boundaries correspond to the invariant GT/AT rule and the splice site discrimination scores lie within the accepted range from 0 to 20 for acceptors and 0 - 11 for donors (Table 6). The resulting ORF of murine *Vmd2L1* consists of 1524 nucleotides rendering a deduced protein of 508 amino acid residues (Fig. 21).

Table 6 Exon sizes, intron sizes and splice sites of murine *Vmd2L1*

Exon No.	Size (bp)	3'-Acceptor Splice Site ^a		5'-Donor Splice Site ^a		Intron	
		Sequence	Score ^b	Sequence	Score ^b	No.	Size (bp)
1 ^c				AAG gtaaag	3.4	1	672
2	205	ttcccttggtcacag G	3.6	TCG gtgaga	3.9	2	97
3	95	attccctaccccacag C	4.8	TTG gtgagg	3.7	3	1691
4	234	tccggttggtccccag G	4.7	CTG gtgagt	1.6	4	85
5	155	ccccgcctccctccag G	2.9	GAG gtgagc	1.9	5	288
6	78	tcctcatccaccctag G	5.9	CAG gtaact	2.8	6	874
7	153	tttgcttggtccctag G	6.4	AAG gtgggt	2.2	7	84
8	81	tcttctctgaaactag G	5.5	CAG gtcagc	4.3	8	145
9	155	ctgtccgcctcctcag G	5.5	AGC gtaagt	4.6	9	1216
10 ^c	424	cctgtccaccctgtag G	5.9				

^a Exonic and intronic sequences are given in upper and lower case letters, respectively.

^b Score of perfect consensus = 0; worst score for acceptors: 42.5 (99 %: 0-20), for donors: 31.1 (99 %: 0-11) (Berg and von Hippel 1988; Penotti 1991). For calculations, an Excel[®]-based spreadsheet is used (Sauer, 2001).

^c Exon size calculations in exon one and ten excludes the 5'-UTR and 3'-UTR, respectively.

```

-180 GGCCACAGGTGAGAAGGGCCAGGTCTGGGAGAATAAATGGCCCTGGACTGGCAGGCTTTGGGCAGGACTCCTGGAGAGAGAGGGGCACGA
      •exon 2
-90  GTGGAAGGCTAGGAGGGGCAGCACGAAAGGAAGAAAGCCCGGACCCAGGCTAAACACCTTCTCCATTGGCCACACTGGCCAGGCGCAGCG
1    ATGACCGTACCTACACAGCCAGAGTGGCGAATGCCCGCTTCGGTGGCTTCTCGCAGCTGCTGCTGTGTGGCGCGGAAGCATCTACAAG
      M T V T Y T A R V A N A R F G G F S Q L L L L L W R G S I Y K 30
      •exon 3
91   CTCCCTGTGGCGAGAGCTGTTATGTTTTCCTGGGACTCTACATGGCACTAAGCGCCGCTATCGCTTCTTACTGGCAGAAGAGCAGAAGCGC
      L L W R E L L C F L G L Y M A L S A A Y R F L L A E E Q K R 60
      •exon 4
181  TACTTCGAGAAGCTTGTATATACTGCGACCAGTACGCCAGCCTCATCCCCGCTCTTTTCGTAAGTGGCTTCTACGTGACTCTGGTGGTG
      Y F E K L V I Y C D Q Y A S L I P V S F V L G F Y V T L V V 90
271  CATCGCTGGTGAACAGTACCTATGCATGCCTCTGCCGGACGCACTCATGTGCATAGTGGCTGGCACCCTGCATGGCGAGACGATCGA
      H R W W N Q Y L C M P L P D A L M C I V A G T V H G R D D R 120
361  GGCCGCTCTACCGGCGCAGCTCATGCGTACGACAGGCTCTCCGCGGTGCTGATCCTTCTGTTAGCACAGCAGTCTTCAAACGG
      G R L Y R R T L M R Y A G L S A V L I L R S V S T A V F K R 150
      •exon 5
451  TTCCCCACTATAGACCAGTGGTCGAGGCTGGATTTATGACCCGAGAAGAGCGCAAGAAGTTCGAGAAGTGAATTCGCTTACAACAAA
      F P T I D H V V E A G F M T R E E R K K F E N L N S S Y N K 180
541  TACTGGGTGCCCTGCGTATGGTTCTCGAGCCTGGCAGCGCAGGCGGGCGAGAGGGGCGCATCCCGCACACAGTGCCTAAAGTTGCTA
      Y W V P C V W F S S L A A Q A R R E G R I R D N S A L K L L 210
      •exon 6
631  CTAGAGGAGCTGAATGTGTTTCGGAGCAAATGTGGGATGCTGTTTCACTACGACTGGATTAGCATAACCCCTCGTCTACACCCAGGTAGTC
      L E E L N V F R S K C G M L F H Y D W I S I P L V Y T Q V V 240
      •exon 7
721  ACTATCGCAGTGTACAGTACTTCTTGGCTTGCCTCATCGCCGCTCAGTTTCTAGACCTGCACAGGGCTACAAAGACCACCCCTGGAC
      T I A V Y S Y F L A C L I G R Q F L D P A Q G Y K D H T L D 270
      •exon 8
811  CTATGCGTACCCATCTTACCTTGCTGCAGTCTTCTTCTACGCTGGCTTGCTTAAGGTAGCAGAGCAGCTTATTAACCCCTTTGGGGAA
      L C V P I F T L L Q F F F Y A G W L K V A E Q L I N P F G E 300
      •exon 9
901  GACGACGACGACTTTGAGACCAACTTCTTATTGACCGCAACTTCCAGGTGTCATGCTAGCTGTAGATGAGATGATGACGACTTGGCC
      D D D D F E T N F L I D R N F Q V S M L A V D E M Y D D L A 330
991  ATGCTGGAGAAAGATCTATACTGGGATGCAGCAGAAGCTCGCGGCCCTACACCGCGCCACCGCTTTCCTGCTTACAGCAGCCCTCCTTC
      M L E K D L Y W D A A E A R A P Y T A A T A F L L Q Q P S F 360
      •exon 10
1081 CAGGGCTCCACCTTTGATATAGCGCTGGCTAAAGAGGACATGCAGTTCACGCGCTGGACGGCGTGGATGGCCCGCTGGGAGAGGTTTAC
      Q G S T F D I A L A K E D M Q F Q R L D G V D G P L G E V H 390
1171 GGGGACTTTCTGCAGCGCTCCTGCCGGCGGGGGCGGTTCTGTGGGTCCGCTGGGGCGGCGCTGTCGCTGTTAAGCGTAAAAACAGC
      G D F L Q R L L P A G A G S V G P L G R R L S L L R R K N S 420
1261 TGCCTGTGACAGGCTCCACTGCTGCCAGCTGTGGCTGTGCAGCGCGGGGATGGCGGAGGCGTTGAGTGGCTTGTGGAGACCCATTG
      C V S E A S T A A S C G C A G A A D G G G V E C G C G D P L 450
1351 CTTGACCCAGCCTGCGGGAGCCTGAGCTGGAGTCTCCCGCATGCTCTGAGCCGCTGCCCCATCCCGGGGCAACTCTGAACCTTTT
      L D P S L R E P E L E S P A C P E P P A P I P G P T P E P F 480
1441 ACCACCGTGTGATTCGGGTCTCGGGCTCCTGCGCCACCCTGGCTGCCAGCCCTATTGGAGAGGAGGAAGAGAGTCCGGCCATGA
      T T V S I P G P R A P A P P W L P S P I G E E E E S P A & 508

```

Fig. 21 cDNA and protein sequence of murine *Vmd2L1*

The cDNA sequence with the corresponding numbering on the left and the deduced amino acid sequence of murine *Vmd2L1* with its numbering on the right are shown. A black dot indicates the position of the respective exon-intron boundaries, while the putative start (ATG) codon at position +1, the upstream stop (TAA) in-frame at position -39 and the stop codon of the gene at position +1525 are framed.

The genomic locus of murine *Vmd2L1* is approximately 7.4 kb in size, containing a single non-coding and nine coding exons. Its genomic organization is partially similar to that found for human *VMD2L1*. Both genes have nine coding exons. Human and murine exons two to nine are identical in size and human exon ten contains one additional codon. Within the highly conserved region spanning from the initiation codon (ATG) in exon two to exon nine, the protein sequence identity between human and mouse *Vmd2L1* is 95 %. Although the sizes

of introns are similar in most cases (introns four, five, seven, eight and nine), some intronic sequence sizes (e.g introns two, three and six) differ greatly (Fig. 22).

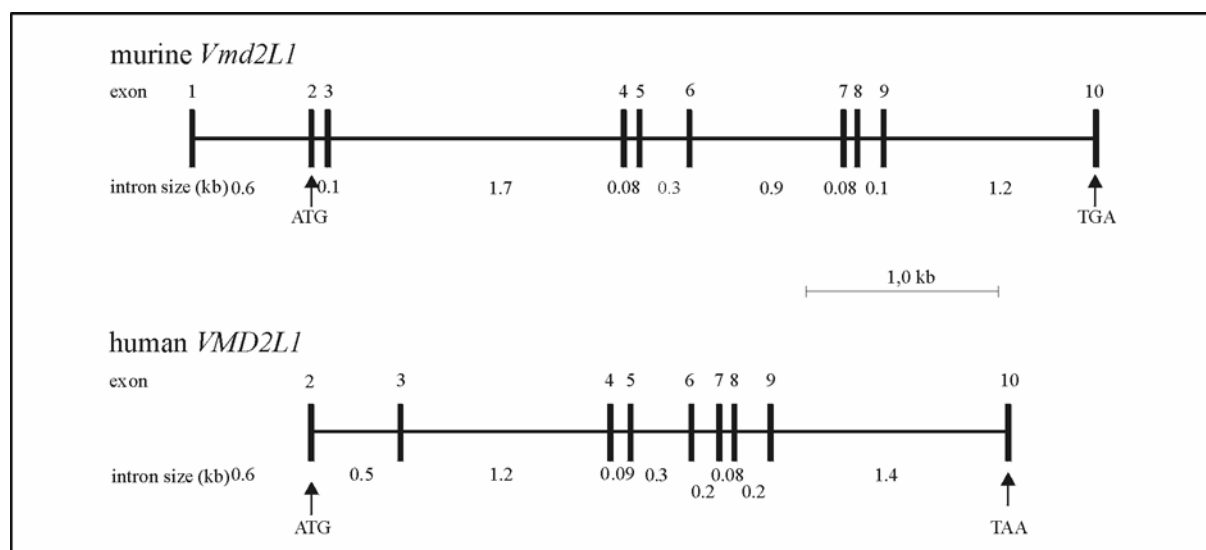


Fig. 22 Comparison between the genomic organization of murine and human *VMD2L1*

The distribution of exons, represented by equally-sized vertical black bars, is illustrated for the murine and human *VMD2L1* gene locus. Intron sizes are given to scale. Arrows indicate the position of start (ATG) and stop codons (TGA/TAA) in mouse and human exons two and ten, respectively. To date, no homologous *Vmd2L1* exon one has been identified in the human gene locus (Marquardt 2001).

3.1.1.3 Murine *Vmd2L2*

Sequence assembly of the murine *Vmd2L2* transcript is predominantly based on *in silico* analysis. Using the entire amino acid sequence of human *VMD2L2* as query sequence, a putative murine genomic sequence on chromosome four with significant homology between human and mouse (>88 %) exons two to seven is identified by BLAT search. No mouse exons homologous to human exons eight, nine and ten are identified. Pairwise sequence alignment (T-Coffee²¹) of the DNA sequence downstream of putative murine *Vmd2L2* with human exons eight, nine and ten individually reveals putative murine exons eight and nine, but not exon ten. In contrast to the other family members of *Vmd2*, neither murine ESTs nor mRNA sequences representing murine *Vmd2L2* are available from NCBI²² database, suggesting that murine *Vmd2L2* is likely to represent a low abundant transcript. Furthermore, several murine hypothetical genes (XM_143934, XM_207579 and XM_205479, predicted by GenomeScan, Yeh et al. 2001) are identified in the NCBI²² database, displaying high sequence similarity to the human *VMD2L2* transcript.

²¹ T-Coffee: <http://www.ch.embnet.org/software/TCoffee.html>

²² NCBI: <http://www.ncbi.nlm.nih.gov:80/>

A direct source of sequence information for murine *Vmd2L2* is explored by RT PCR and direct sequencing. Multiple primers and primer combinations are tested to specifically amplify the murine *Vmd2L2* transcript using cDNA derived from 12 different mouse tissues (brain, spinal cord, eye, heart, lung, liver, spleen, kidney, colon, muscle, trachea and testis). After numerous attempts of PCR amplification with different primer pairs (Fig. 23a), PCR conditions and cDNA templates, a specific PCR product of approximately 340 bp is amplified by nested RT PCR with primers mTU53-F3/mTU53-R4 and mTU53-F3/mTU53-R3 and cDNA from liver tissue (Fig. 23b and 23c). Direct sequencing of this PCR product partially confirms the *in silico* assembled *Vmd2L2* cDNA: the sequence produced by primers mTU53-F3 in exon six and mTU53-R4 in exon nine includes exons six, seven and nine, but skips exon eight. However, the ORF encoded by exons six, seven and nine contains two termination codons in exon seven. Interestingly, GenomeScan predicted that the 3'-acceptor splice site of exon seven is located 60 bp downstream, excluding the two stop codons from the sequence (XM_143934, XM_207579 and XM_205479). Nonetheless, the existence of two consecutive stop codons in exon seven of murine *Vmd2L2* is confirmed by RT PCR. Furthermore, no ORF corresponding to *VMD2L2* is identified in exon four obtained from the UCSC database. Manual editing of murine exon four (i.e. the insertion of 13 bp) would result in an ORF highly homologous to the human orthologous exon. To resolve this, *Vmd2L2* exon four is directly sequenced with primer pair mTU53-F5/R5 and murine genomic DNA as template (Fig. 23b). Interestingly, the 13 nucleotides are indeed deleted in *Vmd2L2* exon four, thus confirming the *in silico* sequence originally obtained from the murine UCSC database.

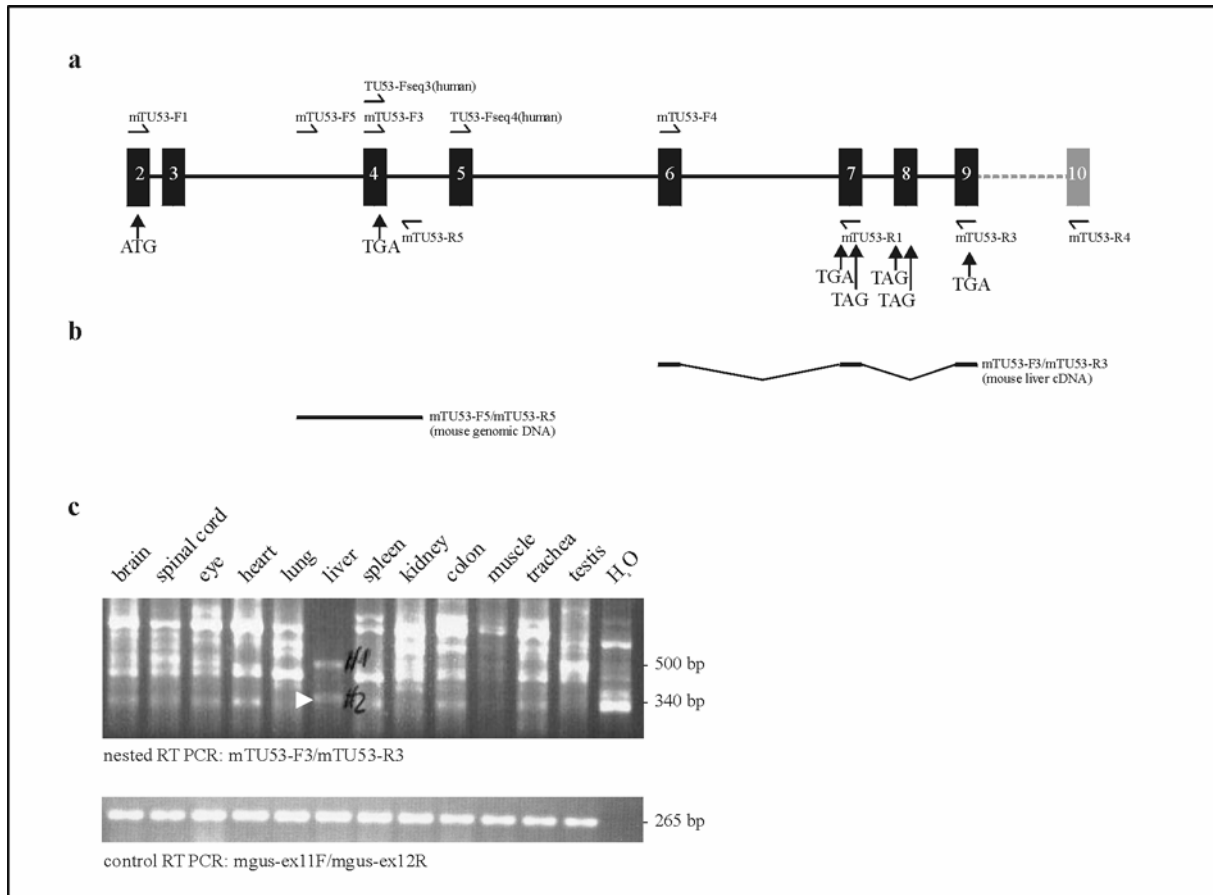


Fig. 23 Genomic organization and expression of murine *Vmd2L2*

(a) In the schematic, the putative exon-intron organization of murine *Vmd2L2* is illustrated and the forward and reverse oligonucleotide primers used for characterizing the *Vmd2L2* cDNA are indicated by arrows above and below the gene, respectively. (b) While no EST or cDNA clones are available from any databases, one RT PCR product was amplified with nested conditions (primers mTU53-F3/mTU53-R4 and mTU53-F3/mTU53-R3) and liver cDNA. Further, the sequence of murine exon four is verified by genomic amplification with primers mTU53-F5/mTU53-R5. (c) Illustrated by agarose gel electrophoresis, nested RT PCR analysis with primers mTU53-F3/mTU53-R4 and subsequently with mTU53-F3/mTU53-R3 results in specific amplification of liver tissue. The specific PCR product of ~340 bp is indicated by an arrow. Due to unstringent PCR conditions and nested amplification, unspecific PCR products are observed in liver tissue (~ 500 bp), in the other mouse tissues as well as in the water control. Amplification of ubiquitously expressed β -*Gus* serves as control to assess quality of RNA.

Taken together, data generated by BLAT searches and RT PCR analyses facilitates the construction of the genomic exon/intron structure of murine *Vmd2L2*, displaying high structural similarity to the human counterpart (Fig. 24). DNA sequence alignment of the putative murine cDNA from exon two to exon nine and human cDNA from exon two to exon nine illustrate a sequence identity of 84 %. However, it is not possible to predict a continuous ORF for murine *Vmd2L2*. The translation of the manually assembled *Vmd2L2* cDNA results in amino acid sequences of high homology in exons two, three, five and six of 78 %, 90 %, 96 % and 96 %, respectively. On the other hand, exons four, seven, eight and nine are interrupted by multiple stop codons due to the presence of a 13 bp deletion in exon four, a 1 bp deletion and a 1 bp insertion in exon seven, a 6 bp deletion in exon seven and a 4 bp

insertion in exon nine (Fig. 25). Features such as small sequence insertions or deletions resulting in premature stop codons and consequently in truncated proteins are commonly seen in genes that have evolved to non-functional pseudogenes during the course of evolution.

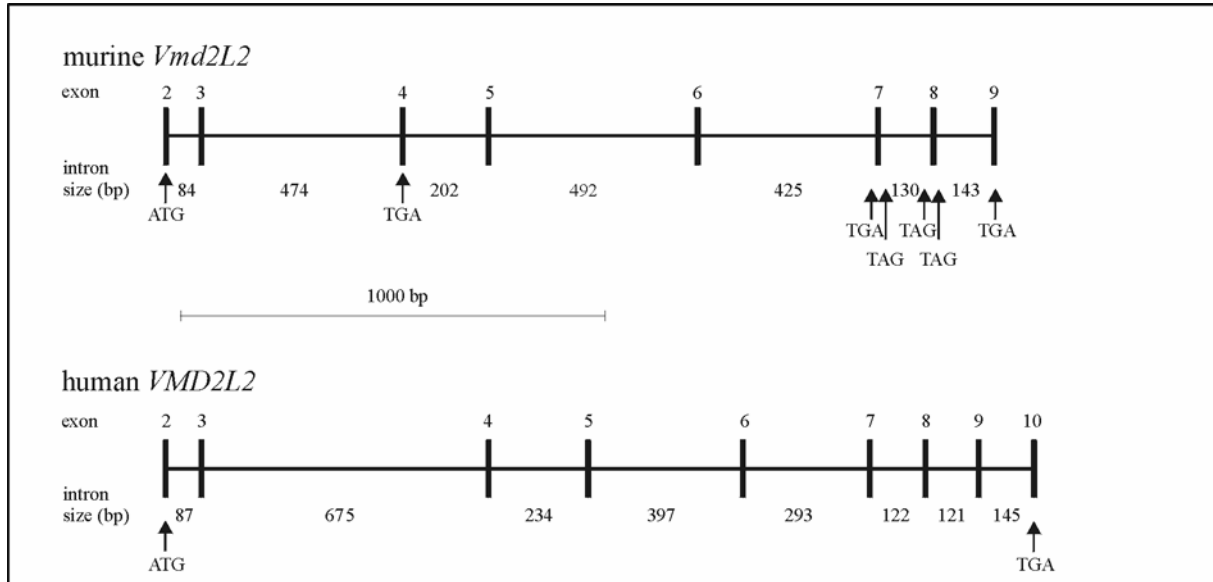


Fig. 24 Comparison between the genomic organization of murine *Vmd2L2* versus human *VMDL2*

The pattern of the human and murine exonic distribution (black vertical bars, not to scale) is shown schematically. Please note that in comparison to the other members of the VMD2 RFP-TM family, both murine and human *VMD2L2* loci contain small intervening sequences (horizontal lines): the murine introns range between 84 bp (IVS2) and 492 bp (IVS5), while the human intron sizes range between 87 bp (IVS2) and 675 bp (IVS3). Arrows indicate the position of predicted start and stop codons in murine and human *VMD2L2*.

```

...exon 2
mouse 1 ATGACGGTGTCTTACACTCTCCAGTGGCAGAGGCGCGCTTCGGAGCCCTTCTCTGGCCTGCTCTTCCA CTGGAGGGGCAG
human 1 ATGACGGTTTCATACACTCTCAAAGTGGCGGAGGCCCGCTTCGGAGGTTTCTCTGGCCTGCTTCTCCGCTGGAGGGGAAG

mouse 81 CATCTACAAGCTCATGTACACGGAGTTCTCTGCTCTTGTGCACCTTGTCTGCTCGCTCAGCATCACCTACCGGCTGTTCG
human 81 CATCTACAAGCTCTCTACAAGGAATTCTCTCTTGTGGGCGCTTGTACGCTGTGCTTAGCATCACCTACCGGCTGTTCG
                                                                                               •exon 3

mouse 161 TGACCCAGGAGCAGAGACACATTTATGCCAGGTGGCCCGTACTGCAACCGCTCAGCAGAGCTCATCCCTTGTCTCTTT
human 161 TGACCCAGGAGCAGAGCTACGTTGATGCTCAGGTGGCCCGTACTGCAACCGCTCAGCAGAGCTCATCCCTTGTCTCTTT
                                                                                               •exon 4

mouse 241 GTGCTGGGTTTCTACTGTGACTTTGGTGGTGAACCGTTGGTGGTCTCAGTACACAAGCATCCCACTGCCAGACCAGTTAAT
human 241 GTATTGGGTTTCTACTGTGACTCTCGTGGTGAACCGTTGGTGGTCTCAGTACACAAGCATCCCGCTGCCAGACCAGCTGAT

mouse 321 GTGTGTCATCTCAGCCAGTGTGCACGGTGTGAACCAGAGTGGTGTGTTGCTACGC-----GCTATGCCAAC
human 321 GTGCGTCATCTCGCTAGCGTGCACGGCGTGAACCAGCGGGGCGCCTGCTCGCCGCACCCTCATCCGCTACGGGAAC

mouse 388 TGGCATCGGTTTGGTGTACTTCCCTGAGCACCCTGTAACAAGCGCTTCCCCACCATGGAGCATGTGGTGGATGCA
human 401 TGGCGTCCGGTGTGGTGTCTCCCTGAGCACCCTGCTTAAGCGCTTCCCCACCATGGAGCACGTGGTGGACGCA
                                                                                               •exon 5

mouse 468 GGTTCATGTCTCAAGAAGAGAGGAAAAAGTTTGAGAGCTTGAATCTGACTTCAACAAGTACTGGGTCCCTTGGCTTTG
human 481 GGTTCATGTCTCCAGGAAGAGAGGAAAAAGTTTGAGAGCTTGAATCTGACTTCAACAAGTACTGGGTCCCTTGGCTCTG
                                                                                               exon 6•

mouse 548 GTTCACTAACCTGGCCGCCAGGCCCTCAGGGATGGACGAATCCGTGACGACATCGCTCTCTGTCTCACTTGGAAAGGC
human 561 GTTCACTAACCTGGCCGCCAGGCCCTCAGGGATGGACGAATCCGTGACGACATTCGCTCTCTGTCTACTTTTGGAAAGGC
                                                                                               exon 7•

mouse 628 TGAACAAGTATCGGGCCAAGTGCAGCATGCTATTCACTATGACTGGATCAGCTTCCCCCTGGTCTACACCAAGTGGTG
human 641 TGAACAAGTATCGAGCCAAGTGCAGCATGCTATTCACTATGACTGGATCAGCTTCCCCCTCTCTACACCAAGTGGTG

mouse 708 ACCATAGGTGTCTATTCTCTTCAACCCTTTCCCTGATTTGGCCGCCAGTTTGTAGAGCCAGAAACGGGGGCTGAAAACT
human 721 ACCATAGCGCTCTACTCTTTCTTTGCCCTCTCCCTGTGTTGGCCGCCAGTTTGTGAGCCAGAGCCAGGGGCTGCCAAAC

mouse 787 TCAGGAGGCTCTGGGAGCCAGGCAGAGAGCCCTGTCCAGCCCTGTGGACGTGGACATGTTCGTGCCTTCACCACTATG
human 801 TCAGAAGCTTCTTGAAGCCAGGCAGGAGCCAGCCAGCCCTGTGGACCCGGACATGTACGTGCCTTCACCACTCTG

mouse 867 CTGCAGTTTTCCTTTTGGCTGGTGGCTCAAGGTGGCTGAACAGCTCACCAACCCCT-----AGAAATGACGAGGACTT
human 880 CTGCAGTTCTTCTTCTGCTGGCTGGCTCAAGGTGGCTGAACAGATCATCAACCCATTTGGTGGAGATGATGACGACTT
                                                                                               •exon 8

mouse 941 TGAGACCAATCAGCTCATAGACTGACACTTGCAGGTGCTCTGCTCTCTGTGGATGATACATACCAGAACCTGCCCTCCA
human 960 TGAGACCAATCAGCTCATAGACCGCAACTTGCAGGTGCTCTGCTATCCGTGGACGAATGTACCAGAACCTTCCCTCCCG

mouse 1021 CTGAGCAGGATCTGTACTGGGATAAGGCCCAACCTCAGCCACTCTATACGGTGGTGGCCATAGGTGCTTAGAGTCTCTGG
human 1040 CTGAGCAGGACCTGACTGGGATGAGGACCAACCCGAGCCACTTACAC-----TGTGGCCACGGCGGCCGAGTCTCTGGC
                                                                                               •exon 10

mouse 1101 TCCCTTCTTCCCTGGATTCACCTTCAACTTGGC-----
human 1116 GCCCTCAATTCCCTGGCTCCACCTTCAACTTGGCATGAGCGACGACCCCTGAGCAGAGCTGCAGGTGGAGGCGTCCCTCC

mouse
human 1196 GATCTGGTCGGCCCGCCCGCCGCGCAGACCCCGTGTCTCGGCCGCTTCTCTGGCGTAGGGGGCCCTCCCCGGCCATC

mouse
human 1276 AGCCTCCGGAACCTTCGGCCCGTGGCAGGACACCCCGCCCGCCCGCATCTGCTGGCTTCCGGGCGGAGAGGGCGCGCA

mouse
human 1356 CCCCAGGCCCGCAGCCCGCATCGAGGAGGAATCGGCGGAGTCCGGGGACGAGGCCCTGGAGCCCTGA

```

Fig. 25 Pairwise sequence alignment of murine and human *VMD2L2* cDNA sequence

Insertions (green bars) and deletions (red bars) of the predicted murine *Vmd2L2* cDNA result in multiple frameshifts leading to downstream stop codons (red and bold). Black dots indicate the beginning of the respective murine and human exons. On the left, the nucleotide numbering of the cDNA sequence is given.

3.1.1.4 Murine *Vmd2L3*

As for *Vmd2L1* and *Vmd2L2*, the same *in silico* gene identification strategy is applied to identify murine *Vmd2L3*. By BLAT homology searches in the UCSC²³ database, a putative murine genomic sequence homologous to human *VMD2L3* is identified on murine chromosome 10. The novel murine *Vmd2L3* sequence spans from exon two to exon nine and contains a putative start codon ATG in exon two but no stop codon. Refined analysis by BLAST searches in the nr- and murine EST-database of NCBI²⁴ reveals little useful sequence information on murine *Vmd2L3*. A single EST clone (BB652397) representing exon four and two hypothetical proteins (XM_137267 and XM_110904) are identified. Alignment of the hypothetical proteins XM_137267 and XM_110904, the murine and the human *VMD2L3* sequence displays high homology from exon two to exon nine. Beyond exon nine, human and hypothetical sequence homology diverge substantially, suggesting that the predictions of the hypothetical murine sequences are probably incorrect. To obtain the complete exon-intron structure of murine *Vmd2L3*, refined *in silico* and *in vitro* RT PCR and 3'-RACE analyses are further pursued.

By means of BLAT searches of single human *VMD2L3* exons instead of entire protein sequences, putative exon one is identified and confirmed by RT PCR with the primer pair mTU52-F3/mTU52-R1 (Fig. 26). In addition to the expected PCR fragment of 567bp, two further PCR products of 396bp and 304bp are identified (Fig. 26b and 26c). These smaller PCR products probably represent splice variants of murine *Vmd2L3*. Interestingly, alternative splicing has previously been described for human *VMD2L3* (Stöhr et al. 2002). The three PCR products of different fragment lengths (567 bp, 396 bp and 304 bp) are expressed exclusively in heart muscle cDNA. The largest PCR fragment, variant one (var 1), includes the entire sequence from exon one to exon four, while variant two (var 2) contains exon one, a partial sequence of exon two and exon four (Fig. 27). In variant three (var 3), exon one splices to exon four, resulting in the skipping of the coding exons two and three. Translation of the three putative splice variants result in the full-length protein with 367 aa residues (variant one) and two protein sequences truncated by 57 aa (variant two) and 106 aa (variant three). Differential splicing does not change the ORF of the deduced amino acid sequence: from exon four onwards, the sequences of variant one, two and three are identical. No further RT PCR analyses were undertaken to inspect murine *Vmd2L3* for further splicing patterns downstream of exon four.

²³ UCSC: <http://genome.ucsc.edu/index.html?org=Human&db=hg13&hgsid=15995042>

²⁴ NCBI: <http://www.ncbi.nlm.nih.gov/80/>

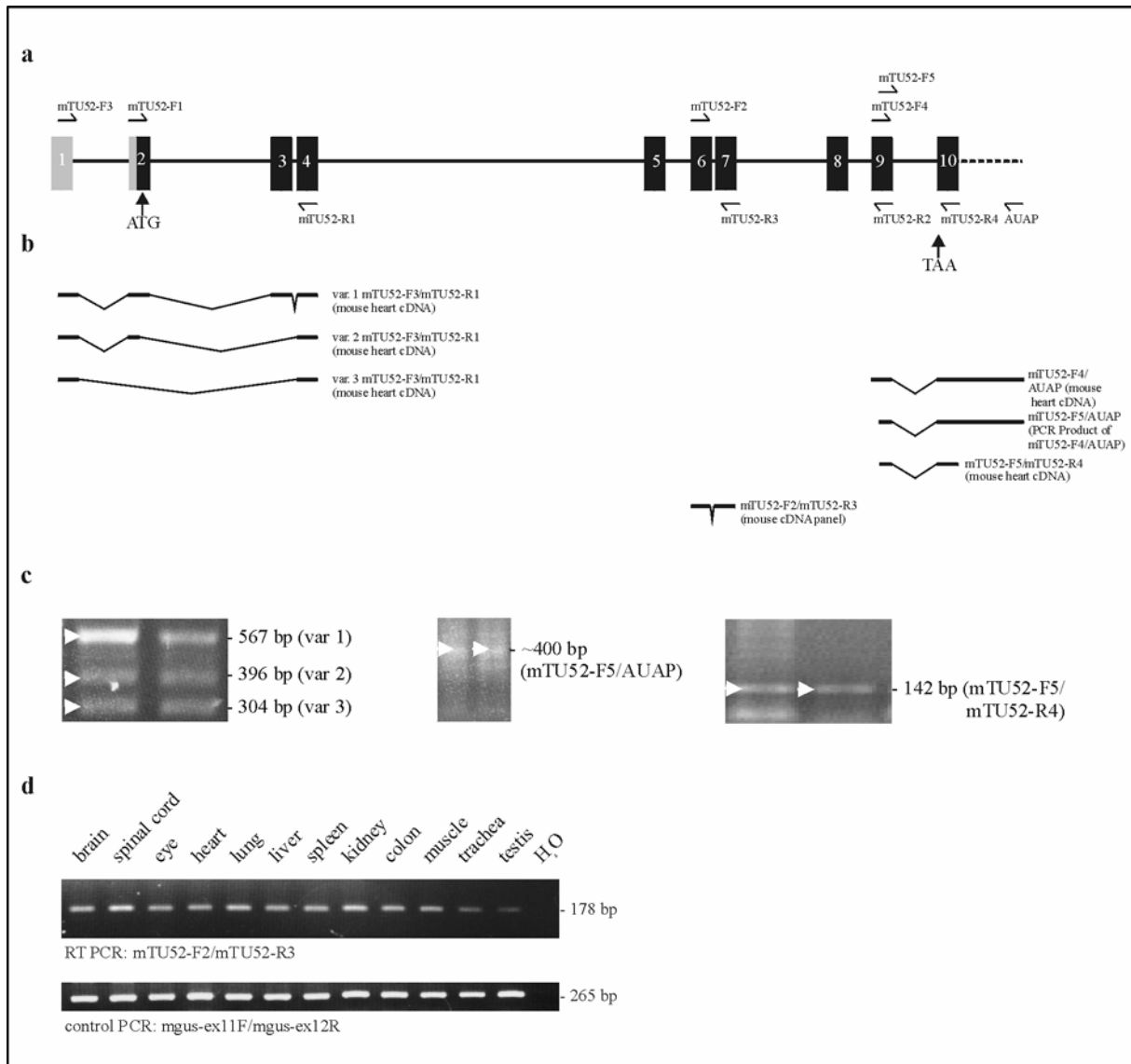


Fig. 26 Genomic organization and expression of murine *Vmd2L3*

(a) In the diagram, equally-sized black and grey boxes represent coding exons and non-coding regions, respectively. Vertical arrows indicate start and stop codon, while horizontal arrows indicated the position of *Vmd2L3*-specific primers. Introns are given to scale. As shown schematically in (b), RT PCR analysis reveals specific amplification with primers mTU52-F3/mTU52-R1, mTU52-F4/AUAP and mTU52-F4/mTU52-R5. (c, left) Three RT PCR products, obtained by amplifying heart muscle cDNA with primers mTU52-F3 and mTU52-R1, correspond to three splice variants of *Vmd2L3*. Var 1 includes exons one, two, three and four, var 2 omits exon two partially and exon three completely and in var 3 exon one is connected to exon four. (c, middle) Exon ten of *Vmd2L3* is identified by means of 3'-RACE using mTU52-F4/AUAP primers and (c, right) is confirmed by RT PCR analysis with mTU52-F4/mTU52-R5. (d) After 33 cycles of amplification, faint PCR products are observed in all 12 murine tissues using primers mTU52-F2 (exon six) and mTU52-R3 (exon seven).

```

•exon 1
var1 gccacagcagcaggagaaactaggaggaaaccagctggtcaccagtgagggtggaagccggcacctcttcagggacggcagatcgttt
var2 gccacagcagcaggagaaactaggaggaaaccagctggtcaccagtgagggtggaagccggcacctcttcagggacggcagatcgttt
var3 gccacagcagcaggagaaactaggaggaaaccagctggtcaccagtgagggtggaagccggcacctcttcagggacggcagatcgttt

•exon 2
var1 gaagatttctcttccttgagagactccaaagaaatagaacaaaaccacccacgatgactgtcacttactccagtaaagtagcaaatg
var2 gaagatttctcttccttgagagactccaaagaaatagaacaaaaccacccacgatgactgtcacttactccagtaaagtagcaaatg
var3 gaagatttctcttccttgagagactccaaagaaatag-----

var1 caacattttttggatttcataggttgccttctcaagtggagaggtagatctacaagctgctgtacaggaatttattgtttttgctgt
var2 caacattttttggatttcataggttgccttctcaagtggagag-----
var3 -----

•exon 3
var1 tctttacacagcaatcagctctggtgtacagattggttaacttacaggagcccaaaaacgttactttgaaaaattatcaatttactgtgac
var2 -----
var3 -----

•exon 4
var1 agatatgctgaacaaattccagtaacctttgtgcttgggttttacgtcactctggttagtgaaccgatggtggaaccagtttgtgaatc
var2 -----gggttttacgtcactctggttagtgaaccgatggtggaaccagtttgtgaatc
var3 -----gggttttacgtcactctggttagtgaaccgatggtggaaccagtttgtgaatc

var1 tgccctggccagacagcgtgatgctcctcatttccagcagtggtccacgggagcgaccagcatggcgctgctcagaaggacgctgat
var2 tgccctggccagacagcgtgatgctcctcatttccagcagtggtccacgggagcgaccagcatggcgctgctcagaaggacgctgat
var3 tgccctggccagacagcgtgatgctcctcatttccagcagtggtccacgggagcgaccagcatggcgctgctcagaaggacgctgat

var1 gcgctacgtcaacctgacgtccctgctcatcttccgctc
var2 gcgctacgtcaacctgacgtccctgctcatcttccgctc
var3 gcgctacgtcaacctgacgtccctgctcatcttccgctc

```

Fig. 27 Alignment of three splice variants identified in murine *Vmd2L3*

Three PCR fragments representing three splice variants of *Vmd2L3* (var1, var2 and var3) are amplified with forward primer mTU52-F3 (underlined sequence in exon one) and reverse primer mTU52-R1 (underlined sequence in exon four) from heart muscle tissue. The putative initiation start codons of variants one, two and three are framed.

Exon ten of murine *Vmd2L3* could not be identified by computer-assisted database searches. Therefore, 3'-RACE experiments are conducted to establish the *Vmd2L3* gene sequence beyond exon nine. A novel murine exon ten sequence is identified with primer pairs mTU52-F4/AUAP and mTU52-F5/AUAP, containing a stop codon at position +2 to +4 in the exon (Fig. 26c). Thereafter, the novel exon ten is independently confirmed with primers mTU52-F5/mTU52-R4 (Fig. 26c). Based on the 3'-RACE and RT PCR data, the final exon of murine *Vmd2L3* consists of four coding nucleotides. The translated hypothetical coding sequence results in a protein which is 32 amino acids shorter than its human counterpart (Fig. 28).

RT PCR analysis of murine *Vmd2L3* is performed to determine the expression profile in 12 different murine tissues. Interestingly, no amplicons are observed after 25 cycles of amplification (semi-quantitative method), while faint amplicon signals are observed in all reaction tubes after 33 amplification cycles. Therefore, it seems that *Vmd2L3* is expressed weakly in all tissues. Alternatively, the weak bands may represent a background noise that is generated by constitutive expression and that does not reflect the *Vmd2L3* expression status in

the respective tissues. Consequently, *Vmd2L3* may be expressed in murine tissues not included in this panel or in a time-dependent manner, for example during embryogenesis. To further elucidate this issue, a more sensitive method to study the expression of genes, in particular low abundant genes, is applied (real time quantitative RT PCR, see Results 3.3).

As shown in Table 7, all intron/exon boundaries conform to the GT/AT rule with acceptor and donor splice scores lying in the expected range between 0 - 20 and 0 - 11, respectively.

Table 7 Exon sizes, intron sizes and splice sites of murine *Vmd2L3*

Exon		3'-Acceptor Splice Site ^a		5'-Donor Splice Site ^a		Intron	
No.	Size (bp)	Sequence	Score ^b	Sequence	Score ^b	No.	Size (bp)
1 ^c				TAG gttagt	4.2	1	1811
2	168	cttcttgctcttct ag A	10.7	CAG gtacct	4.7	2	3725
3	95	tttatttttgctcc ag A	10.1	TTG gtaagt	2.8	3	461
4	234	ctggttatccaac ag G	12.8	CAG gtacgg	2.7	4	9222
5	155	gttattttgtatga ag G	14.4	ACT gtaagt	3.9	5	1210
6	78	tctgttttgggctt ag G	14.0	CAG gtatcg	6.0	6	418
7	153	cttctctctgtccc ag G	8.7	AAG gtaggc	3.0	7	3054
8	81	gtgttctcacctgc ag G	9.8	CAG gtgaga	1.1	8	1221
9	152	cgaccaacgattcc ag G	9.7	GGG gtaagc	3.1	9	1387
10 ^c	4	gtgagcttgctttt ag G	7.2				

^a Exonic and intronic sequences are given in upper and lower case letters, respectively.

^b Score of perfect consensus = 0; worst score for acceptors: 42.5 (99 %: 0-20), for donors: 31.1 (99 %: 0-11) (Berg and von Hippel 1988; Penotti 1991). For calculations, an Excel[®]-based spreadsheet is used (Sauer, 2001).

^c Exon size calculations in exon one and ten excludes the 5'-UTR and 3'-UTR, respectively.

Comparison of the adjacent sequence of initiation codon ATG in exon two (CCCACGATGA) with the Kozak consensus sequence (GCC(A/G)CCATGG) yields sequence differences at positions -6, -1 and +4 (Kozak 1991; Kozak et al. 1996). Nevertheless, the high sequence similarity to human *VMD2L3*, the presence of an upstream in-frame stop codon in exon one and the fact that no alternative start codon is located within a better Kozak context, the ATG codon in exon two is most likely used as initiation start site for translation. As mentioned, the ATG-containing exon two is skipped completely in splice variant two of murine *Vmd2L3*, therefore requiring an alternative ATG. An alternative start codon ATG is located in exon four and is embedded within an acceptable Kozak consensus sequence (CCCACGATGA). This alternative ATG would be in-frame to the coding sequence of murine *Vmd2L3*. Another ATG codon 43 bp upstream of the putative start codon is ruled out as initiation start site, because it is located in a different reading frame resulting in an unknown amino acid sequence of 75 residues. The complete coding sequence (1104 bp) and putative protein product (368 residues) of murine *Vmd2L3* is illustrated in Fig. 28.


```

•exon 1
-147 GGATCGCCACAGCAGCAGGAGAACTAGGAGGAAACCCAGCTGGTCACCAGTGAGGGTGGAAAGCCGGCACCTCTTCAGGGACGGCAGATCG

•exon 2
-57 TTTGAAGATTCTCTCCCTTGAGAGACTCCAAAGAAATAGAACAAAACCCACCGATGACTGTCACTTACTCCAGTAAAGTAGCAAAT
M T V T Y S S K V A N 11
+1

34 GCAACATTTTTGGATTTCATAGGTTGCTTCTCAAGTGGAGAGGTAGTATCTACAAGCTGCTGTACAGGGAATTTATTGTTTTGCTGTT
A T F F G F H R L L L K W R G S I Y K L L Y R E F I V F A V 41

•exon 3
124 CTTTACACAGCAATCAGTCTGGGTACAGATTGTTACTTACAGGAGCCCAAAAACGTTACTTTGAAAAATATCAATTTACTGTGACAGA
L Y T A I S L V Y R L L L T G A Q K R Y F E K L S I Y C D R 71

•exon 4
214 TATGCTGAACAAATCCAGTAACTTTGTGCTTGGGTTTTACGTCACTCTGGTAGTGAACCGATGGTGGAAACAGTTTGTGAATCTGCCT
Y A E Q I P V T F V L G F Y V T L V V N R W W N Q F V N L P 101

304 TGGCCAGACAGGCTGATGCTCCTCATTCCAGCAGTGTCCACGGGAGCGACCAGCATGGGCGCCTGCTCAGAAGGACGCTGATGCGCTAC
W P D R L M L L I S S S V H G S D Q H G R L L R R T L M R Y 131

•exon 5
394 GTCAACCTGACGTCCTGCTCATCTTCCGCTCGGTGAGCACCGCGGTGTACAAGAGTTTCCACCATGGACCAGTGGTTCGAAGCAGGT
V N L T S L L I F R S V S T A V Y K R F P T M D H V V E A G 161

484 TTTATGACGGCAGATGAGAGGAAATATTTCGACCACCTCAAATCGCCTCATCTGAAGTACTGGGTTCCCTTCATTTGGTTTGGAAATCTT
F M T A D E R K L F D H L K S P H L K Y W V P F I W F G N L 191

•exon 6
574 GCAACCAAAGCCCGGAATGAAGGCAGAATCAGAGACAGCGTTGATCTACAATCACTGATGACTGAAATGAATCGGTACCGCTCTTGGTGC
A T K A R N E G R I R D S V D L Q S L M T E M N R Y R S W C 221

•exon 7
664 AGCCTCTTATTTGGTTACGACTGGGTTGGCATTCCGCTGGTTTACACACAGGTCGTCACCCTCGCGTCTACACGTTCTTCTTTCGCTGC
S L L F G Y D W V G I P L V Y T Q V V T L A V Y T F F F A C 251

754 CTGATCGGAAGGCAGTTCCTGGATCCCACCAAAGGCTACGTAGGACATGACTTGGATCTGTACGTTCCCATCTTCACTCTCCTCCAGTTC
L I G R Q F L D P T K G Y V G H D L D L Y V P I F T L L Q F 281

•exon 8
844 TTCTTCTACGCAGGATGGCTCAAGGTTGCAGAGCAGCTGATCAACCCTTTCGGGAAGATGACGATGACTTTGAAACAAACTGGTGCATT
F F Y A G W L K V A E Q L I N P F G E D D D D F E T N W C I 311

•exon 9
934 GACAGAAACCTGCAGGTCTCTCTCTTGGCTGTGGATGAAATGCATATGAGTTTGCCCAAGATGAAGAAGGACATTTACTGGGACGATTCT
D R N L Q V S L L A V D E M H M S L P K M K K D I Y W D D S 341

•exon 10
1024 GCTGCCCGGCCACCGTACACACTGGCGGCTGCCGACTACTGCATACCGTCTTTCTGGGCTCAACGATCCAAATGGGCATAA
A A R P P Y T L A A A D Y C I P S F L G S T I Q M G # 368

```

Fig. 28 cDNA and protein sequence of murine *Vmd2L3*

The nucleotide numbering of *Vmd2L3* cDNA sequence (beginning with +1 = A of ATG) is given on the left; the numbering of the translated protein sequence on the right. A black dot indicates the position of the respective exon-intron boundary, while the putative start (ATG) codon, the upstream stop (TAG) codon and the stop codon of the gene are framed.

The murine *Vmd2L3* gene is structured in ten exons and nine introns spanning a genomic region of approximately 24 kb (Fig. 29). In comparison to human *VMD2*, murine *Vmd2* displays a similar genomic organization from exon one to exon nine. In both murine and human *VMD2L3*, large intervals are found between exons two and three, exons four and five as well as exons seven and eight, and short intervals below 500 bp are found in IVS3 and IVS6. A marked difference between murine and human *Vmd2L3* is displayed by the localization of human and mouse exon ten. Human exon ten is separated from exon nine by a large intervening sequence of 27.7 kb, while putative murine exon ten is located 1.4 kb downstream of exon nine.

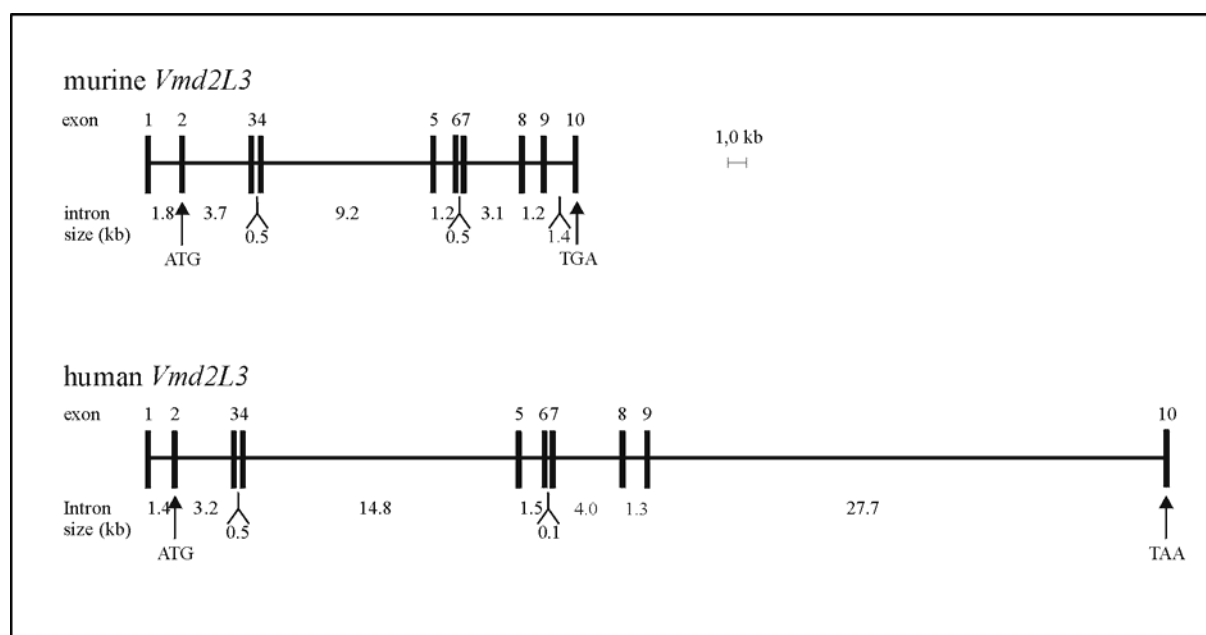


Fig. 29 Comparison between the genomic organization of murine *Vmd2L3* and human *VMD2L3*

With IVS9 as exception, the nucleotide distances between the respective exons (black vertical bars) are similar in mouse and human. For example, exons three and four are separated by a large intervening sequence of 9.2 kb and 14.8 kb in mouse and human, respectively.

3.2 *IN SILICO* CHARACTERIZATION OF THE MURINE RFP-TM PROTEIN FAMILY

To provide further evidence that the above genes are indeed the orthologues to human *VMD2* and *VMD2L1*, *VMD2L2* and *VMD2L3*, numerous bioinformatic tools such as syntenic grouping, multiple sequence alignment, calculation of sequence identity, transmembrane domain prediction and the compilation of a phylogenetic tree are applied.

3.2.1 Syntenic grouping

Despite the fact that mouse and human are separated by approximately 75 million years of evolution (Waterston et al. 2002), murine and human genes often fall into homologous chromosomal regions that share a conserved gene order (synteny). For *VMD2/Vmd2*, the human-mouse homology map from NCBI²⁵ is analyzed to determine the conserved syntenic regions in which the respective genes are located (Fig. 30a). Identical orders of genes are found on the upstream (*DDB1-CD5-FEN1-FADS2-FADS3*) and downstream (*FTH-ROM1-AHNAK*) side of *VMD2* on human chromosome 11 and murine chromosome 19.

²⁵ human-mouse homology map: <http://www.ncbi.nlm.nih.gov/Homology/>

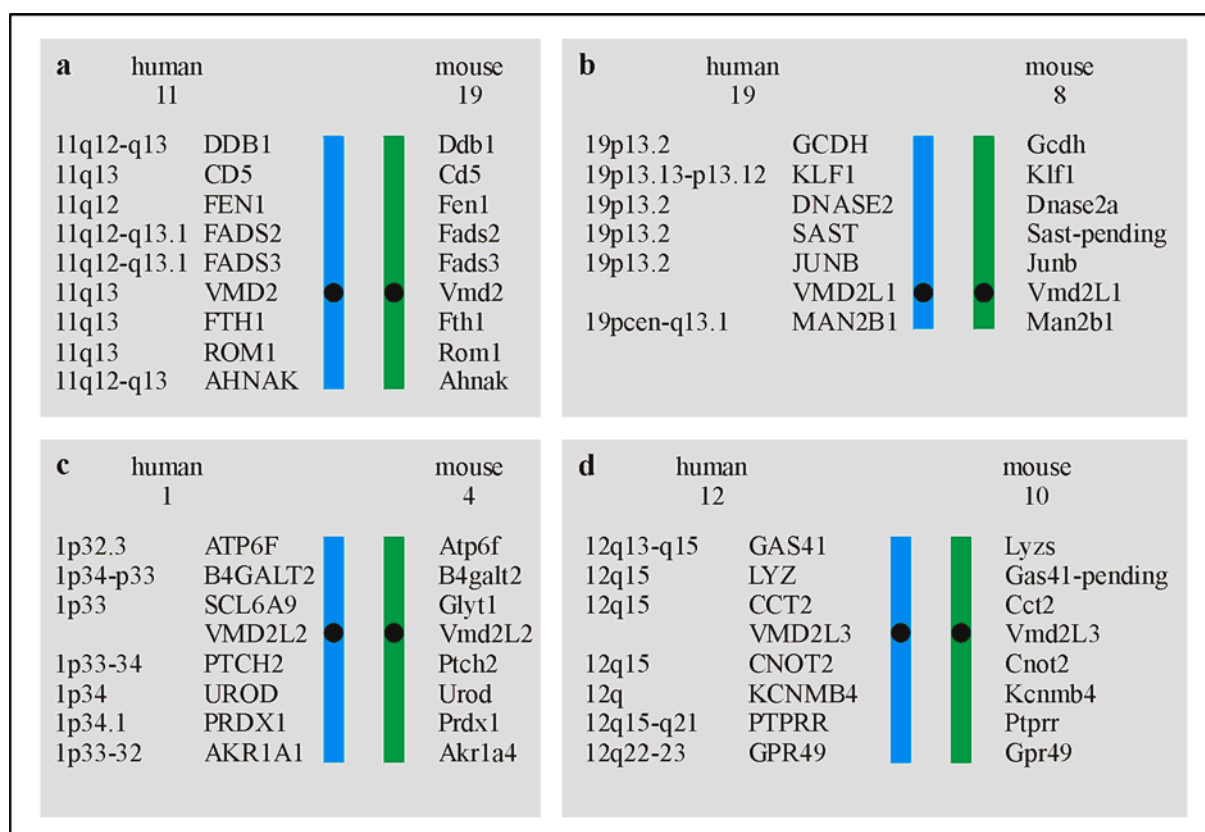


Fig. 30 Conservation of gene order in the human and mouse genome

The mouse *Vmd2* and the human *VMD2* genes (a), the mouse *Vmd2L1* and the human *VMD2L1* genes (b), the mouse *Vmd2L2* and the human *VMD2L2* genes (c) and the mouse *Vmd2L3* and the human *VMD2L3* genes (d) lie within conserved syntenic blocks of genes on the respective chromosomes. Please note that according to BLAT gene assembly the gene order of *GAS41* and *LYZ* is inverted in human and mouse.

In a similar way murine genes flanking the novel genes *Vmd2L1*, *Vmd2L2* and *Vmd2L3* are identified by using GeneView²⁶ and BLAT²⁷ search analysis. Human genes on either side of *VMD2L1*, *VMD2L2* and *VMD2L3* are found by BLAT search analysis. A conserved order of genes is found for *VMD2L1* on human chromosome 19 versus murine chromosome eight, for *VMD2L2* on human chromosome one versus murine chromosome four and for *VMD2L3* on human chromosome 12 versus murine chromosome 10 (Fig. 30b, 30c and 30d). In conclusion, comparison of syntenic groups in human and mouse further confirms that the orthologous genes of the human *VMD2* RFP-TM family are identified in mouse.

3.2.2 Multiple sequence alignment and analysis of transmembrane domains

Because the structure of a protein is critical for its function, structural motifs are often highly conserved across species. In the case of the *VMD2* RFP-TM protein family, it was interesting to compare the putative transmembrane domains between human and murine

²⁶ GeneView: http://www.ensembl.org/Mus_musculus/

²⁷ UCSC: <http://genome.ucsc.edu/index.html?org=Human&db=hg13&hgsid=15995042>

protein sequences. *Vmd2L2* is excluded from this analysis as no ORF could be predicted for the murine gene. First, the putative ORFs of murine *Vmd2*, *Vmd2L1* and *Vmd2L3* are aligned to human *VMD2*, *VMD2L1* and *VMD2L3* using T-Coffee²⁸ and BOXSHADE²⁹. As shown in Fig. 31, human and murine proteins display a high sequence homology from amino acid residue one to 367 (residue one to 368 for murine *Vmd2L1* and human *VMD2L1*) encoded by exons two to nine. Within this protein region, a sequence identity of 82 % is calculated between human and mouse *Vmd2*, 95 % between human and mouse *Vmd2L1* and 98 % between human and mouse *Vmd2L3*. Beyond exon nine, the sequence similarities decrease significantly for protein pairs *VMD2/Vmd2*, *VMD2L1/Vmd2L1* and *VMD2L3/Vmd2L3*.

Three TM domain prediction programs (DAS³⁰, TMpred³¹ and HMMTOP³²), based on different algorithms, are applied to identify putative membrane-spanning regions. Those hypothetical TM sequences predicted by all three programs are designated as consensus TM domains (Fig. 31). The typical features of the human *VMD2* RFP-TM family, i.e. four TM domains and an invariant RFP sequence within the 370 amino acid sequence of the protein, are identified in the murine proteins *Vmd2*, *Vmd2L1* and *Vmd2L3*. In addition to the four highly conserved TM domains identified in all *Vmd2* family members, human and murine *Vmd2L1* possess two further potential transmembrane domains (pTM2a and pTM2b) localized between TM2 and TM3. Interestingly, one of these potential TM domains (pTM2b) is potentially also present in murine *Vmd2* but not in the human orthologue.

²⁸ T-Coffee: <http://www.ch.embnet.org/software/TCoffee.html>

²⁹ BOXSHADE: http://www.ch.embnet.org/software/BOX_form.html

³⁰ DAS: <http://www.sbc.su.se/~miklos/DAS/>

³¹ http://www.ch.embnet.org/software/TMPRED_form.html

³² <http://www.enzim.hu/hmmtop/index.html>

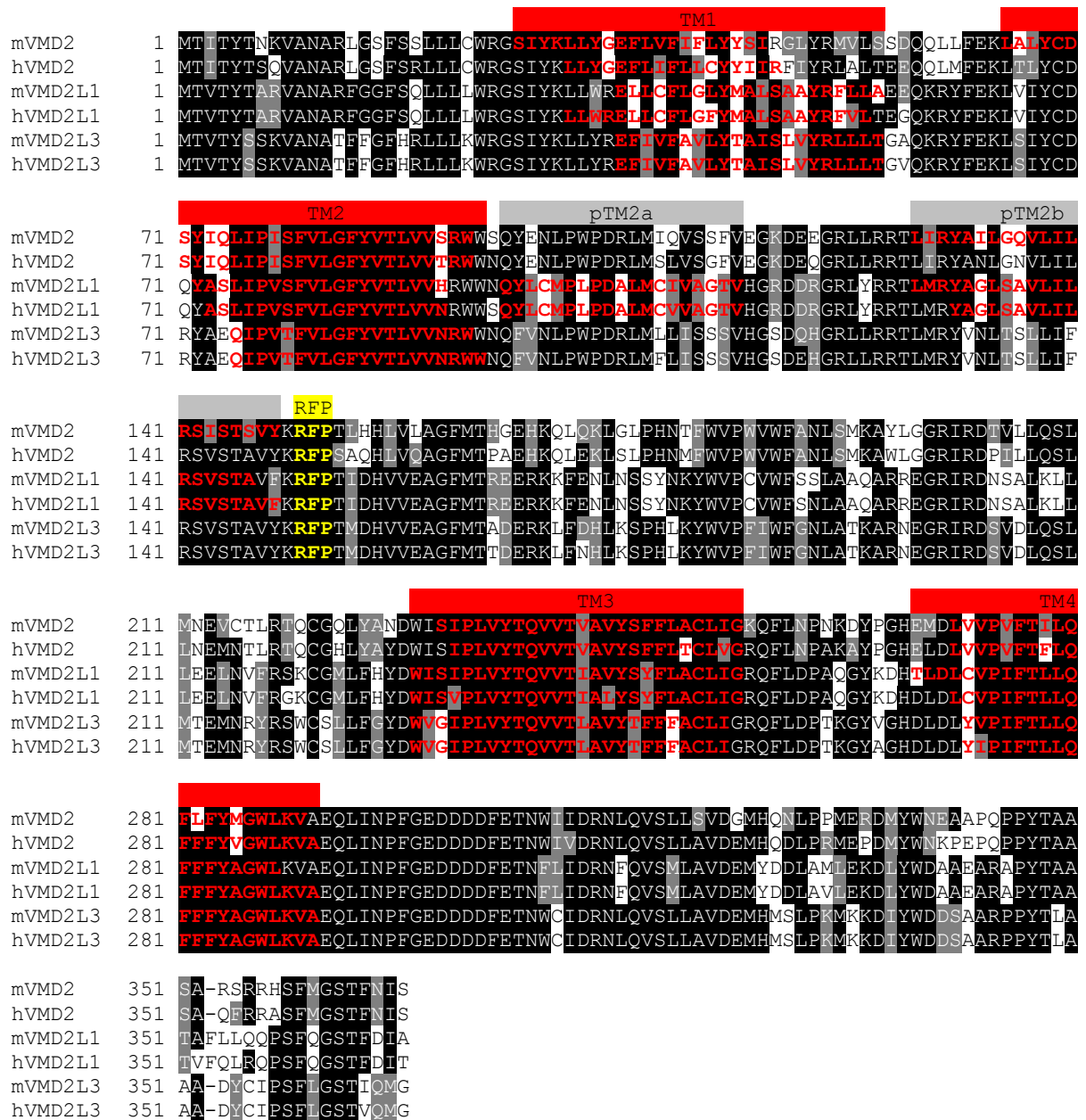


Fig. 31 Multiple sequence alignment of the human and murine Vmd2 RFP-TM protein family

Characteristic motifs of the RFP-TM protein family, encoded by exons two to nine, are indicated by red bars (putative TM domains) and a yellow bar (invariant RFP peptide sequence) as published by Stöhr et al. (2002). Consensus TM domains predicted by multiple programs are shown in red and bold. According to the TM domain predictions, novel TM domains (pTM2a and pTM2b) are identified for murine Vmd2, human VMD2L1 and murine Vmd2L1 (grey bars). Identical amino acid residues are shaded in black and residues with similar chemical property and/or structure are shaded in grey.

3.2.3 Phylogenetic tree

Based on cDNA sequences of murine and human VMD2 RFP-TM family members, a phylogenetic tree is constructed with the bioinformatic programs ClustalW³³ and Phylodendron³⁴. In an unrooted phenogram, the phylogenetic relationship between the orthologous and paralogous genes of the VMD2 RFP-TM family is illustrated (Fig. 32). In all cases, orthologous genes (e.g. human *VMD2* and murine *Vmd2*, etc.) are grouped pairwise together and similar evolutionary distances are observed for the paralogous pairs of genes. Furthermore, the phylogeny suggests that the paralogous genes *VMD2L1/Vmd2L1* and *VMD2L2/Vmd2L2* are related closer to one another than to *VMD2/Vmd2* or *VMD2L3/Vmd3L3*.

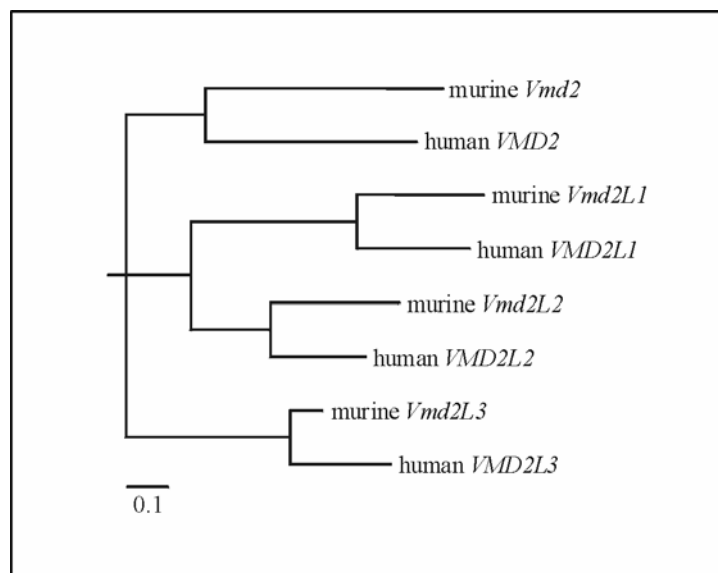


Fig. 32 Phenogram of the murine and human VMD2 RFP-TM family

Paralogous and orthologous cDNAs of the human and murine VMD2 RFP-TM family are subjected to ClustalW. The Phylip output is then used to generate a phylogenetic tree with the program Phylodendron.

3.3 EXPRESSION PROFILE OF MURINE *VMD2*, *VMD2L1* AND *VMD2L3* BY REAL-TIME QUANTITATIVE REVERSE TRANSCRIPTASE POLYMERASE CHAIN REACTION (QRT PCR)

Real-time quantitative reverse transcriptase (qRT) PCR is the most sensitive technique to quantify gene expression, in particular for low abundant genes (Klein et al. 2002; Liu and Saint 2002). In comparison to the classical RT PCR, real-time assays display higher sensitivity with reliable specificity, good reproducibility as well as less labour-intensity at a high-throughput scale. A SYBR green fluorescent reporter system directly measures the amount of product in the reaction tube during each amplification cycle. Similarly to ethidium bromide staining of dsDNA in agarose gels, SYBR green fluoresces weakly in an unbound state, but emits strong fluorescence signals when incorporated into the minor groove of

³³ ClustalW: <http://www.ebi.ac.uk/clustalw/index.html>

³⁴ Phylodendron: <http://iubio.bio.indiana.edu/treeapp/treeprint-form.html>

dsDNA. A further advantage is that quantification is carried out at the beginning of the linear-log phase of amplification, which is the most stable and efficient segment of amplification. The threshold cycle C_t is defined as the cycle of amplification at which fluorescence rises significantly above background levels. It inversely correlates to the initial amount of target template i.e. mRNA copies. Low C_t values represent an early onset of PCR amplification and higher template concentrations and vice versa, high C_t values represent a late onset of amplification associated with low template concentrations.

The real time qRT PCR protocol consists of two parts. In the first step a regular PCR amplification is performed in which SYBR green is incorporated into dsDNA. In the second step, i.e. after the final PCR elongation step at 72°C, the PCR products are melted by gradually increasing the temperature from 50° to 99°C. Dissociation or melting curves are generated to discriminate between the specific PCR product and undesired by-products or the formation of primer dimers.

Due to distinct PCR amplification kinetics, the accurate evaluation and comparison of C_t values to determine the initial amount of template is only possible if PCR amplification efficiencies lie within similar ranges (Liu and Saint 2002). The amplification efficiency value E lies in the range between one and two, with $E = 1$ being the minimum value and $E = 2$ the maximum and optimum value (Pfaffl et al. 2002).

For control experiments, real time qRT PCR requires endogenous genes such as glyceraldehyde-3-phosphate dehydrogenase (*GAPDH*), β -glucuronidase (*β -GUS*) or succinate dehydrogenase complex subunit A (*SDHA*). Such ubiquitously expressed genes are used to normalize the template in the PCR reaction (Vandesompele et al. 2002). Ideally, endogenous house-keeping genes should reflect the overall mRNA population of the tissue or cells of interest, and therefore the expression levels of these genes should be constant and not influenced by the experimental setup. This enables the calculation of the relative expression levels of the target gene, the normalized gene expression (NE). The mean normalized gene expression (MNE) averages several independently calculated normalized expression values. For calculating the NE and MNE, the software program Q-Gene (equation two) is applied (Muller et al. 2002).

Here, the expression profile of murine *Vmd2*, *Vmd2L1* and *Vmd2L3*, normalized to a house-keeping gene, is determined via real time qRT PCR. Due to the finding that *Vmd2L2* is possibly a pseudogene, it is excluded from the expression study (see Results 3.1.1.3). Murine succinate dehydrogenase complex subunit A (*Sdha*, XM_127445) and murine β -glucuronidase (*β -Gus*, NM_010368) are selected as reference genes for normalization. A panel of 12 cDNAs (1. brain, 2. spinal cord, 3. whole eye without vitreous body, 4. heart, 5. lung, 6. liver, 7. spleen, 8. kidney, 9. colon, 10. skeletal muscle, 11. trachea and 12. testis) deriving from a male mouse (*Mus musculus domesticus*, BL/6) are analyzed in the following real time qRT PCRs. Prior to the actual expression studies, a series of pre-experiments include the design of appropriate primers as well as several tests to obtain best conditions for highest efficiency values and specific amplification.

Software from MGB EclipseTM probe system (Amersham-Parmacia-Biotech) is used to design oligonucleotide primers to amplify the target genes *Vmd2*, *Vmd2L1* and *Vmd2L3* as well as the control genes *β -Gus* and *Sdha*. Special requirements for qRT PCR include that the resulting PCR product should not exceed 150bp and that one primer should overspan an exon-exon boundary to avoid the amplification of genomic templates. Moreover, all oligonucleotide primer pairs are located in the 3'-region of the gene. While primer pairs of *Vmd2*, *β -Gus* and *Sdha* are located in the final two exons of the respective genes, primer pairs of *Vmd2L1* are located in exons eight and nine and those of *Vmd2L3* are located in exons seven and eight.

The PCR efficiency value E is determined for the murine house-keeping genes *β -Gus* and *Sdha* using testis cDNA and a mixture of muscle, trachea and testis cDNA. In a series of five-fold dilutions (1:1, 1:5, 1:25, 1:125 and 1:625) of the cDNA, an optimal efficiency value E is determined for *β -Gus* ($E_{\beta\text{-Gus}}=1.995$). However, the calculated efficiency value of *Sdha* is too low ($E_{Sdha}=1.6721$) and therefore *Sdha* is excluded from further analysis. Similarly, the PCR efficiency value E is determined for the murine genes *Vmd2* (testis cDNA), *Vmd2L1* (mixture of eye and colon cDNA) and *Vmd2L3* (mixture of muscle, trachea and testis cDNA). SYBR green incorporation is monitored in a series of five-fold dilutions of the respective cDNAs, amplifying with primers mVMD2-RT-F1/-R1, mTU51-RT-F1/-R1 and mTU52-RT-F1/-R1 the murine genes *Vmd2*, *Vmd2L1* and *Vmd2L3*. High PCR efficiency values are determined for *Vmd2* ($E_{mVmd2}=1.99$) and *Vmd2L1* ($E_{mVmd2L1}=2.00$) and a lower efficiency value is calculated for murine *Vmd2L3* ($E_{mVmd2L3}=1.88$).

To demonstrate specific PCR amplification, a post-PCR gradual temperature increase from 50°C to 99°C is performed. The resulting heat dissociation plots of all five genes display distinct peaks, indicating that each gene is specifically amplified (Fig. 33). The heat dissociation peaks of the reference genes *β-Gus* (82.8°C) and *Sdha* (79.5°C), as well as those of the genes of interest *Vmd2* (82.6°C), *Vmd2L1* (81.5°C) and *Vmd2L3* (80.4°C) are distinct and are clearly distinguishable from the dimer signals at lower melting temperatures (approximately between 70°C and 80°C). The melt curves display no additional dissociation peaks, demonstrating that no unspecific products are amplified. To circumvent the measurement of SYBR green fluorescence signals generated by dimer formation, data acquisition of the subsequent real time qRT PCRs is performed at higher temperatures (Table 8). Furthermore, in Table 8 the conditions of the real time qRT PCR experiments as well as the temperature of data acquisition, the threshold values and the efficiency values are summarized. The threshold values of fluorescence intensity to determine the Ct value of each expressed gene in each tissue is generated by the program RotorGene 4.6 (Corbett Research).

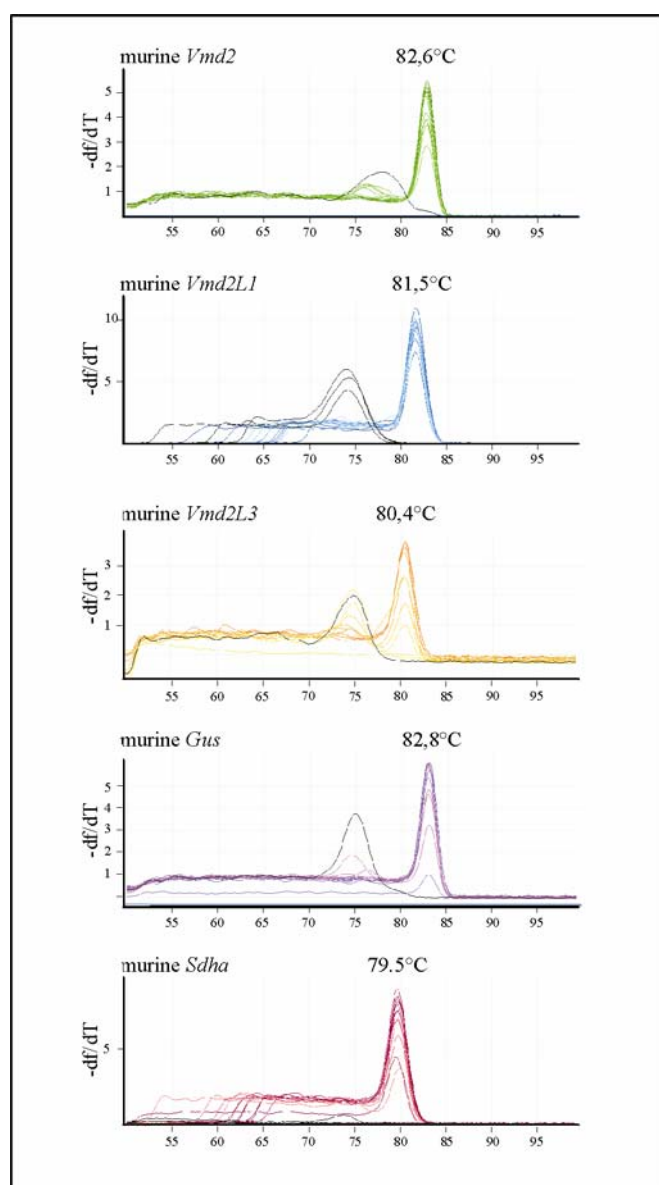


Fig. 33 Heat dissociation plot following the final PCR cycle

Melting curves generated by a stepwise temperature increase of the final PCR products are converted into melting peaks by taking the negative derivative of fluorescence with respect to temperature. Distinct peaks of the murine *Vmd2* (green), *Vmd2L1* (blue), *Vmd2L3* (yellow), β -*Gus* (purple) and *Sdha* (red) amplicons demonstrate that specific amplification takes place in the PCR reaction. Primer dimer formation is only seen in control amplicons without template DNA (black lines). A mix of cDNA's from muscle, trachea and testis tissue is used to amplify *Sdha* and *Vmd2L3*. cDNA extracted from eye and colon is used as template to amplify *mVmd2L1* and testis cDNA is the template for amplifying *Vmd2* and β -*Gus*.

Table 8 Real time qRT PCR conditions

murine gene	primer pair	PCR annealing temperature (°C)	PCR fragment size (bp)	RT PCR ^a temperature of data acquisition (°C)	RT PCR threshold	RT PCR Efficiency
<i>β-Gus</i>	β -Gus-RT-F1/R1	56	108	72; 79; 80	0.01	1.99
<i>Sdha</i>	m <i>Sdha</i> -RT-F1/R1	56	68	72; 80	0.1	1.67
<i>Vmd2</i>	m <i>Vmd2</i> -RT-F1/R1	56	111	72; 79; 80	0.1	1.99
<i>Vmd2L1</i>	mTU51-RT-F1/R1	56	89	72; 78	0.1	2.00
<i>Vmd2L3</i>	mTU52-RT-F1/R1	56	64	72; 77; 80	0.025	1.88

For the reference genes β -*Gus* and *Sdha*, real time qRT PCR yields similar but subtle differences in expression in the panel of 12 murine tissues. In comparison, the less sensitive, conventional RT PCR analysis demonstrates equal expression levels in all 12 tissues (Fig. 34).

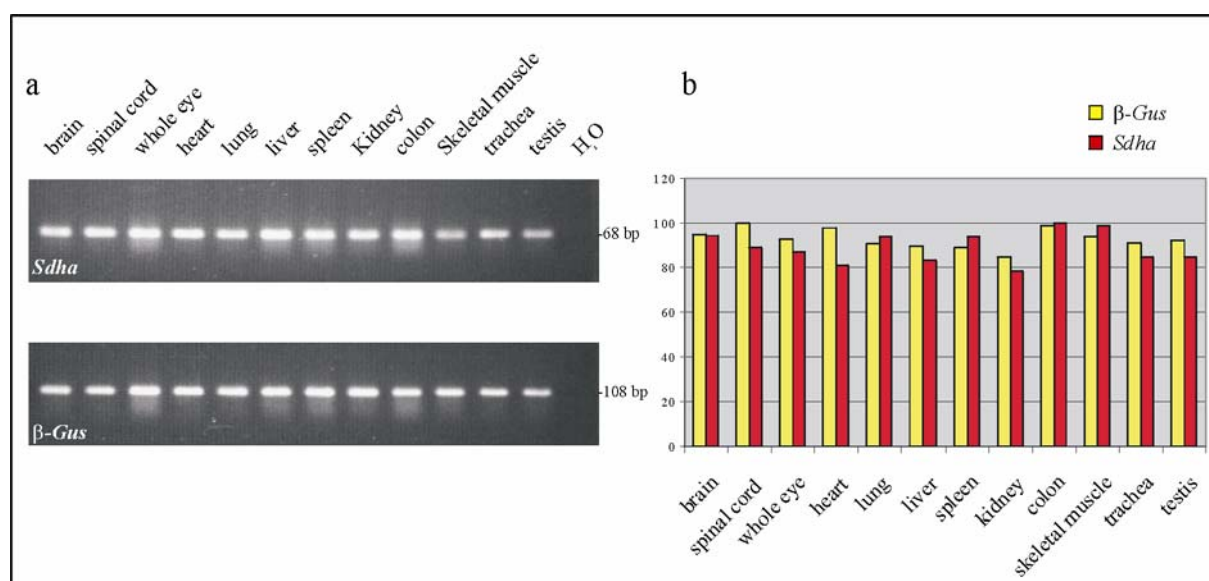


Fig. 34 RT PCR versus real time qRT PCR

Quantitative expression of the murine house-keeping genes β -*Gus* and *Sdha* is analyzed by RT PCR (a) and real time qRT PCR (b) in a panel of 12 mouse tissues. In (b), the expression of β -*Gus* (yellow) and *Sdha* (red) is given in percentage by relating the Ct values of β -*Gus* and *Sdha* to the Ct_{max} values of β -*Gus* (spinal cord) and *Sdha* (colon). The tissues termed ‘whole eye’ includes all tissues of the murine eye except the vitreous body.

For the target genes, unequivocal differences of *Vmd2*, *Vmd2L1* and *Vmd2L3* expression levels are found in the murine cDNA panel by real time qRT PCR. Because of the low amplification efficiency of the reference gene *Sdha*, the target genes are exclusively normalized to the reference gene β -*Gus*. The E values of the target genes and β -*Gus* lie within an accepted range (1.87 and 2.00), meaning that the amplification efficiencies are similar in the exponential phase. Therefore it would have been possible to directly compare the Ct values by using the broadly adopted comparative $\Delta\Delta Ct$ method. However, more exact expression data are generated by using equation two of the software program Q-Gene (Muller et al. 2002), which takes the respective E values into account. A tabular and graphical representation of the MNE of *Vmd2*, *Vmd2L1* and *Vmd2L3* is given in Table 9 and Fig. 35.

Table 9 MNE of murine *Vmd2*, *Vmd2L1* and *Vmd2L3*

tissue	MNE of m <i>Vmd2</i>	MNE of m <i>Vmd2L1</i>	MNE of m <i>Vmd2L3</i>
brain	0.0828	0.0025	0.0021
spinal cord	4.6112	0.0066	0.0009
eye	0.1144	0.0300	0.0001
heart	0.0057	0.0033	0.0043
lung	0.0632	0.0021	0.0025
liver	0.0013	0.0001	-
spleen	0.0049	0.0011	0.0002
kidney	0.0157	0.0003	0.0010
colon	0.0310	0.2879	-
skeletal muscle	0.0076	-	0.1068
trachea	0.0430	0.0121	0.0081
testis	43.1975	0.0002	0.0189

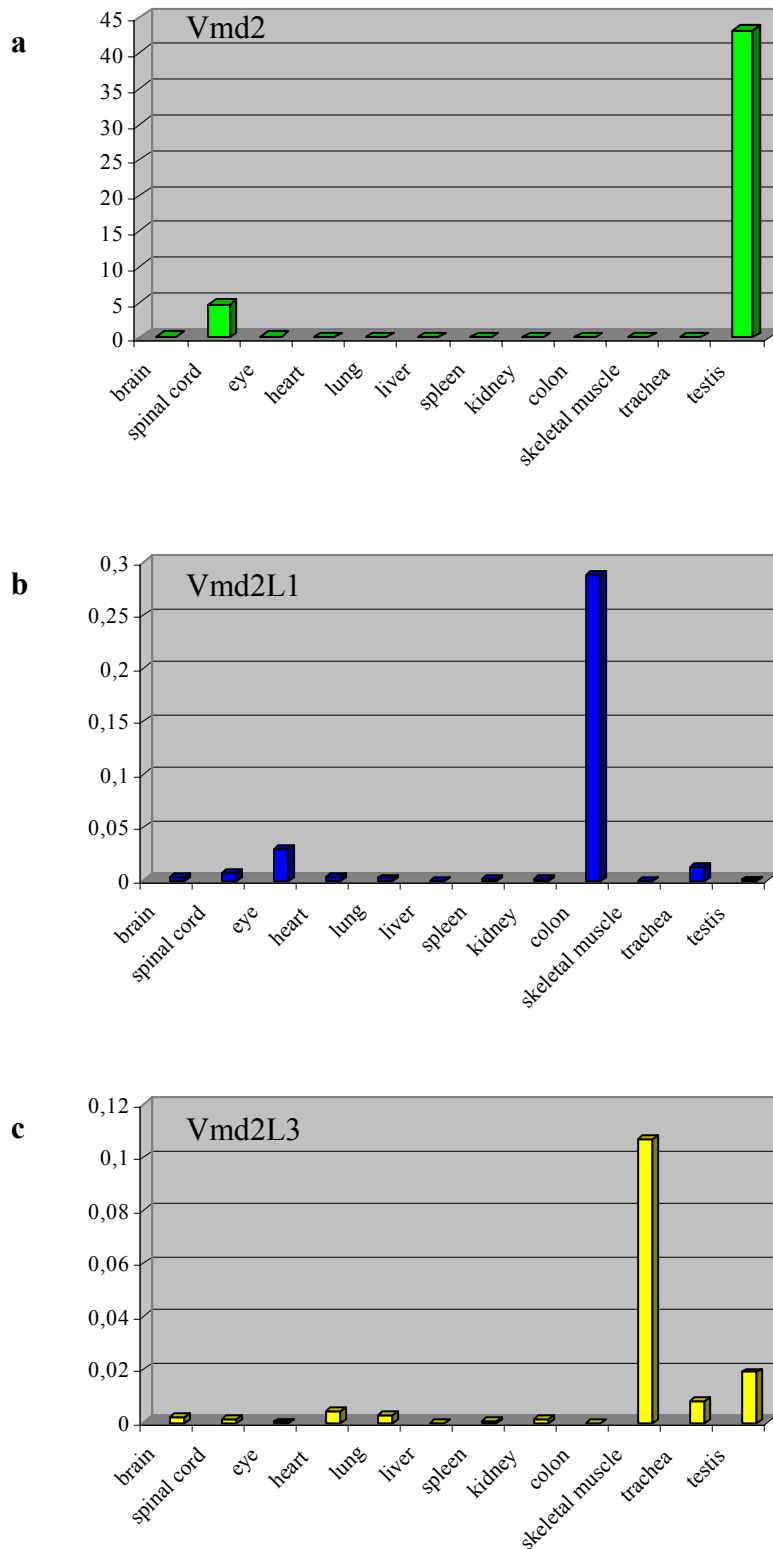


Fig. 35 Mean normalization expression (MNE) profile of murine *Vmd2*, *Vmd2L1* and *Vmd2L3* in a panel of 12 murine tissues

In this graphical representation, the acquired Ct values of murine *Vmd2* (green, a), *Vmd2L1* (blue, b) and *Vmd2L3* (yellow, c) are normalized to the Ct values of β -Gus (Q-Gene program). The graphs demonstrates a 43.2-fold (testis), 4.6-fold (spinal cord) and 0.1-fold (whole eye without vitreous) increase of murine *Vmd2* expression (a), a 0.28-fold increase of murine *Vmd2L1* expression in colon tissue (b) and a 0.1-fold increase of murine *Vmd2L3* expression in muscle. Please note, that the scale of the y-axis is different in the three graphs.

Highest MNE levels of *Vmd2* are detected in testis tissue (43.2-fold), spinal cord (4.6-fold) and eye (0.1-fold). A 0.3-fold increase of *Vmd2L1* expression is determined in colon tissue, and lower MNE values are found in spinal cord (0.006-fold), eye (0.03-fold) and trachea (0.04-fold). Except for a 0.1-fold expression increase in skeletal muscle (0.1-fold), *Vmd2L3* is not expressed in the 12 murine tissues analyzed.

Especially for low abundant genes, quantitative real time RT PCR facilitates the detection of minor differences in expression previously not observed with conventional RT PCR. Prior to real time qRT PCR, the expression of *Vmd2*, *Vmd2L1* and *Vmd2L3* was analyzed by classical RT PCR (data not shown). For *Vmd2*, both RT PCR and real time qRT PCR yield similar results, although the ten-fold difference in expression between testis and spinal cord is not detectable with the conventional technology. For *Vmd2L1*, both methods display highest expression in colon tissues. In comparison to the remaining tissues, a 0.1-fold increase of *Vmd2L3* transcript levels are detectable in skeletal muscle by utilizing real time qRT PCR. In contrast, this difference is not seen by regular RT PCR. After 33 cycles of regular RT PCR amplification, weak PCR products are amplified in all tissues falsely suggesting ubiquitous but weak expression of *Vmd2L3* (Fig. 26d). The feasibility of real time PCR to measure amplification during the linear log phase instead of endpoint concentrations permits more refined analysis with higher accuracy of the cellular expression status.

4 VMD2 KNOCK-IN AND KNOCK-OUT MICE

The generation of *Vmd2*-targeted mice will play a prominent role in unravelling the function of bestrophin. Therefore, the goal of the following project was to create two genetically manipulated mouse lines in which (i) a mutation equivalent to a missense mutation found in human Best disease patients is introduced into an orthologous position of exon six of the murine *Vmd2* gene and (ii) the functional murine *Vmd2* gene is interrupted resulting in complete deficiency of bestrophin.

4.1 GENERATION OF MURINE KNOCK-IN AND KNOCK-OUT CONSTRUCTS

The rationale behind the knock-in model is to generate a mouse line carrying an alteration identified in affected subjects in several unrelated Best disease pedigrees. Provided that the mouse line will develop a phenotype similar to that of Best disease, this animal model will facilitate further studies to better understand the pathological role of mutant VMD2. The tyrosine to asparagine exchange at residue position 227 (Tyr227Asn) in exon six was selected to be introduced into murine *Vmd2*. The important functional significance of the region in which the mutation is located is underscored by several facts. Firstly, exon six shows high sequence conservation even in distantly related species (e.g. *Drosophila melanogaster* and *Ceanorhabditis elegans*) and codon 227 is an invariant residue in all of these (Fig. 36). Secondly, the missense mutation segregates with the Best disease phenotype in three independent families, i.e. in two Dutch and one Canadian pedigrees (Bakall et al. 1999, Lotery et al. 2000, Marquardt et al. 1998 and Petrukhin et al. 1998). Thirdly, at codon 227 a further missense mutation (Tyr227Cys) is identified in another two independent families (a German family, Marquardt et al. 1998; family of unknown origin, Lotery et al. 2000). Lastly, Lotery et al. (2000) report that the Tyr227Asn exchange is correlated with a highly variable Best disease phenotype, ranging from mild to severe in one and the same family. The authors suggest that using this mutation in transgenic animals may make the identification of mitigator genes in various murine backgrounds feasible.

mouse	213	E	V	C	T	L	R	T	Q	C	G	Q	L	Y	A	Y	D	W	I	S	I	P	L	V	Y	T	Q	238
bovine	213	.	M	N	238
human	213	.	M	N	H	238
pig	213	.	M	N	H	V	238
fruit fly	217	.	L	N	K	F	.	G	.	.	.	L	.	I	S	.	T	.	.	V	242
worm	213	D	I	K	K	F	.	.	G	L	A	W	V	C	N	.	.	.	V	.	L	P	I	I	.	P	T	238

Fig. 36 Multialignment of the amino acid sequence deduced from murine Vmd2 exon six and other VMD2 species

The murine amino acid sequence (in bold) encoded by exon six shows highest sequence homology to bovine (93%), and decreasing homology to human (88%), pig (85%), fruit fly (62%) and worm (27%) VMD2. Amino acid residues that are identical to the murine sequence are represented by shaded boxes and only those residues different to the murine sequence are indicated. The black-shaded bar demonstrates the position of tyrosine (Y) 227, which is identical in all species. Mouse and bovine VMD2 sequences are unpublished (Fig. 18 and Appendix), while human, pig and worm VMD2 sequences are available at the NCBI protein database with accession numbers AAC33766, AAL40882 and CAA83005, respectively. The protein sequence of *Drosophila vmd2* is published in the thesis of Matthias Porsch (2002).

The rationale for the knock-out model is to generate a Vmd2-deficient mouse lineage. Vmd2-deficiency, caused by out-of-frame deletions, out-of-frame insertions or deletions of the entire gene, plays a subordinate role in the etiology of Best disease. Thus far, a deletion of two basepairs leading to a premature termination in exon ten and a nonsense mutation in exon four of *VMD2* correlate with Best disease and AMD phenotypes, respectively (Caldwell et al. 1999; Lotery et al. 2000). Nonetheless, Vmd2-deficient mice will be useful animal models to investigate the biochemical and physiological function of Vmd2 *in vivo*. For example, the spatial and temporal expression of Vmd2 in embryonic development and in adulthood may be monitored by comparing homozygous and heterozygous knock-out mice to wild-type mice.

4.1.1 Cloning strategy for the knock-in construct

The final knock-in targeting construct consisted of murine genomic Vmd2 sequence spanning from exon three to intron ten, carrying the Tyr227Asn mutation in exon six with the neomycin-resistant gene as selectable marker nearby. In the following, the engineering process for constructing the knock-in targeting vector will be described in detail (Fig. 37).

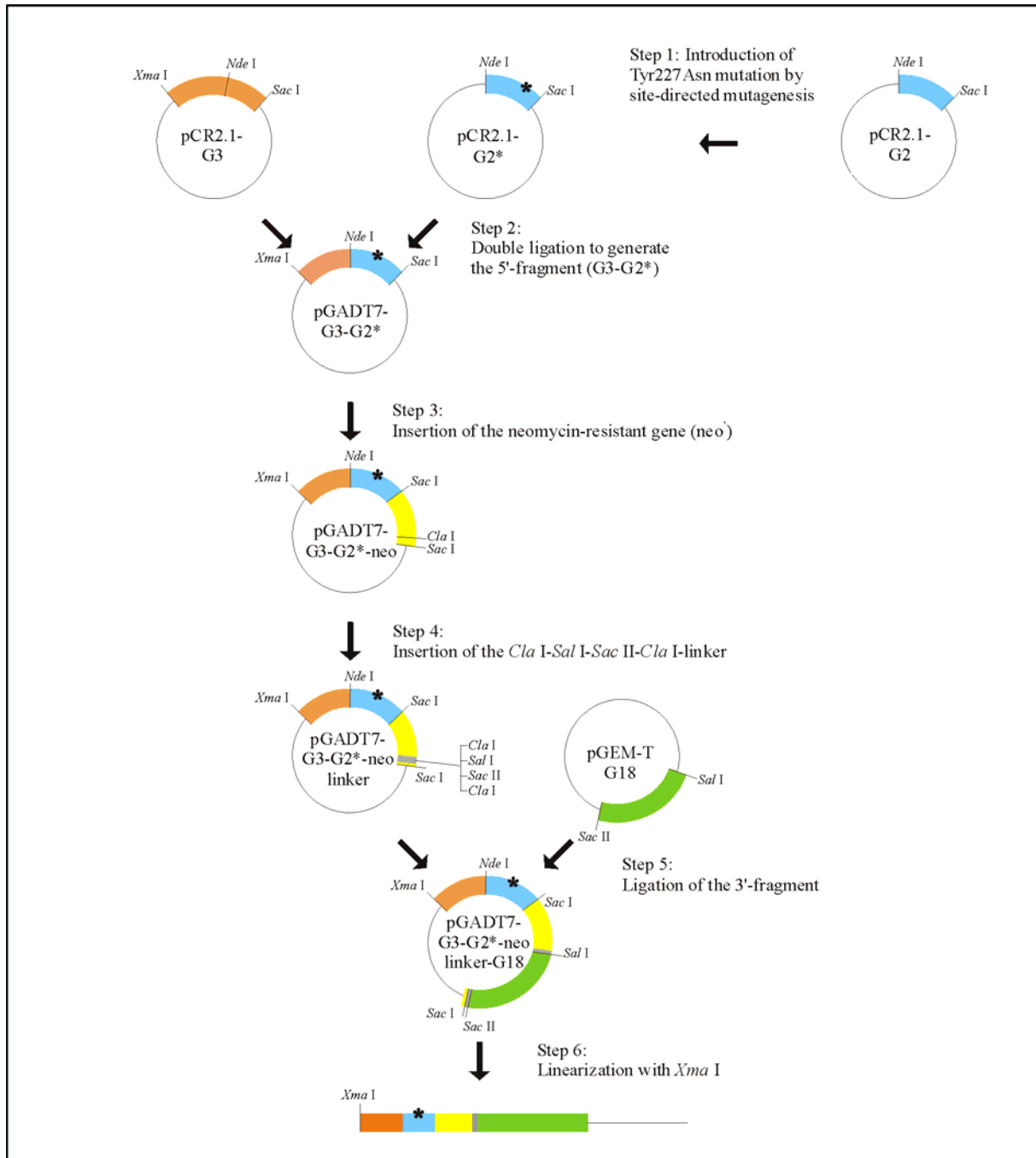


Fig. 37 Schematic representation of the knock-in cloning strategy

Coloured bars indicated the fragments cloned into the respective vectors and only relevant restriction enzyme cutting sites for each step are given. Insert and vector sizes are not to scale. The mutation Tyr227Asn (*) introduced into exon six of murine *Vmd2* by site-directed mutagenesis. See text for details.

PAC clone 586H12 containing the *VMD2* gene (see Results 3.1.1.1) is used as template-DNA for PCR amplification. Partial sequences of the murine *Vmd2* locus are PCR-amplified and subsequently cloned into the pCR2.1 (Invitrogen) or pGEM-T (Promega) by the T-overhang method. In some cases novel restriction enzyme sites are introduced with primers prolonged with the respective recognition sites (*Xma* I and *Cla* I), while in other cases natural restriction sites are used (*Sac* I and *Nde* I).

The 5'-fragment (G3, 1.8 kb), covering exon three to partial intron six, is PCR-amplified with primers mVMD2-XmaI-F and mVMD2-SacI-R and transferred into vector pCR2.1 (pCR2.1-G3). For mutagenesis, the clone pCR2.1-G2 is generated by PCR-amplifying a 371 bp fragment containing parts of intron five, exon six and parts of intron six with the primer pair mVMD2-NdeI-F and mVMD2-SacI-R. Based on the pCR2.1-G2 clone, a modified G2*-fragment is generated by site-directed mutagenesis to introduce the Tyr227Asn mutation into exon six with primers mVMD2-Y227N-F and mVMD2-Y227N-R.

In the next step, a double ligation is performed to correctly connect the fragments G3 and G2* in vector pGADT7 (Clontech). The G3-fragment, digested with *Xma* I and *Nde* I and the G2*-fragment, digested with *Nde* I and *Sac* I, are directionally inserted into the MCS of pGADT7 (*Xma* I/*Sac* I). The correct orientation of the inserts (G3 and G2*) and the presence of the missense mutation Tyr227Asn is confirmed by direct sequencing. 210 bp downstream of the mutation and within intron six, a natural *Sac* I site is used to insert the neomycin-resistant gene (*neo*^r). Later, *neo*^r is utilized to screen for positive ES cells containing the construct. A 1.3 kb *neo*-fragment containing the *neo*^r gene itself, a polyadenylation signal and flanking loxP sites is then transferred from clone Flox-Sac9 (kindly provided by Dr. Heinrich Schrewe and modified by Dr. Biaoyang Lin) into the pGADT7-G3-G2*-construct. The pGADT7-G3-G2*-*neo* construct is further modified by adding a linker sequence of 22 bp (5'-CGATGTCGACATCCCCGCGGAT) which contains two unique restriction sites, *Sal* I and *Sac* II. The linker enables the insertion of the 3'-fragment (G18) constituting the genomic *Vmd2* sequence from intron six to intron nine. First, the 3'-fragment (G18) is PCR-amplified with primer pair mVMD2-ClaI-F/mVMD2-ClaI-R2 and PAC clone 518H12 as template and the resulting 4.2 kb fragment is subcloned into the pGEM-T vector (Promega). Vector-specific cutting sites of the MCS of pGEM-T (*Sal* I and *Sac* II) then allow directional cloning of the G18-fragment into the prepared pGADT7-G3-G2*-*neo*-linker construct. Finally, all exons and adjacent splice sites of the finished pGADT7-G3-G2*-*neo*-linker-G18 construct are confirmed by direct sequencing. Linearization of the final 15.3 kb knock-in construct is achieved with restriction enzyme *Xma* I. The complete knock-in targeting construct pGADT7-G3-G2*-*neo*-linker-G18 (clone #49) is verified by digesting the plasmid DNA with a set of restriction enzymes (Fig. 38). In all cases, the predicted fragment sizes correspond to the sizes determined by agarose gel electrophoresis.

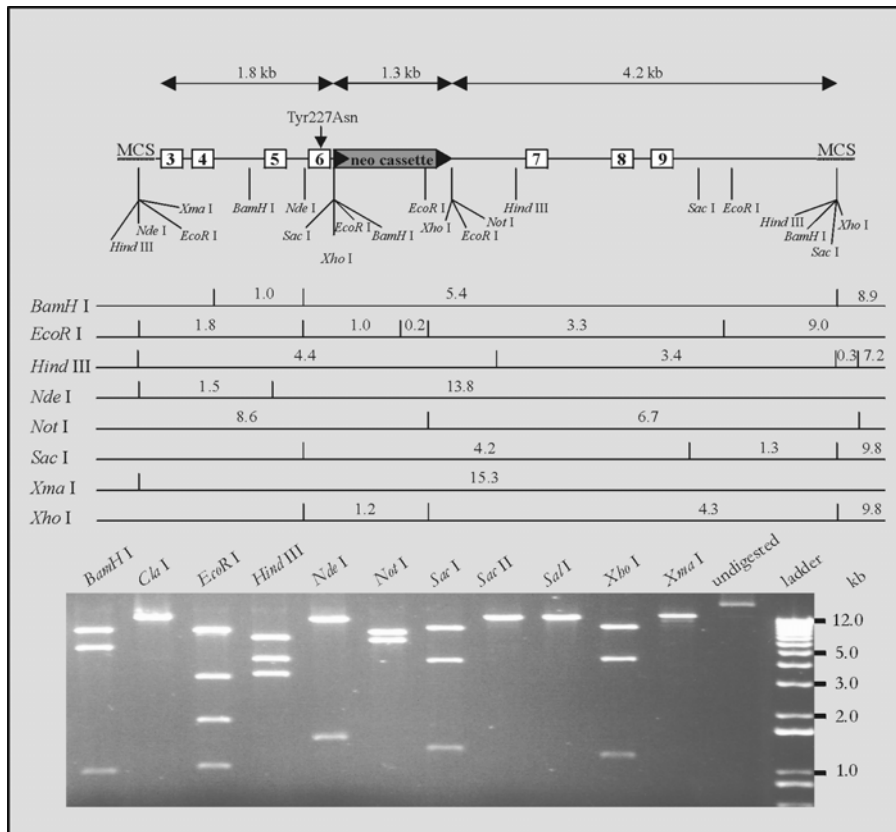


Fig. 38 Restriction map and digest of the final knock-in targeting construct

The 5'-fragment (G3-G2*, 1.8 kb) containing the the Tyr227Asn mutation indicated by an arrow, the neo^r gene (1.3 kb) and the 3'-fragment (G18, 4.2 kb) are introduced stepwise into the multiple cloning site (MCS) of the pGADT7 vector. In the schematic, exon sizes are not to scale, while intron sizes are given to scale. The fragment sizes obtained experimentally in a panel of 11 different restriction enzyme digests match to the respective theoretical predictions.

4.1.2 Cloning strategy for the knock-out construct

The pHM2 vector (a kind gift from Prof. Manfred Gessler) is used as backbone to generate the knock-out construct (Kaestner et al. 1994). pHM2 is specifically developed to be used as gene targeting vector containing important elements like the *lacZ* gene, the neomycin resistant gene (neo^r) and convenient multiple cloning sites. An in-frame connection between a coding exon of the gene of interest and the coding sequence of *lacZ* produces a fused protein. Replacing the gene of interest partially with *lacZ* should disrupt the function of the gene completely in the resulting knock-out mouse. Moreover, it is possible to analyze and characterize the mutant phenotype in the mouse by monitoring the temporal and spatial expression of the gene of interest-*lacZ* fusion protein with X-Gal staining. For engineering the knock-out construct, only two cloning steps are necessary (Fig. 39).

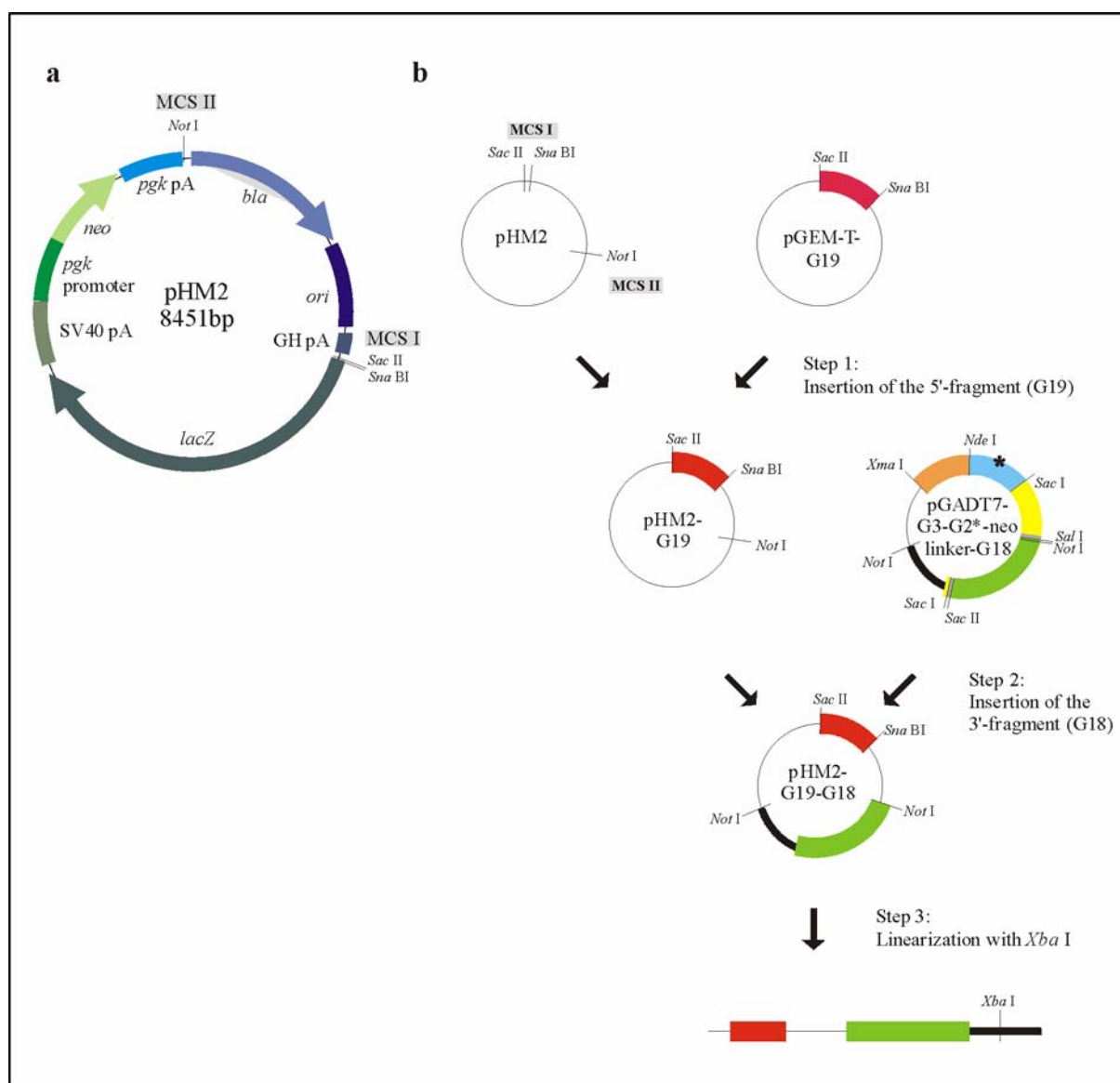


Fig. 39 Schematic representation of the knock-out cloning strategy

(a) The pHM2 vector is especially designed to generate of knock-out constructs, containing specialized feature such as the *lacZ* and the neomycin-resistant gene (*neo*^r). β -galactosidase, encoded by *lacZ*, can be employed as reporter system of expression in the resulting mouse model and *neo*^r is used for as selectable marker in ES cell culture. Conventional features of the cloning vector pHM2 include the ampicillin resistant gene β -lactamase (*bla*), the promoter of phosphoglycerate kinase (*pgk*), the origin of replication (*ori*) and several polyadenylation (pA) sites of the Simian virus 40 (SV40), of the human growth hormone (GH) and of *pgk*. Arrows represent coding sequences. (b) In two cloning steps the final knock-out targeting vector is generated by inserting a 5'-fragment (G19) and 3'-fragment (G18) into MCS I and MCSII of pHM2. Insertion of the 3'-fragment results in an in-frame fusion between exon six of murine *Vmd2* and the coding sequence of *lacZ*. In the third step, the final knock-out targeting vector (clone #4-2) is linearized with restriction enzyme *Xba* I.

Firstly, a 5'-fragment (G19, 1.6 kb) spanning exon three to exon six of murine *Vmd2* is PCR-amplified with primers mVMD2-SacII-F and mVMD2-SnaBI-R using PAC clone 586H12 as template, and is then cloned into the pGEM-T vector (pGEM-T-G19). Both primers contain *Sac*II and *Sna*BI restriction enzyme cutting sites, respectively, enabling a directional transfer of the G19- fragment into the prepared pHM2 vector (pHM2-G19). Secondly, the 3'-fragment spanning from *Vmd2* intron six to intron nine (G18) is excised from

the knock-in construct (pGADT7-G3-G2*-neo-linker-G18, clone 49) with restriction enzyme *Not* I. The G18-insert has a total size of 6.4 kb, because additional pGADT7 vector sequence is included on the 3'-side of the gene-specific sequence. The *Not* I-fragment (G18) was inserted into the second MCS of pHM2 resulting in the final knock-out construct pHM2-G19-G18 (clone #4-2) of 16.8 kb in size. Similar to the knock-in clone, the knock-out plasmid DNA from clone #4-2 is confirmed by 11 different restriction enzyme digests (Fig. 40). Restriction enzyme *Xba* I, with its recognition site located 2.5 kb downstream of *Vmd2* intron nine, is selected for the linearization of the vector prior to electroporation.

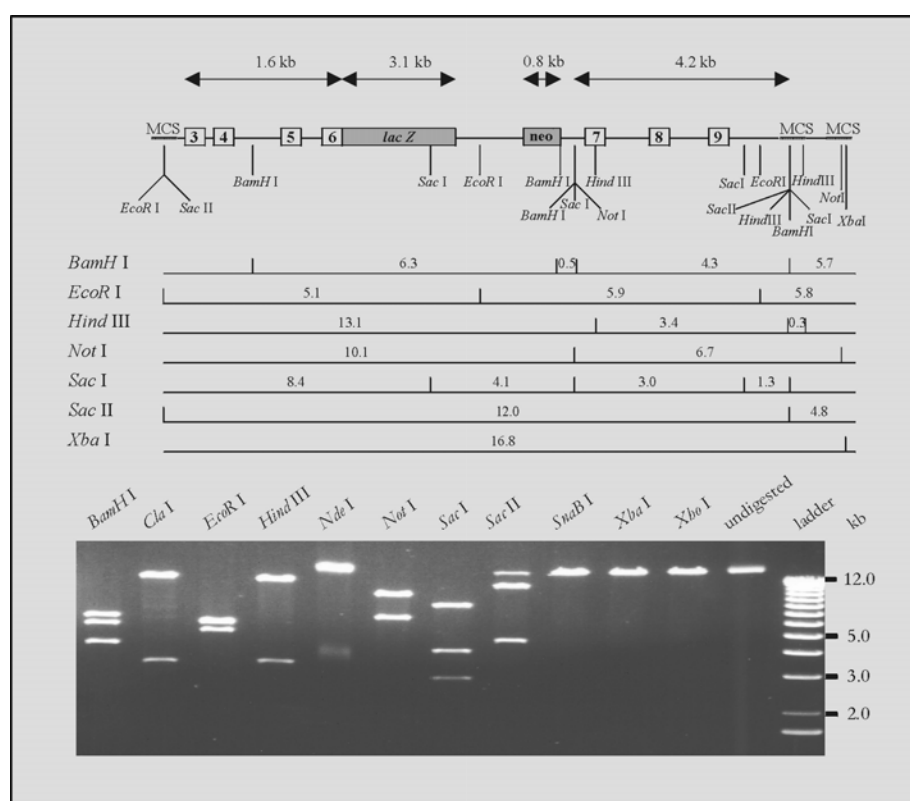


Fig. 40 Restriction map and digest of the final knock-out targeting construct

The final knock-out construct (pHM2-G19-G18) spans a genomic region of 5.8 kb, from exon three to intron nine of murine *Vmd2*. It includes an in-frame fusion of *Vmd2* exon six and the *lacZ* gene. Sizes of exons are not given to scale; sizes of introns are given to scale. Eleven different restriction enzymes, including single cutting enzymes (e.g. *Sna*B I and *Xba* I) and multiple cutters (e.g. *Sac* I and *Sac* II), are used to characterize the final construct by restriction digestion.

4.2 TRANSFECTION OF EMBRYONIC STEM (ES) CELLS WITH MUTANT CONSTRUCTS

Cultivation of embryonic stem (ES) cells and transfection experiments were performed under the guidance and in the laboratory of Dr. Burkard Kneitz. Generally, growth and maintenance, freezing and thawing of ES cells is conducted in a manner to protect the quality of the cells. ES cells should remain in an undifferentiated, pluripotent state, having the ability to develop into the respective fetal and adult cell types. The final goal of successfully transferring the mutation generated in ES cell culture into mouse germline depends on the careful handling of ES cells. Moreover, the selection of serum, the quality of the feeder cells and the supplementation of LIF (Leukemia Inhibitory Factor) have an influence on the

success of the subsequent steps. All stages of ES cell culture are carried out under sterile conditions.

The murine WW6 ES cell lineage is shown to produce a high degree of chimeric progeny and germline transmission (Ioffe et al. 1995) and is therefore selected for transfection experiments of the knock-in and knock-out plasmid constructs. Cultivation of WW6 cells is conducted under optimal conditions (6% CO₂ and 37°C) on monolayers of mitotically inactivated fibroblast feeder cells. For DNA electroporation, 40 µg of either *Xma* I-linearized knock-in plasmid DNA or *Xba* I-linearized knock-out plasmid DNA is prepared at a concentration of 1 µg/µl and in each case 1 x 10⁷ WW6 cells are treated with an electric pulse of 240V. For recovery after electroporation, the WW6 cells are cultivated on prepared feeder dishes in conditioned ES media for two days without selection. Thereafter, drug selection is initiated by supplementing the ES media with Geneticin (G418) at a concentration of 200 µg/ml. This results in the growth of distinct G418-resistant colonies after approximately eight days.

Applying this highly sophisticated technique, including the use of genomic DNA isogenic to the ES cells and the use of positive (e.g. neomycin, hygromycin or puromycin selection cassettes) as well as negative selection markers (e.g. thymidine kinase or hypoxanthine phosphoribosyl transferase selection cassettes), the frequency of homologous targeting events is generally expected to lie between 1/10 and 1/100 (Matise et al. 2000). Because only a positive selection marker (neo^r) is included in both targeting constructs, a lower homologous recombination frequency in the range below 1/100 colonies is expected. A total number of 684 and 408 ES colonies transfected with the knock-in and knock-out construct, respectively, are picked and further cultivated in 24-well feeder plates. For DNA extraction and subsequent screening, a duplicate of each picked ES cell clone is generated on a gelatine-coated 96-well plate. As soon as the ES cells in the 24-well plates reach an optimal growth, they are cryopreserved at -80° C, while the 96-well plates are further cultivated to attain higher cell density. Genomic DNA is isolated from the 96-well plates with a quick-and-easy DNA extraction method. To identify ES cell clones in which homologous recombination with the targeting vector has taken place, the genomic DNA of ES cells is subjected to PCR analysis.

4.3 SCREENING FOR ES CELLS CONTAINING HOMOLOGOUS RECOMBINATION EVENTS WITH MUTANT CONSTRUCTS

A high-throughput, PCR-based technique is used for screening the ES cells for rare homologous recombination events with the introduced targeting vector. In comparison to the well-established screening method by Southern blot analysis, the PCR method is less time- and labor-consuming. In principle, PCR amplification is only possible if the targeted vector is correctly integrated into the genomic DNA of ES cells. One primer binding site is located outside the genomic DNA of the construct, while the other is located within the vector-specific *neo^r* or *lacZ* cassette. No PCR product will result from PCR amplification with wild-type DNA or if integration of the construct has taken place via illegitimate recombination.

4.3.1 Screening for knock-in ES cells

Detection of homologous recombination events of the knock-in targeting vector (*Vmd2*^{+/*Tyr227Asn*}) is conducted by PCR amplification with primer pair mVMD2-F17 and neo-F. In total, 684 ES colonies are picked and screened in two independent transfection experiments, but no positive clones are identified (Fig. 41). To test whether poor DNA quality is the reason for negative PCR results, several isolated DNAs are PCR-amplified with a different primer combination. The control PCR reaction with primers mVMD2-NdeI-F/neo-F reveals PCR products of the expected size, suggesting that the genomic DNA is intact. Consequently, the event of homologous recombination had not occurred among the 684 clones analyzed.

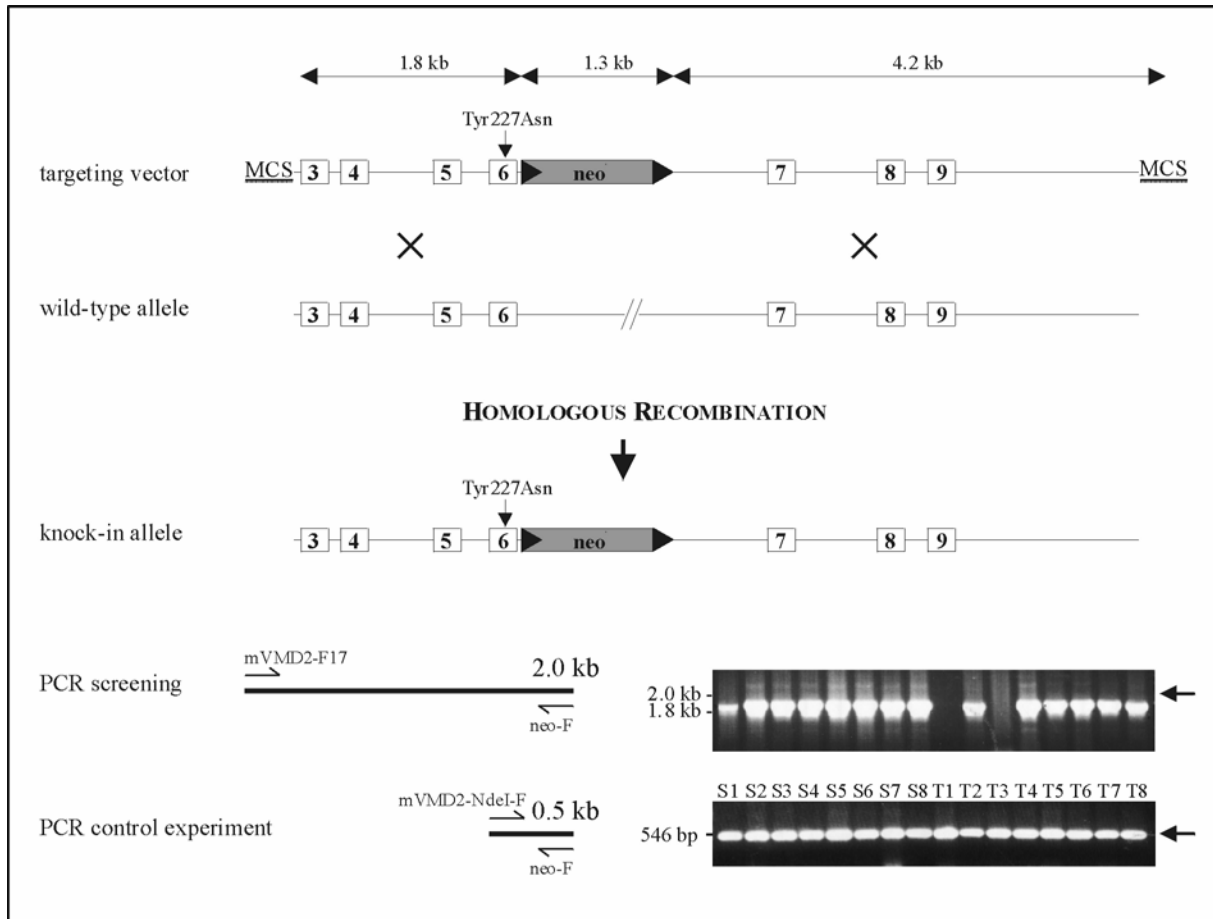


Fig. 41 Homologous recombination between the wild-type *Vmd2* allele and the knock-in construct
 Homologous recombination between the wild-type allele and the targeted allele carrying the missense mutation (Tyr227Asn) and neo^r cassette should have occurred in a low percentage of ES cells. By means of PCR amplification, the primer combination mVMD2-F17/neo-F is used to identify the rare event of homologous recombination (2 kb PCR product), while primers mVMD2-NdeI and neo-F are used for control purposes (546 bp PCR product). In addition to the expected PCR product of 2.0 kb, an unspecific PCR product of 1.8 kb is seen with primers mVMD2-F17/neo-F. The arrows on the left side of the agarose gels indicate the size of the expected PCR products of 2.0 kb and 546 bp.

4.3.2 Screening for knock-out ES cells

Identification of positive ES cell colonies carrying the knock-out construct at the homologous site is performed with PCR using primers mVMD2-F17 and lacZ-R2 (Fig. 42). Genomic DNA is extracted from 246 out of 408 picked ES colonies which are then subjected to screening for positive recombination events. In the initial screen, a PCR product of 1.9 kb is obtained in seven out of 246 (2.8 %) ES colonies.

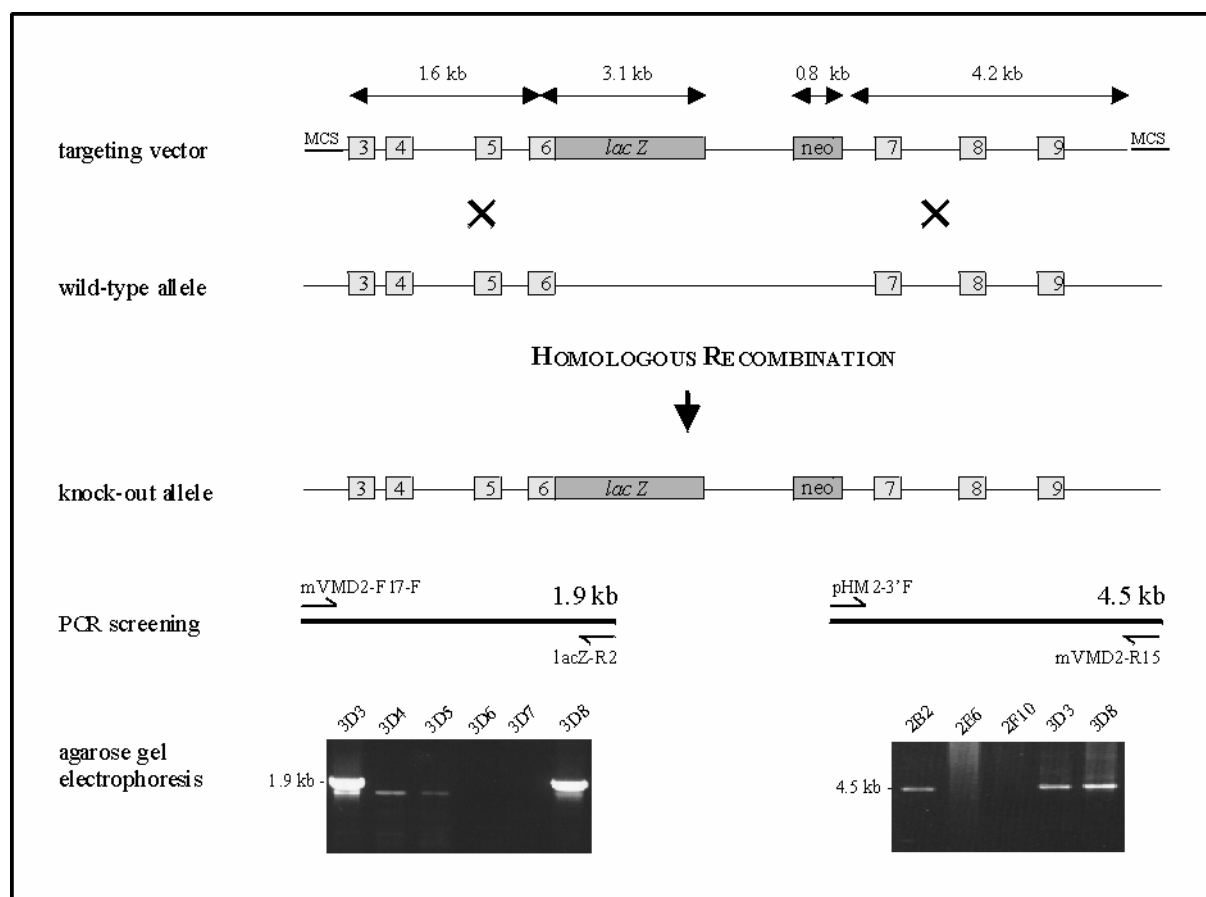


Fig. 42 Introduction of the *Vmd2* knock-out construct into ES cells by homologous recombination

The wild-type allele, the targeting construct and the resulting knock-out allele of *Vmd2* are shown schematically. Screening for positive ES clones by PCR amplification is accomplished with primer pairs mVMD2-F17/lacZ-R2 (5'-PCR) and pHM2-3'F/mVMD2-R15 (3'-PCR), resulting in PCR products of 1.9 kb and 4.5 kb, respectively. Below, some putative positive (3D3 and 3D8) and false-positive (3D4, 3D5, 3D6, 3D7, 3D9) ES clones are depicted by agarose gel electrophoresis in the 5'-PCR screen (left). The 3'-PCR screen confirms the homologous recombination event in ES clones 2B2, 3D3 and 3D8 but not in ES clones 2E6 and 2F10.

Putative positive ES clones (2B2, 2E6, 2F10, 2H12, 3D6, 3D8 and 3E12) and two false-positive ES colonies (4D1 and 4H7) are further tested with a long-range PCR spanning the 3'-region of the insert with primers pHM2-3'F and mVMD2-R15. An expected PCR product of 4.5 kb is observed in ES clones 2B2, 2H12, 3D3 and 3D8, while no PCR product is observed in false-positive ES clones as well as in ES clones 2E6, 2F10 and 3E12. The 3'-PCR delivers additional information, confirming that homologous recombination has taken place with the knock-out construct. However, the screen does not eliminate false-positive clones and therefore the frozen duplicates of all seven clones are thawed and expanded. Of these, ES colonies 2B2, 2H12, 3D8 and 3E12 are successfully re-identified, re-confirmed and preserved in liquid nitrogen for long-term storage, while ES clones 2E6, 2F10 and 3D3 are lost due to inappropriate handling of the cells.

V DISCUSSION

The retinal pigment epithelium (RPE) is a monolayer of cuboidal cells, representing one of ten layers of the neurosensory retina. On the apical side, microvilli of the RPE are in close contact to the rod and cone photoreceptors. The basal side is directly adjacent to the Bruch's membrane and closely associated to the choroid. The lateral sides of the RPE are connected with tight junctions. The extraordinary polarized morphology of the RPE subserves a multitude of functions, including the maintenance of the blood-retina barrier, the vectorial transport of nutrients and metabolites, the creation of ion gradients and the net movement of ions and water. Furthermore, the RPE is involved in the phagocytosis of photoreceptor membranes, the recycling pathway of retinol and the absorption of stray light. It is fascinating that the multifunctional RPE is formed once in life during embryogenesis and is highly active throughout life without renewal by cell division (Gallemore et al. 1998; Bok et al. 1993).

Due to substantial advances of molecular genetics in the past two decades, there is a growing body of knowledge on proteins residing in the RPE. Although the complex network of these proteins performing the vast number of different functions in the RPE is far from being completely understood, the function of some individual proteins and their involvement in various human retinopathies have been elucidated in recent years. For example, RPE65, a highly expressed and developmentally regulated RPE-specific protein, is thought to play a crucial role in the isomerization of 11-*cis* to all-*trans* vitamin A (Redmond et al. 1998). Defective RPE65 impairs the recycling of the visual pigment and is causative for Leber congenital amaurosis and childhood-onset severe retinal dystrophy (Marlhens et al. 1997; Gu et al. 1997). Furthermore, mutations in the cellular retinaldehyde binding protein are responsible for severe retinitis pigmentosa (Maw et al. 1997) and retinitis punctata albescens (Morimura et al. 1999). Finally, mutations in gene encoding 11-*cis* retinol dehydrogenase are associated with fundus albipunctatus (Yamamoto et al. 1999). In both cases, the aberrant proteins are also involved in visual regeneration processes taking place in the RPE.

Bestrophin is preferentially expressed in the RPE (Marquardt et al. 1998), in particular, it is associated with the plasma membrane on the basal and lateral sides of the RPE (Marmorstein et al. 2000). Aside from possible functions of bestrophin as chloride channel or Na/Ca-K exchanger (see below), the exact function and its pathological role in Best disease is not known. This thesis is aimed at further understanding the molecular pathology of Best

disease mutations (see Discussion 1). A second major part included the molecular identification and characterization of the Vmd2 RFP-TM protein family in the mouse, composed of Vmd2 and three Vmd2-like proteins, Vmd2L1, Vmd2L2 and Vmd2L3 (see Discussion 2). Based on the identified mouse *Vmd2* gene, our long-term objective is directed towards generating two mouse models, one mouse lineage deficient in murine bestrophin (knock-out) and one mouse lineage carrying a Best disease-associated mutation (knock-in) in the endogenous murine *Vmd2* gene (see Discussion 3).

1 MOLECULAR STUDIES OF HUMAN VMD2

1.1 MUTATIONAL ANALYSIS OF THE HUMAN VMD2 GENE

Over a three-year period of routine diagnostics for Best disease, the coding sequence of the *VMD2* gene was analyzed in a total number of 47 unrelated patients predominantly affected by Best disease (79 %) as well as in patients suffering from closely related maculopathies (21 %). The analyzed subjects were mainly of West European origin (87 %) and in 14 cases a positive history of Best disease existed in the respective families (30 %). Since *VMD2* mutation screening was performed in the framework of molecular diagnostics, the main goal was to identify sequence changes in the *VMD2* gene and to classify them according to their predicted pathogenic or benign nature. Finding causative mutations is important for the affected patients and their families in defining the ophthalmologic defect, in understanding the course of disease and in respect to family planning. Currently, there is no effective treatment available for Best disease patients, but it is anticipated that the exact molecular defects may be crucial for developing novel therapeutic approaches in the not too distant future. Furthermore, mutation screening may entail the identification of known but also of novel disease-associated mutations, allowing the augmentation of the spectrum of *VMD2* mutations. The growing number of mutation types as well as the location of novel mutations may endorse previous hypotheses and/or provide novel insight into the function of the encoded protein and its dysfunction in Best disease. By searching for *VMD2* mutations in diseases phenotypically similar to Best disease, the role of the gene contributing to maculopathies other than Best disease is further assessed.

A total of 21 heterozygous, disease-associated mutations were identified in the *VMD2* gene in the 47 unrelated subjects (Table 1). Of these, 19 disease-associated mutations were associated with Best disease, and one was each identified in a patient with pattern dystrophy

and Bull's eye maculopathy. Two mutations were recurrently found in unrelated patients and were present in distinct phenotypes: missense mutation Ala243Val was identified in three unrelated Best disease patients and in one pattern dystrophy patient while the in-frame deletion delIle295 was found in four unrelated Best disease patients. Therefore, a total of 15 unique mutations, i.e. 13 non-recurrent and two recurrent mutations fall into the category of „disease-associated mutations”. Six out of 15 mutations (Table 1, not in bold letters), including Leu100Arg, Ala195Val, Arg218Ser, Thr237Arg, Ala243Val and delIle295 have been published previously. The nine novel unique sequence changes, including eight novel missense mutations and one novel out-of-frame deletion, were classified according to a set of criteria as disease-associated mutations. In addition, VMD2 mutation screening revealed six novel rare variants with „unknown pathogenic effect” and nine to date known common polymorphisms.

1.1.1 Novel disease-associated missense mutations

Classification of novel sequence variants according to their pathogenic (disease-associated mutations) or non-pathogenic effect (benign variants) is greatly facilitated by established and well-maintained mutation databases. The plentitude of sequence information gathered in mutation databases aids to directly compare novel sequence changes with previously described disease-associated mutations. For VMD2, such a mutation database was initiated in our laboratory (Fig. 9) and as shown in Fig. 43, most of the known disease-associated mutations are missense mutations (94 %) and deletions of one amino acid residue (4 %). A large fraction of the known disease-associated mutations (90 %) is clustered in four distinct regions of bestrophin, forming four mutational hotspot regions (I - IV). Interestingly, the hotspot regions are located exclusively in the N-terminal half of bestrophin and either within or in close proximity to putative membrane-spanning regions TM1 to TM4 (Fig. 43d). The fourth hotspot, encoded by exon eight, represents a highly conserved sequence motif of 26 residues, spanning from codon 289 to codon 314 (Stöhr et al. 2002). Based on topology model A (Fig. 5), this sequence motif is located beyond the fourth putative TM domain on the intracellular side of bestrophin, bearing the highest density (23) of distinct mutations reported (VMD2 mutation database). Of interest is also that none of the missense mutations are located in exons nine, ten and eleven of *VMD2* (Fig. 43b, 43c).

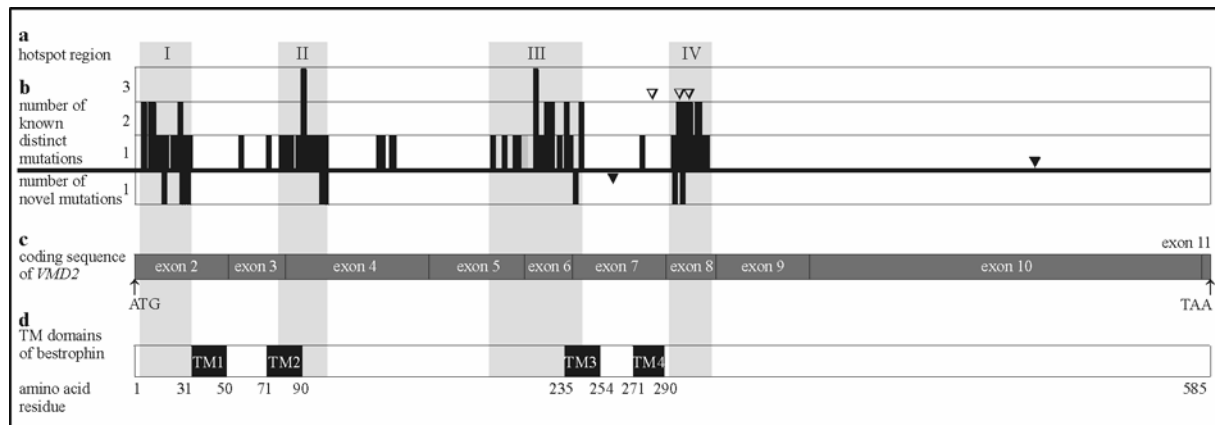


Fig. 43 Distribution of known and novel distinct mutations identified in the *VMD2* gene

(a) To demonstrate the localization of hotspots I – IV within the coding cDNA sequence (c) and the translated protein sequence (d), the hotspots are marked as light-grey vertical bars. (b) Distinct mutations are indicated by black bars (missense mutations), by grey bars (splice site mutation), by black triangles (1 bp or 2 bp out-of-frame deletions) and by open triangles (3 bp in-frame deletions). (c) The size of the ten exons representing the coding sequence of *VMD2* as well as (d) the entire *VMD2* protein with its four putative TM domains according to topological model A (Fig. 5) are given to scale. Except for the novel 1 bp deletion (Pro260fsX288, filled triangle) in exon seven, all novel missense mutations (Table 1) are found within hotspot regions I – IV. Note the location of mutations in the first half of *VMD2* (exons two to eight) coding for TM domains one to four (TM1 – TM4).

The unequal distribution of Best disease-associated mutations, between residue six and 312, pinpoints the location of functionally or structurally active domains. It implies that the entire N-terminal half of bestrophin plays an important role, in particular the four mutational hotspots. This is further underscored by high sequence conservation in the N-terminal region (i) of the orthologous genes in *Drosophila melanogaster*, *Caenorhabditis elegans* or *Mus musculus* (Marquardt et al. 1998; Petrukhin et al. 1998), (ii) of the human paralogues defining the human *VMD2* RFP-TM protein family (Stöhr et al. 2002) and (iii) of the murine paralogues *Vmd2*, *Vmd2L1*, *Vmd2L2* and *Vmd2L3* identified and characterized in the course of this thesis (Fig. 31).

Defined by mutational hotspots, functionally significant domains contribute to the function/dysfunction of the entire protein in different ways: the regions may, for example, play an important role in the formation of hetero/homooligomers (multimers), the regions may contain domains like nucleotide binding domains, calcium binding sites or transmembrane motifs and the regions may be involved in proper protein targeting and/or protein folding. Such disease mechanisms have been associated with retinal diseases. Autosomal dominant cone rod dystrophy (adCORD) is thought to be caused by mutations in the *RetGCI* gene affecting dimerization by forming coiled-coils between two proteins. Both an *in vitro* assay as well as computer-aided predictions indicate that hotspot mutations Arg838His and Arg838Ser of *RetGCI* stabilize the coiled-coil structure and therefore decrease its sensitivity to light-

induced calcium level reduction in photoreceptors (Wilkie et al. 2000). Theoretically, a similar disease-causing mechanism may account for Best disease, as identical amino acid exchanges are found in the *VMD2* gene at codon 92 (Arg92His and Arg92Ser) and codon 218 (Arg218Ser and Arg 218His) and both codons are located intracellularly, nearby TM domains two and three, respectively. To this end, a functional assay is required to test the putative molecular mechanism.

Furthermore, a functional model suggests that the nucleotide binding domains (NBD) of the photoreceptor-specific ATP-binding cassette transporter (ABCA4) is probably involved in an ATP-dependent transport of N-retinylidene-phosphatidylethanolamine across the membrane of the photoreceptor disks. This mechanism is inhibited in defective ABCA4 and appears to be associated with several retinopathies such as autosomal recessive Stargardt disease (Allikmets et al. 1997; Sun et al. 2000) and atypical retinitis pigmentosa (Martinez-Mir et al. 1998; Klevering et al. 1999). Similarly, the presence of NBDs have been suggested for bestrophin (Gomez et al. 2001). Finally, missense and nonsense mutations of *RP2* resulting in aberrant protein targeting and/or loss of the protein have been observed in heterologous expression systems. Such pathways may be the underlying cause of photoreceptor degeneration associated with X-linked retinitis pigmentosa (Schwahn et al. 2001).

In *VMD2*, the localization of missense mutations (and deletions of one amino acid residue) within hotspot regions I to IV is thought to be an important criteria to discern between disease-causative and non-pathogenic mutations. All eight novel missense mutations identified in the *VMD2* gene are located within such hotspots, i.e. Asn11Ile, Gly26Arg and Tyr29His in hotspot I, Trp102Arg and Asp104His in hotspot II, Thr241Asn in hotspot III and Leu294Val and Phe298Ser in hotspot IV (Fig. 43c). Further inclusion criteria for attributing the eight unique missense mutations as disease-associated mutations were partially fulfilled (see Results 1.4). Most codons affected by the eight novel missense mutations are conserved throughout a number of species from bovine to mouse as well as in different family members of the human and mouse *Vmd2* RFP-TM protein family (Table 1). One of the eight novel missense mutations (Asp104His) affects a codon identical to previously described missense mutations (Asp104Glu, Petrukhin et al. 1998). The others are generally direct neighbours of codons known to be mutated, e.g. novel mutation (Phe298Ser) is flanked by previously established mutations Pro297Ser and Gly299Glu. Evidence of disease allele segregation is

demonstrated for Asn11Ile and Thr241Asn. Asn11Ile is found in two affected relatives (mother and son); mutation Thr241Asn which was previously linked by haplotype analysis to the Best disease locus on chromosome 11q13.1 (data not shown) is segregating in three generations of affected individuals.

In summary, all eight novel missense mutations are located in defined hotspot regions, display interspecies as well as protein family conservation and segregate within affected families. Therefore, inclusion criteria are sufficiently fulfilled, corroborating a causative involvement in Best disease pathology. The VMD2 mutation database greatly facilitates such classifications and vice versa, novel sequence changes may aid in classifying known sequence variants with unclear allocation. Initially, Petrukhin et al. (1998) classified Asp104Glu as „change with uncertain pathogenicity”, because segregation was not formerly established. Identification of an independent novel exchange (Asp104His) at the same codon (Asp104Gln), identification of mutations in close vicinity (hotspot region) as well as establishing the absence of Asp104Glu in 200 control alleles (Bakall et al. 1999) provides sufficient evidence to classify a mutation as disease-associated alteration.

1.1.2 Novel disease-causing deletion

A novel heterozygous frameshift deletion (termed 779delC or Pro260fsX288) was identified in exon seven of *VMD2* in an affected Best disease patient (Fig. 43b). Interestingly, Pro260fsX288 not only represents a novel mutation, it also represents a novel type of mutation previously not identified in the N-terminal half of bestrophin. As annotated in the VMD2 mutation database, no frameshift deletions have been identified in *VMD2* exons two to nine and exclusively one 2 bp-frameshift deletion (Leu489fsX513) has been identified in *VMD2* exon ten, resulting in a truncated bestrophin molecule of 513 residues (Caldwell et al. 1999). The novel 779delC deletion is located in exon seven of the *VMD2* gene. This 1 bp-deletion most likely alters the ORF, leading to a premature termination site 28 codons beyond nucleotide 779. Consequently, the resulting protein consists of 287 instead of 585 amino acid residues, encoding a truncated protein which is missing the fourth TM domain as well as the entire C-terminal half. The truncated protein potentially has a devastating impact on the function of bestrophin, suggesting that the 1 bp-deletion is regarded as disease-associated mutation. Pro260fsX288 is the first report of a short deletion resulting in the entire loss of the C-terminal half of bestrophin.

Two further putative disease-causing pathways for the 779delC mutation are conceivable. Exon skipping may result from aberrant exonic splicing enhancer (ESE) or exonic splicing silencer (ESS) motifs (Tian et al. 1994). The one basepair deletion may affect an ESE/ESS motif, leading to an abnormal splicing behaviour of *VMD2* exon seven. For example, a nonsense mutation in the *fibrillin-1* gene causes exon skipping due to a disrupted ESE motif (Caputi et al 2002). Similarly, the 779delC could entail the skipping of exon seven, resulting in an in-frame deletion of 51 residues. In this truncated protein, putative TM domain three would be partially, the short extracellular loop and fourth TM domain would be entirely deleted. As a third scenario, 779delC-carrying mRNAs encoding premature termination codons (PTC) may be recognized and degraded via a pathway called nonsense-mediated mRNA decay (Hentze and Kulozik 1999). Triggered by the 779delC mutation, heterozygous subjects would then produce 50 % intact and 50 % degraded bestrophin. Although exceptions to the rule exist (Carter *et al.*, 1996), nonsense-mediated mRNA decay is primarily elicited if the PTC is located more than 50 – 55 nucleotides upstream of the exon-exon junction (Hentze and Kulozik 1999; Dreyfuss et al. 2002). In the case of the 779delC mutation, the resulting PTC could be located five nucleotides upstream of the following exon-exon boundary.

In summary, the novel deletion (Pro260fsX288) may be involved in a pathological pathway previously not proposed for Best disease. Since missense mutations are predominantly found in the *VMD2* gene, the pathological pathway of Best disease is thought to be of the dominant-negative type. However, the identification of Pro260fsX288 suggests that a loss-of-function mutation and consequently haploinsufficiency may be associated with Best disease as well. Depending on the pathologic mechanism caused by Pro260fsX288, haploinsufficiency may result from non-functional, C-terminally truncated bestrophin (frameshift) or via nonsense-mediated mRNA decay. It cannot be ruled out that the Pro260fsX288 acts in a dominant-negative fashion; the C-terminally truncated bestrophin (frameshift) may retain some aberrant function or an internally truncated protein may be generated by exon skipping.

1.1.3 Novel rare variants identified in human *VMD2*

Of six novel benign sequence changes identified in the *VMD2* gene, (Table 1), five were unequivocally classified as rare variants likely without pathogenic effect, while one sequence change, 624G>A, was further inspected. In spite of a positive family history and the diagnosis of a typical Best disease phenotype, no other mutation except for the 624G>A

sequence variant was identified in the *VMD2* gene of subject G01-1378. Therefore, a functional assay was established to test the 624G>A sequence variant in terms of aberrant splicing (Fig. 6). An *in vitro* pSPL3/COS7 assay displayed normal splicing in both wild-type (624G) and mutant (624A) constructs tested. To a minor degree, exon five was skipped in the mutant construct. Similar to alternative splicing dictated by an exonic silent variant in the *SMN* gene (Lorson et al. 1999), we hypothesized that 624G>A may affect an ESE motif (Fig. 7). Analysis with the ESEfinder© program identified a potential ESE motif (nt 617 - 624 of *VMD2*) located at the same nucleotide position of the 624G>A sequence variant. According to this prediction, the G to A transition affects the ESE motif of the serine/arginine-rich (SR) protein SR35 in a negative sense, underscoring the hypothesis that 624G>A may partially activate exon skipping. The exon five-deficient *VMD2* transcript would encode a 178 amino acid protein, containing two of four putative TM domains.

Taken together, these preliminary data provide a first clue as to a possible pathological effect of the 624G>A substitution. However, the pathogenicity of 624G>A is not yet fully established and as long as substantial evidence of an association between 624G>A and Best disease is not given, it will be regarded as „rare sequence variant with unknown pathologic effect”. Alternatively, the „true” disease-causing mutation may reside in a gene not yet linked to the Best disease phenotype. Despite of high mutation detection rates in *VMD2* in Best disease patients (e.g. 100 % reported by Lotery et al. 2000; 86 % reported by Bakall et al. 1999) the presence of a second gene (genetic heterogeneity) or other genetic factors leading to a Best-like phenotype have previously been suggested (Caldwell et al. 1999; Wadelius et al. 1998). The identification of the „true” *VMD2*-specific mutation may also have been missed due to limitations of the PCR-based screening method. In particular, mutations affecting epigenetic factors, regulatory elements in the 5'-UTR, the 3'-UTR or within intronic sequences and larger structural rearrangements may not be detectable with PCR amplification of exonic sequences.

1.1.4 Topology of bestrophin and the distribution of mutations

Although not yet confirmed by X-ray structure analysis, bestrophin is thought to be an intergral protein, spanning the membrane four (model A) or five (model B) times (Fig. 44). According to model A, both the short N-terminal and large C-terminal part of the protein are located on the intracellular side of the protein. The four TM domain model is supported by *in silico* hydrophobicity predictions performed in this study (data not shown), by previous *in*

silico predictions (Petrukhin et al. 1998; Bakall et al. 1999) as well as by *in vitro* immunological evidence (Marmorstein et al. 2000). Marmorstein and coworkers performed permeabilization experiments, demonstrating an intracellular orientation of the C-terminal half of bestrophin. By using C-terminally specific anti-VMD2 antibodies to label exogenous VMD2 in a heterologous expression system, bestrophin was exclusively detected in permeabilized cells in which access to the antigenic region was granted.

The analysis of the distribution of mutations in relation to the four (A) or five (B) TM domain model of bestrophin reveals a more uniform pattern in the former. It is striking that in model A almost all mutations are located nearby or within each of the putative TM domains and that they are found almost exclusively on the intracellular side of the bestrophin (Fig. 44). Out of a total of 92 mutations (83 mutation entered in the VMD2 mutation database plus nine novel mutations described in this thesis), bestrophin bears two mutations in the extracellular loops (Gln58Leu; Pro260fsX288) and one mutation (Leu489fsX513) in the C-terminal region beyond codon 312. Two of the three exceptions represent atypical out-of-frame deletions (Pro260fsX288 in exon seven and Leu489fsX513 in exon ten), the only out-of-frame deletions identified in *VMD2* of Best disease patients thus far. In contrast, model B would display a rather scattered pattern of mutation distribution. Due to the additional predicted TM domain (2A), hotspots I and II would be located on the intracellular and hotspots III and IV on the extracellular side of the plasma membrane. In this model, almost 50 % of the mutation would reside on the extracellular side of bestrophin (Fig. 44).

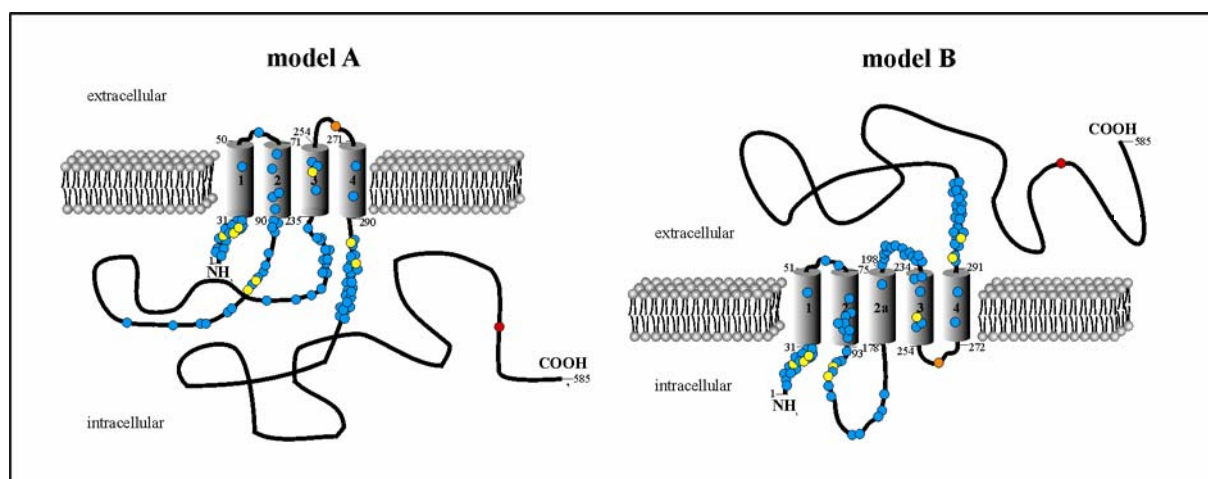


Fig. 44 Distribution of unique mutations in bestrophin topology model A (left) and model B (right) Model A and model B predict four and five membrane-spanning regions for bestrophin, respectively. Known missense mutations detected in the *VMD2* gene are shown as blue filled circles and novel missense mutations identified in this study are highlighted in yellow. Furthermore, the known out-of-frame deletion is indicated by a red circle and the novel out-of-frame deletion is shown as orange circle.

1.2 GENOTYPE/PHENOTYPE CORRELATIONS

Albeit the number of identified *VMD2* mutations is steadily increasing, obvious correlations between the *VMD2* genotype and Best disease phenotype have not yet evolved. Human retinal disorders demonstrating correlations between specific types of mutations and phenotype severity are, for example, different classes of mutations in the rhodopsin gene. While class I mutations are generally causative for a generalized form of retinitis pigmentosa, class II mutations correlate with regionally-restricted types of retinitis pigmentosa (reviewed by Lorenz et al. 2002). Genotype/phenotype correlations are especially helpful in the field of genetic counselling, enabling clinicians to predict the course of disease development. For Best disease such genotype/phenotype correlations have not been identified, in fact, the opposite is frequently observed. There is a striking intrafamilial variability and clinical features of affected relatives carrying identical mutations vary widely with respect to severity and age of onset. Arg218Cys in *VMD2* exon six was identified in a family in which the vision of the mutation-carrying grandmother was normal (20/20), while both affected grandchildren suffered from severe vision impairment by age five (Caldwell et al. 1999). Further reports of highly variable phenotypes within the same family are illustrated for Tyr227Asn and Ala243Thr (Lotery et al. 2000; Park et al. 1997). Highly variable expression and reduced penetrance of causative mutations are typical phenomena seen in dominant traits; a number of reports have documented non-penetrance in obligate carriers of Best disease-causing mutations (Birndorf and Dawson 1973; Graff et al. 1997; Weber et al. 1994c).

These observations suggest that allelic mutations are not the only determinants of clinical severity. Nonetheless, some correlations between *VMD2* mutations and characteristic Best disease phenotypes have been observed. The missense mutations Val89Ala in exon four (Eksandh et al. 2001) and Ala243Val in exon seven of *VMD2* reported in this thesis and elsewhere (Krämer et al. 2000) are generally associated with a mild form of Best disease. It is noteworthy that Val89Ala segregates with an unusually late onset of Best disease (40 – 50 years of age) and all affected individuals display typically reduced EOG recordings. Likewise, Ala243Val was identified multiple times in subjects predominantly associated with a mild phenotype of Best disease (with subnormal EOG) as well as with AVMD, a middle-age onset form of maculopathy closely resembling Best disease (Krämer et al. 2000). In fact, the high incidence of Ala243Val has led to the notion that Ala243Val possibly represents a benign variant of polymorphic nature. This interpretation however may be rejected since the allele

frequency of Ala243Val in a large number of non-affected subjects was determined to be zero out of 502 (Fig. 8).

Based on the topological bestrophin model A, Val89Ala and Ala243Val are located within the second and third TM domain of bestrophin, respectively (Fig. 43 and 44). While most (87 %) missense mutations reside in close proximity to TM domains of bestrophin, the Val89Ala and Ala243Val exchanges are found within membrane-spanning motifs. In both cases, the affected amino acid residues are valine/alanine and alanine/valine exchanges, two hydrophobic residues with very similar chemical properties. These observations suggest that Val89Ala and Ala243Val may represent a subset of mutations correlated with a distinct pathomechanism and resulting in a mild form of Best disease. It would be interesting to assess the degree of disease severity caused by further alanine/valine exchanges (Val9Ala, Ala10Val and Ala195Val) identified in Best disease patients, but unfortunately no detailed phenotypic descriptions of the mutation carriers are given (Bakall et al. 1999; Lotery et al. 2000; Petrukhin et al. 1998). These mutations, however, reside in pre-TM regions and may be responsible for a very different course of disease development.

1.3 VMD2 MUTATIONS CAUSATIVE FOR OTHER MACULOPATHIES

VMD2 mutations may also account for a variety of phenotypic manifestations other than Best disease. Documented in this thesis and by others, *VMD2* mutations have been identified in several cases of AMD, AVMD and Bull's eye maculopathy (Allikmets et al. 1999; Krämer et al. 2000; Lotery et al. 2000; Seddon et al. 2001). Certain *VMD2* mutations, e.g. Thr6Pro and Ala243Val, are causative for two distinct phenotypes (Best disease and AVMD) within the same family (Krämer et al. 2000). Similar findings that multiple retinal disease phenotypes are caused by single genes have been reported previously. Mutant *ABCA4* plays a role in several recessive retinal diseases such as Stargardt macular dystrophy, retinitis pigmentosa and recessive cone-rod dystrophies (Bernstein et al. 2002) and certain *ABCA4* mutations may predispose for AMD (Allikmets 2000). Likewise, *peripherin/RDS* is involved in several types of maculopathies as well as retinitis pigmentosa (Wells et al. 1993; Felbor et al. 1997).

In this study, *VMD2* mutation screening was performed in ten non-Best disease cases, including one case of Bull's eye maculopathy, one case of pattern dystrophy, one case of unclassified macular degeneration, two cases of AVMD and five cases of unspecified

vitelliform macular degeneration. These maculopathies are genetically heterogeneous, displaying phenotypic similarities to Best disease such as an accumulation of lipofuscin-like material and chorioretinal atrophy. Bull's eye maculopathy (Kikawa et al. 1994), pattern dystrophy (Keen et al. 1994; Weleber et al. 1993) and AVMD (Felbor et al. 1997) are associated, for example, with mutations in *peripherin/RDS*. In the ten patients analyzed, disease-associated VMD2 mutations were identified in two patients, one affected by Bull's eye maculopathy (Asn11Ile, novel) and the other affected by pattern dystrophy (Ala243Val, known). The latter mutation, Ala243Val, is associated with both Best disease and AVMD. Similar findings that one distinct mutation accounts for multiple maculopathies, was demonstrated for the VMD2 mutation Glu119Gln which is associated with Bull's eye maculopathy and age-related macular degeneration (Allikments et al. 1999; Lotery et al. 2000). Pattern dystrophy was previously not been related to Best disease. In light of these findings and the growing knowledge of underlying genetic defects, the classification of phenotypically closely related maculopathies into either distinct entities or into a spectrum of mild to severe phenotypic variants of Best disease should be reconsidered and reevaluated.

1.4 MUTATION DETECTION RATES

In total, 21 disease-associated mutations were identified in 47 unrelated patients affected by Best disease and related maculopathies (45 %). Of these, 19 disease-associated mutations were found in 37 Best disease patients (51 %). When including the family history as an important criterion for identifying a related mutation (Lotery et al. 2000; Krämer et al. 2000), the mutation detection rate of the group of patients displaying a positive family history increases markedly. Of the 14 subjects with a positive family history of Best disease, nine (64 %) were found to carry a mutation in the *VMD2* gene. The five subjects without mutation but with a positive familial background may have been misdiagnosed and represent phenocopies, the mutation may reside in another gene or the mutations were not detected with the PCR-based technique applied (discussed above).

In spite of a negative family history in nine patients, three of the patients carry a mutation in the *VMD2* gene (33 %): two novel mutations (Gly26Arg and Tyr29His) and one known mutation (Ile295del) were identified. Although it is highly speculative, the two novel mutations could represent *de novo* mutations. This phenomenon was previously reported by Palomba et al. (2000), who found a novel spontaneous missense mutation (Cys221Trp) in exon six of *VMD2* exclusively in the patient but not in both parents. On the other hand, a

simpler explanation may be that the family history is obscured by incomplete penetrance of the dominant disease trait. For clarification, linkage studies or mutation analyses in further family members would be required.

1.5 FUNCTIONAL ANALYSIS OF BESTROPHIN

1.5.1 VMD2-specific antibodies

Specific antibodies are considered as basic and important tools for carrying out biochemical and immunocytochemical experiments. Therefore polyclonal antibodies were raised in rabbits, against various antigens containing bovine- and human-specific sequences of VMD2. Affinity-purified polyclonal antibody pAB-334(AP3) revealed specific labeling of bestrophin in bovine RPE extracts as well as in COS7 cells transfected with pcDNA3-VMD2 constructs (Fig. 11c). To date, one other laboratory (Marmorstein et al. 2000) has generated polyclonal and monoclonal anti-bestrophin antibodies that are directed against the same C-terminal antigenic region as for pAB-334 (epitope EP001358, Fig. 10). Interestingly, these antibodies (Pab-125 and E6-6) display a different pattern of crossreactivity in different species: they specifically detect human, macaque and porcine but not bovine VMD2. It should be pointed out that the signal intensity of labeled bestrophin in bovine RPE tissue is weak (Fig. 11c) and similarly, immunohistological studies of bestrophin expression on macaque and porcine RPE display weak labeling (Marmorstein et al. 2000). These data indicate that bestrophin may represent low abundantly expressed proteins in the retina.

Besides the pAB-334(AP3) antibody (and pAB-333 which displays identical specificity as pAB-334), two further polyclonal antibodies pAB2 and pAB3 were generated against antigenic regions AB2 (amino acid 92 – 107) and AB3 (amino acid 397 – 412) of human bestrophin, respectively. Although pAB2 and pAB3 specifically recognized the respective fusion proteins, no positive immunoreactivities were seen in human RPE extracts (Fig. 11). The sensitivity of the detection technique may have been too low to specifically detect low abundant bestrophin. Alternatively, access of the antibodies to the antigenic region may be inhibited by structural properties of endogenous bestrophin. For example, the second predicted TM domain of bestrophin is encoded by amino acid residue 73 – 95, overlapping with antigen AB2 (amino acid 92 – 107) in four residues (Fig. 10). This may account for the inability of pAB2 to bind its epitope.

1.5.2 Heterologous expression of mutant and wild-type VMD2

Based on the hypothesis that mutations in bestrophin may result in the mislocalization and/or instability of mRNA or protein molecules, an *in vitro* mammalian heterologous COS7 expression assay was established. To study this potential pathomechanism underlying Best disease, a series of recombinant proteins carrying VMD2 mutations (21 missense mutations and two in-frame deletions) were generated and subjected to the assay (Table 4, Fig. 12). After transient transfection, RNA extracts, whole cell protein lysates as well as membraneous and soluble protein fractions were analyzed (Fig. 13 and 14). By Northern blot analysis, no marked differences were observed in wild-type and mutant *VMD2* transcript levels. Likewise, whole cell extracts and membraneous fractions of wild-type and mutant VMD2 transfectants revealed insignificant differences in protein expression. In the soluble fraction, neither wild-type nor mutant bestrophin was detected. These findings indicate that the mutations have no negative effect on the association or integration of bestrophin into the membranes of COS7 cells. Furthermore, irrelevant of the presence or absence of VMD2 mutations, the indifferent levels of expression imply that bestrophin mutants exert no severe impact on RNA/protein level and stability. Similar observations were reported by Sun et al. (2002) who addressed the issue of bestrophin acting as chloride channel (see below). The authors established a heterologous expression system of mutant and wild-type human VMD2 constructs using the pRK5 vector and HEK293 cells. In agreement with our data, no marked differences of expression levels were noticed between mutant and wild-type bestrophin.

1.5.3 Immunocytochemistry

Besides using the membrane fractionation plus Western blot technique to sublocalize VMD2 as discussed above, refined localization was implemented with fluorescence immunocytochemistry. Fluorescent labeling further confirmed membrane-specific localization of wild-type bestrophin in the COS7 expression system (Fig. 15). By comparing the labeling pattern of bestrophin to numerous specifically labeled Vero cell compartments (Simpson et al. 2000), bestrophin appears to reside in both, the endoplasmatic reticulum (ER) and the plasma membrane of COS7 cells. Initially, computer-based modeling predicted membrane-specific localization of bestrophin to the ER and plasma membrane (Bakall et al. 1999). Sun et al. (2002) also reported that bestrophin localizes to intracellular membranes in the pRK5/HEK293 mammalian expression system. The detection of bestrophin in the ER may be explained by the strong cytomegalovirus (CMV) promoter activity of the pcDNA3 vector, resulting in high biosynthesis rates of bestrophin in the ER. Alternatively, cell-type dependent

protein trafficking may be the cause of bestrophin localized to the ER. Heterologous expression of RP2 revealed a cytosolic localization of RP2 in COS7 cells and plasma membrane-specific localization in HeLa cells. Putative cell-type specific targeting factors may explain the differences in subcellular distribution of RP2 (Schwahn et al. 2001). The observation that bestrophin is localized within the ER and/or other intracellular vesicles probably does not reflect the *in vivo* situation. In its natural physiological context, bestrophin appears to exclusively localize to basal and lateral plasma membranes of the porcine and macaque RPE (Marmorstein et al. 2000).

Because of its polarized phenotype, RPE-derived cell lines may be a more suitable system to analyze the heterologous expression of bestrophin. By using an adenovirus-mediated gene transfer system, Marmorstein et al. (2000) localized exogenous bestrophin to lateral and basal plasma membranes of a rat RPE-derived cell line (RPE-J). In contrast to the COS7 host cell line developed from kidney tissue of the African Green monkey or HEK293 cells cultured from human embryonic kidney, RPE-J or ARPE-19 lineages are derived from rat or human RPE, respectively (Dunn et al. 1996), the tissue in which bestrophin is predominantly expressed. An organization of ARPE 19 cells into basal and apical regions is demonstrated by the distribution of several cell surface markers (Dunn et al. 1998). Although bestrophin is expressed in the RPE, ARPE-19 cells show no bestrophin expression (Marmorstein et al. 2000). Due to the loss of endogenous bestrophin biosynthesis and the polarized structure, ARPE-19 cells may represent a potent expression system to functionally analyze the localization of VMD2 and its mutants *in vitro*. For future studies, ARPE-19 (or RPE-J) cells should be used to clarify whether basolateral targeting of bestrophin is impaired by the mutant forms of bestrophin.

1.6 PROPOSED MOLECULAR MECHANISMS/PATHOMECHANISMS OF HUMAN VMD2

1.6.1 Is bestrophin a subunit of a homo/hetero-oligomeric channel?

Gene dosage (haploinsufficiency) and dominant-negative effects are two common molecular mechanisms underlying dominant disorders (Wilkie et al. 1994). As mentioned above, dominant-negative effects of missense mutations (gain-of-function mutations) in bestrophin probably account for Best disease. To date, the putative non-functional 1 bp-deletion in exon seven (Pro260fsX288), reported in this thesis (Table 1), is the only exception potentially associated with Best disease via haploinsufficiency. The proposed dominant-negative effect of VMD2 mutations is in agreement with recent reports of oligomerization

studies of bestrophin. Sun and co-workers (2002) performed a series of heterologous expression/co-immunoprecipitation experiments showing that four or five bestrophin units assemble to form ion-transporting channels. Oligomerizing transmembrane proteins, for example, the peripherin/RDS-ROM-1 complex, are involved in dominant retinopathies such as retinitis pigmentosa or other maculopathies (Goldberg and Molday 1996). Oligomerization of VMD2 could explain the high degree of variable expression and penetrance frequently observed in Best disease patients. Due to the oligomeric assembly taking place by chance, patients with a mild phenotype may have obtained a certain number of intact channels above a critical level. On the other hand, severe phenotypes may result from the unfortunate occurrence of aberrant channels predominantly consisting of mutant bestrophin.

In the established *in vitro* system by Sun et al. (2002), VMD2 molecules appear to co-assemble with themselves as well as with paralogues of the human VMD2 RFP-TM protein family (VMD2L1) and orthologous VMD2 in *Caenorhabditis elegans* and *Drosophila melanogaster*. The exact *in vivo* composition of the VMD2 oligomeric structure has not been elucidated thus far. Given the potential of VMD2 to form heterooligomers, it will be interesting to determine whether the proposed channels are of homo-oligomeric or hetero-oligomeric nature. Channel diversity seems to be created by heteromeric assembly such as the formation of renal chloride channels consisting of ClC-Ka/b and barttin subunits (Estevez et al. 2001) or heterotetrameric potassium channels (Choe 2002). It may be speculated that VMD2-negative Best disease patients carry a disease-causing mutation residing in such putative unknown oligomeric partners of VMD2. In this study, for 26 out of unrelated 47 patients no VMD2-specific mutations were identified.

1.6.2 Is bestrophin a calcium sensitive chloride channel?

Sun et al. (2002) provides evidence that bestrophin is a calcium-sensitive channel transporting chloride ions across the basolateral plasma membrane of the RPE. The diminished EOG in Best disease patients could be explained by mutant bestrophin forming aberrant chloride channels and resulting in an impaired light-induced depolarization of the RPE. On the other hand, further confirmational evidence is required and several puzzling inconsistencies need to be clarified. Sun and co-workers (2002) performed whole cell recordings, measuring currents of cells transfected with wild-type and mutant VMD2 constructs. Differences of conductance were observed between wild-type and mutant cells; however, it is striking that both display a wide variation of current recordings. Furthermore,

ion selectivity of the analyzed mutants has not yet been established. However, this is indispensable information, because current measurements may result from endogenous channels induced by heterologously expressed proteins (Jentsch 2002). Further controversy is found in the cellular localization of overexpressed proteins. Wild-type VMD2 predominantly localizes to intracellular membranes of transfected HEK cells, but the localization of mutant VMD2 was either not mentioned or not determined. Since only currents of expressed proteins residing exclusively within the plasma membrane are detectable by whole cell recordings, the cellular localization of overexpressed proteins is critical (Buyse et al. 1998).

Data obtained from refined bioinformatic analyses also support the hypothesis that bestrophin is involved in the transportation of ions (Gomez et al 2001), but the authors propose that bestrophin probably functions as Na/Ca-K exchanger. Weak motif homology was found between the N-terminal sequence of bestrophin and ion exchanger motifs (Na/Ca-K exchanger).

1.6.3 Is bestrophin interacting with protein phosphatase 2A?

By applying a very different approach, Marmorstein and co-workers (2002) immunoaffinity purified a complex of bestrophin and protein phosphatase 2A (PP2A) from porcine RPE (Marmorstein et al. 2002). This novel finding requires further independent verification to support the authors' hypothesis that bestrophin is part of a signal transduction pathway, modulating the light peak of the EOG via a phosphorylation cascade. Secretory signals are thought to originate by light induction from the retina and are transmitted via the apical to the basolateral plasma membrane of the RPE. It is unclear, however, in which way mutant bestrophin affects this proposed secretory pathway and how it results in the development of Best disease. Interestingly, the predicted phosphorylation domain is localized to the C-terminal half of bestrophin – this region was formerly regarded as functionally insignificant due to very low evolutionary conservation and the low number of disease-associated mutations (Fig. 43 and 44).

The above described functional implications of normal and mutant bestrophin are primarily based on *in vitro* studies. To further corroborate these findings, there is a great need to develop tools for analyzing bestrophin *in vivo*. Towards this end, the goal was to establish *Vmd2* knock-in and knock-out mice lineages, providing animal models of Best disease. The models will facilitate *in vivo* studies, including the role of bestrophin in retinal development

and physiology, its subcellular localization, the identification of putative interacting partners and the function of the closely related gene family members of *Vmd2*.

2 THE MOUSE VMD2 RFP-TM PROTEIN FAMILY

2.1 THE MOUSE GENOME SEQUENCING CONSORTIUM (MGSC)

„The sequence of the mouse genome is a key informational tool for understanding the contents of the human genome and a key experimental tool for biomedical research”. This citation from the Mouse Genome Sequencing Consortium (Waterston et al. 2002) pinpoints the importance of the mouse genome. In 1990, the time when the Human Genome Project was officially initiated, the mouse was prioritized as one of five model organisms selected for genetic, physical and sequence mapping. The plan was pursued for 12 years and finally the Mouse Genome Sequencing Consortium (MGSC) released a draft version of the mouse genome in 2002 which includes approximately 96 % of the euchromatic portion – a milestone similar to the decoding of the human genome in 2001 (International Human Genome Sequencing consortium 2001; Venter et al. 2001). Due to the immediate public access to novel murine genomic DNA sequences, research in the field of mouse genomics was greatly accelerated. Numerous research goals worldwide as well as one of the major goals of this thesis was to identify and characterize a human protein family in the mouse genome. Prior to the mouse genome era, this was a tedious and time-consuming task.

2.2 THE MURINE VMD2 RFP-TM PROTEIN FAMILY

The objective of identifying and characterizing the orthologous human VMD2 RFP-TM protein family in the mouse genome was accomplished in this project. Initially, the identification of murine *Vmd2* included PAC-library screenings and subsequently repetitive cycles of direct sequencing with walking primers. This way, the murine *Vmd2* genomic sequence was compiled in a step-by-step manner demanding months of benchwork. After mouse genomic sequence data were made available to the public, the manually compiled *Vmd2* DNA sequence was confirmed and supplemented with the novel DNA sequence data obtained from UCSC³⁵. In contrast to the discovery of murine *Vmd2*, the procedure of identifying the three family members *Vmd2L1*, *Vmd2L2* and *Vmd2L3* was greatly facilitated by achievements of the MGSC. By performing BLAT and BLAST searches with the human

³⁵ UCSC: <http://genome.ucsc.edu/>

VMD2L1, VMD2L2 and VMD2L3 protein sequences in UCSC³⁶ and NCBI³⁷ databases, novel murine genomic sequences were identified, providing the basis for subsequent biocomputational analyses and laboratory experiments. However, raw sequence data of the novel Vmd2 RFP-TM protein family were by no means complete. The murine DNA sequences representing putative orthologous genes required both extensive *in silico* inspection as well as *in vitro* RT PCR and RACE experiments to identify additional exons, splice variants and untranslated regions. This resulted in predicted ORFs displaying high homology to the human counterparts. Further computer-assisted analyses such as syntenic grouping (Fig. 30), multiple sequence alignments (Fig. 31), TM domain prediction (Fig. 31) and phylogeny (Fig. 32) contributed to a better understanding of the murine Vmd2 RFP-TM protein family. Sufficient evidence was compiled to confirm that the complete murine Vmd2 RFP-TM protein family was identified. Additional, more distantly related members of the VMD2/Vmd2 proteins could not be identified in human nor in mouse. In the following, the novel murine Vmd2 RFP-TM gene family is first put in context to the entire mouse/human genome and thereafter, noteworthy features of single family members of the novel Vmd2 RFP-TM protein family are discussed.

2.3 COMPARATIVE ANALYSIS OF THE MOUSE AND HUMAN GENOME: GENE, EXON AND INTRON SIZES

The total size of the mouse genome (~2.5 Gb) is approximately 14 % smaller than the human genome (~2.9 Gb). This is generally reflected by the size of genes: often, murine genes are proportionally smaller than their human counterparts. By comparing orthologous mouse and human intervals of 100 kb in size, Waterston et al. (2002) calculated mouse-human expansion ratios (Waterston et al. 2000, see Fig. 6). Autosomes display a mean mouse-human expansion ratio of 0.91, while the mean ratio of the murine X chromosome is slightly above 1.0. In 38 % of the analyzed intervals, murine sequences are larger compared to the human orthologues. Schematically illustrated in Fig. 45, the mouse-human gene size ratios are calculated for the Vmd2 RFP-TM gene family members: the murine *Vmd2* gene is 11 % smaller than the corresponding human gene. Murine *Vmd2L3* is 60 % smaller than human *VMD2L3*, while murine and human *Vmd2L2* are almost identical in size. In contrast, murine *Vmd2L1* is 9 % larger than the human orthologue.

³⁶ UCSC: <http://genome.ucsc.edu/>

³⁷ NCBI: <http://www.ncbi.nlm.nih.gov/BLAST/>

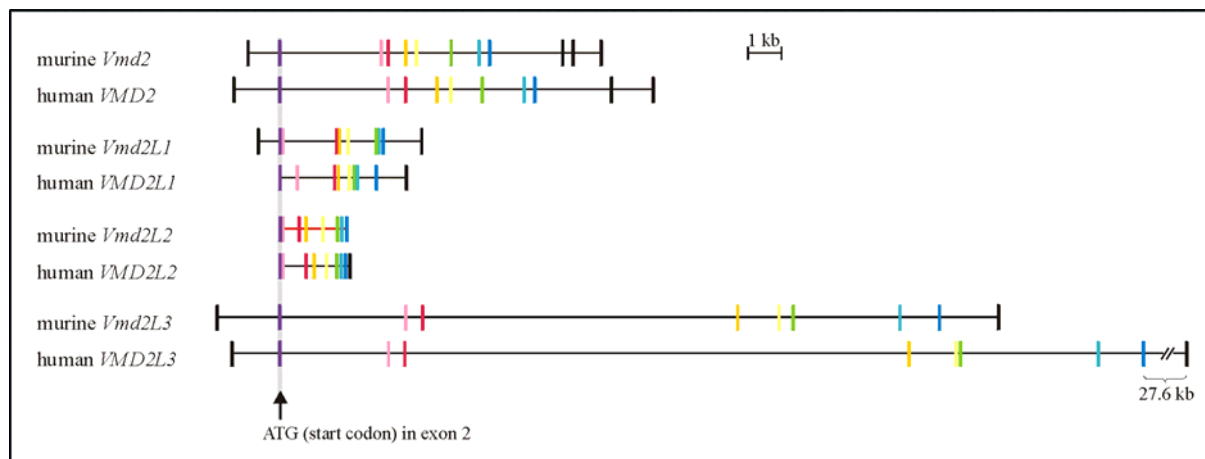


Fig. 45 Genomic Organization of the human and mouse *Vmd2* RFP-TM gene family

Exons are represented by vertical bars (not to scale) and horizontal lines represent intervening sequences given to scale. Indicated by a faint grey vertical bar and by an arrow, the localization of the start codon (ATG) in exon 2 is shown. In some genes (mouse *Vmd2*, human *VMD2*, murine *Vmd2L1*, murine *Vmd2L3* and human *VMD2L3*) putative non-coding exon one was identified. Highly conserved coding exons two to nine are marked in color: exon two (purple), exon three (pink), exon four (red), exon five (orange-yellow), exon six (yellow), exon seven (green), exon eight (turquoise) and exon nine (blue). Please note that the intronic structure of orthologous pairs is more conserved than the paralogues.

A comparative analysis of the mouse/human genome reveals high similarity in gene organization: 86 % of human and murine genes have an identical number of coding exons and in 46 % the length of coding exons are identical (Waterston et al. 2002). Human and mouse *Vmd2L1* and *Vmd2L3*, respectively, contain nine coding exons, whereas human *VMD2* has ten and murine *Vmd2* eleven coding exons. The size of the coding exons in the human and mouse *Vmd2* RFP-TM gene family is also highly conserved. High size conservation exists in exons two to nine, the exons that encode the characteristic transmembrane domains and invariant RFP peptide motif. The orthologous exon pairs of human and mouse *Vmd2*, *Vmd2L1* and *Vmd2L3* are identical in exon length. In particular, the exon length of exons three to eight are identical in all family members analyzed. Exon nine of human and murine *Vmd2L1* was found to be 3 bp longer (155 bp) than that of human and murine *Vmd2/Vmd2L3* (152 bp). The difference of multiples of three is a common feature arising from reading-frame constraints which was observed by Waterston et al. (2002) in 858 out of 930 (92 %) orthologous exons varying in exon length.

Intron sizes are not subjected to selection pressure and therefore conservation of intronic sequence lengths was neither found between orthologous nor paralogous members of the human and murine *Vmd2* RFP-TM protein family. However, an overall correlation between the size of human and murine orthologous introns was observed. Similar to a comparative data set of over ten thousand human-mouse orthologous introns displaying an

average size of murine introns reduced by 17 % (Waterston et al. 2002), the mouse introns of *Vmd2*, *Vmd2L1* and *Vmd2L3* are on average 16 % smaller than the corresponding human introns.

2.4 ESTABLISHMENT OF THE SEQUENCE BEYOND EXON NINE OF THE VMD2 RFP-TM GENE FAMILY

Encoded by exons two to nine, the sequence of ~370 amino acid residues containing several putative TM domains and an invariant RFP tripeptide is the characteristic motif of the RFP-TM protein family. Likely, due to its functional importance, this region is highly conserved and thus, this part of the *Vmd2* RFP-TM genes was readily identified in the murine genome (Fig. 31). Beyond exon nine, the sequence alignment decreased significantly in both orthologous and paralogous *Vmd2* RFP-TM proteins, complicating the identification of novel orthologous coding exons. The putative functional insignificance of the region beyond exon nine (C-terminal region) may be reflected by the low number of disease-associated mutations found in exons ten and eleven of human *VMD2* (1 %). *In silico* evidence for having identified the remaining coding sequence including the termination codon and 3'-UTR was given for *Vmd2* and *Vmd2L1*. For both genes, the predicted ORFs are supported by EST and cDNA clones identified in the respective NCBI databases (Fig. 17 and 20). Murine *Vmd2L2* and *Vmd2L3* are not represented by EST/cDNA clones in the NCBI database, and no orthologous coding exons beyond exon nine were identified by comparative *in silico* searching in the mouse genome. While *Vmd2L2* was not further analyzed as it was recognized as a non-functional pseudogene (see below), the sequence beyond exon nine of *Vmd2L3* was established by 3'-RACE experiments. A novel exon of murine *Vmd2L3* was identified, however, it contains a stop codon after one nucleotide of exon sequence. Opposed to a 27.7 kb distance between human exon nine and ten, the novel murine exon ten is separated from exon nine by 1.4 kb (Fig. 29). Human *VMD2L3* exon ten contains 31 triplets and the termination codon, while in murine *Vmd2L3* the stop codon is positioned at the beginning of the novel exon (Fig. 28). No reasonable comparison of protein sequences was possible, therefore good evidence of having identified murine exon ten is not given and further experiments need to be carried out to finally resolve this issue.

2.5 EXPRESSION PROFILE OF MURINE VMD2 AND ITS FAMILY MEMBERS

The expression of human *VMD2* displayed an overall similar but not identical pattern to that of murine *Vmd2*. In humans, highest transcript levels of *VMD2* were found in the RPE,

followed by testis, retina and the spinal cord (Stöhr et al. 2002). Based on real time qRT PCR, mouse *Vmd2* is highly expressed in testis, moderately expressed in the spinal cord and weakly expressed in the tissue termed „eye”, containing all tissues of the eye except the vitreous body (Fig. 35 and Table 5). The expression pattern of murine *Vmd2* was also determined by a less sensitive technique, RT PCR, revealing high expression in spinal cord and testis tissues and low expression in eye, lung, trachea and possibly in heart. Although *VMD2/Vmd2* transcripts were found in the same types of tissues, highest expression levels were identified in human RPE in contrast to murine testis. The expression level of the murine *Vmd2* transcript in eye was possibly obscured by the technique used to isolate murine eye tissues. Due to the small, pin needle head-sized murine eyes, it was impossible to separate the RPE from the attached retinal layers in a short time-frame minimizing RNA degradation. Here, the vitreous body was removed from the murine eye and the remaining tissues including the corneal epithelium, the iris, the ciliary body, the multilayered retina and the choroid were processed to total RNA and cDNA. In contrast, by applying the brush technique (Marmorstein et al. 2002) on larger porcine, bovine or human donor eyes or by detaching the RPE cells with trypsin or dispase treatment (Holtkamp et al. 1998; Yang et al. 2000), RPE cells could be separated more efficiently from the underlying tissues. A more precise murine expression profile may be obtained either by performing immunological expression studies on murine tissue sections as soon as specific anti-*Vmd2* antibodies are available or by performing RT PCR analysis with non-contaminated RPE tissue.

The same reasoning is applicable for the expression profiles established for *Vmd2L1*. Based on data obtained from RT PCR and real time qRT PCR, the murine *Vmd2L1* transcript is present in the eye cDNA template at low levels (Fig. 20 and 35). This is in concordance with the RPE-specific expression of human *VMD2L1* (Stöhr et al. 2002), however, the low expression level in mouse „eye” is probably generated experimentally by the extraction technique applied.

Opposed to weak signals of human *VMD2L3* in retinal tissues (Stöhr et al. 2002), no murine *Vmd2L3* transcript was detected in the murine „eye” cDNA template by real time RT PCR (Fig. 35). As for *Vmd2* and *Vmd2L1*, the monolayer of the RPE may be „diluted” with other tissues of the eye and therefore the *Vmd2L3* transcript is not detectable using the „eye” cDNA as template. The murine *Vmd2L3* transcript may be present in RPE but below the limit of detection.

2.6 IS MURINE *VMD2L2* A PSEUDOGENE?

Several lines of evidence indicate that murine *Vmd2L2* probably represents an unprocessed pseudogene (see Results 3.1.1.3). The expression profile was determined by RT PCR analysis in a panel of 12 murine tissues. In the first round of RT PCR amplification no distinct PCR products were amplified. Nested RT PCR amplification resulted in specific RT PCR products in liver tissues, while multiple unspecific PCR products were amplified in the other templates (Fig. 23). Because the two liver-specific transcripts did not encode ORFs, these PCR products were regarded as PCR-induced artefacts rather than indicators of *Vmd2L2* expression. In humans, *VMD2L2* is not expressed in liver; it is highly expressed in colon and weakly expressed in spinal cord, retina, lung, trachea and testis (Stöhr et al. 2002). The observation of non-expression is supported by *in silico* analyses of the mouse EST database (NCBI). To date, no EST clones matching to murine *Vmd2L2* have been identified. Furthermore, numerous sequence changes and nonsense mutations were identified in putative exons four, seven, eight and nine (Fig. 25). Therefore, murine *Vmd2L2* is thought to represent a non-functional and non-transcribed pseudogene in which mutations accumulate rather than being eliminated by selective evolutionary pressure. Analysis of conserved synteny between the human and mouse genome was used as tool to confirm orthologous identity between human and mouse *Vmd2L2*. Human *VMD2L2* is located within a syntenic block on human chromosome 12 which corresponds to a syntenic block on murine chromosome ten containing murine *Vmd2L2* (Fig. 30). The alternate explanation that a yet unidentified, but functional orthologous gene exists in the mouse genome was therefore ruled out. In conclusion, human *VMD2L2* seems to have retained its functionality, while murine *Vmd2L2* mutated in the course of evolution to a pseudogene. Deduced from the phenogram of the murine and human VMD2 RFP-TM gene family (Fig. 32), the evolutionary process from functionality to pseudogene most likely took place after the mouse and human lineages diverged approximately 65 – 75 million years ago (Madsen et al. 2001; Murphy et al. 2001). Prior to speciation, the four paralogous RFP-TM genes probably originated from a common ancestor, otherwise, the striking pairing of putative orthologous genes would not be obvious in the phylogenetic tree analysis (Gogarten und Olendzenski, 1999).

Interestingly, the automated gene recognition program GenomeScan (NCBI, Yeh et al. 2001) identified murine *Vmd2L2* as hypothetical gene with an ORF of 259 amino acid residues (XM_143934, XM_207579 and XM_205479). GenomeScan was unable to discriminate the pseudogene *Vmd2L2* from an active gene and therefore, misclassified genes

like *Vmd2L2* are included into the mouse gene catalogue (29 201 transcripts) generated by the MGSC. An even more severe impact on the murine gene and transcript number was illustrated by the murine *Gapdh* gene, which has one functional and more than 400 non-functional pseudogenes (Waterston et al. 2002). More than one quarter of the pseudogenes (118) were identified as functional genes and have not yet been removed from the mouse gene catalogue. Therefore, extensive and more refined biocomputational re-editing strategies on the one hand, and worldwide contributions from scientists who specialize in certain chromosomal regions, genetic diseases or gene families are necessary to eliminate or annotate pseudogenes and to generate a catalogue of genuine murine genes.

2.7 DIFFERENTIAL SPLICING OF MURINE VMD2L3

Based on an EST assembly approach, multiple differentially spliced isoforms were previously identified for human *VMD2L3* (Stöhr et al. 2002). In addition to the „wild-type” transcript with the longest ORF, in some variants the first coding exon (exon two) and in others the first two coding exons (exons two and three) are skipped and two alternative splice acceptor sites in intron four are used. Another group of EST clones displays the skipping of exon seven. Similar results were obtained by nested RT PCR analyses, in which five alternatively spliced variants for human *VMD2L3* have been identified (Marquardt 2001).

RT PCR analysis was performed for murine *Vmd2L3* (Fig. 26). Because the analysis focussed on determining the expression profile rather than on identifying all possible splicing variants of *Vmd2L3*, this set of data is incomplete. However, two splice variants were identified (var2 and var3, Fig. 26 and 27), one skipping exon two partially and the other skipping both exon two and exon three. *Vmd2L3* var2 contains an internal deletion of 57 amino acid residues, encoding putative TM1 and parts of TM2. The potential initiation signal of *Vmd2L3* var3 is located in exon four, resulting in a protein truncated by 106 amino acid residues and lacking the first two TM domains. Further splicing variants were not identified but may exist for the murine *Vmd2L3* transcript. The identified splice variants of murine *Vmd2L3* were exclusively expressed in heart tissue and in none of the other mouse tissues investigated. The generation of mRNA artefacts due to the amplification technique is likely to be rejected, because alternative splicing products have been found in three independent systems: (i) by human EST assembly, (ii) by human RT PCR analysis and (iii) by murine RT PCR analysis. In future, it will be a great challenge to understand the functional significance

of these protein variants that have lost two of their highly conserved transmembrane motifs (i.e. *Vmd2L3* var3).

3 THE RELEVANCE OF KNOCK-IN AND KNOCK-OUT MOUSE MODELS

Mice are one of the best-studied animals in the field of mammalian biology and besides *Drosophila*, *Caenorhabditis* and *Fugu*, mice are often used as model organisms for molecular genetics investigations. The development of gene targeting and embryonic stem cell technology further revolutionized mammalian genetic research and facilitated precise molecular modifications in the mouse genome (Capecchi 1989). Desired alterations are mediated via homologous recombination into murine embryonic stem cells and are then permanently integrated into the mouse germ line. A multitude of useful mouse models representing human diseases, in particular retinal dystrophies, have been generated and are contributing to a better understanding of the underlying pathomechanisms. Some examples are Crx- and Rpe65-deficient mice representing models for Leber congenital amaurosis (Furukawa et al. 1999; Seeliger et al. 2001), rhodopsin-deficient mice as models for retinitis pigmentosa (Humphries et al. 1997), *Abca4*-deficient mice as a model for Stargardt disease (Weng et al. 1999) and *Rs1h*-deficient mice mimicking X-linked juvenile retinoschisis (Weber et al. 2002). Apart from elucidating the respective disease mechanisms, mouse models serve as valuable tools for basic research into photoreceptor function and dysfunction. An interesting finding is that photoreceptor degeneration of distinct mouse models is often triggered by a common pathway, namely apoptosis. Its relevance for developing therapeutic approaches is shown by a recent report, demonstrating a synergistic effect of two apoptosis-inhibitory genes (*Bcl-2* and *BAG-1*), delaying photoreceptor degeneration (Eversole-Cire et al. 2000).

Different mouse models resembling chloride channelopathies have been genetically engineered and insight is gained in their physiological importance. In light of bestrophin potentially acting as multimeric chloride channel (ClC) (Sun et al. 2002), ClC-2, ClC-3 and ClC-7-deficient mouse models display intriguing pathologic features in respect to retinal diseases. Of these, ClC-2 channels are ubiquitously expressed in the plasma membrane of many different human cell types and numerous functions have been proposed, including lung development (Murray et al. 1995; Blaisdell et al. 2000), nephrogenesis (Huber et al. 1998), cell swelling (Xiong et al. 1999) and hyperpolarization (Thiemann et al. 1992). Although ClC-2 is not correlated with any human disease phenotype, in ClC-2 knock-out mice a

degenerative phenotype in two distinct tissues i.e. photoreceptors and male germ cells is observed (Bösl et al. 2001). Both are in close contact to supporting and phagocytosing cells (Sertoli cells and the RPE, respectively) and depend on their blood-organ barrier-forming function. The authors hypothesize that the function of CIC-2 is critical in cells tightly associated with nursing cells and is involved in ion homeostasis. Similarly, human and murine bestrophin is expressed in barrier-forming epithelia (testis and RPE). Therefore, it will be interesting to study the role of *Vmd2* in respect to infertility and/or photoreceptor degeneration in *Vmd2*-deficient mice. As in the CIC-2-deficient mouse model, the onset of potential photoreceptor/Sertoli cell degeneration may also correlate with the development of the blood-retina/blood-testis barrier in *Vmd2*-deficient mice. Furthermore, immunological colocalization studies between *Vmd2* and CIC-2 may resolve the question of a functional interdependence or heterooligomerization between CIC-2 and *Vmd2*. The testis/RPE-restricted phenotype seen in the CIC-2 deficient mice may be functionally related to the testis/RPE-restricted expression of *Vmd2*.

For Best disease, no animal model exists at present. Therefore, part of this work was aimed to generate targeted *Vmd2* mouse lineages. Thus far, two targeting constructs were genetically engineered, a knock-in targeting construct carrying a Best disease-specific missense mutation (Tyr227Asn) in exon six of murine *Vmd2* (Fig. 37 and 38) and a knock-out targeting construct in which the coding sequence of *Vmd2* is interrupted by the *lacZ* gene (Fig. 39 and 40). These targeting constructs are thought to produce a mouse lineage with typical features of Best disease (knock-in) and a *Vmd2*-deficient lineage of yet unknown pathology (knock-out).

The development of features typical for human Best disease in the murine knock-in lineage is unpredictable at this point. The macula, a human-specific (i.e. primate-specific) structure of the retina, is the area of highest cone density, highest visual acuity and the primary site of Best disease etiology. Although a similar structure to the human macula is absent in mice, mouse models representing maculopathies have been generated successfully. Weber et al. (2002) recently reported that *Rs1h* deficient mice display similar degenerative features of the retina as males affected with X-linked juvenile retinoschisis (RS). In humans, however, the RS-typical small cysts are restricted to the macula, while in *Rs1h*^{-Y} mice the cysts are scattered evenly across the retina. Despite the difference in organization of the human and murine retina and the resulting differences in disease manifestation, the *Rs1h*^{-Y}

knock-out mouse lineage serves as an important model to resolve the pathogenic mechanism in retinoschisis. Mouse models of other retinopathies originating in or restricted to the macula, such as Best disease, will similarly display the corresponding phenotype, enabling the elucidation of the underlying disease mechanism.

Vmd2-deficient knock-out mice will be exciting objects to study since its phenotypic outcome is unknown. In humans, no documentation of the homozygous loss of VMD2 exists and the first heterozygous mutation potentially associated with the complete loss of function in 50 % of bestrophin is reported in this thesis (Pro260fsX288, see Discussion 1.1.4). The speculation that the mild, late-onset form of maculopathy (e.g. AMD) may be caused by haploinsufficiency as a result of deleterious VMD2 mutations was not confirmed by mutation analysis in large numbers of AMD patients (Allikmets et al. 1999; Krämer et al. 2000; Lotery et al. 2000).

Presently, four murine embryonic stem cell clones containing the targeted knock-out allele have been isolated and are ready for the subsequent steps in gene targeting technology (Fig. 42). The expanded clones are currently injected into the blastocyst cavity of a pre-implantation mouse embryo and transferred into the uterus of pseudo-pregnant mice. In some of the resulting coat-color chimeras the targeted ES cells will by chance contribute to germline cells and their progeny will then yield heterozygous mutant mice. Further breeding of heterozygous ($Vmd2^{+/-}$) mice should produce a mendelian distribution of wild-type homozygotes ($Vmd2^{+/+}$), heterozygotes ($Vmd2^{+/-}$) and mutant homozygotes ($Vmd2^{-/-}$) at a ratio of 1:2:1 (Joyner 2000). In the case that mutant or absent *Vmd2* affect male viability due to the dominant expression in testis tissue, skewing of sex ratios may be observed in the offspring.

For the knock-in mouse, an additional ES transfection step is required prior to the procedure described above (Fig. 41). ES transfection was previously performed twice, but, no positive clones were identified from 700 ES cell colonies analyzed. Two minor differences between the knock-in and the knock-out constructs may explain the low rate of homologous recombination. Firstly, the backbone of the knock-out construct is the pHM2 vector, a vector exclusively designed to generate knock-out targets. In contrast, a vector designed for the yeast two-hybrid system, pGADT7, is used as backbone for the knock-in construct because of convenient restriction enzyme cutting sites. The latter vector may inhibit homologous

recombination due to an unknown mechanism. Secondly, the knock-out construct is linearized with *XbaI* at the 3'-side of the insert, and conversely, the *XmaI*-linearized knock-in construct is cut at the 5'-side in close proximity to exon three of *Vmd2*. Whether the site of linearization possibly has an effect on DNA conformation and influences the homologous recombination frequency is an issue of speculation. However, homologous recombination frequencies similar to the knock-out transfection (2.8 %) are hopefully obtained by transfecting ES cells with knock-in construct linearized at the 3'-side of the insert. Alternatively, the knock-in construct may be further genetically modified by adding a negative selection marker, a thymidine kinase (*tk*) cassette at the end of the targeting construct. Clones that have incorporated the knock-in construct by non-homologous recombination contain *tk* and thus produce a cell toxin in the presence of gangcyclovir. *Tk*-deficient clones that have integrated the targeting vector by homologous can therefore be selected for. In this way the identification rate of clones carrying the $Vmd2^{Tyr227Asn/+}$ phenotype may increase.

In summary, in this work the groundwork was laid out to generate transgenic knock-out and knock-in mice carrying a $Vmd2^{-/-}$ and $Vmd2^{Tyr227Asn/+}$ genotype, respectively. Once these models are established, a new area of experimental possibilities may be available. Both, a detailed characterization of the individual models as well as in-depth comparative analysis of wild-type mice ($Vmd2^{+/+}$), heterozygous knock-in ($Vmd2^{Tyr227Asn/+}$), homozygous knock-in ($Vmd2^{Tyr227Asn/Tyr227Asn}$), heterozygous knock-out ($Vmd2^{+/-}$) and homozygous knock-out ($Vmd2^{-/-}$) will aid to finally elucidate the role of bestrophin in health and disease.

VI MATERIALS AND METHODS

1 CLINICAL DATA OF PATIENTS

For routine VMD2 molecular diagnostics, a total number of 57 patients (47 unrelated) were referred to our laboratory by ophthalmologic clinicians. Informed consent was obtained from all patients. The 47 unrelated patients include 37 clinically diagnosed cases of BMD, five cases with an unspecified phenotype of vitelliform macular degeneration, two cases with suspected AVMD, one case with Bull's eye maculopathy, one case affected with pattern dystrophy and one case with unclassified macular degeneration. Ophthalmoscopic evaluations of the patients were performed by the respective clinicians and include fundus photography, fluorescein angiography and electrophysiologic testing. If possible, the medical history of the patient's family was ascertained. 14 probands have a positive familial background, in 9 cases the family history is negative and the family history was not stated in the remaining 24 analyzed probands. The 47 patients predominantly originate from Western Europe (41), while five come from Eastern Europe and one from Southern Europe.

2 GENERAL METHODS OF MICROBIOLOGY

Standard protocols described by Sambrook et al. (1989) are applied for the cultivation of bacteria (*Escherichia coli*), for the production of electrocompetent cells (*E. coli* strains DH5 α or XL1-blue) and for the introduction of plasmid DNA into the *E. coli* strains DH5 α or XL1-blue via electroporation. In some exceptional cases, ultracompetent cells (XL-10Gold®, Stratagene, Amsterdam, Netherlands) were purchased and plasmid DNA is transformed by the „heat shock” method following the instruction manual. Bacterial stocks are cryopreserved at -80°C. For cryoprotection, 15 % (v/v) glycerol is added to liquid bacterial LB cultures (LB media: 10 g Bacto-Tryptone, 5 g Bacto-yeast extract, 10 g NaCl; ddH₂O to 1 L).

3 DNA-SPECIFIC METHODS OF MOLECULAR BIOLOGY

3.1. DNA EXTRACTION

3.1.1 *Extraction of human genomic DNA*

Human genomic DNA is isolated from blood lymphocytes. Human EDTA blood is first incubated in lysis buffer (155 mM NH₄Cl, 10 mM KHCO₃, 0.1 mM Na₂EDTA; pH 7.4) and centrifuged twice to separate nuclei-free erythrocytes in the supernatant from DNA-containing leucocytes in the pellet. The leucocyte-containing pellet is then treated with SE

buffer (75 mM NaCl, 25 mM Na₂EDTA; pH 8.0), pronase E (10 mg/ml) and 20 % SDS at 55°C overnight. All proteins are precipitated and removed from the proteolysed leucocytes by adding 6 M NaCl solution. Thereafter, genomic DNA is precipitated and washed with 100 % and 70 % ethanol successively. Finally, DNA is resuspended in TE buffer (10 mM Tris-HCl, 1.0 mM Na₂EDTA; pH 8.0).

3.1.2 Extraction of PAC DNA

PAC DNA is isolated according to the conventional alkaline lysis method (Sambrook et al. 1989). After centrifuging the overnight culture, pelleted bacteria are resuspended in solution I [25 mM Tris-HCl (pH 8.0), 50 mM glucose, 10 mM Na₂EDTA] and lysed in solution II (0.2 N NaOH, 1 % SDS). Denatured genomic DNA and proteins are precipitating with 3 M NaOAc (pH 5.0), while renatured PAC DNA remains soluble. After centrifugation, the supernatant containing soluble PAC DNA is further purified from proteins by phenol/chloroform extraction. PAC DNA is then precipitated in 100 % ethanol, washed in 70 % ethanol and resuspended in TE buffer (10 mM Tris-HCl, 1.0 mM Na₂EDTA; pH 8.0).

3.1.3 Extraction of plasmid DNA

Bacterial plasmid DNA is isolated from bacterial overnight cultures (LB media) supplemented with appropriate antibiotics. For the extraction of plasmid DNA, kits are used that are based on the alkaline lysis method (Sambrook et al. 1989). Generally, these kits make use of centrifugation columns with a high DNA-binding affinity, replacing the time-consuming phenol/chloroform extractions and ethanol precipitation procedures. Depending on the volume of overnight culture, plasmid DNA is extracted by Miniprep or „minipreps” from 1 – 5 ml of saturated *E. coli* culture (Nucleospin[®]Plasmid, Macherey-Nagel, Düren, Germany); „Midipreps” isolate plasmid DNA from approximately 25 ml and „maxipreps” from approximately 100 ml of bacterial culture with high-copy plasmid DNA (QIAfilter[™]Plasmid Midi/Maxi, Qiagen, Hilden, Germany).

3.2 QUANTIFICATION OF DNA

Quantitative and qualitative DNA analysis is performed by agarose gel electrophoresis. Depending of the approximate size of dsDNA, agarose gels with final concentrations of 0.6 % to 4.0 % agarose in 1 x TBE (89mM Tris-HCl, 89mM boric acid, 2mM Na₂EDTA; pH 7.4) are used. While 1.0 % agarose gels generally cover a large spectrum of dsDNA fragment sizes, 0.6 % agarose gels are used to separate „large” (>2 kb) and agarose

gels up to 4 % are used for separating „small” dsDNA fragments (<0.2 kb). dsDNA is separated electrophoretically (~140 Volt, 30 min) and visualized by ethidium bromide intercalation under UV-light. The 1 Kb Plus DNA Ladder (Invitrogen, Karlsruhe, Germany) and the High DNA Mass Ladder (Invitrogen, Karlsruhe, Germany) are used for accurate size and mass estimations, respectively. Alternatively, the concentration of dsDNA is determined by UV spectrophotometry at a wavelength of 260 nm. The absorption value one corresponds to a concentration of 50 µg/ml dsDNA and a concentration of 33µg/ml oligonucleotide primer.

3.3 RESTRICTION ENZYME DIGESTION

Restriction enzymes are purchased from New England Biolabs (New England Biolabs, NEB, Frankfurt am Main, Germany). A typical restriction enzyme digest includes genomic, plasmid or PAC DNA, a 1 x buffer supplied by the company and the restriction enzyme. As a rule of thumb, one unit of enzyme cuts 1 µg DNA in one hour. Depending on the type and quality of DNA, enzyme digests are incubated between 1 hr (plasmid or PAC DNA) and 12 hrs (genomic DNA) at 37°C (or optimal temperatures recommended by the manufacturer).

3.4 SOUTHERN BLOT

Developed by Ed Southern (1975), Southern blotting is the transfer of DNA fragments onto a membrane via an upward capillary action and high salt buffer (Sambrook et al. 1989).

3.4.1 Labeling of DNA probes

Probes for hybridization are generated by PCR amplification (see VI, 3.6) and purified by agarose gel excision using the Nucleospin[®] Extract kit (Macherey-Nagel, Düren, Germany). By means of random priming following a modified protocol of Feinberg and Vogelstein (1984), the purified PCR product is labeled with [α -³²P]dCTP (Hartmann, Braunschweig, Germany). Briefly, 34 µl H₂O containing 20 ng PCR product is denatured (3min, 100°C) and immediately incubated on ice (3 min, 0°C). In a final volume of 50 µl, the labeling reaction contains 20 ng denatured DNA, 1 x OLB buffer [5 x OLB: 250 mM Tris-HCl (pH 8.0), 25 mM MgCl₂, 50 mM β -mercaptoethanol, 96 µM dATP, 96 µM dGTP, 96 µM dTTP, 1 M Hepes (pH 6.6), 50 U (A₂₆₀) pd(N)6], 20 µg BSA, 4 U Klenow fragment and 3 µl [α -³²P]dCTP (3 000 Ci/mmol). The labeling reaction takes place at 37°C for 3 hrs or overnight at room temperature. Afterwards, labeled probes are separated from free [α -³²P]dCTP by gel filtration chromatography using G-25 sephadex columns (Amersham-

Pharmacia-Biotech, Freiburg, Germany). Prior to hybridization, labeled probes are denatured for 5 min at 100°C.

3.4.2 DNA transfer (Southern blotting)

After restriction enzyme digestion of the genomic or PAC DNA, the restriction fragments are electrophoretically separated in a low-percentage (0.6 %) agarose gel. The depurination step (0.25 M HCl, 10 min) is optional – DNA fragments larger than 15 kb are better transferred to the blotting membrane after depurination. Then, the DNA fragments are denatured in an alkaline buffer (0.5 M NaOH, 1.5 M NaCl) twice for 10 min and are subsequently neutralized (25 mM Na₃PO₄, pH 6.5) for 15 min. In the next step, ssDNA fragments are transferred from the gel onto a nylon membrane (Nylon Hybond N⁺, Amersham-Pharmacia-Biotech, Freiburg, Germany) by capillary action. A typical blotting apparatus consists of a buffer reservoir of 10 x SSC (1.5 M NaCl, 150 mM NaCitate; pH 7.0), an elevated glass plate and a wick consisting of the gel, the nylon membrane, dry filter papers and a ~500 g weight. The transfer of ssDNA to the nylon membrane is allowed to proceed overnight. By means of UV-crosslinking, ssDNA is bound irreversibly to the membrane and may be used for several rounds of hybridization.

3.4.3 Hybridization and washing

The immobilized DNA blot is prehybridized with Church buffer [0.5 M Na₂PO₄ (pH 7.4), 1 mM Na₂EDTA (pH 8.0), 7 % SDS) at 65°C for a minimum of 1 hr. Then, a [α -³²P]dCTP labeled probe (see VI, 3.4.1) is added to the Church buffer and hybridization takes place overnight at 65°C in a rotating hybridization oven. After hybridization, the blot is washed at least three times for 15 min, each with SSPE/SDS washing buffer (20 x SSPE: 3 M NaCl, 200 mM NaH₂PO₄, 20 mM Na₂EDTA) at 42°C. Stringency of washing conditions is increased by decreasing the SSPE concentration of the washing buffer stepwise from 2 x SSPE to 0.1 x SSPE. X-ray films (RETINA XBD, Fotochemische Werke, Berlin, Germany) are exposed to the hybridized blots for 1 – 2 weeks.

3.5 ISOLATION OF GENOMIC PAC CLONES

To isolate genomic clones containing the murine *Vmd2* gene, RCPI-21, a 129/SvevTACfBr RPCI-21 murine P1-derived bacterial artificial chromosome (PAC) library (Roswell Park Cancer Institute, Buffalo, USA) is screened with a 1.3 kb probe generated by PCR amplification from murine genomic DNA (oligonucleotide primer pair

TU15newF2/VMD2-R1, Table 10A). The 1.3 kb probe spanning from murine *Vmd2* exon four to exon six is first labeled with [α - 32 P]dCTP and then hybridized at 65°C to the PAC library filters (see VI, 3.4.1 and 3.4.3). The final wash is in 0.5 x SSPE / 0.1% SDS for 15 min. Four positive clones (472E12, 472P7, 586H16 and 599E13) are isolated and PAC DNA is extracted by applying the alkaline lysis method (see VI, 3.1.2).

3.6 PCR AMPLIFICATION

Standard PCR amplification is performed in a volume of 25 μ l in 1 x buffer [50 mM KCl, 10 mM Tris-HCl (pH 8.3), 1.0 mM MgCl₂, 0.01% gelatin] using ~100 ng template DNA, 0.4 μ M forward and reverse primers (Metabion, Martinsried, Germany or MWG Biotech, Ebersberg, Germany), 1 U *Taq* polymerase and 100 μ M dNTPs (Peqlab, Erlangen, Germany). Samples are amplified by PCR in 33 cycles, each cycle consisting of 30 s at 94°C (denaturing temperature), 30 s at the given annealing temperature and 30 s at 72°C (extension temperature). The sequence composition of all forward and reverse oligonucleotide primers used for PCR amplification are listed in Table 10A, 10B, 10C, 11A and 11B. The oligonucleotide-specific annealing temperature is empirically calculated (annealing temperature = {2 x (A + T) + 4 x (C + G)} - 2°C) and experimentally adjusted. Modifications of the standard PCR reaction include differences in Mg²⁺-concentrations (1.0 or 1.5 mM) and supplementation with 4 % formamide. Generally, the extension time of amplicons of 1 kb or smaller is 30 s, but for larger PCR products an additional time of 1 min per 1 kb is added. Especially for cloning PCR products a more accurate, proof-reading *Taq* polymerase with 3' \rightarrow 5' exonuclease activity is used (Platinum® *Taq* DNA Polymerase High Fidelity, Invitrogen, Karlsruhe, Germany).

3.7 DIRECT SEQUENCING OF PCR PRODUCTS

Prior to the cycle sequencing reaction, amplified PCR products are treated with shrimp alkaline phosphatase (USB, Cleveland, USA) and exonuclease I (USB, Cleveland, USA) to remove ssDNA and unincorporated dNTPs, respectively. Alternatively, the PCR products are purified by gel excision after agarose gel electrophoresis with a kit (Nucleospin® Extract, Macherey-Nagel, Düren, Germany). Fluorescence-labeling is performed in 24 cycles of denaturing (96°C, 30 s) and annealing/elongation (60°C, 4 min), using the BigDye terminator kit (Applied Biosystems, Weiterstadt, Germany) and the respective forward or reverse primer. After ethanol precipitation with 0.1 Vol 3 M sodium acetate (pH 4.6) and 2.5 Vol 100 % ethanol, the sequencing products are analyzed on an automated capillary sequencer and

evaluated with Sequencing Analysis version 3.6.1 and the Sequencing Navigator software packages (ABI Prism 310, Applied Biosystems, Weiterstadt, Germany).

Table 10 Oligonucleotide primer sequences and amplicon sizes

A. Generation of radiolabeled hybridization probes

Primer Pair	Sequence (5'→3')	Amplicon Size
TU15-newF2	CAGTACGAGAACCTGCCGTG	1.3 kb
mVMD2-R1	GCATACAGCTGTCCACACTGAG	
hAB3-F	CTGAATCCGGCTCCACCTCAACATCAG	282 bp
hAB3-R	GAAGTAGAGCGGCCGCTTCCAGGCCTTGTGTCTTCC	

B. VMD2 mutation screening

Primer Pair	Sequence (5'→3')	Amplicon Size
TU15-ex2F	CCCTACAAAACCCCAATCG	272
TU15-ex2R	CCAGCCACATCCTTCCCAG	
TU15-ex3F	AGTCTCAGCCATCTCCTCGC	211
TU15-ex3R	TGGCCTGTCTGGAGCCTG	
TU15-ex4F	AGAAAGCTGGAGGAGCCGA	423
TU15-ex4R	TCCACCCATCTCCATTCTCCT	
TU15-ex5F	GCCATCCCTTCTGCAGGTT	239
TU15-ex5R	GCGGCAGCCCTGTCTGTAC	
TU15-ex6F	GGGGCAGGTGGTGTTCAGA	150
TU15-ex6R	GGCAGCCTCACCAGCCTAG	
TU15-ex7F	TGATTTACAGGGTCCCACCTAG	295
TU15-ex7R	CATCCTCGTCTCAGGCAGCT	
TU15-ex8F	AGGGTTTACAGAGCCTCACCTG	158
TU15-ex8R	CACCTTGGGGAAGGTCCATG	
TU15-ex9F	CCTCCAAGTCATCAGGCACATA	289
TU15-ex9R	CTAGGCAGACCCCTGCACTAG	
TU15-ex10_F1	ACTGGCTCAGCCCTGCATC	340
TU15-ex10_R1	GTGGGGCACTGTAGTAGCCTG	
TU15-ex10F_F1H	CCTTCAAGTCTGCCCACTG	417
TU15-ex10F_F1H	CCTTCAAGTCTGCCCACTG	
TU15-ex11F	GGTACCTTCCATACTTATGCTG	149
TU15-ex11.2-R	GTCTATGGCTGTGACTGGAT	

C. Characterization of murine genes *Vmd2* and *Vmd2L2*

Primer Name	Sequence (5'→3')	Gene
bov4-b	GAAGTAGAGCGGCCGCTTAGGAATGTGCTTCATCCC	<i>Vmd2</i>
TU15newR2	ATCTCATCCACGCCAACAG	<i>Vmd2</i>
mVMD2-F3	AGCTACATCCAGCTCATCCC	<i>Vmd2</i>
mVMD2-F5	TACAGCTTTTTCCTTGCATG	<i>Vmd2</i>
mVMD2-F6	GCGTACTCAGTGTGGACAGCTGTATGC	<i>Vmd2</i>
mVMD2-F8	TCTATTGGCTACCACTTCGG	<i>Vmd2</i>
mVMD2-F11	CTAGTGGCCTGAGTGTGTGT	<i>Vmd2</i>
mVMD2-F12	TTGGAATCCCTGACTAGCCC	<i>Vmd2</i>
mVMD2-R1	GCATACAGCTGTCCACACTGAG	<i>Vmd2</i>
mVMD2-R2	TGGCAAACCACACCCAGGGC	<i>Vmd2</i>
mVMD2-R3	CCACCGGACCCGAACAGCC	<i>Vmd2</i>
mVMD2-R4	CACCTGATTCTGACCTGCC	<i>Vmd2</i>
mVMD2-R5	CATGCAAGGAAAAAGCTGTA	<i>Vmd2</i>
mVMD2-R7	AACAGCCAGTTGTACCTGACTC	<i>Vmd2</i>
mVMD2-R8	TCTCAAAATCATCATCGTCCTC	<i>Vmd2</i>
mVMD2-R9	CCTCATCCTTGCCCTCCACG	<i>Vmd2</i>
mVMD2-R10	GAGATAAATGCTGAGGCTGG	<i>Vmd2</i>
mVMD2-R12	AACACAAGTTTCCCCACAG	<i>Vmd2</i>
mVMD2-R13	AGTGTCTTGGTAGGGCTGT	<i>Vmd2</i>
mTU53-F5	CTGTTACCCATGGAAGCTCA	<i>Vmd2L2</i>
mTU53-R5	GTCAGACCTTCCATCACGG	<i>Vmd2L2</i>

Table 11 Oligonucleotide primer sequences for cloning (A) and screening (B)**A. Generation of PCR-based clone inserts**

Purpose	Primer Pair	Enzyme	Sequence (5'→3')	Cloning Vector ^a
GST / MBP fusion protein	AB2-F	<i>EcoR</i> I	CTGAATTCATTTCCTTCGTGCTGG	pGEX-4T3 / pMal-cxh
	AB2-R	<i>Not</i> I	GAAGTAGAGCGGCCGCTTCGACGAAGCCCGACAC	
GST / MBP fusion protein	AB3-F	<i>EcoR</i> I	CTGAATTCGGCTCCACCTTCAACATCAG	pGEX-4T3 / pMal-cxh
	AB3-R	<i>Not</i> I	GAAGTAGAGCGGCCGCTTCAGGCCTTGTTGCTTCC	
GST / MBP fusion protein	bov4-a	<i>EcoR</i> I	CTGAATTCGAGTTTAACCTGATGGACATG	pGEX-4T3 / pMal-cxh
	bov4-b	<i>Not</i> I	GAAGTAGAGCGGCCGCTAGGAATGTGCTTCATCCC	
partial knock-in construct	mVMD2-XmaI-F	<i>Xma</i> I	GTCCCCCGGGAGCTACATCCAGCTCATCCC	pCR2.1
	mVMD2-SacI-R	<i>Sac</i> I	ACCACCCAATGAGCTCTACC	
partial knock-in construct	mVMD2-NdeI-F	<i>Nde</i> I	GTCTAGGGAGCTGCATATGG	pCR2.1
	mVMD2-SacI-R	<i>Sac</i> I	ACCACCCAATGAGCTCTACC	
partial knock-in construct	mVMD2-ClaI-F	<i>Cla</i> I	GCTGATCGATATTGGGTGGTGTGCCATG	pGEM-T
	mVMD2-ClaI-R2	<i>Cla</i> I	GCTGATCGATGGGTCTCCTACTGGCCTGAA	
partial knock-out construct	mVMD2-SacII-F	<i>Sac</i> II	TACGTCCGCGGAGCTACATCCAGCTCATCCC	pGEM-T
	mVMD2-SnaBI-R	<i>SnaB</i> I	AGCTTTACGTACGCTGTGTGTACACCAATGGGA	

^a Cloning vectors pGEX-4T3, pMAL-cxh, pCR2.1 and pGEM-T are purchased from Amersham-Pharmacia-Biotech (Freiburg, Germany) NEB (Frankfurt am Main, Germany), Invitrogen (Karlsruhe, Germany) and Promega (Mannheim, Germany), respectively.

B. Screening of ES clones

Purpose	Primer Pair	Sequence (5'→3')	Amplimer Size
screening for positive knock-in ES clones (5'-PCR analysis)	mVMD2-F17	GATCAGCAGCTGTTGTTTGA	2.0 kb
	neo-F	CATCGCCTTCTATCGCCTTC	
testing the quality of neomycin-resistant knock-in ES clones	mVMD2-NdeI-F	GTCTAGGGAGCTGCATATGG	0.5 kb
	neo-F	CATCGCCTTCTATCGCCTTC	
screening for positive knock-out ES clones (5'-PCR analysis)	mVMD2-F17	GATCAGCAGCTGTTGTTTGA	1.9 kb
	lacZ-R2	GCTGCAAGGCGATTAAGTTGGGT	
verification of positive knock-out clones (3'-PCR analysis)	pHM2-3'-F	CAACGCGTTGGAGTACCGAG	4.5 kb
	mVMD2-R15	CAGCCTCCTCTTTTGACCAA	

3.8 MUTATION SCREENING OF HUMAN VMD2

Genomic DNA is extracted from blood lymphocytes of patients subjected to *VMD2* mutation screening (see VI, 3.1). All ten coding exons of *VMD2* are screened by using a PCR-based method. PCR amplification of *VMD2* exons 2 – 9, 10I and 10II is accomplished with the respective pairs of forward and reverse oligonucleotide primers (Table 10B), and include the exonic sequences as well as sequences of the flanking splice donor and acceptor sites (see VI, 3.6). Identification of sequence variants is performed on an automated sequencing system by sequencing with both forward and reverse oligonucleotide primers (see VI, 3.7).

3.9 CLONING OF PCR PRODUCTS**3.9.1 T-overhang cloning**

If using Taq Polymerase for PCR amplification, the enzyme leaves single A overhangs at the ends of replicated molecules. To take advantage of this, a pre-prepared vector with T-overhangs simplifies the ligation of such PCR products. By using kits from Promega (pGEM[®]-T vector, Mannheim, Germany) or Invitrogen (pCR[™] 2.1/pCR[™] II vector, Karlsruhe,

Germany), the amplified A-overhang PCR products (< 2 kb) are directly ligated with the respective T-overhang vectors and transformed into *E. coli* XL1-blue electrocompetent cells.

3.9.2 Cloning by introducing restriction sites

It is possible to introduce restriction sites to either side of the PCR product during amplification. For this, oligonucleotide primers are designed containing a template specific sequence as well as an additional restriction enzyme specific sequence at their 5'-ends. Usually two different cutting sites of restriction enzymes are used to ensure directional insertion of the PCR product into the prepared vector. After amplification, the PCR product is digested with the relevant restriction enzymes to generate cohesive or blunt ends (see VI, 3.3). The vector is treated with the same restriction enzymes. In order to ensure ligation with inserts and decrease self-ligation, the linearized vector ends are dephosphorylated (see VI, 3.9.3). Then, complementary ends of vector and insert are ligated (see VI, 3.9.4) and subsequently transformed into electrocompetent *E. coli* XL1-blue cells. Table 11A lists all oligonucleotide primers used for restriction enzyme-based PCR cloning the corresponding vectors.

3.9.3 Vector modifications

Novel restriction enzyme cutting sites are introduced into vectors by adding linkers. A linker is a pair of complementary primers containing one or more desired enzyme sites. For example, two novel sites *Sac* II (CCGCGG) and *Sal* I (GTCGAC) are added to the plasmid construct pGADT7-G3-G2*-neo (clone # 23) via one unique cutting site (*Cla* I) present within the vector. First, 1 µg of forward primer (Linker-CSSC-F 5'-CGATCCGCGGGGATGTCGACAT) and 1 µg of reverse primer (Linker-CSSC-R 5'-CGATGTCGACATCCCCGCGGAT) plus 1 x ligation buffer (NEB, Frankfurt am Main, Germany) are denatured at 75°C (3 min) in a final volume of 10 µl. A gradual decrease of the temperature from 75°C to 25°C results in reannealing of the complementary primers, forming double-stranded oligomers (linkers) with sticky *Cla* I restriction sites on either end. Thereafter, the linkers are inserted into the *Cla*I-linearized vector by ligation (see VI, 3.9.4).

In most cases, linearized vectors are dephosphorylated to prevent self-ligation. This step is important if a single enzyme is used to perform non-directional cloning. In a final volume of 100 µl, the dephosphorylation reaction includes 88 µl linearized vector DNA (~10 µg), 10 µl 10 x shrimp alkaline phosphatase buffer and 2 µl shrimp alkaline phosphatase

(USB, Cleveland, USA). The reaction is incubated for 2 hrs at 37°C. Prior to ligation (see VI, 3.9.4), enzyme and buffer are removed by using the Nucleospin[®] Extract kit (Macherey-Nagel, Düren, Germany).

3.9.4 Ligation

The ligation reaction is incubated overnight at 14°C – 16°C in a final volume of 10 µl, including a 1:3 ratio of vector to insert DNA template, 1µl T4 ligase and 1 x ligation buffer (NEB, Frankfurt am Main, Germany). By electroporation, 1 µl ligated product is transformed into electrocompetent *E. coli* XL1-blue cells.

3.10 SITE-DIRECTED MUTAGENESIS

For generating a set of constructs carrying Best disease-associated *VMD2* mutations, QuikChange[™] site-directed mutagenesis is applied (Stratagene, Amsterdam, Netherlands). A total number of 23 mutations, including 21 missense mutations and two in-frame deletions are introduced into the cDNA of human *VMD2*. Following a four-step protocol, the wild-type gene of interest (here, the full-length cDNA of human *VMD2*) is first cloned into an appropriate vector (pcDNA3.1, Invitrogen, Karlsruhe, Germany). In the second step, the supercoiled dsDNA construct (pcDNA3-VMD2) as template, a set of complementary primers (Table 12) containing the desired mutation and PfuTurbo[™] DNA polymerase (Stratagene, Amsterdam, Netherlands) are the main components of 16 cycles of amplification. Thirdly, the reaction mix is digested with *Dpn* I, an enzyme which exclusively digests methylated DNA. Due to its unmethylated status, nicked circular strands with incorporated mutagenic primers are not affected by *Dpn* I digestion. However, the parental non-mutated dsDNA is methylated, therefore digested and removed. Finally, the remaining mutated dsDNA is transformed into commercially available XL-10Gold[®] ultracompetent cells by heat-shock (Stratagene, Amsterdam, Netherlands) or into electrocompetent XL10-blue cells by electroporation (Stratagene, Amsterdam, Netherlands). The entire coding sequence (2.2 kb) of manipulated *VMD2* is checked by direct sequencing (see VI, 3.7).

Table 12 Oligonucleotide primer sequences for site-directed mutagenesis

<i>Forward Primer</i>		<i>Reverse Primer</i>	
<i>Name</i>	<i>Sequence (5'→3')</i>	<i>Name</i>	<i>Sequence (5'→3')</i>
hVMD2-T6P-F	ATGACCATCACTTACCCAAGCCAAGTGGCT	hVMD2-T6P-R	AGCCACTTGGCTTGGGTAAGTGTGGTCAT
hVMD2-A10T-F	ACACAAGCCAAGTGACTAATGCCCGCTTAG	hVMD2-A10T-R	CTAAGCGGGCATTAGTCACTTGGCTTGTGT
hVMD2-L21V-F	CCTTCTCCCGCTGGTGTGTGTGGCGGG	hVMD2-L21V-R	CCC GCCAGCACAGCACCAGGCGGGAGAAGG
hVMD2-W24C-F	CCTGCTGTGTGCTGTGCGGGCAGCATCTA	hVMD2-W24C-R	TAGATGCTGCCCGACAGCACAGCAGCAGG
hVMD2-R25Q-F	TGCTGTGTGCTGGCAGGGCAGCATCTACA	hVMD2-R25Q-R	TGTAGATGCTGCCCTGCCAGCACAGCAGCA
hVMD2-R47H-F	CTACTACATCATCCACTTTATTATAGGCT	hVMD2-R47H-R	AGCCTATAAATAAAGTGGATGATGTAGTAG
hVMD2-L82V-F	CCATTTCTCTCGTGGTGGGCTTCTACGTGA	hVMD2-L82V-R	TCACGTAGAAGCCCACCACGAAGGAAATGG
hVMD2-Y85H-F	TCGTGTGGGCTTCCACGTGACGCTGGTCG	hVMD2-Y85H-R	CGACCAGCGTCACGTGGAAGCCCAGCACGA
hVMD2-R92S-F	CGCTGGTCGTGACCAGCTGGTGGAAACCAGT	hVMD2-R92S-R	ACTGGTTCCACCAGCTGGTCCAGCACCAGCG
hVMD2-P101T-F	AGTACGAGAACCTGACGTGGCCCGACCGCC	hVMD2-P101T-R	GGCGGTGCGGGCCACGTGAGTTCTCGTACT
hVMD2-R218C-F	AGATGAACACCTTGTGTACTCAGTGTGGAC	hVMD2-R218C-R	GTCCACTGAGTACACAAGGTGTTTCATCT
hVMD2-L224M-F	CTCAGTGTGGACACATGTATGCCTACGACT	hVMD2-L224M-R	AGTCGTAGGCATACATGTGTCCACACTGAG
hVMD2-Y227N-F	GGACACCTGTATGCCAACGACTGGATTAGT	hVMD2-Y227N-R	ACTAATCCAGTCGTTGGCATAACAGGTGTC
hVMD2-V235M-F	ATTAGTATCCCACTGATGTATACACAGGTG	hVMD2-V235M-R	CACCTGTGTATACATCAGTGGGATACTAAT
hVMD2-T237R-F	TCCCACTGGTGTATAGACAGGTGGTGACTG	hVMD2-T237R-R	CAGTCACCACCTGTCTATACACCAGTGGGA
hVMD2-A243V-F	CAGGTGGTACTGTGACGGTGTACAGCTTC	hVMD2-A243V-R	GAAGCTGTACACCGTCACAGTACCACCTG
hVMD2-F276L-F	CGTTGTGCCCGTCTGACGTTCTGCAGTT	hVMD2-F276L-R	AACTGCAGGAACGTCAAGACGGGCACAACG
hVMD2-delF281-F	CTTCACGTTCTGCAGTTCTTCTATGTTGGCTGG	hVMD2-delF281-R	CCAGCCAACATAGAAGAAGTGCAGGAACGTGAAG
hVMD2-delI295-F	AGGTGGCAGAGCAGCTCAACCCCTTTGGAGAGG	hVMD2-delI295-R	CCTCTCCAAAGGGTTGAGCTGCTCTGCCACCT
hVMD2-P297A-F	GAGCAGCTCATCAACGCCTTTGGAGAGGAT	hVMD2-P297A-R	ATCCTCTCCAAAGCGTTGATGAGCTGCTC
hVMD2-D301E-F	CCCCTTTGGAGAGGAGGATGATGATTTTGA	hVMD2-D301E-R	TCAAATCATCATCCTCCTCTCCAAAGGGG
hVMD2-F305S-F	AGGATGATGATGATCTGAGACCAACTGGA	hVMD2-F305S-R	TCCAGTTGTTCTCAGAATCATCACATCCT
hVMD2-V311G-F	AGACCAACTGGATTGGCGACAGGAATTTGC	hVMD2-V311G-R	GCAAATCCTGTGCCAATCCAGTTGGTCT
mVMD2-Y227N-F	ACTTATCCAGTCGTTGGCATAACGCTGTCC	mVMD2-Y227N-R	GGACAGCTGTATGCCAACGACTGGATAAGT

4 RNA-SPECIFIC METHODS

4.1 TOTAL RNA ISOLATION

Total RNA is isolated from (i) 12 tissues (brain, spinal cord, eye, heart, lung, liver, spleen, kidney, colon, skeletal muscle, trachea, testis) of a sacrificed male mouse (*Mus musculus domesticus*, BL/6) and from (ii) transiently transfected COS7 cells. In the former case, total RNA is then analyzed by RT PCR, real time quantitative RT PCR and 3'-RACE experiments; in the latter case, total RNA is analyzed by Northern blotting. Generally, total RNA is prepared from murine tissues and transfected monolayers of COS7 cells by using the standard guanidin isothiocyanate method (Pqqlab, Erlangen, Germany). According to the manufacturer's instructions, cells or tissues are homogenized in peqGOLD RNAPure™ buffer, separated from proteins by adding chloroform and precipitated with 0.7 vol isopropanol. RNA pellets are washed in 70 % ethanol and resuspended in RNase-free H₂O. Quality and quantity of isolated total RNA is controlled in an 1.2 % agarose gels containing formaldehyde.

4.2 NORTHERN BLOTTING

RNA samples (extracted from transiently transfected COS7 cells, see VI, 4.1) are electrophoretically separated in an 1.2 % (w/v) agarose gel containing 1 % (v/v) formaldehyde at 50 – 70 V for 3 hrs. For the gel solution and as electrophoresis buffer, MOPS buffer (10 x Morpholinopropanesulfonic acid (MOPS): 0.2 M MOPS, 50 mM NaOAc, 10 mM Na₂EDTA; pH 7.0) is used. 2 µl total RNA and 18 µl RNA loading buffer (1 x MOPS, 50 % formamide, 18.5 % formaldehyde, 0.04 % bromphenol blue, 10 µg ethidium bromide) are mixed and denatured for 10 min at 65°C. To estimate the size of the RNA transcripts, 3 µl RNA Standard (Promega, Mannheim, Germany) is run parallel to the probes. Integrity of total RNA is checked by UV illumination: intact, non-degraded RNA displays a RNA smear as well as two intensive RNA signals of 4.8 kb (28S ribosomal RNA) and 1.9 kb (18S ribosomal RNA). Total RNA is then transferred overnight to a Nylon Hybond N⁺ membrane (Amersham-Pharmacia-Biotech, Freiburg, Germany) by an upward capillary force in 20 x SSC buffer (3 M NaCl, 0.3 M NaCitrate; pH 7.0) identical to Southern blotting (see VI, 3.4.2). From here onwards, the procedure of hybridization with a [α -³²P]dCTP-labeled probe, the washing of filters and autoradiography does not differ from the Southern blot protocol (see VI, 3.1). A [α -³²P]dCTP-labeled probe is generated with primers AB3-F and AB3-R (Table 10A) to detect human *VMD2* transcripts.

4.3 FIRST STRAND cDNA SYNTHESIS

First strand cDNA synthesis is catalyzed by the reverse transcriptase (RT) enzyme Superscript™ II (Gibco-BRL, Karlsruhe, Germany). Reverse transcription is performed in a total volume of 20 µl, containing 2 µl total RNA (~5 µg), 1 µl oligo(dT)₁₂₋₁₈ primer (0.5 µg), 1 µl dNTPs (10 mM dATP, 10 mM dCTP, 10 mM dGTP, 10 mM dTTP), 9 µl DEPC-H₂O, 4 µl 5 x reaction buffer [250 mM Tris-HCl (pH 8.3), 375 mM KCl, 15 mM MgCl₂], 2 µl DTT (0.1 M) and 1 µl Superscript™ II (200 U).

The AP primer, 5' GGCCACGCGTCGACTAGTACTTTTTTTTTTTTTTTTTTTT, is used as oligo(dT)₁₂₋₁₈ primer. A mixture of total RNA, water, primer and dNTPs is denatured for 2 min at 70°C and immediately chilled on ice. Then, the remaining components are added (5 x reaction buffer, DTT and RT enzyme) and the reaction is incubated for 50 min at 42°C. The reaction is stopped by inactivating the enzyme for 15 min at 70°C. To degrade the original RNA template, the first strand cDNA is treated with RNase H (2 U) for 20 min at

37°C. First strand cDNA is stored at -20°C and cycles of freezing and thawing are minimized as far as possible.

4.4 3'-RAPID AMPLIFICATION OF cDNA ENDS (3'-RACE)

To extend the *Vmd2L3* cDNA transcript, 3'-extension PCR (see VI, 3.6) is performed on cDNA isolated from murine heart tissue. According to a modified version of the manufacturer's protocol (Life Technologies, Karlsruhe, Germany), 3'-RACE consists of two steps of PCR amplification. The first PCR reaction includes one gene-specific primer mTU52-F4 (Table 13D) and the AUAP-primer (5'-GGCCACGCGTCGACTAGTAC) as well as a murine heart cDNA as template. In the second amplification step the first PCR product is diluted 1:100 and used as template DNA. The DNA is then amplified with a nested gene-specific forward primer mTU52-F5 (Table 13D) and AUAP as reverse primer. Sequence analysis of nested RT PCR product(s) is performed by utilizing the BigDye terminator kit and the ABI 310 automated sequencer (see VI, 3.7).

4.5 REVERSE TRANSCRIPTASE (RT) PCR

For RT PCR experiments, a regular PCR (see VI, 3.6) is carried out using first strand cDNA (see VI, 4.3) as template and multiple sets of forward and reverse primers as given in Table 13.

Table 13 Oligonucleotide primer sequences for RT PCR analysis

A. Murine <i>Vmd2</i> and β -Gus			B. Murine <i>Vmd2L1</i>		
Gene	Primer Name	Sequence (5'→3')	Gene	Primer Name	Sequence (5'→3')
<i>Vmd2</i>	mVMD2-F18	ATGTACTGGAACGAGGCAGC	<i>Vmd2L1</i>	mTU51-NotI-F	AAGGAAAAAAGCGGCCGCCCTTCTCCATTGGCCACACT
<i>Vmd2</i>	mVMD2-F19	GACCCAAGCCCACCTACTGC	<i>Vmd2L1</i>	mTU51-F1	ACCGTCACCTACACAGCCAG
<i>Vmd2</i>	mVMD2-R14	ATGTTCTGTGGGGCTCTCTG	<i>Vmd2L1</i>	mTU51-F2	GCTACAAAGACCACACCCTG
<i>Vmd2</i>	mVMD2-R15	CAGCCTCCTCTTTGACCAA	<i>Vmd2L1</i>	mTU51-F3	CAGGTCTGGGAGAATAAATG
<i>Vmd2</i>	mVMD2-R18	CTTGTGTGCCTTTGACTGGG	<i>Vmd2L1</i>	mTU51-F6	ATGTGTTTCGGAGCAAATGTG
β -Gus	mgus-ex11F	GACCCGCTCGCATGTTTACG	<i>Vmd2L1</i>	mTU51-NotI-R	AAGGAAAAAAGCGGCCGCTAGGTAGGTGTCCGTAGGGG
β -Gus	mgus-ex12R	GCCCTGAACCGTGACCTCC	<i>Vmd2L1</i>	mTU51-R1	TTGAAGACTGCTGTGCTAAC
			<i>Vmd2L1</i>	mTU51-R3	AGTTGGTCTCAAAGTCGTCGTCG
			<i>Vmd2L1</i>	mTU51-R4	GCTTTCTGAAGGCCTAGCTA
			<i>Vmd2L1</i>	mTU51-R6	TGTGCAGGGTCTAGGAACTGA
C. Murine <i>Vmd2L2</i>			D. Murine <i>Vmd2L3</i>		
Gene	Primer Name	Sequence (5'→3')	Gene	Primer Name	Sequence (5'→3')
<i>Vmd2L2</i>	mTU53-F1	GGAGGGGCAGCATCTACAAG	<i>Vmd2L3</i>	mTU52-F1	CTCCAGTAAAGTAGCAAATG
<i>Vmd2L2</i>	mTU53-F3	CATCGGTTTTGGTGCTACGT	<i>Vmd2L3</i>	mTU52-F2	GCAGCCTCTTATTTGGTTAC
<i>Vmd2L2</i>	mTU53-F4	CTGAACAAGTATCGGGCCAA	<i>Vmd2L3</i>	mTU52-F3	GCCACAGCAGCAGGAGAAGT
<i>Vmd2L2</i>	TU53-Fseq3	CAGCTGATGTGCGTCATCTC	<i>Vmd2L3</i>	mTU52-F4	TTGCCAAAGATGAAGAAGGA
<i>Vmd2L2</i>	TU53-Fseq4	TCGCTCTGTGTACTTTTGG	<i>Vmd2L3</i>	mTU52-F5	CCGTCCTTCTGGGCTCAAC
<i>Vmd2L2</i>	mTU53-R1	AAAGGGTGAAGAGGAATAGA	<i>Vmd2L3</i>	mTU52-R1	GAGCGGAAGATGAGCAGGGA
<i>Vmd2L2</i>	mTU53-R3	GCGACTCAGCAGCTATGGCC	<i>Vmd2L3</i>	mTU52-R2	GTTGAGCCAGAAAAGGACGG
<i>Vmd2L2</i>	mTU53-R4	ATAGCAGGCGAGGGCACACC	<i>Vmd2L3</i>	mTU52-R3	TGGAGGAGAGTGAAGATGGG
			<i>Vmd2L3</i>	mTU52-R4	CTCTGGCTGTGAAGTCTGCT

4.6 REAL TIME QUANTITATIVE RT PCR

Real time quantitative RT PCR is performed on the RotorGene 4.6 system (Corbett Research, Sydney, Australia), either using the 72-well-rotor and a reaction volume of 10 μ l or the 36-well-rotor and a reaction volume of 25 μ l. For each 10 μ l (25 μ l) SYBR green PCR reaction (Schneeberger et al. 1995), 0.8 μ l (2 μ l) cDNA template, each 0.3 μ l (0.75 μ l) forward primer and reverse primers (10 pmol), 2 μ l (5 μ l) SYBR green (2.5 x concentrated, Sigma-Aldrich, München, Germany), 1 μ l (2.5 μ l) 10 x PCR buffer [500 mM KCl, 100 mM Tris-HCl (pH 8.3), 10 mM MgCl₂, 0.1% gelatin], 0.2 μ l (0.5 μ l) *Taq* polymerase and 0.4 μ l (1 μ l) dNTPs (100 μ M, Peqlab, Erlangen, Germany) and 5 μ l (12.5 μ l) PCR-grade water are mixed. The tested cDNA samples are derived from 12 different murine tissues by RNA isolation (see VI, 4.1) and cDNA synthesis (see VI, 4.3). Each PCR reaction was performed in triplicate and repeated at least twice. Suitable oligonucleotide primers sequences are designed according to suggestions from the MGB Eclipse™ software³⁸ (Amersham-Pharmacia-Biotech, Freiburg, Germany); primers are synthesized by MWG Biotech (Ebersberg, Germany) (Table 14).

Table 14 Oligonucleotide primer sequences for real time quantitative RT PCR

<i>Gene</i>	<i>Primer Pair</i>	<i>Sequence (5'→3')</i>	<i>Amplimer Size</i>
murine <i>β-Gus</i>	mGUS-RT-F1 mGUS-RT-R1	ATGACGAACCAGTCACC TTTGCAGAGAGATACTGGAGG	108 bp
murine <i>Sdha</i>	mSDHA-RT-F1 mSDHA-RT-R1	CAAGACTGGCAAGGTTAC GAATGAGGCTGACTGTG	68 bp
murine <i>Vmd2</i>	mVMD2-RT-F1 mVMD2-RT-R1	AGAGCCCCACAGAACAT TACAGGGATGAAGCTGGCA	111 bp
murine <i>Vmd2L1</i>	mTU51-RT-F1 mTU51-RT-R1	CAACTTCCAGGTGTCCAT ATACTGGGATGCAGCAGAAG	89 bp
murine <i>Vmd2L3</i>	mTU52-RT-F1 mTU52-RT-R1	TTCCCATCTTCACTCTCC AAGGTTGCAGAGCAGCT	64 bp

PCR cycling conditions comprise an initial denaturation step at 94°C for 5 min, 45 cycles of denaturation (30 s at 94°C), annealing (30 s at 56°C) and elongation (30 s at 72°C) and a hold at 50°C for 3 min. During cycling, fluorescence data are acquired at 72°C or at higher temperatures depending on primer dimer formation (77°C – 80°C). After PCR amplification, the samples are immediately heated in 0.5°C intervals for each 5 s, from 50°C to 99°C. The change in fluorescent energy is monitored and the differential of the fluorescence curve reveals the melting temperature for each amplicon.

³⁸ MGB Eclipse™ software: <http://www.syntheticgenetics.com/ordering/Ordering.htm>

The Q-Gene program, an Excel[®]-based spreadsheet developed by Muller et al. (2002), is used to determine the PCR amplification efficiency value ($E = 10^{(-1/\text{slope})}$) as well as the mean normalized gene expression (MNE), based on the following equation:

$$\text{MNE} = \frac{\frac{(E_{\text{target}})^{\text{CT}(\text{target well 1})}}{(E_{\text{ref}})^{\text{CT}(\text{ref well 1})}} + \frac{(E_{\text{target}})^{\text{CT}(\text{target well 2})}}{(E_{\text{ref}})^{\text{CT}(\text{ref well 2})}} + \frac{(E_{\text{target}})^{\text{CT}(\text{target well 3})}}{(E_{\text{ref}})^{\text{CT}(\text{ref well 3})}}}{3}$$

5 MAMMALIAN CELL CULTURE

5.1 COS7 CELL CULTURE

Maintenance and cultivation of COS7 cells is performed according to standard protocols (Lindl and Bauer 1989). COS7 cells are cultured in 175 cm² flasks at 37°C in a 5 % CO₂ atmosphere, in Dulbecco's modified Eagle's medium (DMEM) supplemented with 15 % (v/v) foetal calf serum (FCS). Optionally, the culture media contained 50 U/ml penicillin and 50 U/ml streptomycin. For long-term storage, stock cells are kept in liquid nitrogen in DMEM containing 10 % (v/v) FCS and 10 % (v/v) dimethyl sulfoxide (DMSO).

5.1.1 Transient Transfection of COS7 cells

Transient transfection of COS7 cells is performed by means of electroporation following a modified protocol of Korn et al. (1999). A day prior to electroporation, 100 % confluent COS7 cells are passaged 1:3, to obtain cell cultures between 70 and 80 % confluency. COS7 cells are trypsinized (Gibco-BRL, Karlsruhe, Germany), rinsed in phosphate-buffered saline (1 x PBS: 137 mM NaCl, 0.3 mM KCl, 8.1 mM Na₂HPO₄, 6.7 mM KH₂PO₄; pH 7.4) and resuspended in equal aliquots of prechilled PBS-Hepes (18 mM Hepes in 1 x PBS). To each 4 mm electrode gap electroporation cuvette (BioRad, München, Germany), 800 µl cell suspension (8×10^6 cells) and 20 – 50 µg sterile plasmid DNA (pcDNA3 constructs encoding wild-type and mutant bestrophin, see VI, 3.10) are added. The cells are incubated on ice for 10 min, electroporated at 250 V and 25 µF using a GenePulser electroporator (BioRad, München, Germany) and then incubated for another 10 min on ice. Transfected COS7 cells are transferred to prewarmed tissue culture flasks containing DMEM media supplemented with 15 % (v/v) foetal calf serum, 18 mM Hepes and 50 U/ml penicillin

and 50 U/ml streptomycin. After an incubation period of 48 hrs, total RNA is isolated (see VI, 4.1), protein extracts are made (see VI, 6.1.2) and the transfected cells are stained by immunocytochemistry (see VI, 6.3).

5.1.2 The Exon Trapping System

The expression vector pSPL3b from the Exon Trapping System (Gibco-BRL, Karlsruhe, Germany) is used to evaluate the consequences of a putative splice site mutation (624 G>A) in exon 6 of *VMD2*. Genomic DNA of the affected patient carrying the heterozygous 624 G>A variant and oligonucleotide primers VMD2-EcoRI-Ex5F/VMD2-BamHI-Ex6R are used to PCR-amplify the region of interest. The resulting PCR product contains either wild-type or mutant sequence. Addition of the *EcoR* I and *BamH* I recognition sites to the oligonucleotide primers enables directional cloning of the PCR product into the pSPL3b vector which is also linearized with *EcoR* I and *BamH* I (see VI, 3.3). Wild-type (WT) and mutant (MUT) clones are selected by direct sequencing with vector-specific primers pSPL3-F and pSPL3-R (see VI, 3.7). COS7 cells are transiently transfected (see VI, 5.1.1) with the wild-type (pSPL3b-VMD2-WT) and mutant constructs (pSPL3b-VMD2-MUT), incubated for a period of 48 hours and subsequently total RNA is isolated (see VI, 4.1). A vector-/vector-specific set of primers (SD6/SA2) and a vector-/insert-specific primer pair (SD6/mVMD2-R1) is used for RT PCR analysis. After electrophoresis of the RT PCR products on a 1 % agarose gel, the PCR-fragments are excised from the gel and directly sequenced. All primers used for the exon trapping system, including for PCR-amplification, direct sequencing, cloning and RT PCR analysis are listed in Table 15.

Table 15 Oligonucleotide primer sequences for the Exon Trapping System

<i>Gene</i>	<i>Name</i>	<i>Sequence (5'→3')</i>
vector-specific	SA2	ATCTCAGTGGTATTTGTGAGC
vector-specific	SD6	TCTGAGTCACCTGGACAACC
vector-specific	pSPL3-F	CTCCTTGGGATGTTGATGAT
vector-specific	pSPL3-R	GGTTGCTTCCTTCCACACAG
human <i>VMD2</i>	VMD2 EcoRI Ex5F	CCGGAATTCGCCATCCCTTCTGCAGGTT
human <i>VMD2</i>	VMD2 BamHI Ex6R	CGACGGATCCGGCAGCCTCACCAGCCTAG
human <i>VMD2</i>	mVMD2-R1	GCATACAGCTGTCCACACTGAG
human <i>TP53</i>	p53 EcoRI Ex5F	CCGGAATTCCAGATAGCGATGGTGAGC
human <i>TP53</i>	p53 BamHI Ex6R	CGACGGATCCCCTGACAACCACCCTTA
human <i>TP53</i>	p53-Ex6-R3	AGGCGGCTCATAGGGCACCA

The efficiency of the exon trapping system is controlled by genomic DNA isolated from a Li Fraumeni syndrome patient carrying a 11 bp deletion in the splice acceptor site of IVS5 of *TP53*. Oligonucleotide primers p53-EcoRI-Ex6F/p53-BamHI-Ex6R are used for PCR

amplification/cloning and RT PCR analyses are performed with primers SD6/SA2 and SD6/p53-Ex6R3.

5.2 EMBRYONIC STEM CELL CULTURE

The production of targeted embryonic stem (ES) cells is performed according to a protocol by Maise et al. (2000). Generally, ES cells are cultured at 37°C and 6 % CO₂, on a monolayer of mitotically inactivated feeder cells. To inhibit ES cell differentiation, leukemia inhibitory factor (LIF, Gibco-BRL, Karlsruhe, Germany) is added to ES media. ES and feeder cells are cryopreserved in DMEM containing 10 % (v/v) FCS and 10 % (v/v) DMSO and frozen in liquid nitrogen.

5.2.1 Handling of feeder cells

Feeder cells are derived from primary mouse embryo fibroblasts (STO) and have been transfected with expression constructs for neo^r and LIF. Generally, feeder cells are cultured in ES media (see below) without LIF and nucleosides. When using feeder monolayers for ES cell passaging, feeder cells are first inactivated by means of mitomycin C treatment and subsequently are cultured in ES media on gelatin-coated plates. To inactivate feeder cells, 100 µl mitomycin C (1 mg/ml) (Sigma-Aldrich, München, Germany) is added to the feeder cells and incubated for 2.5 – 3 hrs at 37°C. Prior to trypsination and replating, cells are rinsed several times to remove toxic mitomycin C. The optimum time to seed ES cells on feeder cells is approximately 12 hrs after feeder cell inactivation.

5.2.2 Handling of ES cells

WW6 ES cells (Ioffe et al. 1995) are cultured in ES media containing high glucose, pyruvate-free DMEM (Gibco-BRL, Karlsruhe, Germany) supplemented with 10 % (v/v) ES-qualified FCS (Gibco-BRL, Karlsruhe, Germany), 10 mM each of non-essential amino acids (Gibco-BRL), 100 U/ml penicillin (Gibco-BRL, Karlsruhe, Germany), 100 µg/ml streptomycin (Gibco-BRL, Karlsruhe, Germany), 1 % (v/v) nucleoside mix (Sigma-Aldrich, München, Germany), 50 µM β-mercaptoethanol (Sigma-Aldrich, München, Germany) and 1000 U/ml LIF (Gibco-BRL, Karlsruhe, Germany). Since ES cells are fast-growing cells dividing every 12 – 24 hrs, ES media need to be exchanged daily. It is important to generate single ES cell suspensions during passaging. Aggregating cells tend to differentiate, producing endoderm-like cells.

5.2.3 Establishment of stable cell lines

5.2.3.1 Preparation of targeting DNA

100 µg targeting plasmid DNA (knock-in clone #49 and knock-out clone #4-2, see Results 4, Fig. 2 and 4) is digested with a single cutting enzyme to linearize the circular targeting plasmid DNA. The linearized DNA is extracted twice with phenol/chloroform, precipitated by adding 0.1 Vol 3 M sodium acetate (pH 4.6) and 2.5 Vol 100 % ethanol, pelleted by centrifugation and washed in 70 % ethanol. The DNA pellet is resuspended in sterile 1 x PBS at a concentration of 1 µg/µl. Quality and quantity of DNA is determined by agarose gel electrophoresis using the High DNA Mass Ladder (Invitrogen, Karlsruhe, Germany).

5.2.3.2 Electroporation

Highest transfection efficiencies are obtained using exponentially growing ES cells. Therefore, ES cells are subcultured the day preceding electroporation. ES cells are harvested by trypsin digestion, rinsed in 1 x PBS, resuspended in 10 ml 1 x PBS and counted using a Neubauer hemacytometer. Per electroporation, 2×10^7 ES cells are needed. The concentration of ES cells is adjusted and a mixture of 700 µl ES suspension (2×10^7 ES cells) and 40 µg linearized plasmid DNA is added to the cuvette (4 mm, BioRad, München, Germany). Then, the ES cells are incubated for 10 min on ice, electroporated at 240 V and 500 µF using the GenePulser apparatus with capacitance extender (BioRad, München, Germany) and incubated again for 10 min on ice. Transformed ES cells are transferred on 5 – 6 previously prepared inactivated feeder plates containing ES medium. 48 hrs post-transfection, drug selection is initiated by adding 200 µg/ml Geneticin (Gibco-BRL, Karlsruhe, Germany) to ES media. Selection media (ES media plus Geneticin) is replaced on a daily basis. Six days after drug selection, extensive cell death is observed. Eight days after drug selection, surviving ES cells form colonies and are macroscopically visible. On the following day, Geneticin-resistant clones are picked.

Briefly, single ES colonies are dislodged from the plate by using a pipette tip and are broken up into a single cell suspension by trypsin treatment and by repetitive pipetting. Each stable ES cell line is cultured in duplicate, (i) on previously prepared gelatine-coated 24-well plates containing inactivated feeder cells and (ii) on gelatine-coated 96-well plates for cryopreservation and for subsequent DNA extraction and screening, respectively.

5.2.3.3 DNA extraction of stable ES cell lines

DNA is extracted from ES colonies in 96-well plates after 100 % confluency is reached. Cells are rinsed twice with 1 x PBS and lysed overnight in a 60°C humid atmosphere in 50 µl lysis buffer [10 mM Tris-HCl (pH 7.5), 10 mM Na₂EDTA, 10 mM NaCl, 0.5 % (w/v) SDS] containing proteinase K at a final concentration of 1 mg/ml. The following day, precipitation of a filamentous network of DNA is achieved by adding a mix of 1.5 µl NaCl and 100 µl 100 % cold ethanol to each well. By inverting the plates, the solution is discarded while the filamentous DNA remains attached to the plates. The DNA is rinsed three times with 70 % ethanol, dried and resuspended in 100 µl H₂O.

5.2.3.4 Screening for homologous recombination events in stable ES cell lines

A PCR-based approach (see VI, 3.6) is applied to distinguish „positive” ES clones that have correctly incorporated the targeting plasmid DNA by homologous recombination from „false positive” ES clones that have included the targeting plasmid DNA randomly. For the knock-in lineage, the primer combination mVMD2-F17 and neo-F is used for PCR amplification to identify ES clones harbouring the correct homologous recombination event. Furthermore, genomic DNA quality of knock-in cells is inspected by PCR amplification using primers mVMD2-NdeI-F and neo-F. For the knock-out lineage, mVMD2-F17 and lacZ-R2 primers are used to amplify the 5'-region of the gene. Positive clones are further confirmed by testing the 3'-region of the gene using primers pHM2-3'F and mVMD2-R15. Sequences of oligonucleotide primers are found in Table 11B.

6 PROTEIN BIOCHEMISTRY

6.1 PREPARATION OF PROTEIN EXTRACTS

Protein extracts isolated from transformed *E. coli* bacteria, from transfected COS7 cells and from human and bovine RPE tissues are dissolved in a β-mercaptoethanol-containing SDS sample buffer [62.5 mM Tris-HCl (pH 6.8), 2 % SDS, 10 % glycerol, 5 % β-mercaptoethanol, 0.001 % bromphenol blue] and are denatured for 5 min at 99°C. The heating of the sample as well as β-mercaptoethanol and SDS in the sample buffer have reducing effects on the proteins. Both SDS and β-mercaptoethanol are denaturing reagents, disrupting non-covalent protein interactions and reducing disulfide bonds.

6.1.1 Bacterial lysates

Recombinant fusion proteins (Table 11A) are expressed in bacteria by IPTG induction. According to the manufacturers' instructions (NEB, Frankfurt am Main, Germany), *E. coli* strain XL1-blue is transformed with pGEX-4T3 and pMAL-cxh constructs and cultured until an A_{600} of 0.5 is reached. Expression of recombinant protein is then induced by adding IPTG to a final concentration of 0.3 mM. The cultures are grown for 2.5 hrs, collected by centrifugation and resuspended in the β -mercaptoethanol-containing SDS-PAGE sample buffer.

6.1.2 Whole cell protein extracts of COS7 cells

Two days after heterologous expression of wild-type and mutant bestrophin in COS7 cells, the cells are trypsinized, pelleted and washed twice in 1 x PBS. Thereafter, a whole cell protein lysate is obtained by resuspending the cells in β -mercaptoethanol-containing SDS-PAGE sample buffer.

6.1.3 Membrane fractionation of COS7 cells

Membrane isolation procedure is obtained by ultracentrifugation of COS7 cells in two distinct layers of sucrose concentration. 48 hrs posttransfection, COS7 cells are harvested from two 175 cm² flasks in hypotonic buffer (10 mM Tris-HCl, 0.5 mM Na₂EDTA; pH 7.4) and are pelleted by centrifugation (2800 x g, 10 min). The cells are washed twice in hypotonic buffer, and are then resuspended in the same hypotonic buffer containing a mix of serine and cysteine protease inhibitors (Complete Mini EDTA-free, Roche, Mannheim, Germany). After an incubation time of 1 hr, the cells are homogenized by using a glass homogenizer and by passing them through a 28-G needle. The cells are added to a sucrose column, consisting of 5 % and 60 % (w/v) sucrose in gradient buffer (10 mM Tris-HCl, 150 mM NaCl, 1 mM MgCl₂, 1 mM CaCl₂, 0.1 mM Na₂EDTA; pH 7.4), representing the top and bottom layers, respectively. For 1 hr and at 4°C, the samples are centrifuged at 70 000 x g (SW-28 rotor, Beckman, München, Germany). The membrane fraction (forming a cloudy band in the interphase between 5 % and 60 % sucrose layer) and the soluble fraction (above the 5 % sucrose solution) are collected and centrifuged for 20 min and 4°C at 135 000 x g (TLA100.4 rotor, Beckman, München, Germany). Finally, the pellets are resuspended in the β -mercaptoethanol-containing SDS-PAGE sample buffer.

6.1.4 RPE tissue extracts

RPE tissue extracts are prepared from human and bovine donor eyes within 2 – 3 hrs postmortem. All steps are performed at 4°C. By circumferential incision above the ora serrata of the eye, the anterior segment, the vitreous body and the neurosensory retina are removed from the eye cup. Single bovine RPE cells are detached from the underlying choroid by gently brushing the eye cup in 10 mM Tris-HCl. The human RPE is isolated as membranous fraction together with the choroid. Bovine RPE and human RPE/choroid cells are pelleted by centrifugation and homogenized in chilled RIPA buffer (1 % Nonidet P-40, 0.5 % sodium deoxycholate, 0.1 % SDS in 1 x PBS) containing a complete protease inhibitor cocktail (Complete Mini EDTA-free, Roche, Mannheim, Germany). Lysates are vortexed for 5 min, incubated on ice for 15 min, centrifuged for 5 min at 14 000 g to remove cell debris and finally the protein supernatant is diluted 1:1 in 2 x β -mercaptoethanol-containing SDS-PAGE sample buffer.

6.2 WESTERN BLOTTING

6.2.1 Sodium dodecyl sulfate polyacrylamide gel electrophoresis (SDS-PAGE)

Protein extracts are separated by SDS-PAGE, which is based on the electrophoretic mobility of proteins according to their size. Prior to SDS-PAGE, protein samples are boiled for 5 min. Per lane, 20 – 30 μ l protein sample and 4 μ l prestained SDS-PAGE Standards, broad range (BioRad, München, Germany) are loaded. 10 % acrylamide SDS gels are run for 1 hr at a constant voltage of 100 V in a Tris-glycine buffer (25 mM Tris-Base, 192 mM glycine, 1 % SDS), using the BioRad Mini-protean[®] 3 system (BioRad, München, Germany). The polyacrylamide-SDS gels are composed of two layers, a separating gel [10 % 30:0.8 % (w/v) acrylamide:bisacrylamide, 0.1 % SDS, 375 mM Tris-HCl (pH 8.8)] as bottom layer and a stacking gel [4 % 30:0.8 % (w/v) acrylamide:bisacrylamide, 0.1 % SDS, 125 mM Tris-HCl, (pH 6.8)] as top layer. To activate polymerization, 16 μ l TEMED and 16 μ l APS are added to the 10 ml gel solutions. The stacking gel ensures that the proteins enter the separating gel simultaneously. After electrophoresis, the separated proteins are either directly stained with a Coomassie[®] solution (0.025 % (w/v) Coomassie[®] Brilliant Blue R250, 50 % (v/v) methanol, 10 % (v/v) acetic acid) for 30 min and subsequently destained with 10 % (v/v) acetic acid or the protein gel is further processed and subjected to immunoblotting (see VI, 6.2.4).

6.2.2 *Antibody generation*

The work was performed by two commercial providers, BioScience (Göttingen, Germany) and Eurogentec (Seraing, Belgium). Polyclonal antibodies are raised in New Zealand rabbits, immunized with human antigens AB2 (NH₂-RWWNQYENLPWPDRLM-COOH), AB3 (NH₂-QSHDHHPPRANSRTKL-COOH and EP001358 (NH₂-CDPYWALENRDEAHS-COOH) as well as with the bovine antigen EP001359 (NH₂-CQSLDRQSPRTNSKTK-CONH₂). For each immunization, 15 – 25 mg of peptide is synthesized and coupled to keyhole limpet hemocyanin (KLH) via m-maleimidobenzoyl-N-hydroxysuccinimide ester (MBS). The standard immunization schedule includes an initial immunization and three successive boosts at 14 day intervals.

6.2.3 *Purification of antibodies by affinity chromatography*

First, a bacterial lysate containing the fusion protein MBP-hbov4 (8-1) is generated by IPTG-induced overexpression of the pMAL-cxh-h-bov4 construct (see VI, 6.1.1). Following the manufacturers' instructions (NEB, Frankfurt am Main, Germany), the soluble fusion protein is coupled to an amylose resin column. From the pool of polyclonal antibodies (pAB-334) raised in rabbit 334, antibodies directed against epitope EP001358 bind specifically to the column. After repetitive washing steps, specifically bound antibodies are released from the column by decreasing the pH value. In this way a purified antibody, termed pAB-334(AP3), is obtained.

6.2.4 *Immunoblotting*

The transfer of proteins to a PVDF membrane (Immobilon-P, Millipore, Eschborn) takes place at a constant current of 40 mA for 2 hrs in transfer buffer (25 mM Tris-Base, 192 mM glycine, 15 % methanol) using a BioRad Mini Trans-Blot[®] cell (BioRad, München, Germany). The PVDF membrane is then blocked with 2 % dry milk in 1 x PBS (137 mM NaCl, 0.3 mM KCl, 8.1 mM Na₂HPO₄, 6.7 mM KH₂PO₄; pH 7.4) for a minimum of 1 hr. Thereafter, the membrane is incubated for 1 hr in 0.2 % dry milk/1 x PBS with the primary antibody at dilutions between 1:500 and 1:1000. After three rounds of washing the membrane in 0.05 % Tween/1 x PBS, the membrane is incubated for 30 min in 0.2 % dry milk/1 x PBS with the secondary antibody dilutions between 1:5000 and 1:10000. Secondary anti-rabbit antibodies are conjugated to horseradish peroxidase (Calbiochem, San Diego, USA) and are detected with the ECL detection system (Amersham-Pharmacia-Biotech, Freiburg, Germany).

6.3 IMMUNOCYTOCHEMISTRY

After transient expression of bestrophin in COS7 cells (see VI, 5.1.1), the cells are incubated for a period of 48 hrs at 37°C and 5 % CO₂ on sterile glass coverslips. Adherent cells are rinsed three times with 1 x PBS, fixed with cold acetone for 5 min and washed again three times with 1 x PBS. To reduce non-specific antibody binding and to permeabilize the plasma membrane, cells are treated with a blocking/permeabilization solution (10 % (v/v) normal goat serum, 0.5 % (v/v) Triton X-100 in 1 x PBS) for 30 min. Cells are then labeled for 4 hrs with the primary antibody (pAB-334) diluted 1:500 in 2 % normal goat serum, 0.1 % (v/v) Triton X-100 in 1 x PBS. Then, the cells are washed three times with washing solution (0.5 % Tween in 1 x PBS). From here onwards, all steps are performed in the dark. The cells are incubated for 45 min with the secondary antibody, diluted 1:500 in 2 % normal goat serum, 0.1 % (v/v) Triton X-100 in 1 x PBS. The secondary antibody, Alexa Fluor[®] 488 goat anti-rabbit IgG (Molecular Probes, Leiden, Netherlands) is coupled to light-sensitive FITC. After washing the cells with 1 x PBS, the cellular nuclei are stained for 15 min with DAPI dyes (Applichem, Darmstadt, Germany) at a final concentration of 0.1 µg/ml in 1 x PBS. DAPI staining is performed to determine the transfection efficiency. Three steps of PBS rinsing follow, a drop of mounting medium is added and the cells are examined by using the FITC filter on a conventional fluorescent microscope.

7 METHODS OF BIOCOMPUTATION

Created by NCBI in 1988, the public database NCBI³⁹ GenBank database contains entries of DNA sequences of e.g. genes, EST, mRNA. Those relevant for this thesis are found under the accession numbers given in Table 16.

Table 16 GenBank Accession Numbers

<i>Accession Number</i>	<i>Species</i>	<i>Gene</i>	<i>Type of Sequence</i>
NT_033241	human	VMD2	genomic DNA sequence
AF073501	human	VMD2	cDNA sequence
AAC33766; NP_004174	human	VMD2	protein sequence
AAL40882	pig	VMD2	protein sequence
CAA83005	worm	VMD2	protein sequence
XM_127445	mouse	Sdha	cDNA sequence
NM_010368	mouse	β-gus	cDNA sequence

Today's standard molecular and cellular biology techniques are complemented and facilitated by modern bioinformatic tools. Those tools utilized in this thesis include homology sequence searches (BLAST, BLAT, GeneView), the generation of multiple sequence

³⁹ <http://www.ncbi.nlm.nih.gov:80/>

alignments (T-Coffee, boxshade) and phylogenetic trees (Clustalw, phylodendron), the identification of putative ESE motifs (ESEfinder[©]), and the search for syntenic groupings (Human-Mouse Homology Map) (Table 17).

Table 17 Bioinformatic tools

<i>Name</i>	<i>URL</i>	<i>Purpose</i>
BLAST search	http://www.ncbi.nlm.nih.gov/BLAST/	sequence homology searches
BLAT search	http://genome.ucsc.edu/cgi-bin/hgBlat?org=Mouse&hgsid=13334871	sequence homology searches
boxshade	http://www.ch.embnet.org/software/BOX_form.html	multiple alignment design
Clustalw	http://www.ebi.ac.uk/clustalw/index.html	alignment
DAS	http://www.sbc.su.se/~miklos/DAS/	TM domain prediction
ESEfinder [©]	http://exon.cshl.edu/ESE/	identification of ESE's
GeneView	http://www.ensembl.org/Mus_musculus/	sequence homology searches
HMMTOP	http://www.enzim.hu/hmmtop/index.html	TM domain prediction
Human-Mouse Homology Map	http://www.ncbi.nlm.nih.gov/Homology/	human-mouse homology
Phylodendron	http://iubio.bio.indiana.edu/treeapp/treeprint-form.html	phylogenetic tree
SOSUI	http://sosui.proteome.bio.tuat.ac.jp/sosuiframe0.html	TM domain prediction
T-Coffee	http://www.ch.embnet.org/software/TCoffee.html	multiple sequence alignments
TMHMM	http://www.cbs.dtu.dk/services/TMHMM/	TM domain prediction
TMpret	http://www.ch.embnet.org/software/TMPRED_form.html	TM domain prediction

VII REFERENCES

- Allikmets R, Seddon JM, Bernstein PS, Hutchinson A, Atkinson A, Sharma S, Gerrard B, Li W, Metzker ML, Wadelius C, Caskey CT, Dean M and Petrukhin K. 1999. **Evaluation of the Best disease gene in patients with age-related macular degeneration and other maculopathies.** Hum Genet. 104(6):449-453
- Allikmets R, Shroyer NF, Singh N, Seddon JM, Lewis RA, Bernstein PS, Peiffer A, Zabriskie NA, Hutchinson A, Dean M, Lupski JR and Leppert M. 1997. **Mutation of the Stargardt disease gene (ABCR) in age-related macular degeneration.** Science 277:1805-1807
- Allikmets R. 2000. **Further evidence for an association of ABCR alleles with age-related macular degeneration. The International ABCR Screening Consortium.** Am J Hum Genet. 67(2):487-491
- Altschul SF, Madden TL, Schaffer AA, Zhang J, Zhang Z, Miller W and Lipman DJ. **Gapped BLAST and PSI-BLAST: a new generation of protein database search programs.** Nucleic Acids Res. 25:3389-3402
- Arden GB, Barrada A and Kelsey JH. 1962. **New clinical test of retinal function based on the standing potential of the eye.** Br J Ophthalmol. 46:449-467
- Bakall B, Marknell T, Ingvast S, Koisti MJ, Sandgren O, Li W, Bergen AA, Andreasson S, Rosenberg T, Petrukhin K and Wadelius C. 1999. **The mutation spectrum of the bestrophin protein - functional implications.** Hum Genet. 104(5):383-389
- Berg OG and von Hippel PH. 1988. **Selection of DNA binding sites by regulatory proteins.** J Mol Biol. 200(4):709-723
- Bernstein PS, Leppert M, Singh N, Dean M, Lewis RA, Lupski JR, Allikmets R and Seddon JM. 2002. **Genotype-phenotype analysis of ABCR variants in macular degeneration probands and siblings.** Invest Ophthalmol Vis Sci. 43(2):466-473
- Berson EL. 1992. **Electrical phenomena in the retina.** In: Hart WMJ (editor) Adlers physiology of the eye. Mosby Year Book. St Louis. pp 641-685
- Best F. 1905. **Ueber eine hereditaere Maculaaffektion.** Z Augenheilk. 13:199-212
- Birndorf LA and Dawson WW. 1973. **A normal electrooculogram in a patient with a typical vitelliform macular lesion.** Invest Ophthalmol. 12:830
- Blaisdell CJ, Edmonds RD, Wang XT, Guggino S and Zeitlin PL. 2000. **pH-regulated chloride secretion in fetal lung epithelia.** Am J Physiol Lung Cell Mol Physiol. 278:1248-1255
- Bok D. 1993. **The retinal pigment epithelium: a versatile partner in vision.** J Cell Sci Suppl. 17:189-195
- Buyse G, Trouet D, Voets T, Missiaen L, Droogmans G, Nilius B and Eggermont J. 1998. **Evidence for the intracellular location of chloride channel (Cl⁻)-type proteins:**

- co-localization of CIC-6a and CIC-6c with the sarco/endoplasmic-reticulum Ca^{2+} pump SERCA2b.** *Biochem J.* 330:1015–1021
- Caldwell GM, Kakuk LE, Griesinger IB, Simpson SA, Nowak NJ, Small KW, Maumenee IH, Rosenfeld PJ, Sieving PA, Shows TB and Ayyagari R. 1999. **Bestrophin gene mutations in patients with Best vitelliform macular dystrophy.** *Genomics.* 58(1):98-101
- Capecchi MR. 1989. **The new mouse genetics: altering the genome by gene targeting.** *Trends Genet.* 5:70-76
- Caputi M, Kendzior RJ Jr and Beemon KL. 2002. **A nonsense mutation in the fibrillin-1 gene of a Marfan syndrome patient induces NMD and disrupts an exonic splicing enhancer.** *Genes Dev.* 16(14):1754-1759
- Cartegni L, Zhu Z, Zhang MQ, and Krainer AR. 2002. **ESEfinder web interface .** <http://exon.cshl.edu/ESE/>
- Carter MS, Li S and Wilkinson MF. 1996. **A splicing-dependent regulatory mechanism that detects translation signals.** *EMBO J.* 15:5965–5975
- Cavallerano AA, Gutner RK and Oshinskie LJ. 1997. **Macular Disorders: An illustrated diagnostic guide.** Butterworth-Heinemann, Newton. pp 3-8
- Choe S. 2002. **Potassium channel structures.** *Nat Rev Neurosci.* 3(2):115-121
- Cooper PR, Nowak NJ, Higgins MJ, Simpson SA, Marquardt A, Stöhr H, Weber BHF, Gerhard DS, De Jong PJ and Shows TB. 1997. **A sequence-ready high-resolution physical map of the Best's macular dystrophy gene region in 11q12-q13.** *Genomics.* 41:185-192
- den Dunnen JT and Antonarakis SE. 2001. **Nomenclature for the description of human sequence variations.** *Hum Genet.* 109(1):121-124
- Dreyfuss G, Kim VN and Kataoka N. 2002. **Messenger-RNA-binding proteins and the messages they carry.** *Nat Rev.* 3:195-205
- Dunn KC, Aotaki-Keen AE, Putkey FR and Hjelmeland LM. 1996. **ARPE-19, a human retinal pigment epithelial cell line with differentiated properties.** *Exp Eye Res.* 62(2):155-169
- Dunn KC, Marmorstein AD, Bonilha VL, Rodriguez-Boulan E, Giordano F and Hjelmeland LM. 1998. **Use of the ARPE-19 cell line as a model of RPE polarity: basolateral secretion of FGF5.** *Invest Ophthalmol Vis Sci.* 39(13):2744-9
- Eksandh L, Bakall B, Bauer B, Wadelius C and Andreasson S. 2001. **Best's vitelliform macular dystrophy caused by a new mutation (Val89Ala) in the VMD2 gene.** *Ophthalmic Genet.* 22(2):107-115

- Estevez R, Boettger T, Stein V, Birkenhager R, Otto E, Hildebrandt F and Jentsch TJ. 2001. **Barttin is a Cl⁻ channel beta-subunit crucial for renal Cl⁻ reabsorption and inner ear K⁺ secretion.** *Nature* 414(6863):558-561
- Eversole-Cire P, Concepcion FA, Simon MI, Takayama S, Reed JC and Chen J. 2000. **Synergistic effect of Bcl-2 and BAG-1 on the prevention of photoreceptor cell death.** *Invest Ophthalmol Vis Sci* . 41(7):1953-1961
- Feinberg AP and Vogelstein B. 1984. **A technique for radiolabeling DNA restriction endonuclease fragments to high specific activity.** *Addendum Anal Biochem.* 137(1):266-7
- Felbor U, Schilling H and Weber BHF. 1997. **Adult vitelliform macular dystrophy is frequently associated with mutations in the Peripherin/RDS gene.** *Hum Mutat.* 10:301-309
- Forsman K, Graff C, Nordström S, Johannson K, Westermark E, Lundgren E, Gustavson KH, Wadelius C and Holmgren G. 1992. **The gene for Best's macular dystrophy is located at 11q13 in a Swedish family.** *Clin Genet.* 42:156-159
- Furukawa T, Morrow EM, Li T, Davis FC and Cepko CL. 1999. **Retinopathy and attenuated circadian entrainment in Crx-deficient mice.** *Nat Genet.* 23(4):466-470
- Gallempore RP, Hughes BA and Miller SS. 1998. in **The Retinal Pigment Epithelium.** (Marmor MF, and Wolfensberger TJ, eds). Oxford University Press, 175-198
- Godel V, Chaine G, Regenbogen L and Coscas G. 1986. **Best's vitelliform macular dystrophy.** *Acta Ophthalmol Suppl.* 175:1-31
- Gogarten JP and Olendzenski L. 1999. **Orthologs, paralogs and genome comparisons.** *Curr Opin Genet Dev.* 9(6):630-636
- Goldberg AF and Molday RS. 1996. **Subunit composition of the peripherin/rds-rom-1 disk rim complex from rod photoreceptors: hydrodynamic evidence for a tetrameric quaternary structure.** *Biochemistry.* 35(19):6144-6149
- Gomez A, Cedano J, Oliva B, Pinol J and Querol E. 2001. **The Gene causing the Best's Macular Dystrophy (BMD) encodes a putative Ion Exchanger.** *DNA Seq.* 12(5-6):431-435
- Gorin MB, Breitner JCS, De Jong PTVM, Hageman GS, Klaver CCW, Kuehn MH and Seddon JM. 1999. **The Genetics of Age-related Macular Degeneration.** *Mol Vis.* 5:999
- Graff C, Eriksson A, Forsman K, Sandgren O, Holmgren G and Wadelius C. 1997. **Refined genetic localization of the Best disease gene in 11q13 and physical mapping of linked markers on radiation hybrids.** *Hum Genet.* 101:263-270
- Graff C, Forsman K, Larsson C, Nordström S, Lind L, Johannson K, Sandgren O, Weissenbach J, Holmgren G, Gustavson KH and Wadelius C. 1994. **Fine mapping**

- of Best's macular dystrophy localizes the gene in close proximity but distinct from the D11S480/ROM1 loci.** *Genomics*. 24:425-434
- Gu SM, Thompson DA, Srikumari CR, Lorenz B, Finckh U, Nicoletti A, Murthy KR, Rathmann M, Kumaramanickavel G, Denton MJ and Gal A. 1997. **Mutations in RPE65 cause autosomal recessive childhood-onset severe retinal dystrophy.** *Nat Genet*. 17:194-197
- Hentze MW and Kulozik AE. 1999. **A perfect message: RNA surveillance and nonsense-mediated decay.** *Cell*. 96(3):307-310
- Holtkamp GM, Van Rossem M, de Vos AF, Willekens B, Peek R and Kijlstra A. 1998. **Polarized secretion of IL-6 and IL-8 by human retinal pigment epithelial cells.** *Clin Exp Immunol*. 112(1):34-43
- Hou YC, Richards JE, Bingham EL, Pawar H, Scott K, Segal M, Lunetta LK, Boehnke M and Sieving PA. 1996. **Linkage Study of Best's vitelliform macular dystrophy (VMD2) in a large North American family.** *Hum Hered*. 46:211-220
- Huber S, Schroppe B, Kretzler M, Schlöndorff D and Horster M. 1998. **Single cell RT-PCR analysis of CIC-2 mRNA expression in ureteric bud tip.** *Am J Physiol*. 274:951-957
- Humphries MM, Rancourt D, Farrar GJ, Kenna P, Hazel M, Bush RA, Sieving PA, Sheils DM, McNally N, Creighton P, Erven A, Boros A, Gulya K, Capecchi MR and Humphries P. 1997. **Retinopathy induced in mice by targeted disruption of the rhodopsin gene.** *Nat Genet*. 15(2):216-219
- International Human Genome Sequencing consortium. 2001. **Initial sequencing and analysis of the human genome.** *Nature*. 409:860-921
- Ioffe E, Liu Y, Bhaumik M, Poirier F, Factor SM and Stanley P. 1995. **WW6: an embryonic stem cell line with an inert genetic marker that can be traced in chimeras.** *Proc Natl Acad Sci U S A*. 92(16):7357-7361
- Jentsch TJ, Stein V, Weinreich F and Zdebik AA. 2002. **Molecular structure and physiological function of chloride channels.** *Physiol Rev*. 82(2):503-568
- Kaestner KH, Montoliu L, Kern H, Thulke M and Schutz G. 1994. **Universal beta-galactosidase cloning vectors for promoter analysis and gene targeting.** *Gene*. 148(1):67-70
- Kazazian HH, Boehm MS and Seltzer WK. The ACMG Laboratory Practice Committee Working Group. 2000. **ACMG recommendations for standards for interpretation of sequence variations.** *Genet Med*. 2(5):302-303
- Keen TJ, Inglehearn CF, Kim R, Bird AC and Bhattacharya S. 1994. **Retinal pattern dystrophy associated with a 4 bp insertion at codon 140 in the RDS-peripherin gene.** *Hum Mol Genet*. 3(2):367-8
- Kellner U. 1997a. **Hereditäre Netzhautdystrophien.** *Ophthalmologe*. 94:164-183

- Kellner U. 1997b. **Hereditäre Netzhautdystrophien, Teil 2: Differentialdiagnose.** Ophthalmologe. 94:450-465
- Kikawa E, Nakazawa M, Chida Y, Shiono T and Tamai M. 1994. **A novel mutation (Asn244Lys) in the peripherin/RDS gene causing autosomal dominant retinitis pigmentosa associated with bull's-eye maculopathy detected by nonradioisotopic SSCP.** Genomics. 20(1):137-139
- Kim TS, Reid DM and Molday RS. 1998. **Structure-function relationships and localization of the Na/Ca-K exchanger in rod photoreceptors.** J Biol Chem. 273(26):16561-16567
- Klein D. 2002. **Quantification using real-time PCR technology: applications and limitations.** Trends Mol Med. 8(6):257-260
- Klevering BJ, van Driel M, van de Pol DJ, Pinckers AJ, Cremers FP and Hoyng CB. 1999. **Phenotypic variations in a family with retinal dystrophy as result of different mutations in the ABCR gene.** Br J Ophthalmol. 83(8):914-918
- Korn B, Yaspo ML, Lehrach H and Pouska A. 1999. **Positional Cloning by Exon Trapping and cDNA Selection.** ISBN: 0-471-29797-6
- Kozak M. 1991. **Structural features in eukaryotic mRNAs that modulate the initiation of translation.** J Biol Chem 255:19867-19870
- Kozak M. 1996. **Interpreting cDNA sequences: some insights from studies on translation.** Mamm Genome. 7(8):563-574
- Krämer F, White K, Pauleikhoff D, Gehrig A, Passmore L, Rivera A, Rudolph G, Kellner U, Andrassi M, Lorenz B, Rohrschneider K, Blankenagel A, Jurklies B, Schilling H, Schutt F, Holz FG and Weber BH. 2000. **Mutations in the VMD2 gene are associated with juvenile-onset vitelliform macular dystrophy (Best disease) and adult vitelliform macular dystrophy but not age-related macular degeneration.** Eur J Hum Genet. 2000. 8(4):286-92
- Leydhecker W. 1988. **Augenheilkunde.** 23. Auflage. Berlin, Heidelberg. Springer-Verlag
- Lindl T and Bauer J. 1987. **Zell- und Gewebekultur.** Stuttgart, New York. Gustav Fischer Verlag
- Liu W and Saint DA. 2002. **Validation of a quantitative method for real time PCR kinetics.** Biochem Biophys Res Commun. 294:347-353
- Lorenz B, Preising M and Kretschmann U. 2001. **Molekulare und klinische Ophthalmogenetik.** Deutsches Ärzteblatt. 51-52:2698-2704
- Lorson CL and Androphy EJ. 2000. **An exonic enhancer is required for inclusion of an essential exon in the SMA-determining gene SMN.** Hum Mol Genet. 9(2):259-265
- Lotery AJ, Munier FL, Fishman GA, Weleber RG, Jacobson SG, Affatigato LM, Nichols BE, Schorderet DF, Sheffield VC and Stone EM. 2000. **Allelic variation in the VMD2**

- gene in best disease and age-related macular degeneration.** Invest Ophthalmol Vis Sci. 41(6):1291-1296
- Madsen O, Scally M, Douady CJ, Kao DJ, DeBry RW, Adkins R, Amrine HM, Stanhope MJ, de Jong WW and Springer MS. 2001. **Parallel adaptive radiations in two major clades of placental mammals.** Nature. 409:610-614
- Marlhens F, Bareil C, Griffoin JM, Zrenner E, Amalric P, Eliaou C, Liu SY, Harris E, Redmond TM, Arnaud B, Claustres M and Hamel CP. 1997. Mutations in RPE65 cause Leber's congenital amaurosis. Nat Genet. 17:139-141
- Marmorstein AD, Marmorstein LY, Rayborn M, Wang X, Hollyfield JG and Petrukhin K. 2000. **Bestrophin, the product of the Best vitelliform macular dystrophy gene (VMD2), localizes to the basolateral plasma membrane of the retinal pigment epithelium.** Proc Nat Acad Sci. 97:12758-12763
- Marmorstein LY, McLaughlin PJ, Stanton JB, Yan L, Crabb JW and Marmorstein AD. 2002. **Bestrophin interacts physically and functionally with protein phosphatase 2A.** J Biol Chem. 277(34):30591-7
- Marquardt A, Stöhr H, Passmore LA, Krämer F, Rivera A and Weber BHF. 1998. **Mutations in a novel gene, VMD2, encoding a protein of unknown properties cause juvenile-onset vitelliform macular dystrophy (Best's disease).** Hum Mol Genet. 7(9):1517-25
- Marquardt A. 2001. Dissertation. **Positionsklonierung des Morbus Best-Gens VMD2.** Universität Würzburg.
<http://opus.bibliothek.uni-wuerzburg.de/opus/volltexte/2002/41>
- Martinez-Mir A, Paloma E, Allikmets R, Ayuso C, del Rio T, Dean M, Vilageliu L, Gonzalez-Duarte R and Balcells S. 1998. **Retinitis pigmentosa caused by a homozygous mutation in the Stargardt disease gene ABCR.** Nat Genet. 18:11-12
- Matise MP, Auerbach W and Joyner A. 2000. **Production of targeted embryonic stem cell clones.** In: Joyner A (editor) Gene Targeting: A practical approach. Oxford University Press, Oxford. pp 101-132
- Maw MA, Kennedy B, Knight A, Bridges R, Roth KE, Mani EJ, Mukkadan JK, Nancarrow D, Crabb JW and Denton MJ. 1997. **A Mutation of the gene encoding cellular retinaldehyde-binding protein in autosomal recessive retinitis pigmentosa.** Nat Genet. 17:198-200
- Mohler CW and Fine SL. 1981. **Long-term evaluation of patients with Best's vitelliform dystrophy.** Ophthalmology. 88(7):688-692
- Morimura H, Berson EL and Dryja TP. 1999. **Recessive mutations in the RLBP1 gene encoding cellular retinaldehyde-binding protein in a form of retinitis punctata albescens.** Invest Ophthalmol Vis Sci. 40:1000-1004

- Muller PY, Janovjak H, Miserez AR and Dobbie Z. 2002. **Processing of gene expression data generated by quantitative real-time RT-PCR.** *Biotechniques*. 32(6):1372-4, 1376, 1378-9
- Murphy WJ, Eizirik E, Johnson WE, Zhang YP, Ryder OA, and O'Brien SJ. 2001. **Molecular phylogenetics and the origins of placental mammals.** *Nature*. 409(6820):614-618
- Murray CB, Morales MM, Flotte TR, McGrath-Morrow SA, Guggino WB and Zeitlin PL. 1995. **CIC-2: a developmentally dependent chloride channel expressed in the fetal lung and downregulated after birth.** *Am J Respir Cell Mol Biol*. 12:597-604
- Nichols BE, Bascom R, Litt M, McInnes R, Sheffield VC and Stone EM. 1994. **Refining the locus for Best vitelliform macular dystrophy and mutation analysis of the candidate gen ROM1.** *Am J Hum Genet*. 54:95-103
- Palomba G, Rozza C, Angius A, Pierottet CO, Orzalesi N and Pirastu M. 2000. **A novel spontaneous missense mutation in VMD2 gene is a cause of a Best macular dystrophy sporadic case.** *Am J Ophthalmol*. 129:260-262
- Park DW, Polk, TD and Stone EM. 1997. **Fluctuating vision in Best disease.** *Arch Ophthalmol*. 115:1469-1470
- Penotti FE. 1991. **Human pre-mRNA splicing signals.** *J Theor Biol*. 150(3):385-420
- Petrukhin K, Koisti MJ, Bakall B, Li W, Xie G, Marknell T, Sandgren O, Forsman K, Holmgren G, Andreasson S, Vujic M, Bergen AA, McGarty-Dugan V, Figueroa D, Austin CP, Metzker ML, Caskey CT and Wadelius C. 1998. **Identification of the gene responsible for Best macular dystrophy.** *Nat Genet*. 19(3):241-247
- Pfaffl MW, Horgan GW, Dempfle L. 2002. **Relative expression software tool (REST) for group-wise comparison and statistical analysis of relative expression results in real-time PCR.** *Nucleic Acids Res*. 30(9):36
- Porsch M. 2002. Dissertation. **OMB and ORG-1: Homologous Drosophila T-box proteins with functional specificity.** Universität Würzburg. <http://opus.bibliothek.uni-wuerzburg.de/opus/volltexte/2002/361/>
- Redmond TM, Yu S, Lee E, Bok D, Hamasaki D, Chen N, Goletz P, Ma JX, Crouch RK and Pfeifer K. 1998. **Rpe65 is necessary for production of 11-cis-vitamin A in the retinal visual cycle.** *Nat Genet*. 20(4):344-351
- Sambrook J, Fritsch EF and Maniatis, T. 1989. **Molecular cloning: A laboratory manual.** 2nd Edition. Cold Spring Harbor, New York: Cold Spring Harbor Laboratory Press
- Sauer C. 2001. Dissertation. **Untersuchungen zu den genetischen Ursachen hereditärer Netzhautdegenerationen des Menschen.** Universität Würzburg. <http://opus.bibliothek.uni-wuerzburg.de/opus/volltexte/2002/193/>
- Schneeberger C, Speiser P, Kury F and Zeillinger R. 1995. **Quantitative detection of reverse transcriptase-PCR products by means of a novel and sensitive DNA stain.** *PCR Methods Appl*. 4(4):234-8

- Schwahn U, Paland N, Techritz S, Lenzner S and Berger W. 2001. **Mutations in the X-linked RP2 gene cause intracellular misrouting and loss of the protein.** Hum Mol Genet. 10(11):1177-1183
- Seddon JM, Afshari MA, Sharma S, Bernstein PS, Chong S, Hutchinson A, Petrukhin K and Allikmets R. 2001. **Assessment of mutations in the Best macular dystrophy (VMD2) gene in patients with adult-onset foveomacular vitelliform dystrophy, age-related maculopathy, and bull's-eye maculopathy.** Ophthalmology. 108(11):2060-2067
- Seeliger MW, Grimm C, Stahlberg F, Friedburg C, Jaissle G, Zrenner E, Guo H, Reme CE, Humphries P and Hofmann F. 2001. **New views on RPE65 deficiency: the rod system is the source of vision in a mouse model of Leber congenital amaurosis.** Nat Genet. 29:70-74
- Simpson JC, Wellenreuther R, Poustka A, Pepperkok R and Wiemann S. 2000. **Systematic subcellular localization of novel proteins identified by large-scale cDNA sequencing.** EMBO Reports. 1(3):287-292
- Sonnhammer EL and Durbin R. 1997. **Analysis of protein domain families in Caenorhabditis elegans.** Genomics. 46(2):200-216
- Southern EM. 1975. **Detection of specific sequences among DNA fragments separated by gel electrophoresis.** J Mol Biol 98:503-517
- Spalton DJ, Hitchings RA and Holder GE. 1994. **Methods of ocular examination.** In: Spalton DJ, Hitchings RA and Hunter PA (editors) Atlas of clinical ophthalmology. Wolfe Publishing, Mosby-Year Book Europe Limited. pp 1.1-1.30
- Stöhr H and Weber BHF. 1995. **A recombination event excludes the ROM1 locus from the Best's vitelliform macular dystrophy region.** Hum Genet. 95:219-222
- Stöhr H, Marquardt A, Rivera A, Cooper PR, Nowak NJ, Shows TB, Gerhard DS and Weber BHF. 1998. **A gene map of the Best's vitelliform macular dystrophy region in chromosome 11q12-11q13.1.** Genome Research. 8:48-56
- Stöhr H, Marquardt A, Nanda I, Schmid M and Weber BHF. 2002. **Three novel human VMD2-like genes are members of the evolutionary highly conserved RFP-TM family.** Eur J Hum Genet. 10(4):281-284
- Stone EM, Nichols BE, Streb LM, Kimura AE and Sheffield VC. 1992. **Genetic linkage of vitelliform macular dystrophy (Best's disease) to chromosome 11q13.** Nat Genet. 1:246-250
- Sun H, Smallwood PM and Nathans J. 2000. **Biochemical defects in ABCR protein variants associated with human retinopathies.** Nature Genet. 26:242-246
- Sun H, Tsunenari T, Yau KW and Nathans J. 2002. **The vitelliform macular dystrophy protein defines a new family of chloride channels.** Proc Natl Acad Sci U S A. 99(6):4008-4013

- Thiemann A, Gründe S, Pusch M and Jentsch TJ. 1992. **A chloride channel widely expressed in epithelial and non-epithelial cells.** *Nature.* 356:57–60
- Tian M and Maniatis T. 1994. **A splicing enhancer exhibits both constitutive and regulated activities.** *Genes Dev.* 8(14):1703-1712
- Vandesompele J, De Preter K, Pattyn F, Poppe B, Van Roy N, De Paepe A and Speleman F. 2002. **Accurate normalization of real-time quantitative RT-PCR data by geometric averaging of multiple internal control genes.** *Genome Biol.* 3(7):1-12
- Venter JC, Adams MD, Myers EW, Li PW, Mural RJ, Sutton GG, Smith HO, Yandell M, Evans CA, et al. 2001. **The sequence of the human genome.** *Science.* 291(5507):1304-1351
- Wadelius C, Koisti MJ, Bakall B, Marknell T, Ingvast S, Sandgren O, Li W, Xie G, McGarty-Dugan V, Figueroa D, Austin CP, Metzger M, Caskey CT and Petrukhin K. 1998. **Clustering of mutations in the positionally cloned gene for Best macular dystrophy.** *Am J Hum Genet.* 63(s):2273
- Wain HM, Bruford EA, Lovering RC, Lush MJ, Wright MW and Povey S. 2002. **Guidelines for human gene nomenclature.** *Genomics.* 79(4):464-470
- Waterston RH and the Mouse Genome Sequencing Consortium. 2002. **Initial Sequencing and comparative analysis of the mouse genome.** *Nature.* 420(6915):520-562
- Weber BHF and Mar L. 1994a. **Best's vitelliform dystrophy (VMD2) maps between D11S903 and PYGM: no evidence for locus heterogeneity.** *Genomics.* 20:267-274
- Weber BHF, Vogt G, Stöhr H, Sander S, Walker D and Jones C. 1994b. **High-resolution meiotic and physical mapping of the Best vitelliform macular dystrophy (VMD2) locus to pericentromeric chromosome 11.** *Am J Hum Genet.* 55:1182-1187
- Weber BHF, Walker D and Müller B. 1994c. **Molecular evidence for non-penetrance in Best's disease.** *J Med Genet.* 31:388-392
- Weber BHF, Schrewe H, Molday LL, Gehrig A, White KL, Seeliger MW, Jaissle GB, Friedburg C, Tamm E, and Molday RS. 2002. **Inactivation of the murine X-linked juvenile retinoschisis gene, Rs1h, suggests a role of retinoschisin in retinal cell layer organization and synaptic structure.** *Proc Natl Acad Sci USA.* 2002. 99(9):6222-6227
- Weingeist TA, Kobrin JL and Watzke RC. 1982. **Histopathology of Best's macular dystrophy.** *Arch Ophthalmol.* 100:1108-1114
- Weleber RG, Carr RE, Murphey WH, Sheffield VC and Stone EM. 1993. **Phenotypic variation including retinitis pigmentosa, pattern dystrophy, and fundus flavimaculatus in a single family with a deletion of codon 153 or 154 of the peripherin/RDS gene.** *Arch Ophthalmol.* 111(11):1531-1542
- Wells J, Wroblewski J, Keen J, Inglehearn C, Jubb C, Eckstein A, Jay M, Arden G, Bhattacharya S, Fitzke F, et al. 1993. **Mutations in the human retinal degeneration**

- slow (RDS) gene can cause either retinitis pigmentosa or macular dystrophy.** Nat Genet. 3(3):213-218
- Weng J, Mata NL, Azarian SM, Tzekov RT, Birch DG and Travis GH. 1999. **Insights into the function of Rim protein in photoreceptors and etiology of Stargardt's disease from the phenotype in abcr knockout mice.** Cell. 98(1):13-23
- White K, Marquardt A and Weber BH. 2000. **VMD2 mutations in vitelliform macular dystrophy (Best disease) and other maculopathies.** Hum Mutat. 15(4):301-308
- Wilkie AO. 1994. **The molecular basis of genetic dominance.** J Med Genet. 31(2):89-98
- Xiong H, Li C, Garami E, Wang Y, Ramjeesingh M, Galley K and Bear CE. 1999. **CIC-2 activation modulates regulatory volume decrease.** J Membr Biol. 167:215-221
- Yamamoto H, Simon A, Eriksson U, Harris E, Berson EL and Dryja TP. 1999. **Mutations in the gene encoding 11-cis retinol dehydrogenase cause delayed dark adaptation and fundus albipunctatus.** Nat Genet. 22(2):188-191
- Yang M, Wang XG, Stout JT, Chen P, Hjelmeland LM, Appukuttan B and Fong HK. 2000. **Expression of a recombinant human RGR opsin in Lentivirus-transduced cultured cells.** Mol Vis. 18(6):237-242
- Yeh RF, Lim LP and Burge CB. 2001. **Computational inference of homologous gene structures in the human genome.** Genome Res. 11(5):803-816

VIII APPENDIX**1 cDNA AND PUTATIVE AMINO ACID SEQUENCE OF BOVINE VMD2**

1 ATGACCGTACCTACTCGAGCCAAGTGGCCAATGCCCGTTTAGGCTCCTTCTCCCGCTTG
 M T V T Y S S Q V A N A R L G S F S R L 20
 61 CTGCTGTGCTGGCGAGGCAGCATCTACAAACTGCTCTATGGCGAGTTTCTCATCTTTCTG
 L L C W R G S I Y K L L Y G E F L I F L 40
 121 CTCTGCTACTACATCATCCGCTTCATTTACAGGATGGCCCTCACAGATGAACAGCAAGTG
 L C Y Y I I R F I Y R M A L T D E Q Q V 60
 181 ATTTTTGAGAAGCTGACTCTGTATTGCGACAGCTACATCCAGCTCATCCCCATCTCCTTC
 I F E K L T L Y C D S Y I Q L I P I S F 80
 241 GTGCTGGGCTTCTACGTGACGCTAGTCGTGACCCGCTGGTGGAAACCAGTATGAGAACCTG
 V L G F Y V T L V V T R W W N Q Y E N L 100
 301 CCTTGGCCCGACCGCCTCATGAACCTGGTGTGCTCCTTCGTTGAGGGCAAGGACGAGCAA
 P W P D R L M N L V S S F V E G K D E Q 120
 361 GGCCGGATGCTGCGGCGCACGCTCATGCGCTATGCCAACCTAGGCAACGTGCTCATCCTG
 G R M L R R T L M R Y A N L G N V L I L 140
 421 CGCAGCGTCAGCGCTGCGGTCTACAAACGCTTTCCAGCCACAGCACCTGGTGAAAGCA
 R S V S A A V Y K R F P S P Q H L V K A 160
 481 GGCTTCATGACACCCTCGGAACACAAGCACTTACAAAACTGAGCTTACCACACAACCTCG
 G F M T P S E H K H L Q K L S L P H N S 180
 541 TTCTGGATGCCCTGGGTGTGGTTTTGCCAACTTGTCAACAAAGGCATGGATTGGAGGTCGA
 F W M P W V W F A N L S T K A W I G G R 200
 601 ATCCGGGACCCTATCCTGCTCCAGAGCCTGCTCAACGAAATGAACACCTTGCCTACTCAG
 I R D P I L L Q S L L N E M N T L R T Q 220
 661 TGTGGACAGCTGTATGCCTACGACTGGATCAGTATCCCACTGGTGTACACTCAGGTGGTG
 C G Q L Y A Y D W I S I P L V Y T Q V V 240
 721 ACCGTGGCAGTATACAGCTTCTTCTGCTTGCCTGATTGGGCGGCAGTTTCTGAACCCA
 T V A V Y S F F L A C L I G R Q F L N P 260
 781 GCCAAGGCCTACCCCGGCCACGAGATGGACCTCGTTGTACCCCTCTTACGTTTCTGCAG
 A K A Y P G H E M D L V V P L F T F L Q 280
 841 TTCTTCTTCTATGCCGGCTGGTTGAAGGTGGCAGAGCAGCTCATCAACCCATTTGGAGAG
 F F F Y A G W L K V A E Q L I N P F G E 300
 901 GATGACGATGACTTTGAGACCAACTGGATTGTGACAGGAGCTTGCAGGTGTCCCTATTG
 D D D D F E T N W I V D R S L Q V S L L 320
 961 GCTGTAGACGAGATGCACCAGGACTTGCCACCGATGGAGAGAGATATGTACTGGAATGAG
 A V D E M H Q D L P P M E R D M Y W N E 340
 1021 CCAGAACCACATCCTCCGTACACAGCCGCTTCTGCCAGTCTCGTCGACCCTCCTTTTTT
 P E P H P P Y T A A S A Q S R R P S F F 360

1081 GGCTCCACCTTCAACATCAGTCTGGATAAGGAAGACATGGAGTTTCAGCCAGATCTAGAG
G S T F N I S L D K E D M E F Q P D L E 380

1141 GAGCAAGAGGGTGCTCACTCTGGCATCATTGGCCGCTTCTTAGGGCTGCAATCCCTCGAC
E Q E G A H S G I I G R F L G L Q S L D 400

1201 CGCCAGTCCCCTAGGACAAACTCAAAGACCAAACACTACTGTGGCCCAAGAAAGAAGTCCTT
R Q S P R T N S K T K L L W P K K E V L 420

1261 TCACATGAGAACCAGCCCCAAGAACCTTGAGAGGGGCCGGACAGAACAACACTAGTGACCAGGAA
S H E N Q P K N L G G A G Q N T S D Q E 440

1321 GACAGCAAGGCCTGGAAGGGGAAGATGTTTTCAAGTCTGCGGTGCTCTACGGAAAGGTCA
D S K A W K G E D V F K S A V L Y G R S 460

1381 GGCATCCACAGTGCCCCACAGACACCCCTCAGCCACACCCCTATGGTCTTTCCACCTGGA
G I H S A P Q T P L S H T P M V F P P G 480

1441 CAGTCAGCACCCCTCAAGTCTTCGCAGAATCTCGGGCATAGATGACCCTGTCAAAGATCAA
Q S A P S S L R R I S G I D D P V K D Q 500

1501 AGCCTTCAGCCTGCAACCCCCAGGTCCAAGAAGAGTTTTGAATTGCTCCCAGAGAATGCT
S L Q P A T P R S K K S F E L L P E N A 520

1561 GGGGCCTCAACGGAGCACCCAGAAGTTATTCACATGAGAAGGAAAACGTGCGAGTTTAAC
G A S T E H P E V I H M R R K T V E F N 540

1621 CTGATGGACATGTCAGAGGCCCTGAACATCTCAGAGAACCACACTTGGGACAATCGACA
L M D M S E A P E H L R E P H L G Q S T 560

1681 AGCAACATACACACTATACTCAAAGATCATGGAGATCCTTACTGGGACTTGGAAAAACAGG
S N I H T I L K D H G D P Y W D L E N R 580

1741 GATGAAGCACATTCCTAG
D E A H S * 585

2 ABBREVIATIONS

3'-RACE	rapid amplification of cDNA ends	pAB	polyclonal antibody
5'-, 3'-UTR	3'-untranslated region	PAC	P1-derived bacterial artificial chromosome
A	optic density	PCR	polymerase chain reaction
aa	amino acid	qRT	quantitative reverse transcriptase
AD	activating domain	RFP-TM	arginine (R) phenylalanine (F) proline (P) transmembrane
AMD	age-related macular degeneration	RPE	retinal pigment epithelium
APS	ammonium persulphate	RT PCR	reverse transcriptase PCR
AVMD	adult vitelliform macular dystrophy	s	seconds
<i>β-Gus</i>	<i>β-glucoronidase</i>	SDS	sodium dodecyl sulfate
BLAST	Basic Local Alignment Search Tool	SDS-PAGE	SDS-polyacrylamide gel electrophoresis
BLAT	Basic Local Alignment Tool	SNP	single nucleotide polymorphism
bp	base pair	SR proteins	serine/arginine-rich proteins
BSA	bovine serum albumine	ssDNA	single stranded DNA
cGMP	cyclic guanosine monophosphate	STR	short tandem repeat
cM	centiMorgan	SV40	Simian virus 40
CMV	cytomegalovirus	TEMED	N,N,N',N'-Tetramethylethylenediamine
DAPI	4',6-diamidine-2'-phenylindole dihydrochloride	TF	transcription factor
dNTP	desoxynucleosidtriphosphate	TM	transmembrane
dsDNA	double stranded DNA	Tris	Tris-(hydroxymethyl) aminomethane
EDTA	ethylenediaminetetraacetic acid	U	units
EOG	electro-oculography	URL	Unique Recource Locator
ERG	electro-retinography	VMD2	vitelliform macular dystrophy type 2
ER	endoplasmatic reticulum	Vol	volumes
ES	embryonic stem cells		
EST	expressed sequenced tags		
Gb	giga base pairs		
goi	gene of interest		
GST	gluthathione S-transferase		
HEK	human embryonic kidney		
HeLa	Henrietta Lacks		
Hepes	4-(2-hydroxyethyl)-1-piperazine ethanesulfonic acid		
hrs	hours		
HUGO	Human Genome Organisation		
IPTG	Isopropyl-β-D-thiogalactopyranoside		
IVS	interveneing sequence		
kb	kilo base pairs		
kDa	kilo Dalton		
LIF	lukemia inhibitory factor		
MALDI-TOF	matrix-assisted laser desorption ionization time-of-flight		
MBP	maltose binding protein		
MCS	multiple cloning site		
MD	macular degeneration		
min	minute		
ml	mililiter		
MOPS	Morpholinopropanesulfonic acid		
neo ^r	neomycin-resistant gene		
nt	nucleotide		
nt	nucleotide		
OMIM	Online Mendelian Inheritance in Man		
ORF	open reading frame		
PAA	polyacrylamid		

IX CURRICULUM VITAE**Personal data****Franziska Ingeborg Krämer**

Date of birth: 05.05.72
 Place of birth: Marktredwitz, Oberfranken
 Nationality: German
 Marital status: single
 E-mail: fkraemer@biozentrum.uni-wuerzburg.de

School Education

1979 – 1985 Primary School
 De Kuilen Primary School (Kuilsvier, South Africa)
 Grundschule Neusorg (Germany)
 Bellpark Primary School (Durbanville, South Africa)
 1986 – 1991 High School
 Fairmont High School (Durbanville, South Africa)
 Gymnasium Selb (Germany)
 1991 „Allgemeine Hochschulreife“

University education

1992 – 1999 Studies of „Diplom“-Biology at the Bavarian Julius-Maximilians-
 University of Würzburg:
 1994 „Vordiplom“ Examination
 1998 „Diplom“ Examination (Biochemistry, Human Genetics and Plant
 Physiology)
 1999 „Diplom“ Thesis
 (Title: Molekulargenetische Untersuchungen zur Charakterisierung des
 Morbus Best Gens VMD2)
 1999 – 2003 PhD student at the Institute of Human Genetics (University of Würzburg)
 (Title: Molecular and biochemical investigations into VMD2,
 the gene associated with Best Disease)

University work experience

1995 Practical experience in tropical ecology, in the Comoe National Park
 (Ivory Coast)
 1996 – 1997 Studies of Biology at the University of Texas, Austin (USA)
 (DAAD scholarship)
 1997 Practical laboratory experience in molecular genetics, in the Laboratory of
 Robert Jansen (University of Texas, USA)

X LIST OF PUBLICATIONS

Thesis-related publications

Marquardt, A., Stöhr, H., Passmore, L.A., Krämer, F., Rivera, A. and Weber, B.H.F. 1998. **Mutations in a novel gene, VMD2, encoding a protein of unknown properties cause juvenile-onset vitelliform macular dystrophy (Best's disease).** Hum Mol Genet. 7(9):1517-1525

Krämer, F., White, K., Pauleikhoff, D., Gehrig, A., Passmore, L.A., Rudolph, G., Kellner, U., Andrassi, M., Lorenz, B., Rohrschneider, K., Blankenagel, A., Jurklies, B., Schilling, H., Holz, F.G. and Weber, B.H.F. (2000) **Mutations in the VMD2 gene are associated with juvenile-onset vitelliform macular dystrophy (Best's disease) and adult vitelliform macular dystrophy but not age-related macular degeneration.** Eur J Hum Genet. 8:286-292

Thesis-related publications – in preparation

Krämer F, Götz T and Weber BHF. **Genomic organization, chromosomal localization and gene expression of the murine VMD2 gene family.**

Krämer F, Mohr N, Kellner U, Jurklies B and Weber BHF. **Nine Novel Mutations in the VMD2 gene in Patients with Best Vitelliform Macular Dystrophy (BMD).**

Oral presentations at meetings

Krämer F, Gehrig A, Marquardt A, Rivera A and Weber BHF. 1999. **The Cloning of the VMD2 Gene: Mutation Analysis in Best disease and Adult Vitelliform Macular Dystrophy.** 11. Jahrestagung der Deutschen und Österreichischen Gesellschaft für Humangenetik, Nürnberg, Germany

Krämer F. 1999. **Genetische Ursachen des Morbus Best.** Würzburger Augenärztliche Fortbildung, Würzburg, Germany

Poster presentations at meetings

Marquardt, A., Stöhr, H., Krämer, F., Rivera, A. and Weber, B.H.F. 1998. **Genomic Characterization of 9 Novel Genes within the Core Region of the Best's Disease Locus in 11q12-q13.1.** 48th Annual Meeting of the American Society of Human Genetics, Denver, USA

Marquardt A, Stöhr H, Krämer F, Rivera A and Weber BHF. 1999. **Best's Vitelliform Macular Dystrophy: Refinement of the Chromosomal Locus and Analysis of Candidate Genes.** 10. Jahrestagung der Deutschen und Österreichischen Gesellschaft für Humangenetik, Nürnberg, Germany

Kellner U, Krämer F, Gehrig A, Kraus H, Foerster MH and Weber BHF. 1999. **Clinical Variability in Patients with Mutations in the VMD2 Gene.** Annual Meeting of the Society for Research in Vision and Ophthalmology, Fort Lauderdale, USA

Marquardt, A, Stöhr, H, Krämer, F, Rivera A and Weber BHF. 1999. **Genomic Characterization of 11 Genes in 11q12-q13.1.** 11. Jahrestagung der Deutschen und Österreichischen Gesellschaft für Humangenetik, Nürnberg, Germany

Krämer F, Kubbies M, Swisshelm K, Nanda I, Schmid M and Weber BHF. 2000. **Human claudin-1 (CLDN1): mapping, gene structure and assessment of its role in breast cancer.** 12. Jahrestagung der Deutschen und Österreichischen Gesellschaft für Humangenetik, Lübeck, Germany

Krämer F, Milenkovic H, Stöhr H and Weber B. 2001. **Towards understanding the molecular pathology of vitelliform macular dystrophy (Best disease).** 10th International Congress of Human Genetics, Vienna, Austria

Krämer F, Kneitz B and Weber BHF. 2002. **Generation of a mouse model for Best vitelliform macular dystrophy.** 13. Jahrestagung der Deutschen und Österreichischen Gesellschaft für Humangenetik, Leipzig, Germany

Milenkovic V, Krämer F, Gehrig A and Weber BHF. 2002. **The search of proteins interacting with bestrophin.** 13. Jahrestagung der Deutschen und Österreichischen Gesellschaft für Humangenetik, Leipzig, Germany

Further publications

Krell FT and Krämer F. 1998. **Chemical Attraction of Crab Spiders (Araneae, Thomisidae) to a Flower Fragrance Component.** The Journal of Arachnology. 26:117-119

Ferguson CJ, Krämer F and Jansen RK. **Relationships of Eastern Phlox (Polemoniaceae) based on ITS sequence data.** 1999. Systematic Botany. 24(4):616-613

Krämer F, White K, Kubbies M, Swisshelm K, Weber BHF. 2000. **Genomic organization of claudin-1 and its assessment in hereditary and sporadic breast cancer.** Hum Genet. 107(3):249-56